THE UNIVERSITY *of* EDINBURGH

Mast cell ontogeny and functions in tissue development

Simran Kapoor
Thesis submitted for Doctor of Philosophy
The University of Edinburgh
2026

Acknowledgements

Here I go, writing the hardest part of this thesis. It is nearly impossible to put into words how lucky and fortunate I feel to have had support from so many kind people during this PhD.

First and foremost, I would be nowhere without the guidance of my supervisors. Starting from my earlier years, I am immensely grateful to my undergraduate mentor Dr Dietmar Zaiss, who inspired me to take up immunology all the way back in my third year, and continues to excite me about the field with the ongoing journal club meetings every week. His continued guidance has always been such an important support system to me since, and I would not be where I am without it. I am incredibly thankful to my PhD supervisor Dr Rebecca Gentek for providing me with so many opportunities to learn and develop the scientific confidence I have now. I deeply appreciate her continued trust in me from the very beginning to be able to carry this forward, and it provided me with the best exposure I could have ever asked for. I will always be grateful towards her for her kind support and constant efforts to help me grow out of my comfort zone and challenge myself to learn more. I would also like to extend a massive thank you to my co-supervisor Dr Amy Pedersen, who has been incredibly kind and supportive to me from the very beginning to help navigate through this journey. Her support has been invaluable and endlessly reassuring at so many instances in this PhD, and I am thankful to have had her kind support throughout.

To my wonderful lab: the Gentek lab has been my favorite experience in academia so far. I cannot express how lucky I feel to have had the best lab colleagues. Anna, my lab bestie; Marlene and Cyril, my French-Portuguese lab parents; Bert, my research twin, all of whom

have been so supportive and have become so close to me since I joined the lab. I cannot even begin to express my gratitude to Clara, who provided immense practical support (and emotional support as you know) in this project. I truly could not have even imagined doing this without her. A huge thank you to Solvig for her research and life assistance throughout, chief! I also want to thank Holly for being the best voice of sanity and reason every time. And last but not least in the IRR, I would like to thank the BEG crew as well as the man & bus crew for all the fun side quests! A massive thank you also to Mike and Will, who have made animal work training significantly less daunting and have been so kind and helpful in teaching me to work with mice. On the other side of the world, I would like to thank all my support systems sk and all my closest friends for always being there for me and checking in on me. I am also so grateful to have the nicest PhD cohort to graduate with. Thank you to Adam, Kate, Sam, Ifeanyi and Ruth - our nature walks and expeditions, HPGH retreat reunions, and random get togethers have always been so much fun and helped push us all through. And of course, thank you to Kate for always being there for me, and for our coffee runs and dinners.

I am also very grateful to my funder Wellcome Trust and my programme Hosts, Pathogens and Global Health for their support towards my PhD, and all the opportunities I have had.

Importantly, I would like to thank my family, especially my parents for their constant push and encouragement in my career and in finishing my PhD. I also want to thank my aunt for her unwavering support throughout. And last but not least, I will finally do something out of character and give myself some credit for showing up everyday and making it to this point. This thesis would not have been possible without all the support I have been so privileged to receive, and I am very grateful for everyone I have met during this time.

Abstract

Mast cells (MCs) are granulocytic immune cells classically recognised for their detrimental roles in allergic disease. Widely distributed throughout almost all tissues in the body, MCs are tissue-resident cells that release various mediators during allergic responses, driving pathological tissue remodelling. However, these same effector mechanisms may also participate in beneficial tissue remodelling during development and homeostasis. Emerging studies have proposed that MCs influence vascularisation and innervation processes which are re-shaped during allergy and anaphylaxis. Yet, whether they play a critical role in normal tissue development remain largely unexplored.

Despite their early emergence during fetal development, the prevailing view is that MCs are dispensable for essential tissue development and organogenesis, largely based on observations from conventionally used MC-targeting mice models that appear phenotypically normally without overt developmental defects. However, it remains possible that these genetic models may not sufficiently ablate MCs at developmental windows where they play a critical function. Genetic MC-deficiencies have not yet been identified in humans, lending support to the controversial yet plausible hypothesis that MCs play a critical role in tissue development and survival, and therefore, remain strongly evolutionarily conserved. The aim of this thesis is to re-define the paradigm of the developmental significance of MCs in tissue development.

Previously, conventional *cKit*-based MC-targeting models were used to report the critical developmental function of MCs for mammary gland morphogenesis during puberty. Using newly developed MC-targeting mouse models, I demonstrate that MCs are not critical for

tissue development postnatally in the mammary gland at least, indicating that the previously used *cKit*-based approach may be unsuitable for evaluating MC function in this context. Investigating the critical functions of MCs during development therefore remains and requires a clear understanding of MC identity during development. To address this, I combined single cell RNA sequencing approaches to comprehensively characterise MC ontogeny as they emerge during embryonic days 15.5 to 18.5 in the fetal liver and peripheral tissues. This work revealed that MC developmental kinetics follow a conserved developmental programme, and tissue-specific cues shape the heterogeneity of MCs across tissues as they develop in situ, suggesting potentially important roles in organogenesis. Building on the early expression of *Cpa3* in MCs as they develop during embryogenesis, we newly generated a Cre-based targeting model in which *Cpa3*-Cre driven diphtheria toxin expression in cells may enable direct disruption of MC development in utero to assess its developmental consequences. In contrast to previous assumptions, perturbation of MC development in this novel genetic approach resulted in severe neonatal lethality. This phenotype was associated with altered haematopoiesis and reduced platelets, impaired tissue development, and dysfunctional fetal lungs leading to respiratory distress in these mice shortly after birth. These findings demonstrated that early *Cpa3*-based disruption has profound consequences for developmental homeostasis.

Collectively, this work introduces new genetic tools for developmental immunology in the field of MC biology and uncovers key insights into MC haematopoietic development and functions in organogenesis and tissue development.

Lay Summary

Mast cells are a type of immune cell that are most known for their harmful roles in allergy and anaphylaxis. They are found throughout the body in nearly all tissues, where they can mistakenly respond to harmless substances like allergens and release potent substances like histamine. These substances trigger inflammation and can remodel the surrounding tissue, which contributes to disease in allergic reactions. However, mast cells first emerge very early during fetal development, at a time when tissues and organ systems are actively developing. Yet, the fetus is not directly exposed to the external environment. This raises the question: why do mast cells arise so early? While mast cell activation may remodel and damage tissue in allergy, the same mechanisms may also play a helpful role in shaping tissue development during normal growth and maintenance. Yet, it has remained largely elusive whether mast cells play such a role.

Most previous studies have used mice that have genetic mutations causing them to lack mast cells. However, these models may fail to target mast cells at precise stages of development where they could be essential. Interestingly, no humans have been identified who completely lack mast cells, raising the possibility that the absence of mast cells may be required to support survival after birth. As such, we hypothesise that mast cells may play a critical role in development. The aim of this thesis is to re-evaluate the role of mast cells in tissue development.

To better understand the role of mast cells in tissue development, we generated new mouse models to investigate whether targeting mast cells more specifically in developmental windows resulted in impaired tissue development. Previously, mast cells were shown to play

an important, yet transient role in promoting mammary gland development during puberty. However, these models attempted to target mast cells using a gene that is also expressed on the surface of cells lining the mammary epithelial tissue making it difficult to distinguish whether the observed defects in mammary gland development were due to mast cells or the mammary tissue itself. Using new models that targeted mast cells more specifically showed that mast cells are not essential for pubertal mammary gland development after birth, indicating that earlier conclusions were likely driven by the limitations of the genetic model used.

To investigate whether mast cells play an essential role in tissue development earlier in life, I performed an analysis to map how mast cells develop in the fetus. Using advanced sequencing techniques, this work revealed that mast cells develop in the fetus by first acquiring a shared mast cell programme, and subsequently mature at different rates in different tissues, where the local tissue may shape the identity of mast cells. These findings suggests that mast cells may play an integral role to tissue development during this period. Finally, we created a new genetic model to target mast cell development during birth. Contrary to previous genetic models, the genetically targeted newborn mouse pups in this model succumbed to lethality shortly after birth due to respiratory distress. These newborn mice showed defects in lung development, resulting in poorly functioning lungs and breathing difficulties. Although mast cell populations were replenished in number, they appeared less activated. At the same time, platelets were also reduced, which may have contributed to the observed developmental defects.

Overall, this work collectively introduces new genetic models which can serve as tools to study mast cells and their development, and provides new insights into the role of mast cells in supporting tissues during normal development and growth.

Table of contents

Table of figures

Chapter 3

List of abbreviations

4-OHT	4-hydroxytamoxifen
AGM	Aorta-gonadal-mesonephros
AREG	Amphiregulin
Baso/BasoP(s)	Basophil/Basophil progenitor(s)
BMCP(s)	Basophil mast cell progenitor(s)
c-Kit (*W^v/W^v*)	KIT receptor tyrosine kinase (CD117)
Cebpa	CCAAT/enhancer binding protein alpha
Cma1 (Mcpt5)	Chymase 1/Mast cell protease 5
CMC	Connective tissue mast cell
CMP(s)	Common myeloid progenitor(s)
Cpa3	Carboxypeptidase 3
CSF1	Colony stimulating factor 1
Cx3cl1	CX3C chemokine ligand 1
Cx3cr1	CX3C chemokine receptor 1
DEG(s)	Differentially expressed gene(s)
DTA	Diphtheria toxin A
E	Embryonic day
ECM	Extracellular matrix
EMP(s)	Erythro-myeloid progenitor(s)
Ery/EryP(s)	Erythrocyte/Erythrocyte progenitor(s)
FCERI	High affinity IgE receptor
GDF15	Growth differentiation factor 15
GMP(s)	Granulocyte monocyte progenitor(s)
Gpr141b (Karma)	G protein coupled receptor
HSC(s)	Haematopoietic stem cell(s)
IgE	Immunoglobulin E
IL-3/4/9/10/13	Interleukin 3/4/9/10/13
Itgae/Itgb7/Itga2a	Integrin alpha E/beta7/alpha2
MC(s)	Mast cell(s)
Mcl-1	Myeloid cell leukemia-1
MCP	Mast cell progenitor
Mcpt 1/2/4/7/9	Mast cell protease 1/2/4/7/9
MDP	Monocyte-dendritic cell progenitor(s)
MEP(s)	Megakaryocyte-erythrocyte progenitor(s)
Mitf	Microphthalmia-associated transcription factor

Mk/MkP(s)	Megakaryocyte/Megakaryocyte progenitor(s)
MMC	Mucosal tissue mast cell
MPP(s)	Multipotent progenitor(s)
Mrg/Mrgprb2	Mas-related G-protein coupled receptor (b2)
NK cell	Natural killer cell
PCA	Principal Component Analysis
PGD_2	Prostaglandin D_2
RAG1	Recombination activating gene 1
scRNA-seq	Single cell RNA sequencing
Sl/Sl^d	Steel locus mutation
ST2 (Il1rl1)	IL-33 receptor subunit
TEB(s)	Terminal end bud(s)
TED(s)	Terminal end duct(s)
Tgfb	Transforming growth factor beta
TNFa	Tumour necrosis factor alpha
Tpsb2	Tryptase beta 2
TRPV1	Transient receptor potential vanilloid 1
TSLP	Thymic stromal lymphopoietin
udP(s)	Undefined progenitor(s)
UMAP	Uniform Manifold Approximation and Projection
VEGF	Vascular endothelial growth factor

Literature Review

Mast cell ontogeny and functions in tissue development

Mast cells (MCs) are a type of immune cell that reside within nearly all vascularised tissues in the body (Krystel-Whittemore et al., 2016). They are particularly enriched within barrier tissues, where they are poised to respond to the environmental stimuli. MCs exhibit a diverse range of effector functions (Krystel-Whittemore et al., 2016), underpinned by heterogeneity in MC phenotype (Derakhshan et al., 2022; Tauber et al., 2023; Dwyer et al., 2016). Yet, MCs remain most widely known in the context of allergen-induced hypersensitivity reactions, where MCs are the main effector cells that orchestrate pathological tissue remodelling reactions (Dougherty et al., 2023; Galli and Tsai, 2010; Williams and Galli, 2000). It is conceivable that the mechanisms underlying these responses may fundamentally be important in homeostasis and become pathological when the outcome is detrimental. Consistent with this, there is increasing evidence that MC effector mechanisms may operate beyond pathological allergic reactions. Many of the “type 2” immunological mechanisms in which MCs may play a central role, while important during allergic reactions, also underpin the immunological responses against toxins and pathogens (McSorley et al., 2018; Ogulur et al., 2025).

However, MCs are evolutionarily conserved and their origins pre-date the adaptive immune system which coordinates “type 2” responses (St. John et al., 2023). Nonetheless, the tissue remodelling processes that drive these responses may reflect fundamental mechanisms of tissue development (Zeisberg and Kalluri, 2012). MCs first emerge during embryogenesis (Gentek et al., 2018; Z. Li et al., 2018; Ma et al., 2025), raising the possibility that MC-driven

tissue remodelling functions represent the adaptation of evolutionarily conserved developmental programmes that contribute to tissue formation during development (Chia et al., 2023).

This literature review first addresses the heterogeneity of MCs, and how this may be shaped by their developmental origin. It then provides a detailed overview of their established roles in allergic disease. An evolutionary framework is then applied to consider proposed physiological roles of mast cells in host defence. Finally, the review explores emerging evidence that MCs may play a fundamental role in tissue development, which forms the central focus of this thesis.

Mast cell heterogeneity and development

Early recognition of mast cell heterogeneity

MCs were first described by Paul Ehlrich as early as the 19th century (Beaven, 2009; Crivellato et al., 2003; Ribatti, 2025). Using histological staining techniques, MCs were described to have unique granules that stained metachromatically – like basophils, but residing within tissues instead of blood (Beaven, 2009; Crivellato et al., 2003; Ribatti, 2025). Subsequent discoveries revealed that MCs are not a homogenous cell population. Enerbäck identified a distinct subset of MCs within the intestinal mucosa tissues (Enerbäck, 1966a, 1966b). Although granulated, the MCs within this mucosal tissue showed distinct morphological and staining properties, appearing smaller, less densely granulated (hypogranular), with red-toned metachromasia. Moreover, they also responded differently to activation in response to compound 48/80, showing distinct biological reactivity from MCs in connective tissues (Enerbäck, 1966c).

Transcriptional profiling of mast cell heterogeneity

More recently with the advent of single cell sequencing, cross-tissue transcriptomic datasets have demonstrated that mucosal and connective MCs differ fundamentally at a transcriptomic level. Although they may share core MC signature characterised by genes like *Cpa3* and *Kit,* MCs within connective tissues share a core signature that is largely distinct from MCs in mucosal tissues (Derakhshan et al., 2022; Dwyer et al., 2016; Tauber et al., 2023). The canonical "connective tissue signature" includes expression of genes encoding receptors of the Mrg family (*Mrgprb2, Mrgprb1),* MC proteases (*Cma1, Mcpt4, Tpsb2)* as well as high levels of *Cpa3*. In contrast, MCs in the gut mucosa with "mucosal tissue signatures" typically express distinct MC proteases (*Mcpt1, Mcpt2, Mcpt9),* integrins (*Itgae, Itgb7, Itga2a)* and chemokine receptor (*Cx3cr1).* Notably, these transcriptional profiles have been identified in MCs isolated across adult tissues. MCs detected in connective tissues during fetal development also express *Itgb7* and *Cx3cr1* (Gentek et al., 2018a; Z. Li et al., 2018), raising the possibility that some features of "mucosal" and "connective" MC identity may reflect migratory capacity during trafficking as part of their developmental state, rather than fixed MC subtypes.

These observations establish that MCs exhibit tissue-specific heterogeneity, which may underpin functional specialization in distinct immunological contexts. Importantly, this tissue-specific heterogeneity may itself be shaped by the developmental continuum through which MCs arise and mature. In the following sections, I outline our current understanding of MC development, and discuss how MC developmental states may contribute to the establishment of MC identity and heterogeneity.

Revisiting mast cell developmental origin

At the time of their discovery, MCs were believed to be metamorphosed mesenchymal cells that arose directly from differentiation of the tissue mesenchyme itself (Beaven, 2009; Crivellato et al., 2003; Ribatti, 2025). It was therefore postulated that MCs may reflect the phenotype of the tissue they arise from. However, it is now well established that MCs have a haematopoietic origin. This paradigm shift raises a new possibility: that differences in the developmental origin (or "ontogeny") of MCs taking residence in distinct tissues may contribute to and shape MC heterogeneity. As such, MC identity may be shaped by the developmental context in which they develop within tissues.

Seminal studies in the 1970s began to challenge the notion that MCs are differentiated mesenchymal cells, and laid the foundational proof that MCs are haematopoietic in origin. Following the use of irradiation to ablate host haematopoietic stem cells (HSCs), MCs could be reconstituted in tissues by transplanting donor bone marrow from mutant "beige" mice, which are characterised by large granules in HSC-derived cells like neutrophils (Kitamura et al., 1977). The derived tissue-resident MCs in recipient host tissues in these experiments comprised of similar large granules, indicating that MCs have (donor) haematopoietic origin.

However, reconstitution efficiency differed markedly between tissues. MCs residing in mucosal tissues appeared to be re-constituted most efficiently by donor bone marrow haematopoiesis, whereas MCs within connective tissue like the skin largely remained of the host type. In the skin, MC precursors of host origin were found to be fixed within the tissue and exhibited greater radioresistance than bone marrow haematopoietic progenitors (Hatanaka et al., 1979; Kitamura et al., 1983a). These precursors may therefore remain within the skin even after irradiation and may be capable of locally maintaining MCs, independently of the bone marrow. *cKit* deficient W^v/W^v mice lack MCs across tissues,

thereby generating an empty niche devoid of MCs and their precursors (Kitamura et al., 1978). In this model, subsequent donor bone marrow transplantation could contribute to replenishing MCs in mucosal tissues as well as connective tissues (Kitamura et al., 1978). Indeed, *Kit* signaling may be essential for precursors in the connective tissues, as the precursors fixed in the skin were also depleted in this model (Matsuda et al., 1981). In the absence of precursors seeded within the connective tissue, MCs could be replenished from the bone marrow. Thus, MC precursors were established to be of haematopoietic origin but contribute to mucosal and connective MCs with different kinetics.

Specifically, MCs within mucosal tissues are radiosensitive and show fast turnover kinetics (Fukuzumi et al., 1990), consistent with their reliance on continuous input from precursors deriving from the bone marrow under steady state (Kitamura et al., 1977). In contrast, MCs within connective tissues rely on tissue-seeding precursors that remain relatively radioresistant following differentiation in the tissue and show slow turnover under steady state (Fukuzumi et al., 1990; Kitamura et al., 1983b). Moreover, these precursors do not enter skin tissue in the presence of sufficient mature MCs and precursors (Matsuda et al., 1981). As such, MCs in connective tissues may be able to maintain themselves independent of the bone marrow under steady state.

These observations, demonstrating differential reliance of connective and mucosal MCs on bone marrow haematopoiesis under steady state raised a fundamental question: from which haematopoietic tissue do MCs arise, and at what stages of development are distinct MC populations seeded? Interestingly, MCs can already be detected in connective tissues during embryogenesis, even prior to the onset of bone marrow haematopoiesis, whereas MCs in mucosal tissues emerge predominantly after birth (Combs et al., 1965; Gamble & Stempak, 1961; Kitamura et al., 1979; Kitamura et al., 1978). These findings suggest that the

distinct MC subpopulations may be seeded at different developmental stages, potentially reflecting their distinct haematopoietic origins. In the subsequent section, I discuss early experimental evidence that addressed this question.

Layered haematopoietic development of mast cells: early experiments

Early experimental studies examined the anatomical origin of MCs within embryogenesis and revealed that MC development is embedded within the layered haematopoietic waves that establish during embryonic development. Granular MCs could be detected as early as embryonic day (E)15 within mesenchymal tissues and rapidly increase to the level found in newborns by E18-19 (Combs et al., 1965; Gamble & Stempak, 1961; Kitamura et al., 1979; Kitamura et al., 1978). In contrast, MCs in mucosal tissues were largely undetectable until later postnatal stages of life (Kitamura et al., 1978), suggesting that connective tissue MCs may arise from alternative embryonic haematopoietic sources, prior to the establishment of definitive bone marrow haematopoiesis.

During embryonic development, the yolk sac is the earliest source of haematopoeisis (Palis et al., 1999). Primitive haematopoiesis is initiated in the yolk sac as early as E7.5, which give rise to erythrocytes and megakaryocytes to establish the circulatory system for subsequent development (Palis et al., 1999). Following this, definitive haematopoietic progenitors become active by E8.5, and are associated with the development of definitive erythroid, mast cell and macrophage progenitors (Palis et al., 1999; McGrath et al., 2003; McGrath et al., 2015). These erythro-myeloid progenitors (EMPs) expand within circulation prior to colonising the fetal liver. Definitive haematopoietic stem cells (HSCs) capable of replenishing haematopoietic compartments in adult recipients arise around E10.5-E11, within the aorta-gondal-mesonephros region and subsequently colonise the fetal liver (Medvinsky and Dzierzak, 1996; Müller et al., 1994) and undergo expansion and/or maturation (Ema and

Nakauchi, 2000). Such layered haematopoiesis occurs during embryogenesis, within which MC development must be considered.

Consistent with this framework, early studies established that layered haematopoietic activity within the embryo may contribute to the generation of MCs in a temporally ordered manner. The earliest precursors with mast cell potential could be detected in the yolk sac at E8.5, reaching maximum level by E11 and dropping markedly by E13 (Moore and Metcalf, 1970; Palis et al., 1999; Sonoda et al., 1983). Subsequently, precursors in the fetal liver with MC potential can be first detected at E11, and become the main source of precursors by E13 to E15 (Y. Kitamura et al., 1979). Intriguingly, MC precursors could be detected in the yolk sac as early as E8.5 and were found in higher numbers in the embryo proper, specifically the tail region of the developing liver, rather than in the blood, reflecting that they are preferentially homed to the haematopoietic niche of the fetal liver before colonising peripheral tissues (Palis et al., 1999). Intriguingly a MC-precursor like cell could already be detected within fetal blood at E14.5, peaking at E15.5 and subsequently declining in the period leading to birth (Rodewald et al., 1996). These cells had mast cell potential both *in vitro* and *in vivo,* and already express MC proteases *Cpa3* and to a lesser extent *Mcpt4* and *Mcpt2*. These precursors may represent precursors that are migrating in fetal blood and undergoing partial differentiation prior to seeding tissue. Alternatively, they may be a transient population of circulating fetal MCs restricted to these fetal stages. Nonetheless, these observations established that MC precursor-like cells could be detected with embryonic yolk sac and liver haematopoietic tissues prior to the emergence of mature MCs within fetal connective tissues.

Functional evidence supporting the MC potential of embryonic haematopoietic progenitors was provided by early transplantation studies. MC precursors from the yolk sac and fetal

liver could give rise to MCs in tissues of adult *cKit* deficient W^v/W^v mice (Sonoda et al., 1983a), indicating their ability to generate MCs during embryonic development. The ability of the haematopoietic progenitors to seed peripheral tissues was shown to depend on *Kit* signalling. In *cKit* deficient W^v/W^v mice, MCs as well as their precursors were markedly declined in fetal skin in the absence of the *Kit* receptor, which suggested failure of the precursors to migrate and seed into peripheral tissue, and could not differentiate into MCs in the skin (Hayashi et al., 1985). However, precursors could still be detected in *Kit* ligand (stem cell factor) deficient Sl/Sl^d mice, and transfer of bone marrow from Sl/Sl^d mice to c*Kit* deficient W^v/W^v mice could replenish MCs in connective and mucosal tissues (Kitamura & Go, 1979). Nonetheless, bone marrow transplantation from wild type bone marrow to Sl/Sl^d mice could not replenish MCs in either mucosal nor connective tissues, indicating that *Kit* ligand signaling were thought to be important to support either the recruitment of precursors to tissues, their differentiation into MCs within the tissues, or both (Kitamura & Go, 1979). Fibroblasts express *Kit* (Flanagan and Leder, 1990), and may support the differentiation of connective tissue MCs from precursors derived from Sl/Sl^d mice (Fujita et al., 1989). These findings indicate that stromal niches within tissues may provide essential cues that enable MCPs to differentiate into MCs following seeding of peripheral tissues.

While these studies collectively provided a framework to study MCs as part of the embryonic layered haematopoiesis programme, these studies relied heavily on the use of *in vitro* differentiation assays or adoptive transfer of embryonic haematopoietic cells into adult hosts. Moreover, these adult hosts were subject to irradiation pre-conditioning or were constitutively deficient in signalling *Kit*. However, *Kit* deficiency may also impair HSC maintenance (Fantin et al., 2021; Keller et al., 1995), such that bone marrow transplanted from the donor may be able to outcompete host haematopoietic progenitors. Consistent with this, bone marrow transplantation in *Kit* deficient mice does not require irradiation

conditioning (Waskow et al., 2009). These limitations prompted a re-evaluation of the developmental origin of MCs using genetic fate-mapping approaches, which are discussed in the following section.

Layered haematopoietic development of mast cells: fate mapping

Genetic fate mapping studies have been instrumental in resolving the developmental origins of tissue-resident immune cells *in vivo*. By labelling haematopoietic progenitors at defined developmental stages of haematopoietic activity and tracking their progeny over time, fate mapping enables direct lineage tracing of the immune cell *in vivo,* overcoming limitations associated with transplantation, genetic knockout models and *in vitro* assays. Macrophages provide a well-established paradigm for this approach: fate-mapping experiments have demonstrated that tissue-resident macrophages in adult tissues originate from early embryonic haematopoietic waves and persist into adulthood through self-maintainence within their niches, independently from bone marrow haematopoiesis (Gomez Perdiguero et al., 2014;Hoeffel et al., 2015; Ginhoux & Guilliams, 2016).

Two complementary fate-mapping studies subsequently revealed that MCs also follow a similar “layered” developmental programme. MCs first originate from yolk sac-derived EMPs which seed connective tissues such as the skin, followed by gradual replacement by fetal liver-derived definitive HSC precursors (Gentek et al., 2018a; Z. Li et al., 2018). Connective MCs in adulthood are therefore established during embryogenesis that may persist and self-maintain with minimal input from bone marrow haematopoiesis (Gentek et al., 2018a; Kitamura et al., 1983b, 1977).

While both Gentek et al. (2018a) and Li et al. (2018) clearly support embryonic origin of MCs, they differ in their interpretation of which progenitors contribute to MC waves. Using

a *Cdh5-CreERT2* fate mapping strategy, Gentek and colleagues were able to label the *Cdh5*-expressing hemogenic endothelium in a temporally restricted manner. Early induction (E7.5) could label yolk sac-derived EMPs, and later induction (E10.5) could label HSCs which start emerging from the aorta-gonadal-mesonephros (Gentek et al., 2018a). Based on this, the authors proposed that the second wave of MCs are definitive HSC derived. In contrast, Li and colleagues used the *Runx1-CreERT2* model, which labels haematopoietic progenitors from early EMPs (E7.5), late EMPs (E8.5) and definitive HSCs (E9.5). Instead, they concluded that the second MC wave originates largely from late EMPs and a minor contribution from fetal-HSCs.

These differing interpretations may be reconciled by considering the overlapping nature of the "layered" haematopietic waves. EMPs, fetal-HSCs and adult-type HSCs all originate in close succession between E8.25 and E10.5, and each population generates haematopoietic output over extended periods (McGrath et al., 2015; Palis et al., 2001). However, both of the aforementioned fate mapping approaches rely on temporally restricted labelling using 4-hydroxytamoxifen (4-OHT), which itself remains bioavailable for at least 24 hours. As a result, labelled progenitors may not be cleanly segregated into distinct types if they arise within adjacent induction time points, and the distinction between "early" and "late" EMPs may reflect differences in labelling windows rather than distinct biological populations (Chia et al., 2023). Indeed, EMPs from the yolk sac and fetal liver at these timepoint show comparable haematopoietic potential in clonogenic assays *in vitro* (Dege et al., 2020; Gomez Perdiguero et al., 2014). Likewise, the two fate mapping strategies may label both fetal-restricted type and definitive-type HSCs, depending on timing of induction. Recent evidence suggests that MC potential is restricted to the earliest HSCs and is lost during the transition to adult type HSCs (Yoshimoto et al., 2022), which may explain the limited contribution of adult bone marrow haematopoiesis to connective tissue MCs *in vivo* (Gentek et al., 2018a).

A layered haematopoietic programme for MC development therefore encompasses embryonic haematopoietic contributions which seed MCs in the emerging connective tissues during fetal development, as well as from bone marrow haematopoiesis which predominantly supplies MCs in mucosal tissues or to replenish MCs in *Kit* deficient niches. Nonetheless, progenitors with MC potential are clearly present in the adult bone marrow (Hatanaka et al., 1979; Kitamura et al., 1978). Understanding when and how these progenitors may contribute to maintaining and replenishing MCs is therefore central to understanding MC maintenance kinetics. In the next section, I provide current insights into how MCs are maintained after their initial establishment.

How mast cells are maintained after being established

The recognition that mast cell populations arise from distinct developmental waves and persist with tissue-specific kinetics raises an important question: how are mast cells maintained postnatally once these populations are established?

Bone marrow haematopoietic progenitors with MC potential have been identified by expression of Kit, integrin α4β7 and ST2 (Jamur et al., 2005; Chen et al., 2005). Upon migration into peripheral tissues like the gut mucosa, they also begin to express low levels of FCER1 and gradually mature into MCs (Abonia et al., 2006; Arinobu et al., 2005; Bankova et al., 2015; Gurish et al., 2001). Decades of work have led to the establishment of a model in which bone marrow HSCs generate progenitors in a stepwise manner from multipotent (MPP) to lineage committed MCps via common myeloid (CMP) and subsequent granulocyte-monocyte progenitors (Dahlin et al., 2018; Dahlin and Hallgren, 2015). Within the GMP fraction of the bone marrow, Kit^{+} $ST2^{+}$ $\beta7^{hi}$ progenitors were identified as bipotential basophil/MC progenitors (BMCPs) which differed from other GMPs based on *FceR1* and

Ms4a2 gene expression (Dahlin et al., 2018). Commitment to the MC lineage is subsequently promoted by downregulating expression of *Cebpa* and upregulating expression of transcription factors like *Mitf* (Arinobu et al., 2005; Qi et al., 2013; Tojima et al., 2024). Although these progenitors with mast cell potential exist in the adult bone marrow, their contribution to tissue-resident mast cells *in vivo* is strikingly heterogeneous, depending on the tissue niche.

Maintenance kinetics of mucosal tissue mast cells

Mucosal tissue MCs generally have higher turnover rates from bone marrow, and this has been attributed to differences in radiosensitivity (Fukuzumi et al., 1990; Kitamura et al., 1983b). While these cell-intrinsic differences may contribute, environmental factors are also key drivers of MC turnover. MCs in the intestinal mucosa are continuously exposed to food antigens and microbiome as well as inflammatory triggers, which could explain their high turnover rates, as seen in intestinal macrophages (Bain et al., 2014). Consistent with this mucosal MCs in the gut mucosa are sparse right after birth (Kitamura et al., 1977), when postnatal cues that influence their development are not yet established. One such postnatal cue is the microbiota, as MCs do not develop in mucosal tissues in germ-free mice (Schwarzer et al., 2019; Tauber et al., 2023). Moreover, inflammatory triggers encountered postnatally in the respiratory and gastrointestinal mucosal tissues further influence the recruitment and development of mucosal MCs (Derakhshan et al., 2021; Knight et al., 2000).

Maintenance kinetics of connective tissue mast cells

Unlike in the case of mucosal MCs, MC-competent progenitors in the bone marrow show limited actual contribution to tissue-resident MCs in connective tissues under steady state. Bone marrow transplantation experiment, even in irradiated newborns, revealed marked radioresistance of connective tissue MCs (Z. Li et al., 2018), supporting the notion that

connective tissue MCs and their precursors may have already seeded the tissues by birth. The low turnover of these connective tissue MCs from bone marrow progenitors under steady state (Kitamura et al., 1977; Li et al., 2018) may be explained by self-maintenance mechanisms established by MCs (Matsuda et al., 1981; Waki et al., 1990). According to this proposal, when mature MCs are present within a tissue, they may suppress recruitment and differentiation of progenitors. Recent lineage-tracing studies further support this model. MCs in connective tissue like the skin are labelled by fluorescent protein expressed under the control of *Mcpt5-Cre* (Weitzmann et al., 2020). Under steady state, these *Mcpt5*-expressing mature MCs themselves clonally expand to form stable clusters under steady state that self-maintain in the absence of bone marrow haematopoiesis. These findings suggest that MCs may be able to sense the presence of other MCs in the niche, perhaps through sending chemokines or growth factors, although the mechanisms still remain unknown. Patients with mastocytosis have a gain-of-function mutation in *Kit* and exhibit a pronounced increase in MC densities and flux even under steady state (Akin et al., 2025), suggesting that *Kit* may be one of important signals involved in defining MC clonal territories. Understanding the mechanisms that underlie MC maintenance under steady state will therefore be important from a clinical standpoint.

Nonetheless, donor bone marrow could contribute to MC replenishment in a MC deficient niche in *Kit* deficient W^v/W^v mice (Kitamura et al., 1978; Z. Li et al., 2018). However, as mentioned previously, *Kit* deficiency may also impair HSC maintenance (Fantin et al., 2021; Keller et al., 1995), such that bone marrow transplanted from the donor may be able to outcompete host haematopoietic progenitors. Inducible depletion of MCs in adult tissues followed by irradiation revealed that MCs in connective tissues like the skin were poorly replenished from donor bone marrow (Gentek et al., 2018a). These findings indicate that skin MCs in the adult tissue are long lived and exhibit slow recovery kinetics with limited

bone marrow contribution not just in steady state but also upon recovery in an empty depleted niche. Nonetheless, post depletion, by 6 months MCs eventually are replenished (Gentek et al., 2018a), likely from host precursors that remain radioresistant. Notably, these did not derive from yolk sac progenitors labelled at E7.5 but may be from later definitive precursors that replace them (Gentek et al., 2018a).

While cell-intrinsic differences in radiosensitivity may similarly contribute to MC maintenance kinetics, the local tissue microenvironment plays an important role in shaping connective tissue MC maintenance mechanisms, as is reflected by the heterogeneity in maintenance kinetics of MCs across various connective tissues. For instance, contrary to skin MCs, MCs in the peritoneum could be recovered eventually from donor bone marrow following inducible depletion in adulthood (Gentek et al., 2018a). Peritoneal MCs exhibit differences in their transcriptional profile from skin MCs, and exhibit much higher expression of cell cycling even in steady state and therefore retain proliferative capacity (Sonoda et al., 1984; Dwyer et al., 2016). We speculate that the variations may be driven by the anatomical differences between the tissues that MCs reside in. Peritoneal MCs line the serosal gut wall and may therefore experience different signals than MCs seeded within tissue like the skin.

Taken together, MC developmental origin may determine how MCs develop distinctly within mucosal and connective tissues. Differences in their maintenance strategies – ranging from short-lived, continuously replenished mucosal MCs and long-lived, self-maintaining connective MCs – define the temporal window during which MCs are exposed to environmental cues within the tissue they develop in. Insights from other immune cell populations suggests that stromal niches play a central role in regulating maintenance. At least for macrophages, their niche is maintained by signals – most prominently CSF1 –

derived from stromal cells including fibroblasts, epithelial cells, endothelial cells as well as glial cells (Guilliams et al., 2020). A refined understanding of what tissue-specific factors promote MC maintenance will be important to better understand how MCs are maintained in health and disease. These factors may shape establishment and plasticity of MC identity and contribute to MC heterogeneity. In the next section, I provide a framework for how different developmental cues may contribute to shaping MC identity and phenotype.

Influence of developmental origin in shaping mast cell identity

Early experimental evidence of the tissue microenvironment in shaping MC identity initially came from c*Kit* deficiency models, where bone marrow cultured MCs differentiated into either connective tissue-type or mucosal tissue-type MCs depending on the type of tissue they were injected into (Kitamura et al., 1987; Nakano et al., 1985). Fibroblasts express *Kit* ligand (stem cell factor) (Flanagan and Leder, 1990), and may support the differentiation of connective tissue MCs from precursors derived from *Kit* ligand deficient *Sl/Sl*^{d} mice (Fujita et al., 1989). In addition, cytokines like IL-3 further promote MC differentiation towards connective tissue phenotypes (Levi-Schaffer et al., 1991). These early findings indicated that stromal niches within tissues may provide essential cues that enable MCPs to differentiate into MCs following seeding of peripheral tissues.

Importantly however, the dichotomy between mucosal and connective tissue type MCs may not be so strict. Considerably plasticity can exist between MC subtypes, and MC identity can switch from strict MMC signatures and can also comprise transcriptional profiles of MC subtypes found in connective and mucosal tissues. MCs expressing varying combinations of Mcpt1, Mcpt2 and Mcpt5 have been detected in response to different stimuli encountered over the course of inflammation and resolution as they migrate and localise within different tissues in the gut (Friend et al., 1998) (Friend et al., 1996). Similarly, MCs in various locations

along the lung and trachea broadly express proteases Mcpt1, Mcpt2 as well as Mcpt4, Mcpt7 and Cpa3 (Xing et al., 2011), going beyond the classical connective/mucosal MC dichotomy. These studies profoundly demonstrate how MC identity is strongly influenced by tissue context.

However, the *cKit* deficiency model does not reflect the naturally occurring layered developmental model of MCs, and therefore does not capture how MC identity is established under physiological conditions as they emerge in the spatio-temporally "layered" manner. In adulthood, bone marrow MCPs first commit to MCs through transcriptional factors like *Gata2* and *Mitf* (Arinobu et al., 2005; Kitamura et al., 2002a; Qi et al., 2013; Tojima et al., 2024). Following lineage commitment, these progenitors then migrate to tissues and mature within the tissue environment (Bankova et al., 2015; Derakhshan et al., 2021; Gurish et al., 2001), and therefore their development may be influenced by the state of the tissue it encounters during differentiation.

Factors determining mucosal tissue mast cell identity

Mucosal MCs which emerge postnatally likely are shaped by postnatal cues. One of the earliest cues which emerges after birth is the microbiome, and its importance in shaping mucosal MC identity is reflected by the absence of mucosal type MCs but not connective tissue type MCs in germ-free mice (Schwarzer et al., 2019; Tauber et al., 2023). Nonetheless, MMCs are generally sparse in the steady state, and they are more robustly induced by inflammatory stimuli triggered by insults encountered postnatally. Type 2 T-cell responses induce MMC development which underpin helminth infections (McSorley et al., 2018; Lützelschwab et al., 1988; MacDonald et al., 1980; Abe, 1988; Mayrhofer, 1979; Ruitenberg & Elgersma, 1976; Arizono et al., 1996), as well as allergic inflammatory conditions such as asthma (Reber et al., 2015) and food allergies (Hagel et al., 2013; Yang et al., 2013). Key

mediators of this response, including Notch signalling as well as cytokines like IL-10 and Tgfb (McSorley et al., 2018; Tu et al., 2005), play a key role in generating an “MMC” type of signature. These signals directly promote an increase in serine proteases like Mcpt1 and Mcpt2 and concomitantly repressing other proteases like Mcpt5 and cathepsin G (Derakhshan et al., 2021, 2025; Meurer et al., 2025; Nakano et al., 2021). MMCs therefore acquire their identity depending on their local microenvironment during their emergence postnatally.

Factors determining connective tissue mast cell identity

In contrast, connective tissue MCs emerge prenatally, they are likely exposed to different prenatal cues which may shape their development differently. Moreover, their longevity and self-maintenance mechanisms under steady state highlight the importance of understanding how the identity of these MCs is first established. Adult connective tissue MCs exhibit transcriptional diversity across distinct sites such as the peritoneum, skin, tongue, trachea and oesophagus (Dwyer et al., 2016). In other tissue-resident immune lineages such as macrophages, EMPs first commit to the core macrophage programme prior to migrating and seeding tissues in the embryo, after which local tissue-specific microenvironmental cues direct transcriptional diversification (Mass et al., 2016). One open question is whether MCs may follow a similar programme. MCPs with immature MC phenotypes were previously detected in the fetal liver and circulation as early as E11.5 (Guiraldelli et al., 2013; Z. Li et al., 2018; Ma et al., 2025). Although hypogranular, they already begin to transcriptionally express certain MC proteases like *Cpa3*, as well as *Kit* at this stage (Guiraldelli et al., 2013; Z. Li et al., 2018; Ma et al., 2025). This indicates that MCps may also commit to lineage prior to tissue colonization and final maturation may occur after seeding in the tissue. However, key questions remain unresolved. It remains unknown what transcription factors drive this commitment to a core MC programme in fetal stages and

whether it is conserved across tissues. Moreover, it is also unclear how developing MCs integrate their core signature with tissue-specific signals to drive heterogenous MC identity in distinct tissues. Spatio-temporal transcriptomic mapping of MC development in embryonic tissues may address these questions. In addition, postnatal cues may also affect MCs in connective tissues. For instance, skin MCs in adult mice appear reduced and functionally immature in germ-free conditions, as the microbiota normally promotes Kit ligand (Stem cell factor) expression from keratinocytes and shapes skin MC identity postnatally (Wang et al., 2017).

The layered developmental origin of MCs therefore also provides a framework for not only their identity, but also their functional heterogeneity. Connective tissue MCs are long lived and self maintaining, and are poised to mediate rapid responses within the stromal, neurovascular rich niches they occupy. Mucosal MCs in contrast, are replenished from adult bone marrow progenitors, exhibiting higher plasticity in response to inflammation. This framework helps reconcile longstanding observations of tissue-specific MC functions. In the following sections, I will discuss the effector functions of MCs, and how these two subsets may differ in functional specialisation.

Mast cell effector functions

When MCs were first discovered by Ehrlich, they could be detected at higher densities in chronically inflamed tissues and tumours, especially surrounding blood vessels and areas of actively growing, developing tissues (Crivellato et al., 2003). Since these tissues have high nutritional requirements, he accordingly termed them as “Mastzellen” derived from the german word relating to nourishment, proposing that these granular MCs may serve a “nutritional” function within the tissue. Although it is now established that MCs do not

directly provide nutrients to tissues, this early hypothesis anticipated their intimate association with tissue development and regeneration functions. Indeed, many of the MC effector functions are associated with trophic effects on stromal mesenchymal cells, neurons and vascular endothelial cells (Krystel-Whittemore et al., 2016; Metcalfe et al., 1997).

Mast cells as effector cells of allergy

Active research on allergy was already underway at the time MCs were discovered, and their link to allergy became clear early on. Histamine and eicosanoids derived from degranulating mast cells were associated with the symptoms of allergic reactions (Mota & Vugman, 1956; Roberts et al., 1979). The discovery of the IgE antibody within the sera of allergic patients (Stanworth, 1993; Platts-Mills et al., 2016) established that IgE-mediated activation was thought to drive allergy. The high affinity IgE-receptor FcERI (Turner and Kinet, 1999) was subsequently identified on MCs as well as other granulocytic immune cells including basophils, neutrophils and eosinophils, indicating that these cells may be effectors of IgE-mediated allergic reactions (Kawakami and Galli, 2002; Galli and Tsai, 2012). Consistent with this, constitutive depletion of the FCERI receptor abrogates IgE-driven anaphylactic reactions (Dombrowicz et al., 1993).

However, MCs are uniquely poised to initiate immediate hypersensitivity responses in allergy. They express FcERI at high levels and constitutively reside in tissues, and are therefore uniquely poised to trigger allergic reactions as part of the immediate hypersensitivity response (Stone et al., 2010). In contrast, basophils remain in circulation and need to first be recruited within tissues, while FCER1 expression is lower in neutrophils (Mora et al., 2009) and eosinophils (Kayaba et al., 2001). These features support the primary

role of MCs in initiating allergic reactions, whereas other granulocytes may amplify and sustain the allergic reaction (Stone et al., 2010; Galli and Tsai, 2012).

Upon exposure to allergens, antigen(allergen)-specific IgE bind to FCERI which subsequently aggregate on the MC surface to trigger activation (Metcalfe et al., 2009). This leads to the rapid release of pre-formed granular content including serotonin, histamine, proteoglycans like heparin and proteases (tryptase, chymase, Cpa3) as well as de novo lipid mediators. These mediators act within minutes on surrounding tissue components including the neurons, stroma and vasculature to driving a broad range of changes within the tissue (Galli and Tsai, 2012). Mechanistically, MC mediators promote a range of responses, including vasodilation and vascular permeability (Galli & Tsai, 2012; Norrby, 2002; Nakamura & Murata, 2018; Nuñez-Borque et al., 2022), as well as smooth muscle contraction (Charles A Janeway et al., 2001). In parallel, IgE-activated MCs also engage neurons in close proximity. The release of chymase Mcpt4 – expressed by connective tissue MCs - activates proximal Trpv1 sensory neurons and depolarizes them, transmitting signals to the brainstem thermoregulatory circuit and driving hypothermia, which may further exacerbate vasodilation (Bao et al., 2023). Consistent with this, selective targeting connective tissue type MCs but not mucosal tissue MCs protects against the temperature drop in anaphylactic shock (Tauber et al., 2023). Another aspect of an allergic response is pruritus (itch), whereby histamine secreted from MCs binds to TRPV1 neurons and results in histaminergic itch (Wang et al., 2020).

These ‘early phase’ changes are typically localized to the site of the tissue where the MCs were exposed to the allergen. For example, exposure to allergens in the respiratory tract manifests as rhinitis and asthma, in the gastrointestinal tract as food allergy, and in the skin as dermatitis (Berni Canani et al., 2024). The symptoms associated with the site begin to

resolve within a few hours, fully resolving within 1-2 days (Galli et al., 2008; Galli and Tsai, 2012, 2010). This quick resolution reflects the short half-life of MC mediators like histamine and tryptase (Mandola et al., 2019; Schwartz, 1990). Moreover, MC proteases like tryptase also have the potential to cleave IgE (Rauter et al., 2008) which may reduce its half-life in sera and contribute to self-resolution of allergic responses (Lawrence et al., 2016). However, if the release of these mediators occurs at high concentrations systemically, for instance following ingestion or intraveneous exposure to the allergen at large doses, it results in a potentially fatal shock reaction called anaphylaxis and requires immediate treatment (Kemp and Lockey, 2002; Metcalfe et al., 2009).

Beyond immediate responses MCs may also contribute to 'late phase' responses depending on the strength of the initial reaction. Hours after exposure, MCs are able to release a broad range of cytokines, chemokines and growth factors which may further interact with the immune system to drive the 'late phase' response (Galli et al., 2008; Galli and Tsai, 2012). This results in the recruitment of leukocytes including neutrophils and eosinophils, as well as T-cells. Repeated or prolonged exposure to allergens amplifies these responses and is associated with chronic allergic inflammation. While mucosal type MCs are sparse at baseline, the onset of the adaptive immune responses, especially T-cells, drive enhanced recruitment and differentiation of mucosal MCs (Derakhshan et al., 2021; Oishi et al., 2025).

Whilst MC mediators may contribute to unfavourable responses to benign antigens like allergens, the mediator-driven immune responses may be beneficial if appropriately mounted. Yet, MC effector functions have largely been recognised in the context of pathological allergic reactions. This pathological context alone cannot explain their remarkable evolutionary conservation. Indeed, mast cells predate the adaptive immune system and emerged prior to when IgE-mediated immunity first evolved (Crivellato and

Ribatti, 2010; Metcalfe and Boyce, 2006; St. John et al., 2023), suggesting that allergic responses may represent a specialized use of an older effector program. Given their strategic tissue localisation and capacity for immediate activation, it has been proposed that MCs may play an important role in host defence. Indeed, most components of the immune system play an important role in host defence, and it is conceivable that MCs may also be key players in this response. To understand why mast cells and their potent mediators have been retained despite the risk of allergy and anaphylaxis, it is necessary to consider their functions within an evolutionary framework. In these next sections, MC effector functions beyond their role in allergic disease are discussed under the framework of an evolutionary context.

Evolutionary perspectives on mast cell functions: an ancient mode of host defence?

MCs are evolutionary ancient cells, which evolved prior to the adaptive immune system which orchestrates IgE mediated immunity. MC-like cells can be detected in early chordates including tunicates (Brunelli et al., 2025) (Cavalcante et al., 2000; García-García et al., 2014; Wong et al., 2014). Intriguingly, these MC-like cells share features with connective tissue type MCs found in mammals, including the expression of histamine, heparin, prostaglandin D2 and serine proteases (tryptase and chymase) and can also degranulate upon activation (Brunelli et al., 2025; Cavalcante et al., 2000; De Barros et al., 2007; Wong et al., 2014)(Akula et al., 2015; Hellman and Thorpe, 2014; Hellman et al., 2017). Moreover, like present day MCs, these early MC-like cells are also enriched in barrier tissues (Cavalcante et al., 2000). Localised within these tissues, they appear to module vascular permeability and hemagglutination (Cavalcante et al., 2000; De Barros et al., 2007), suggesting potentially conserved roles of connective tissue type MCs in tissue remodelling, most likely in the

context of host defence. Indeed, upon exposure to bacteria, these cells are able to degranulate and secrete heparin, histamine and TNFa (Cima et al., 2018).

However, these early MC-like cells do not get activated by IgE in the absence of the adaptive immune response, but instead respond to basic secretagogues via G-protein coupled receptors on the cell surface, including members of the Mrg receptors (Ferry et al., 2002; Kashem et al., 2011; Tatemoto et al., 2006). This mode of activation is retained even in connective tissue MCs found in present day mammals (Tauber et al., 2023). Through their Mrg receptors, they interact with nociceptive peptidergic neurons (Starkl et al., 2024) to regulate pain and non-histaminergic IgE-independent pruritus responses (Meixiong et al., 2019). Nociception itself is evolutionarily ancient (Baraniuk, 2012; Smith and Lewin, 2009), further underscoring the importance of MCs in response to early danger sensing.

One possibility is that these receptors may have evolved in connective tissue MCs early on to expand their responsiveness to a range of diverse physiological substances – including neuropeptides, venoms, anti-microbial peptides and other basic secretagogues that they may encounter directly in the exposed environment (Grimbaldeston, 2015). From an evolutionarily perspective, the “ancient” MCs may have selected for this even before the evolution of the IgE pathway, as such broad responsiveness would enhance early danger sensing and rapid defence. Nonetheless, even in the absence of IgE, these basic secretagogue receptors inadvertently trigger a MC response to benign antigens and result in pseudo-allergic responses (McNeil et al., 2014; Kumar et al., 2021). In this framework allergy may simply reflect the evolutionary cost associated with expanding the repertoire of MC responsiveness.

The most potent forms of allergic disease are predominantly observed in mammals, coinciding with the emergence of IgE dependent mechanisms (Daschner and González Fernández, 2020; Fitzsimmons and Dunne, 2014; Pritchard et al., 2021). IgE is present at low levels in circulation, is unable to fix complement and relies on cellular effector functions by binding to its high affinity FCERI receptor (Galli and Tsai, 2012). This suggests that IgE-dependent immune mechanisms rather likely represent an adaptive layer that may have co-opted the ancient MC effector system and amplified it through antigen-specificity. Consistent with this, the FCER1 receptor evolved around a similar time to IgE in early mammals (Akula et al., 2014; Hellman et al., 2017).

Notably, activation and degranulation via the Mrgprb2 receptor compared to the FCER1 receptor triggers distinct responses (Gaudenzio et al., 2016). Basic secretagogues such as substance P which activate Mrg receptors, trigger a rapid, yet transient release of small granules and limited de novo synthesis of inflammatory mediators. In contrast, activation through FCER1 receptor results in enhanced de novo inflammatory mediator synthesis, as well as the exocytosis of larger granules that persist for longer and more likely to travel to lymph nodes and activate the adaptive arm of immunity (Gaudenzio et al., 2016). This suggests that the FCER1 function does not define evolutionary origin of MCs but rather represents a coupling mechanism that enhances the antigen-specificity of MCs as part of adaptive immunity. Importantly, the ancestral IgE-independent pathways are still retained and co-exist alongside IgE-dependent responses in allergic reactions. For example, allergens like house dust mite directly activate nociceptors and form physical contacts with Mrgprb2^{+} connective tissue MCs, resulting in their activation and type 2 immunity in allergic reactions (Serhan et al., 2019). In this evolutionary framework, it is conceivable that allergies are a pathological manifestation of an immunological strategy that evolved to enhance MC

defence mechanisms at barrier tissues (Artis et al., 2012; Palm et al., 2012). In the next section, we will discuss how MCs effector mechanisms play a key role in host defence.

The role of mast cells in defence against toxins

Although the type 2 immune response associated with IgE drives allergic responses, these immune responses are also activated in response to environmental challenges that represent a genuine threat to the host, including macroparasitic helminths as well as noxious toxins (Palm et al., 2012). These toxins may be encountered at barrier sites – including the skin, lung as well as the gut (Florsheim et al., 2021; Palm et al., 2012; Profet, 1991) (Mukai et al., 2016). In these contexts, MC mediators can directly contribute to host protection by enzymatically cleaving and neutralising a range of toxins, including venoms and even toxins produced by bacterial pathogens (Metz et al., 2006) (Akahoshi et al., 2011; Anderson et al., 2018; Schneider et al., 2007; Starkl et al., 2020a). Furthermore, the vasoactive and proteolytic mediators such as heparin, when released by MCs, may act as anti-coagulants to prevent the spread of the noxious substance (Palm et al., 2012). Other protective MC-mediated effector functions includes pruritus (Meixiong et al., 2019; F. Wang et al., 2020) which may be beneficial in this context to promote scratching and physical removal of irritants, as well as regulating pain responses which may similarly drive behaviours to reduce exposure (Starkl et al., 2024). These protective roles provide a plausible explanation for why the rapid and systematically potent responses of MCs may have been evolutionarily selected for, given the significant and immediate risk of these toxins (Palm et al., 2012; Profet, 1991).

Importantly, IgE-dependent mechanisms can further enhance protection against these toxins (Marichal et al., 2013; Starkl et al., 2020a, 2016). However, these toxins also existed prior to the onset of the adaptive immune system (Pritchard et al., 2021). It has been

proposed that the integration of the adaptive immune system may have provided an evolutionarily advantage of supporting a form of “allergic” memory, such that the organism can sense the quality of the external environmental stimuli and upon sensitisation to avoid the antigen in the future (Plum et al., 2024). Indeed, at least for food toxins, MCs sense antigens that might be noxious and be activated, which promoted their avoidance of the antigen overtime after being sensitized to the toxin (Florsheim et al., 2023; Plum et al., 2023). Importantly, antigen avoidance behaviour was abrogated in the absence of IgE and FCER1 receptor, indicating the importance of the adaptive arm in sensitising MCs. In this model, MC-derived leukotrienes induce intestinal epithelial cells to release GDF15 which engage neuro-immune circuits converging in the brain to activate area postrema, the nucleus of tractus solitarius as well as the central amygdala – brain areas linked to food intake and avoidance behaviour. Whether MCs elicit similar mechanisms of avoidance for noxious stimuli encountered in other barrier sites remain to be explored.

The role of mast cells in defence against parasites

An alternative, yet related, evolutionary explanation proposes that IgE receptors and MCs have co-evolved to facilitate host defence against metazoan parasites. Helminths are multicellular macroparasites that infect most vertebrates (Dobson et al., 2008). Unlike pathogenic micro-organisms like viruses and bacteria, the large size and multicellular complexity of helminthic parasites represent a challenge to the host immune system. For the former category of infections, type 1 immune responses tend to prevail, whereby cell-mediated immunity is orchestrated to facilitate killing of the micro-parasite within host tissue (Fenton et al., 2008). However, such immune responses are pro-inflammatory and can be quite damaging to host tissue if prolonged. If such immune responses are prolonged against large helminthic infections, the extent of damage to the host tissue may outweigh the benefit of eliciting an immune response (Maizels and Yazdanbakhsh, 2003). As such, the

type 2 immune response is preferentially elicited against helminth infections. These immune responses are characterised by tissue remodelling processes that can promote expulsion of the parasite (McSorley et al., 2018).

The relationship between vertebrates and helminths is ancient, and helminths exert a significantly negative effect on host nutrition and fitness, which impairs reproductive fitness (Fitzsimmons and Dunne, 2009; Jackson et al., 2009; King and Li, 2018). Widespread exposure to helminths may therefore have exerted a significant selection pressure for the type 2 immune response (Fitzsimmons & Dunne, 2009; Cooper & Alder, 2006; Jackson et al., 2009; McSorley et al., 2018). The sensitivity and speed of immune responses offered by IgE and MCs, as described earlier for toxins, may also apply to helminthic parasites which may quickly invade barrier tissues to infect the host (Artis et al., 2012). It has been proposed that the ability to mount IgE-mediated responses is a mis-directed response to helminths. Consistent with this parasite defence hypothesis, many environmental allergens actually share structural and biochemical features with parasite-derived proteins (Tyagi et al., 2015). The homology between parasitic antigens and allergens support the idea that allergen responsiveness may arise from immune mechanisms that originally arose to detect parasite-derived molecules. Moreover, the mechanisms that underpin the type 2 immune responses to allergens is very similar to the immune responses to metazoan multicellular parasites (Ryan and Oghumu, 2019; McSorley et al., 2018).

Early histochemical analyses revealed that MCs underwent local proliferation in tissues where heminth infections occurred – including the skin, lung and gastrointestinal tract (Lützelschwab et al., 1988; MacDonald et al., 1980; Abe, 1988; Mayrhofer, 1979; Ruitenberg & Elgersma, 1976; Arizono et al., 1996). Evidence from experimental models supports an important role for MCs as protective effector cells against helminths. Upon activation, MCs

degranulate and release mediators which promote serotonin release and contraction of smooth muscle (Vermillion et al., 1988), as well as mediators that can directly target the nematode proteins (Mckean and Pritchard, 1989). Moreover, MCs may induce epithelial cells to release "damage" signals via cytokines like IL-25, IL-33 and TSLP which further promote Th2 responses to expel parasites (Shimokawa et al., 2017) (Hepworth et al., 2012). MC-driven tissue remodelling may also contribute to host protection. While tissue hypertrophy are pathological features of allergic disease, these same processes may be beneficial in promoting parasite expulsion (Gause et al., 2013). For instance, an epidermal growth factor ligand called amphiregulin (AREG) is secreted by MCs (Zaiss et al., 2013). AREG is upregulated in allergic lung disease and correlated to goblet cell hyperplasia (Okumura et al., 2005). However, in helminth infections, AREG may also promote the proliferation and turnover of epithelial cells to promote parasite displacement (Zaiss et al., 2006), reflecting shared effector pathways between parasite defence and allergic pathogenesis.

Importantly however, different MC subsets may contribute differently towards protective immunity in this context. In helminth infections, connective tissue MCs may be more important in contributing to early responses, whereas mucosal MCs are often essential for complete expulsion of the parasite (Reitz et al., 2017). Consistent with this, *RAG1* deficient mice lacking adaptive immunity did not impair initial response to helminths but were essential for full resolution of infection (Reitz et al., 2017). This impaired immunity against helminths may be, at least in part, due to reduced MC responses. The development of mucosal MCs is impaired in the absence of T-cell responses to helminths in the intestine (Abe and Nawa, 1988). Type 2 T-cell cytokines like IL-4, IL-9, IL-13 promote mucosal MC hyperplasia (Mukai et al., 2016; Pennock and Grencis, 2006). Given that the development of mucosal MCs depends on T-cell signals, it is conceivable that mucosal MCs have been preferentially co-opted to facilitate these responses in conjunction with adaptive immunity

to facilitate removal of these parasites. Upon infection, mucosal MC associated proteases like Mcpt1 increase significantly in sera (Hepworth et al., 2012), and genetic deficiency of the protease results in impaired expulsion of intestinal parasites (Knight et al., 2000) (Yang et al., 2024) (Lawrence et al., 2004; McDermott et al., 2003). As such, mucosal MCs may be important for protecting against intestinal helminths, at least in experimental models of intestinal helminth infections like *S. ratti* (Reitz et al., 2017), as well as *S. venezuelensis (Mukai et al., 2017), H. polygyrus* and *T.muris* (Hepworth et al., 2012). Although connective tissue MCs do not play a critical role in intestinal parasite expulsion, they may play a more prominent role in restoring the homeostatic epithelial barrier function (Groschwitz et al., 2009).

It has been argued that since no known corelations exist between non-allergic individuals and protection against toxins, defence against multicellular parasites may represent the primary evolutionary benefit driving the retention of MCs and IgE-mediated immunity (Artis et al., 2012). In line with this theory, allergic reactions, which share these type 2 immune responses, have been thought to be a misdirected response as part of an evolutionarily trade off for the protective benefits of MCs in host defence. Nonetheless, the relationship between the protective response of IgE and worm infections is also inconsistent across species and infections (Baker and Gershwin, 1993).

Epidemiological observations linking the inverse relationship between helminth prevalence with allergic occurrence, termed as the “hygiene hypothesis”, have been proposed to support this view (Briggs et al., 2016; Elston, 2006; Lau and Matricardi, 2006; McSorley et al., 2018). However, this hypothesis often falls through in more systematic analyses in human populations where the effects are not always consistent (Santiago and Nutman, 2016). Moreover, even laboratory mice that are brought up in “wild” pathogenic

environments are not better protected from allergic disease compared to specific pathogen free mice (Ma et al., 2023), reflecting that the hygiene hypothesis may be an oversimplification. One explanation is that the protective role of mast cells is not universal. MC deficiency of either subset did not impair protection against other nematodes like *L. sigmodontis* (Linnemann et al., 2020). The difference may lie in the anatomical location that the parasite infects. *L. sigmodontis* is a tissue dwelling filarial nematode which occupies a different anatomical niche where connective mast cells such as those in the skin and peritoneal cavity are more locally available to respond than mucosal MCs. Since mucosal MCs play a more important role in driving tissue remodelling for parasite expulsion, the differential contribution of MC subsets may explain these differences in MC-driven protective responses. Thus, protection from helminths (and perhaps against allergy in the context of hygiene hypothesis) may reflect a mix of factors including the type of infection.

A more unifying interpretation is that type 2 responses – including MC activation - may protect against tissue damage in response to diverse environmental insults, including toxins and parasites (Artis et al., 2012; Palm et al., 2012). Viewed in this context, IgE-dependent mast cell activation can be interpreted as an adaptive extension of an evolutionarily older mast cell danger-sensing programme to enhance specificity and memory. Host defence therefore represents an important function of MCs in postnatal life, and the persistence of mast cells across evolution thus implies that their core functions precede, and extend beyond, their role in type 2 immunity.

However, the emergence of MCs during embryonic development indicates that additional roles must have shaped their evolutionary conservation. In particular, MCs already establish within connective tissues during fetal development and persist through adulthood. Yet, during fetal development, the organism is largely protected from pathogen exposure, and

adaptive immunity is not fully developed. This raises an important challenge to the previous hypotheses: if MCs evolved primarily to facilitate host immune defence against environmental insults, then why might they arise during fetal development when such functions are unlikely to be required? Fetal development involves tissue formation, remodelling and organogenesis. Consequently, a "demand driven" model of haematopoiesis has been proposed, whereby fetal haematopoietic waves give rise to immune cells to facilitate and support tissue development (Mass and Gentek, 2021). For instance, microglia are among the first macrophages to arise during fetal development and are long lived, with important functions associated with synaptic pruning and neurogenesis in the adult brain (Zhao et al., 2024). However, recent work has shown that microglia are already functional during embryogenesis where they facilitate structural morphogenesis and synaptic pruning for proper fetal brain development (Cabirol et al., 2022; Lawrence et al., 2024). Given the potent tissue remodelling effector functions of MCs shown in adult tissues, it is plausible that these cells may contribute to tissue developmental processes as they emerge. In the subsequent section, I discuss the hypothesis that MCs are critical for tissue development.

The role of mast cells in tissue development

Accumulating evidence indicates that MCs are already functionally equipped during fetal stages. Granulated MCs can be detected as early as E14.5, and already express MC proteases and other mediators at least at a transcriptomic level (Gentek et al., 2018a; Z. Li et al., 2018). By E18.5, MCs already express FCERI and can already be primed in utero through maternal IgE, resulting in neonatal sensitization to allergens (Msallam et al., 2020). One interpretation of these findings is that MCs acquire functional competance during fetal stages in preparation for immunological challenges encountered after birth.

However, fetus life is largely restricted from exposure to external pathogens as the placenta serves as a defense barrier and the uterine environment is largely immune privileged (Kanellopoulos-Langevin et al., 2003). This raises the question about whether immune defense alone can explain the early acquisition of MC functional programmes. The presence of these MC mediators may instead actively participate in tissue-level processes.

As described in previous sections, mucosal MCs largely arise postnatally in mucosal tissue sites and rely on bone marrow haematopoiesis in response to postnatal cues, including the microbiome and inflammatory signals. As such, their identity is co-opted to facilitate functional specialisation in response to these cues. However, unlike mucosal MCs, MCs arise early during embryonic development in connective tissues and are often independent from bone marrow haematopoietic turnover. Connective tissues are among the earliest tissues to arise during embryogenesis and play a critical role in supporting organ development (Nassari et al., 2017). Yet, it remains largely elusive how prenatal cues in developing tissues may specify MC identity and whether MCs may be co-opted to have a functional specialisation towards development, the major function of these tissues.

Insights from pathological contexts suggest that connective tissue MCs may be intrinsically linked to tissue remodelling and repair. While mucosal MCs contribute to inflammatory pathology during chronic allergic disease, connective tissue MCs are associated with a beneficial outcome in tissue repair. Chymase-expressing “connective tissue” type MCs play an essential role in regulating homeostatic epithelial barrier repair in the gastrointestinal tract by regulating transmembrane proteins like claudin-3 (Groschwitz et al., 2009b). Chymase-expressing MCs may also play similar protective roles in the respiratory tract. During chronic allergic inflammation such as asthma, chymase-expressing MCs have been associated with beneficial airway tissue remodelling, likely via exerting effects on

vascularisation and extracellular matrix remodelling (Balzar et al., 2012; Zhao et al., 2022). These observations raise the possibility that is MCs in connective tissues possess an intrinsic capacity to modulate tissue architecture, a function that may represent co-opting of a developmentally conserved MC programme.

Accumulating evidence supports a physiological role for MCs towards tissue remodelling in development. Although conventional *cKit* deficiency mice lack any gross physiological defects, some studies have shown that these mice have defects in the development of organs that characteristically undergo continued and extensive tissue remodelling even postnatally. For example, *cKit* deficient mice that lack MCs exhibit impaired hair follicle cycling (Paus et al., 1994). Importantly, IgE-independent activation of MCs through basic secratagogues was shown to facilitate MC-mediated degranulation to stimulate hair follicle growth and cycling, highlighting the importance of IgE-independent mechanisms in development and tissue remodelling contexts. In addition, the bones of cKit deficient mice have reduced density and increased risk of fracturing, driven by delayed bone tissue remodelling cycles and impaired synthesis of bone tissue matrix (Cindik et al., 2000).

Reproductive tissues are yet another example of tissues undergoing active tissue remodelling postnatally, where they develop in response to hormones at distinct stages of reproductive cycle. In the uterus, spiral artery remodelling is essential during pregnancy to meet the nutritional and oxygen demands of the developing fetus after implantation. MCs respond to estrous cycle and pregnancy hormones and increase in numbers during these stages (Schmerse et al., 2014). Using the *cKit* deficiency models, mice that lacked MCs had implantation defect which could be rescued by bone marrow transplant (Woidacki et al., 2013a). Studies using MC specific deficiency models like the *Cpa3*$^{Cre/Cre}$ revealed functional redundancy between MCs and NK cells which could compensate for each other's functions

(Woidacki et al., 2017). Given the fundamental importance of uterine implantation in mammalian pregnancy, it is perhaps unsurprising that such compensatory measures exist. Mammary gland morphogenesis is another conserved developmental process in mammalian reproduction, which is essential to support lactation. During puberty, mammary gland branching is initiated to prepare for pregnancy and lactation during adulthood (Hinck and Silberstein, 2005). *cKit* deficient mice exhibit a transient delay in branching in the absence of MCs (Lilla and Werb, 2010). However, whether this transient defect is due to compensation by another cell type is unknown. MCs also play an important role in triggering mammary gland involution post lactation (Lilla et al., 2009). While the mechanisms that MCs may use to facilitate these developmental processes are not entirely clear, MCs produce proteases like plasma kallikrein during puberty and involution which activates the plasminogen cascade and facilitates stromal remodelling (Lilla et al., 2009). MC proteases may also promote stromal remodelling via the secretion of cytokines like IL-4 and IL-13 (Wu et al., 2021).

While the above examples highlight the role of MCs in tissue development postnatally, MCs can already be detected in fetal tissues prenatally and have a functional transcriptome expressing MC mediators (Gentek et al., 2018a; Z. Li et al., 2018; Perçin et al., 2025). It is therefore conceivable that MCs may also exert developmental functions at these fetal stages where active tissue development is ongoing. Moreover, as MCs emerge through the fetal haematopoietic waves during embryogenesis, their phenotype varies as they mature. MCs seeding connective tissues in the fetus, such as the skin, appear granulated only later by E16.5, yet hypogranulated MCs can be detected already by E14.5 (Gentek et al., 2018a). Hypogranulated MCPs and mucosal type MCs have distinct functions in postnatal tissues (Gurish and Austen, 2012), and it is plausible that distinct MC subsets in fetal tissues also exhibit functional heterogeneity depending on their developmental stage and identity.

In line with this, MC lysates at E15.5 (comprising hypogranulated MCs) do not degranulate in response to fetal wounding, whereas by E18.5 MCs degranulate and secrete cytokines driving scarred fetal wound formation (Wulff et al., 2012). In adult tissues, MCs have been shown to interact with fibroblasts and promote wound contraction and angiogenesis, resulting in scars (Ng, 2010). Moreover, *cKit* deficient mice lacking MCs retain scarless wound healing features, indicating that granulated MCs appearing in late-stage fetal development and adult stages may be specialized in promoting scarred wound formations (Wulff et al., 2012). However, this does not exclude the role of hypogranulated MCs earlier in development. In the fetal cornea, MCs support the innervation and vascularization in two distinct developmental waves as they emerge (Liu et al., 2015a). A first wave of hypogranulated fetal MCs colonise the cornea stroma at E12.5 and disappear postnatally, while a second wave of MCs settle in the corneal limbus around the blood vessels within the first postnatal week and stabilize in number after postnatal day 21. Importantly, *cKit* deficiency models lacking MCs exhibit reduced nerve fibers and limbal blood vessels, reflecting a functional requirement for MCs at different developmental stages. MCs produce several growth factors such as VEGF and neurturin which may be relevant in supporting these processes during fetal stages (Gentek et al., 2018; Liu et al., 2015). In adulthood, MC derived VEGF results in pathological corneal neovascularisation and blindness (Cho et al., 2020), suggesting that pathological angiogenesis may reflect dysregulated activation of a developmental process orchestrated by MCs.

These findings warrant re-investigation using *cKit* independent genetic model systems to ascertain the role of MCs. Intriguingly, transcriptomic analyses revealed the MCs also develop as part of a layered haematopoietic developmental programme in human fetuses, and MCs already express many of these mediators at these stages, at least at a

transcriptomic level (Suo et al., 2022). We speculate that fetal MCs may also be important in fetal tissue development in humans. Nevertheless, no known human deficiencies in MCs are known, and one hypothesis is that human MC deficiencies are embryonically lethal (Rodewald and Feyerabend, 2012). This may reflect a previously underappreciated role of MCs in tissue development.

Hypothesis and Aims

Based on the above, I hypothesise that MCs may play a critical role in tissue development. I propose that reliance on *cKit* deficiency models have several limitations that have obscured key developmental functions of MCs, leading to an underestimation of their contribution to tissue morphogenesis and remodelling. The central aim of this thesis is therefore to re-evaluate the development and functions of MCs in c*Kit* independent models.

Aim 1: To re-investigate the role of MCs in pubertal mammary gland branching, as an example of postnatal tissue development. This aim will be addressed using c*Kit* independent genetic MC targeting models.

Aim 2: To perform spatial-temporal transcriptomic analysis of MC development as they emerge and establish their identity during fetal development. This aim will be addressed using single cell sequencing analyses of transcriptomic datasets from fetal liver as well as peripheral tissues.

Aim 3: To re-investigate the role of MCs in fetal tissue development. This aim will be addressed using *Kit* independent genetic models which target *Cpa3*, a gene expressed early in MC development during fetal stages.

References

Abe, T. (1988) “Worm expulsion and mucosal mast cell response induced by repetitive IL-3 administration in Strongyloides ratti-infected nude mice,” *Immunology*, 63, pp. 181–185.

Abe, T. and Nawa, Y. (1988) “Worm expulsion and mucosal mast cell response induced by repetitive IL-3 administration in Strongyloides ratti-infected nude mice,” *Immunology*, 63(2), p. 181. Available at: https://pmc.ncbi.nlm.nih.gov/articles/PMC1454520/ (Accessed: December 26, 2025).

Abonia, J.P. *et al.* (2006) “Alpha-4 integrins and VCAM-1, but not MAdCAM-1, are essential for recruitment of mast cell progenitors to the inflamed lung,” *Blood*, 108(5), pp. 1588–1594. Available at: https://doi.org/10.1182/BLOOD-2005-12-012781.

Akahoshi, M. *et al.* (2011) “Mast cell chymase reduces the toxicity of Gila monster venom, scorpion venom, and vasoactive intestinal polypeptide in mice,” *The Journal of clinical investigation*, 121(10), pp. 4180–4191. Available at: https://doi.org/10.1172/JCI46139.

Akin, C. *et al.* (2025) “Mastocytosis,” *Nature reviews. Disease primers*, 11(1). Available at: https://doi.org/10.1038/S41572-025-00611-8.

Akula, S. *et al.* (2015) “Granule Associated Serine Proteases of Hematopoietic Cells – An Analysis of Their Appearance and Diversification during Vertebrate Evolution,” *PLoS ONE*, 10(11), p. e0143091. Available at: https://doi.org/10.1371/JOURNAL.PONE.0143091.

Anderson, E. *et al.* (2018) “Human Mast Cell Tryptase Is a Potential Treatment for Snakebite Envenoming Across Multiple Snake Species,” *Frontiers in immunology*, 9(JUL). Available at: https://doi.org/10.3389/FIMMU.2018.01532.

Arinobu, Y. *et al.* (2005) “Developmental checkpoints of the basophil/mast cell lineages in adult murine hematopoiesis,” *Proceedings of the National Academy of Sciences of the*

United States of America, 102(50), pp. 18105–18110. Available at: https://doi.org/10.1073/PNAS.0509148102;PAGEGROUP:STRING:PUBLICATION.

Arizono, N. *et al.* (1996) "Lung granulomatous response induced by infection with the intestinal nematode Nippostrongylusbrasiliensis is suppressed in mast cell-deficient Ws/Ws rats," *Clinical and Experimental Immunology*, 106(1), p. 55. Available at: https://doi.org/10.1046/J.1365-2249.1996.D01-803.X.

Artis, D., Maizels, R.M. and Finkelman, F.D. (2012) "Allergy challenged," *Nature 2012 484:7395*, 484(7395), pp. 458–459. Available at: https://doi.org/10.1038/484458a.

Bain, C.C. *et al.* (2014) "Constant replenishment from circulating monocytes maintains the macrophage pool in the intestine of adult mice," *Nature immunology*, 15(10), pp. 929–937. Available at: https://doi.org/10.1038/NI.2967.

Baker, D.G. and Gershwin, L.J. (1993) "Inverse relationship between IgE and worm burdens in cattle infected with Ostertagia ostertagi," *Veterinary Parasitology*, 47(1–2), pp. 87–97. Available at: https://doi.org/10.1016/0304-4017(93)90179-Q.

Balzar, S. *et al.* (2012) "Relationship of Small Airway Chymase-Positive Mast Cells and Lung Function in Severe Asthma," *https://doi.org/10.1164/rccm.200407-949OC*, 171(5), pp. 431–439. Available at: https://doi.org/10.1164/RCCM.200407-949OC.

Bankova, L.G. *et al.* (2015) "Maturation of mast cell progenitors to mucosal mast cells during allergic pulmonary inflammation in mice," *Mucosal Immunology*, 8(3), pp. 596–606. Available at: https://doi.org/10.1038/mi.2014.91.

Bao, C. *et al.* (2023) "A Mast Cell-Thermoregulatory Neuron Circuit Axis Regulates Hypothermia in Anaphylaxis," *Science immunology*, 8(81), p. eadc9417. Available at: https://doi.org/10.1126/SCIIMMUNOL.ADC9417.

Baraniuk, J.N. (2012) "Rise of the Sensors: Nociception and Pruritus," *Current allergy and asthma reports*, 12(2), p. 104. Available at: https://doi.org/10.1007/S11882-012-0245-8.

de Barros, C.M. *et al.* (2007) “The Hemolymph of the Ascidian Styela plicata (Chordata-Tunicata) Contains Heparin inside Basophil-like Cells and a Unique Sulfated Galactoglucan in the Plasma,” *Journal of Biological Chemistry*, 282(3), pp. 1615–1626. Available at: https://doi.org/10.1074/JBC.M604056200.

Beaven, M.A. (2009) “Our perception of the mast cell from Paul Ehrlich to now,” *European journal of immunology*, 39(1), p. 11. Available at: https://doi.org/10.1002/EJI.200838899.

Berni Canani, R. *et al.* (2024) “Skin, gut, and lung barrier: Physiological interface and target of intervention for preventing and treating allergic diseases,” *Allergy*, 79(6), pp. 1485–1500. Available at: https://doi.org/10.1111/ALL.16092.

Briggs, N. *et al.* (2016) “The Hygiene Hypothesis and Its Inconvenient Truths about Helminth Infections,” *PLoS Neglected Tropical Diseases*, 10(9), p. e0004944. Available at: https://doi.org/10.1371/JOURNAL.PNTD.0004944.

Brunelli, N., Dalle Palle, S. and Cima, F. (2025) “Possible Evolutionary Precursors of Mast Cells: The ‘Granular Cell’ Immunocyte of Botrylloides leachii (Tunicata; Ascidiacea),” *Journal of Marine Science and Engineering 2025, Vol. 13, Page 811*, 13(4), p. 811. Available at: https://doi.org/10.3390/JMSE13040811.

Cabirol, M.J. *et al.* (2022) “Microglia shape the embryonic development of mammalian respiratory networks,” *eLife*, 11. Available at: https://doi.org/10.7554/ELIFE.80352.

Cavalcante, M.C.M. *et al.* (2000) “Occurrence of heparin in the invertebrate Styela plicata (Tunicata) is restricted to cell layers facing the outside environment: An ancient role in defense?,” *Journal of Biological Chemistry*, 275(46), pp. 36189–36196. Available at: https://doi.org/10.1074/jbc.M005830200.

Charles A Janeway, J. *et al.* (2001) “Effector mechanisms in allergic reactions.” Available at: https://www.ncbi.nlm.nih.gov/books/NBK27112/ (Accessed: December 24, 2025).

Chen, C.C. *et al.* (2005) “Identification of mast cell progenitors in adult mice,” *Proceedings of the National Academy of Sciences*, 102(32), pp. 11408–11413. Available at: https://doi.org/10.1073/PNAS.0504197102.

Chia, S.L. *et al.* (2023) “Mast cell ontogeny: From fetal development to life-long health and disease,” *Immunological Reviews*. John Wiley and Sons Inc, pp. 31–53. Available at: https://doi.org/10.1111/imr.13191.

Cho, W.K. *et al.* (2020) “Activation of ocular surface mast cells promotes corneal neovascularization,” *Ocular Surface*, 18(4), pp. 857–864. Available at: https://doi.org/10.1016/j.jtos.2020.09.002.

Cima, F. *et al.* (2018) “Immunological response to bacterial infection in a pelagic tunicate: Inflammation in the salp Thalia democratica,” *Journal of Invertebrate Pathology*, 159, pp. 28–40. Available at: https://doi.org/10.1016/j.jip.2018.10.012.

Cindik, E.D. *et al.* (2000) “Phenotypical characterization of c-kit receptor deficient mouse femora using non-destructive high-resolution imaging techniques and biomechanical testing,” *Technology and Health Care*, 8(5), pp. 267–275. Available at: https://doi.org/10.3233/THC-2000-8502.

Combs, J.W., Lagunoff, D. and Benditt, E.P. (1965) “DIFFERENTIATION AND PROLIFERATION OF EMBRYONIC MAST CELLS OF THE RAT,” *The Journal of Cell Biology*, 25(3), p. 577. Available at: https://doi.org/10.1083/JCB.25.3.577.

Cooper, M.D. and Alder, M.N. (2006) “The Evolution of Adaptive Immune Systems,” *Cell*, 124(4), pp. 815–822. Available at: https://doi.org/10.1016/J.CELL.2006.02.001.

Crivellato, E. *et al.* (2003) “Paul Ehrlich’s doctoral thesis: A milestone in the study of mast cells,” *British Journal of Haematology*, 123(1), pp. 19–21. Available at: https://doi.org/10.1046/J.1365-2141.2003.04573.X;WGROUP:STRING:PUBLICATION.

Crivellato, E. and Ribatti, D. (2010) “The mast cell: an evolutionary perspective,” *Biological Reviews*, 85(2), pp. 347–360. Available at: https://doi.org/10.1111/J.1469-185X.2009.00105.X.

Dahlin, J.S. *et al.* (2018) “A single-cell hematopoietic landscape resolves 8 lineage trajectories and defects in Kit mutant mice,” *Blood*, 131(21), p. e1. Available at: https://doi.org/10.1182/BLOOD-2017-12-821413.

Dahlin, J.S. and Hallgren, J. (2015) “Mast cell progenitors: Origin, development and migration to tissues,” *Molecular Immunology*, 63(1), pp. 9–17. Available at: https://doi.org/10.1016/J.MOLIMM.2014.01.018.

Daschner, A. and González Fernández, J. (2020) “Allergy in an Evolutionary Framework,” *Journal of molecular evolution*, 88(1), pp. 66–76. Available at: https://doi.org/10.1007/S00239-019-09895-3.

Derakhshan, T. *et al.* (2021) “Lineage-specific regulation of inducible and constitutive mast cells in allergic airway inflammation,” *Journal of Experimental Medicine*, 218(1). Available at: https://doi.org/10.1084/JEM.20200321.

Derakhshan, T. *et al.* (2025) “Human intraepithelial mast cell differentiation and effector function are directed by TGF-β signaling,” *The Journal of Clinical Investigation*, 135(1). Available at: https://doi.org/10.1172/JCI174981.

Derakhshan, T., Boyce, J.A. and Dwyer, D.F. (2022) “Defining mast cell differentiation and heterogeneity through single cell transcriptomics analysis,” *The Journal of allergy and clinical immunology*, 150(4), p. 739. Available at: https://doi.org/10.1016/J.JACI.2022.08.011.

Dobson, A. *et al.* (2008) “Homage to Linnaeus: How many parasites? How many hosts?,” *Proceedings of the National Academy of Sciences of the United States of America*, 105(SUPPL. 1), pp. 11482–11489. Available at: https://doi.org/10.1073/PNAS.0803232105,.

Dombrowicz, D. *et al.* (1993) “Abolition of anaphylaxis by targeted disruption of the high affinity immunoglobulin E receptor α chain gene,” *Cell*, 75(5), pp. 969–976. Available at: https://doi.org/10.1016/0092-8674(93)90540-7.

Dougherty, J.M., Alsayouri, K. and Sadowski, A. (2023) “Allergy,” *Instant Wisdom for Gps: Pearls from all the Specialties: Second Edition*, pp. 9–14. Available at: https://doi.org/10.1201/9781003304586-2.

Dwyer, D.F. *et al.* (2016a) “Expression profiling of constitutive mast cells reveals a unique identity within the immune system,” *Nature Immunology*, 17(7), pp. 878–887. Available at: https://doi.org/10.1038/ni.3445.

Dwyer, D.F. *et al.* (2016b) “Expression profiling of constitutive mast cells reveals a unique identity within the immune system,” *Nature Immunology*, 17(7), pp. 878–887. Available at: https://doi.org/10.1038/ni.3445.

Elston, D.M. (2006) “The hygiene hypothesis and atopy: Bring back the parasites?,” *Journal of the American Academy of Dermatology*, 54(1), pp. 172–179. Available at: https://doi.org/10.1016/j.jaad.2005.09.020.

Ema, H. and Nakauchi, H. (2000) “Expansion of hematopoietic stem cells in the developing liver of a mouse embryo,” *Blood*, 95(7), pp. 2284–2288. Available at: https://doi.org/10.1182/BLOOD.V95.7.2284.

Enerbäck, L. (1966a) “Mast cells in rat gastrointestinal mucosa. 2. Dye-binding and metachromatic properties,” *Acta pathologica et microbiologica Scandinavica*, 66(3), pp. 303–312. Available at: https://doi.org/10.1111/APM.1966.66.3.303.

Enerbäck, L. (1966b) “Mast cells in rat gastrointestinal mucosa. 3. Reactivity towards compound 48/80,” *Acta pathologica et microbiologica Scandinavica*, 66(3), pp. 313–322. Available at: https://doi.org/10.1111/APM.1966.66.3.313.

Enerbäck, L. (1966c) “Mast cells in rat gastrointestinal mucosa. I. Effects of fixation.,” *Acta pathologica et microbiologica Scandinavica*, 66(3), pp. 289–302. Available at: https://doi.org/10.1111/APM.1966.66.3.289;WGROUP:STRING:PUBLICATION.

Fantin, A. *et al.* (2021) “KIT Is Required for Fetal Liver Hematopoiesis,” *Frontiers in Cell and Developmental Biology*, 9, p. 648630. Available at: https://doi.org/10.3389/FCELL.2021.648630/BIBTEX.

Fenton, A., Lamb, T. and Graham, A.L. (2008) “Optimality analysis of Th1/Th2 immune responses during microparasite-macroparasite co-infection, with epidemiological feedbacks,” *Parasitology*, 135(7), pp. 841–853. Available at: https://doi.org/10.1017/S0031182008000310.

Ferry, X. *et al.* (2002) *G protein-dependent activation of mast cell by peptides and basic secretagogues*, *Peptides*.

Fitzsimmons, C.M. and Dunne, D.W. (2009) “Survival of the fittest: allergology or parasitology?,” *Trends in Parasitology*, 25(10), pp. 447–451. Available at: https://doi.org/10.1016/j.pt.2009.07.004.

Flanagan, J.G. and Leder, P. (1990) “The kit ligand: A cell surface molecule altered in steel mutant fibroblasts,” *Cell*, 63(1), pp. 185–194. Available at: https://doi.org/10.1016/0092-8674(90)90299-T.

Florsheim, E.B. *et al.* (2021) “Food allergy as a biological food quality control system,” *Cell*, 184(6), pp. 1440–1454. Available at: https://doi.org/10.1016/J.CELL.2020.12.007.

Florsheim, E.B. *et al.* (2023) “Immune sensing of food allergens promotes avoidance behaviour,” *Nature*, 620(7974), pp. 643–650. Available at: https://doi.org/10.1038/s41586-023-06362-4.

Friend, D.S. *et al.* (1996) “Mast cells that reside at different locations in the jejunum of mice infected with Trichinella spiralis exhibit sequential changes in their granule ultrastructure

and chymase phenotype," *Journal of Cell Biology*, 135(1), pp. 279–290. Available at: https://doi.org/10.1083/jcb.135.1.279.

Friend, D.S. *et al.* (1998) "Reversible Expression of Tryptases and Chymases in the Jejunal Mast Cells of Mice Infected with Trichinella spiralis," *The Journal of Immunology*, 160(11), pp. 5537–5545. Available at: https://doi.org/10.4049/JIMMUNOL.160.11.5537.

Fujita, J. *et al.* (1989) "In vitro duplication and in vivo cure of mast-cell deficiency of Sl/Sl(d) mutant mice by cloned 3T3 fibroblasts," *Proceedings of the National Academy of Sciences of the United States of America*, 86(8), pp. 2888–2891. Available at: https://doi.org/10.1073/PNAS.86.8.2888;WGROUP:STRING:PUBLICATION.

Fukuzumi, T. *et al.* (1990) "Differences in irradiation susceptibility and turnover between mucosal and connective tissue-type mast cells of mice.," *Experimental Hematology*, 18(7), pp. 843–847. Available at: https://europepmc.org/article/med/2379550 (Accessed: December 21, 2025).

Galli, S.J. and Tsai, M. (2010) "Mast cells in allergy and infection: Versatile effector and regulatory cells in innate and acquired immunity," *European journal of immunology*, 40(7), p. 1843. Available at: https://doi.org/10.1002/EJI.201040559.

Galli, S.J. and Tsai, M. (2012) "IgE and mast cells in allergic disease," *Nature medicine*, 18(5), p. 693. Available at: https://doi.org/10.1038/NM.2755.

Galli, S.J., Tsai, M. and Piliponsky, A.M. (2008) "The development of allergic inflammation," *Nature*, 454(7203), p. 445. Available at: https://doi.org/10.1038/NATURE07204.

Gamble, H.J. and Stempak, J.G. (1961) "Observations upon the mast cells of rat foetal tissues," *Experientia*, 17(10), pp. 460–461. Available at: https://doi.org/10.1007/BF02158289.

García-García, E. *et al.* (2014) "Histamine regulates the inflammatory response of the tunicate Styela plicata," *Developmental & Comparative Immunology*, 46(2), pp. 382–391. Available at: https://doi.org/10.1016/J.DCI.2014.05.017.

Gaudenzio, N. *et al.* (2016) “Different activation signals induce distinct mast cell degranulation strategies,” *The Journal of clinical investigation*, 126(10), pp. 3981–3998. Available at: https://doi.org/10.1172/JCI85538.

Gause, W.C., Wynn, T.A. and Allen, J.E. (2013) “Type 2 immunity and wound healing: evolutionary refinement of adaptive immunity by helminths,” *Nature reviews. Immunology*, 13(8), pp. 607–614. Available at: https://doi.org/10.1038/NRI3476.

Gentek, R. *et al.* (2018) “Hemogenic Endothelial Fate Mapping Reveals Dual Developmental Origin of Mast Cells,” *Immunity*, 48(6), pp. 1160-1171.e5. Available at: https://doi.org/10.1016/j.immuni.2018.04.025.

Ginhoux, F. and Guilliams, M. (2016) “Tissue-Resident Macrophage Ontogeny and Homeostasis,” *Immunity*, 44(3), pp. 439–449. Available at: https://doi.org/10.1016/J.IMMUNI.2016.02.024.

Gomez Perdiguero, E. *et al.* (2015) “Tissue-resident macrophages originate from yolk-sac-derived erythro-myeloid progenitors,” *Nature*, 518(7540), pp. 547–551. Available at: https://doi.org/10.1038/NATURE13989.

Grimbaldeston, M.A. (2015) “Mast cell-MrgprB2: Sensing secretagogues or a means to overreact?,” *Immunology and Cell Biology*, 93(3), pp. 221–223. Available at: https://doi.org/10.1038/ICB.2015.10;PAGE:STRING:ARTICLE/CHAPTER.

Groschwitz, K.R. *et al.* (2009) “Mast cells regulate homeostatic intestinal epithelial migration and barrier function by a chymase/Mcpt4-dependent mechanism,” *Proceedings of the National Academy of Sciences of the United States of America*, 106(52), pp. 22381–22386. Available at: https://doi.org/10.1073/PNAS.0906372106.

Guilliams, M. *et al.* (2020) “Establishment and Maintenance of the Macrophage Niche,” *Immunity*, 52(3), pp. 434–451. Available at: https://doi.org/10.1016/J.IMMUNI.2020.02.015.

Gurish, M.F. *et al.* (2001) “Intestinal mast cell progenitors require CD49dbeta7 (alpha4beta7 integrin) for tissue-specific homing,” *The Journal of experimental medicine*, 194(9), pp. 1243–1252. Available at: https://doi.org/10.1084/JEM.194.9.1243.

Gurish, M.F. and Austen, K.F. (2012) “Developmental Origin and Functional Specialization of Mast Cell Subsets,” *Immunity*, 37(1), pp. 25–33. Available at: https://doi.org/10.1016/j.immuni.2012.07.003.

Hagel, A.F. *et al.* (2013) “Mast cell tryptase levels in gut mucosa in patients with gastrointestinal symptoms caused by food allergy,” *International archives of allergy and immunology*, 160(4), pp. 350–355. Available at: https://doi.org/10.1159/000341634.

Hatanaka, K., Kitamura, Y. and Nishimune, Y. (1979) “Local Development of Mast Cells From Bone Marrow-Derived Precursors in the Skin of Mice,” *Blood*, 53(1), pp. 142–147. Available at: https://doi.org/10.1182/BLOOD.V53.1.142.142.

Hayashi, C. *et al.* (1985) *Mast-Cell Precursors in the Skin of Mouse Embryos and Their Deficiency in Embryos of S//SF’ Genotype*, *DEVELOPMENTAL BIOLOGY*.

Hellman, L. and Thorpe, M. (2014) “Granule proteases of hematopoietic cells, a family of versatile inflammatory mediators - An update on their cleavage specificity, in vivo substrates, and evolution,” *Biological Chemistry*, 395(1), pp. 15–49. Available at: https://doi.org/10.1515/HSZ-2013-0211/XML.

Hellman, L.T. *et al.* (2017) “Tracing the Origins of IgE, Mast Cells, and Allergies by Studies of Wild Animals,” *Frontiers in immunology*, 8(DEC). Available at: https://doi.org/10.3389/FIMMU.2017.01749.

Hepworth, M.R. *et al.* (2012) “Mast cells orchestrate type 2 immunity to helminths through regulation of tissue-derived cytokines,” *Proceedings of the National Academy of Sciences of the United States of America*, 109(17), pp. 6644–6649. Available at: https://doi.org/10.1073/PNAS.1112268109.

Hinck, L. and Silberstein, G.B. (2005) “The mammary end bud as a motile organ,” *Breast Cancer Research*, pp. 245–251. Available at: https://doi.org/10.1186/bcr1331.

Hoeffel, G. and Ginhoux, F. (2015) “Ontogeny of Tissue-Resident Macrophages,” *Frontiers in Immunology*, 6(SEP), p. 486. Available at: https://doi.org/10.3389/FIMMU.2015.00486.

Jackson, J.A. *et al.* (2009) “Review series on helminths, immune modulation and the hygiene hypothesis: Immunity against helminths and immunological phenomena in modern human populations: Coevolutionary legacies?,” *Immunology*, 126(1), pp. 18–27. Available at: https://doi.org/10.1111/J.1365-2567.2008.03010.X;ISSUE:ISSUE:DOI.

Jamur, M.C. *et al.* (2005) “Identification and characterization of undifferentiated mast cells in mouse bone marrow,” *Blood*, 105(11), pp. 4282–4289. Available at: https://doi.org/10.1182/BLOOD-2004-02-0756.

st. John, A.L., Rathore, A.P.S. and Ginhoux, F. (2023) “New perspectives on the origins and heterogeneity of mast cells,” *Nature Reviews Immunology*, 23(1), pp. 55–68. Available at: https://doi.org/10.1038/S41577-022-00731-2;SUBJMETA.

Kanellopoulos-Langevin, C. *et al.* (2003) “Tolerance of the fetus by the maternal immune system: role of inflammatory mediators at the feto-maternal interface,” *Reproductive biology and endocrinology : RB&E*, 1, p. 121. Available at: https://doi.org/10.1186/1477-7827-1-121.

Kashem, S.W. *et al.* (2011) “G protein coupled receptor specificity for C3a and compound 48/80-induced degranulation in human mast cells: Roles of Mas-related genes MrgX1 and MrgX2,” *European Journal of Pharmacology*, 668(1–2), pp. 299–304. Available at: https://doi.org/10.1016/j.ejphar.2011.06.027.

Kawakami, T. and Galli, S.J. (2002) “Regulation of mast-cell and basophil function and survival by IgE,” *Nature Reviews Immunology 2002 2:10*, 2(10), pp. 773–786. Available at: https://doi.org/10.1038/nri914.

Kayaba, H. *et al.* (2001) “Human Eosinophils and Human High Affinity IgE Receptor Transgenic Mouse Eosinophils Express Low Levels of High Affinity IgE Receptor, but Release IL-10 upon Receptor Activation,” *The Journal of Immunology*, 167(2), pp. 995–1003. Available at: https://doi.org/10.4049/JIMMUNOL.167.2.995,.

Keller, J.R., Ortiz, M. and Ruscetti, F.W. (1995) “Steel Factor (c-kit Ligand) Promotes the Survival of Hematopoietic Stem/Progenitor Cells in the Absence of Cell Division,” *Blood*, 86(5), pp. 1757–1764. Available at: https://doi.org/10.1182/BLOOD.V86.5.1757.BLOODJOURNAL8651757.

Kemp, S.F. and Lockey, R.F. (2002) “Anaphylaxis: A review of causes and mechanisms,” *Journal of Allergy and Clinical Immunology*, 110(3), pp. 341–348. Available at: https://doi.org/10.1067/MAI.2002.126811.

King, I.L. and Li, Y. (2018) “Host–Parasite Interactions Promote Disease Tolerance to Intestinal Helminth Infection,” *Frontiers in Immunology*, 9(SEP), p. 2128. Available at: https://doi.org/10.3389/FIMMU.2018.02128.

Kitamura, Y. *et al.* (1977) “Development of mast cells from grafted bone marrow cells in irradiated mice,” *Nature*, 268(5619), pp. 442–443. Available at: https://doi.org/10.1038/268442A0.

Kitamura, Y. *et al.* (1983) “Different Radiosensitivities of Mast-Cell Precursors in the Bone Marrow and Skin of Mice,” *Radiation Research*, 93(1), pp. 147–156. Available at: https://doi.org/10.2307/3575950.

Kitamura, Y. *et al.* (1987) “Mutual phenotypic changes between connective tissue type and mucosal mast cells,” *International Archives of Allergy and Immunology*, 82(3–4), pp. 244–248. Available at: https://doi.org/10.1159/000234198.

Kitamura, Y., Go, S. and Hatanaka, K. (1978) *Decrease of Mast Cells in W/ W" Mice and Their Increase by Bone Marrow Transplantation*, *Blood*. Available at: http://ashpublications.org/blood/article-pdf/52/2/447/581579/447.pdf.

Kitamura, Y., Shimada, M. and Go, S. (1979) “Presence of mast cell precursors in fetal liver of mice,” *Developmental Biology*, 70(2), pp. 510–514. Available at: https://doi.org/10.1016/0012-1606(79)90042-3.

Knight, P.A. *et al.* (2000) “Delayed expulsion of the nematode Trichinella spiralis in mice lacking the mucosal mast cell-specific granule chymase, mouse mast cell protease-1,” *The Journal of experimental medicine*, 192(12), pp. 1849–1856. Available at: https://doi.org/10.1084/JEM.192.12.1849.

Krystel-Whittemore, M., Dileepan, K.N. and Wood, J.G. (2016) “Mast cell: A multi-functional master cell,” *Frontiers in Immunology*. Frontiers Media S.A. Available at: https://doi.org/10.3389/fimmu.2015.00620.

Kumar, M., Duraisamy, K. and Chow, B.K.C. (2021) “Unlocking the Non-IgE-Mediated Pseudo-Allergic Reaction Puzzle with Mas-Related G-Protein Coupled Receptor Member X2 (MRGPRX2),” *Cells*, 10(5). Available at: https://doi.org/10.3390/CELLS10051033.

Lau, S. and Matricardi, P.M. (2006) “Worms, asthma, and the hygiene hypothesis,” *Lancet*, 367(9522), pp. 1556–1558. Available at: https://doi.org/10.1016/S0140-6736(06)68670-4.

Lawrence, A.R. *et al.* (2024) “Microglia maintain structural integrity during fetal brain morphogenesis,” *Cell*, 187(4), p. 962. Available at: https://doi.org/10.1016/J.CELL.2024.01.012.

Lawrence, C.E. *et al.* (2004) “Mouse mast cell protease-1 is required for the enteropathy induced by gastrointestinal helminth infection in the mouse,” *Gastroenterology*, 127(1), pp. 155–165. Available at: https://doi.org/10.1053/j.gastro.2004.04.004.

Lawrence, M.G. *et al.* (2016) “Half-life of IgE in serum and skin: Consequences for anti-IgE therapy in patients with allergic disease,” *The Journal of allergy and clinical immunology*, 139(2), p. 422. Available at: https://doi.org/10.1016/J.JACI.2016.04.056.

Levi-Schaffer, F., Segal, V. and Shalit, M. (1991) “Effects of interleukins on connective tissue type mast cells co-cultured with fibroblasts,” *Immunology*, 72(2), p. 174. Available at: https://pmc.ncbi.nlm.nih.gov/articles/PMC1384480/ (Accessed: December 17, 2025).

Li, Z. *et al.* (2018) “Adult Connective Tissue-Resident Mast Cells Originate from Late Erythro-Myeloid Progenitors,” *Immunity*, 49(4), pp. 640-653.e5. Available at: https://doi.org/10.1016/j.immuni.2018.09.023.

Lilla, J.N. *et al.* (2009) “Active plasma kallikrein localizes to mast cells and regulates epithelial cell apoptosis, adipocyte differentiation, and stromal remodeling during mammary gland involution,” *Journal of Biological Chemistry*, 284(20), pp. 13792–13803. Available at: https://doi.org/10.1074/jbc.M900508200.

Lilla, J.N. and Werb, Z. (2010) “Mast cells contribute to the stromal microenvironment in mammary gland branching morphogenesis,” *Developmental Biology*, 337(1), pp. 124–133. Available at: https://doi.org/10.1016/j.ydbio.2009.10.021.

Linnemann, L.C. *et al.* (2020) “Limited role of mast cells during infection with the parasitic nematode Litomosoides sigmodontis,” *PLoS Neglected Tropical Diseases*, 14(7), p. e0008534. Available at: https://doi.org/10.1371/JOURNAL.PNTD.0008534.

Liu, J. *et al.* (2015) “Mast Cells Participate in Corneal Development in Mice,” *Scientific reports*, 5. Available at: https://doi.org/10.1038/SREP17569.

Lützelschwab, C. *et al.* (1988) “A kinetic analysis of the expression of mast cell protease mRNA in the intestines of Nippostrongylus brasiliensis-infected rats.” Available at: https://doi.org/10.1002/(SICI)1521-4141(199811)28:11.

Ma, W. *et al.* (2025) “Embryonic mast cells arise from the Cpa3-expressing precursors but not granulocyte-monocyte progenitors,” *Science China Life Sciences* [Preprint]. Available at: https://doi.org/10.1007/s11427-024-2891-1.

MacDonald, T.T., Murray, M. and Ferguson, A. (1980) “Nippostrongylus brasiliensis: Mast cell kinetics at small intestinal sites in infected rats,” *Experimental Parasitology*, 49(1), pp. 9–14. Available at: https://doi.org/10.1016/0014-4894(80)90050-8.

Maizels, R.M. and Yazdanbakhsh, M. (2003) “Immune Regulation by helminth parasites: cellular and molecular mechanisms,” *Nature Reviews Immunology 2003 3:9*, 3(9), pp. 733–744. Available at: https://doi.org/10.1038/nri1183.

Mandola, A., Nozawa, A. and Eiwegger, T. (2019) “Histamine, histamine receptors, and antihistamines in the context of allergic responses,” *https://doi.org/10.14785/lymphosign-2018-0016*, 6(2), pp. 35–51. Available at: https://doi.org/10.14785/LYMPHOSIGN-2018-0016.

Marichal, T. *et al.* (2013) “A beneficial role for immunoglobulin E in host defense against honeybee venom,” *Immunity*, 39(5), pp. 963–975. Available at: https://doi.org/10.1016/j.immuni.2013.10.005.

Mass, E. *et al.* (2016) “Specification of tissue-resident macrophages during organogenesis,” *Science*, 353(6304). Available at: https://doi.org/10.1126/SCIENCE.AAF4238/SUPPL_FILE/MASS.SM.PDF.

Mass, E. and Gentek, R. (2021) “Fetal-Derived Immune Cells at the Roots of Lifelong Pathophysiology,” *Frontiers in Cell and Developmental Biology*, 9, p. 648313. Available at: https://doi.org/10.3389/FCELL.2021.648313/FULL.

Matsuda, H. *et al.* (1981) “Precursor of mast cells fixed in the skin of mice,” *Journal of Cellular Physiology*, 108(3), pp. 409–415. Available at: https://doi.org/10.1002/jcp.1041080315.

Mayrhofer, G. (1979) “The nature of the thymus dependency of mucosal mast cells: I. An adaptive secondary response to challenge with Nippostrongylus brasiliensis,” *Cellular Immunology*, 47(2), pp. 304–311. Available at: https://doi.org/10.1016/0008-8749(79)90340-X.

McDermott, J.R. *et al.* (2003) “Mast cells disrupt epithelial barrier function during enteric nematode infection,” *Proceedings of the National Academy of Sciences of the United States of America*, 100(13), pp. 7761–7766. Available at: https://doi.org/10.1073/PNAS.1231488100.

McGrath, K.E. *et al.* (2003) “Circulation is established in a stepwise pattern in the mammalian embryo,” *Blood*, 101(5), pp. 1669–1675. Available at: https://doi.org/10.1182/BLOOD-2002-08-2531.

McGrath, K.E. *et al.* (2015) “Distinct sources of hematopoietic progenitors emerge before HSCs and provide functional blood cells in the mammalian embryo,” *Cell reports*, 11(12), p. 1892. Available at: https://doi.org/10.1016/J.CELREP.2015.05.036.

McKEAN, P.G. and PRITCHARD, D.I. (1989) “The action of a mast cell protease on the cuticular collagens of Necator americanus,” *Parasite immunology*, 11(3), pp. 293–297. Available at: https://doi.org/10.1111/J.1365-3024.1989.TB00667.X.

McNeil, B.D. *et al.* (2014) “Identification of a mast cell specific receptor crucial for pseudo-allergic drug reactions,” *Nature*, 519(7542), p. 237. Available at: https://doi.org/10.1038/NATURE14022.

McSorley, H.J., Chayé, M.A.M. and Smits, H.H. (2018) “Worms: Pernicious parasites or allies against allergies?,” *Parasite Immunology*, 41(6), p. e12574. Available at: https://doi.org/10.1111/PIM.12574.

Medvinsky, A. and Dzierzak, E. (1996) “Definitive Hematopoiesis Is Autonomously Initiated by the AGM Region,” *Cell*, 86(6), pp. 897–906. Available at: https://doi.org/10.1016/S0092-8674(00)80165-8.

Meixiong, J. and Dong, X. (2017) “Mas-Related G Protein-Coupled Receptors and the Biology of Itch Sensation,” *Downloaded from www.annualreviews.org. Guest* [Preprint]. Available at: https://doi.org/10.1146/annurev-genet-120116.

Metcalfe, D.D., Baram, D. and Mekori, Y.A. (1997) “Mast cells,” *Physiological reviews*, 77(4), pp. 1033–1079. Available at: https://doi.org/10.1152/PHYSREV.1997.77.4.1033.

Metcalfe, D.D. and Boyce, J.A. (2006) “Mast cell biology in evolution,” *Journal of Allergy and Clinical Immunology*, 117(6), pp. 1227–1229. Available at: https://doi.org/10.1016/j.jaci.2006.03.031.

Metcalfe, D.D., Peavy, R.D. and Gilfillan, A.M. (2009) “Mechanisms of mast cell signaling in anaphylaxis,” *The Journal of allergy and clinical immunology*, 124(4), p. 639. Available at: https://doi.org/10.1016/J.JACI.2009.08.035.

Metz, M. *et al.* (2006) “Mast cells can enhance resistance to snake and honeybee venoms,” *Science (New York, N.Y.)*, 313(5786), pp. 526–530. Available at: https://doi.org/10.1126/SCIENCE.1128877.

Meurer, S.K. *et al.* (2025) “TGF-β1 Induces Mucosal Mast Cell Genes and is Negatively Regulated by the IL-3/ERK1/2 Axis,” *Cell Communication and Signaling : CCS*, 23(1), p. 76. Available at: https://doi.org/10.1186/S12964-025-02048-8.

Meyer, N. *et al.* (2017) “Safeguarding of Fetal Growth by Mast Cells and Natural Killer Cells: Deficiency of One Is Counterbalanced by the Other,” *Frontiers in Immunology*, 8(JUN), p. 711. Available at: https://doi.org/10.3389/FIMMU.2017.00711.

Moore, M.A.S. and Metcalf, D. (1970) “Ontogeny of the haemopoietic system: yolk sac origin of in vivo and in vitro colony forming cells in the developing mouse embryo,” *British journal of haematology*, 18(3), pp. 279–296. Available at: https://doi.org/10.1111/J.1365-2141.1970.TB01443.X.

Mora, J. *et al.* (2009) “Expression of the high affinity IgE receptor by neutrophils of individuals with allergic asthma is both minimal and insensitive to regulation by serum IgE,” *Clinical Immunology*, 132(1), pp. 132–140. Available at: https://doi.org/10.1016/j.clim.2009.03.513.

Mota, I. and Vugman, I. (1956) “Effects of anaphylactic shock and compound 48/80 on the mast cells of the guinea pig lung,” *Nature*, 177(4505), pp. 427–429. Available at: https://doi.org/10.1038/177427A0.

Msallam, R. *et al.* (2020) “Fetal mast cells mediate postnatal allergic responses dependent on maternal IgE,” *Science*, 370(6519), pp. 941–950. Available at: https://doi.org/10.1126/SCIENCE.ABA0864;WEBSITE:WEBSITE:AAAS-SITE;JOURNAL:JOURNAL:SCIENCE;WGROUP:STRING:PUBLICATION.

Mukai, K. *et al.* (2016) “IgE and mast cells in host defense against parasites and venoms,” *Seminars in immunopathology*, 38(5), pp. 581–603. Available at: https://doi.org/10.1007/S00281-016-0565-1.

Müller, A.M. *et al.* (1994) “Development of hematopoietic stem cell activity in the mouse embryo,” *Immunity*, 1(4), pp. 291–301. Available at: https://doi.org/10.1016/1074-7613(94)90081-7.

Nakamura, T. and Murata, T. (2018) “Regulation of vascular permeability in anaphylaxis,” *British Journal of Pharmacology*, 175(13), p. 2538. Available at: https://doi.org/10.1111/BPH.14332.

Nakano, N. *et al.* (2021) “Mucosal Mast Cell–Specific Gene Expression Is Promoted by Interdependent Action of Notch and TGF-β Signaling,” *The Journal of Immunology*, 207(12), pp. 3098–3106. Available at: https://doi.org/10.4049/JIMMUNOL.2100112.

Nakano, T. *et al.* (1985) “Fate of bone marrow-derived cultured mast cells after intracutaneous, intraperitoneal, and intravenous transfer into genetically mast cell-deficient W/Wv mice. Evidence that cultured mast cells can give rise to both connective tissue type and mucosal mas…,” *The Journal of experimental medicine*, 162(3), pp. 1025–1043. Available at: https://doi.org/10.1084/JEM.162.3.1025.

Nassari, S., Duprez, D. and Fournier-Thibault, C. (2017) “Non-myogenic Contribution to Muscle Development and Homeostasis: The Role of Connective Tissues,” *Frontiers in Cell*

and Developmental Biology, 5(MAR), p. 22. Available at: https://doi.org/10.3389/FCELL.2017.00022.

Ng, M.F. (2010) "The role of mast cells in wound healing," *International Wound Journal*, 7(1), p. 55. Available at: https://doi.org/10.1111/J.1742-481X.2009.00651.X.

Norrby, K. (2002) "Mast cells and angiogenesis," *APMIS : acta pathologica, microbiologica, et immunologica Scandinavica*, 110(5), pp. 355–371. Available at: https://doi.org/10.1034/J.1600-0463.2002.100501.X.

Nuñez-Borque, E. *et al.* (2022) "Pathophysiological, Cellular, and Molecular Events of the Vascular System in Anaphylaxis," *Frontiers in immunology*, 13. Available at: https://doi.org/10.3389/FIMMU.2022.836222.

Ogulur, I. *et al.* (2025) "Type 2 immunity in allergic diseases," *Cellular & Molecular Immunology 2025 22:3*, 22(3), pp. 211–242. Available at: https://doi.org/10.1038/s41423-025-01261-2.

Oishi, K. *et al.* (2025) "MHC Class II-Expressing Mucosal Mast Cells Promote Intestinal Mast Cell Hyperplasia in a Mouse Model of Food Allergy," *Allergy: European Journal of Allergy and Clinical Immunology*, 80(8), pp. 2297–2309. Available at: https://doi.org/10.1111/ALL.16477;PAGE:STRING:ARTICLE/CHAPTER.

Okumura, S. *et al.* (2005) "FcεRI-mediated amphiregulin production by human mast cells increases mucin gene expression in epithelial cells," *Journal of Allergy and Clinical Immunology*, 115(2), pp. 272–279. Available at: https://doi.org/10.1016/j.jaci.2004.10.004.

Palis, J. *et al.* (1999) "Development of erythroid and myeloid progenitors in the yolk sac and embryo proper of the mouse," *Development (Cambridge, England)*, 126(22), pp. 5073–5084. Available at: https://doi.org/10.1242/DEV.126.22.5073.

Palm, N.W., Rosenstein, R.K. and Medzhitov, R. (2012) "Allergic Host Defenses," *Nature*, 484(7395), p. 10.1038/nature11047. Available at: https://doi.org/10.1038/NATURE11047.

Paus, R. *et al.* (1994) “Mast cell involvement in murine hair growth,” *Developmental Biology*, 163(1), pp. 230–240. Available at: https://doi.org/10.1006/dbio.1994.1139.

Pennock, J.L. and Grencis, R.K. (2006) “The mast cell and gut nematodes: damage and defence,” *Chemical immunology and allergy*, 90, pp. 128–140. Available at: https://doi.org/10.1159/000088885.

Perçin, G. *et al.* (2025) “Embryonic macrophages orchestrate niche cell homeostasis for the establishment of the definitive hematopoietic stem cell pool,” *Nature Communications 2025 16:1*, 16(1), pp. 4428-. Available at: https://doi.org/10.1038/s41467-025-59059-9.

Platts-Mills, T.A.E. *et al.* (2016) “The discovery of IgE 50 years on,” *Annals of allergy, asthma & immunology : official publication of the American College of Allergy, Asthma, & Immunology*, 116(3), p. 179. Available at: https://doi.org/10.1016/J.ANAI.2016.01.003.

Plum, T. *et al.* (2023) “Mast cells link immune sensing to antigen-avoidance behaviour,” *Nature*, 620(7974), pp. 634–642. Available at: https://doi.org/10.1038/s41586-023-06188-0.

Plum, T., Feyerabend, T.B. and Rodewald, H.R. (2024) “Beyond classical immunity: Mast cells as signal converters between tissues and neurons,” *Immunity*, 57(12), pp. 2723–2736. Available at: https://doi.org/10.1016/J.IMMUNI.2024.11.016.

Pritchard, D.I., Falcone, F.H. and Mitchell, P.D. (2021) “The evolution of IgE-mediated type I hypersensitivity and its immunological value,” *Allergy: European Journal of Allergy and Clinical Immunology*, 76(4), pp. 1024–1040. Available at: https://doi.org/10.1111/ALL.14570;SUBPAGE:STRING:FRAMEDPDF;PAGE:STRING:ARTICLE/CHAPTER.

Profet, M. (1991) “The function of allergy: immunological defense against toxins,” *The Quarterly review of biology*, 66(1), pp. 23–62. Available at: https://doi.org/10.1086/417049.

Qi, X. *et al.* (2013) “Antagonistic regulation by the transcription factors C/EBPα and MITF specifies basophil and mast cell fates,” *Immunity*, 39(1), p. 97. Available at: https://doi.org/10.1016/J.IMMUNI.2013.06.012.

Reber, L.L. *et al.* (2015) “Potential effector and immunoregulatory functions of mast cells in mucosal immunity,” *Mucosal Immunology*, 8(3), pp. 444–463. Available at: https://doi.org/10.1038/MI.2014.131.

Reitz, M. *et al.* (2017) “Mucosal mast cells are indispensable for the timely termination of Strongyloides ratti infection,” *Mucosal Immunology*, 10(2), pp. 481–492. Available at: https://doi.org/10.1038/mi.2016.56.

Ribatti, D. (2025) “The Discovery of Mast Cells: An Historical Note,” *Clinical Anatomy*, 0, pp. 1–4. Available at: https://doi.org/10.1002/CA.70043;SUBPAGE:STRING:FULL.

Roberts, L.J. *et al.* (1979) “Prostaglandin thromboxane, and 12-hydroxy-5,8,10,14-eicosatetraenoic acid production by ionophore-stimulated rat serosal mast cells,” *Biochimica et biophysica acta*, 575(2), pp. 185–192. Available at: https://doi.org/10.1016/0005-2760(79)90020-1.

Rodewald, H.R. *et al.* (1996) “Identification of a committed precursor for the mast cell lineage,” *Science*, 271(5250), pp. 818–822. Available at: https://doi.org/10.1126/SCIENCE.271.5250.818.

Rodewald, H.R. and Feyerabend, T.B. (2012) “Widespread Immunological Functions of Mast Cells: Fact or Fiction?,” *Immunity*, pp. 13–24. Available at: https://doi.org/10.1016/j.immuni.2012.07.007.

Ruitenberg, E.J. and Elgersma, A. (1976) “Absence of intestinal mast cell response in congenitally athymic mice during Trichinella spiralis infection,” *Nature*, 264(5583), pp. 258–260. Available at: https://doi.org/10.1038/264258A0.

Ryan, N.M. and Oghumu, S. (2019) “Role of mast cells in the generation of a T-helper type 2 dominated anti-helminthic immune response,” *Bioscience Reports*, 39(2), p. BSR20181771. Available at: https://doi.org/10.1042/BSR20181771.

Santiago, H.C. and Nutman, T.B. (2016) “Human Helminths and Allergic Disease: The Hygiene Hypothesis and Beyond,” *The American Journal of Tropical Medicine and Hygiene*, 95(4), p. 746. Available at: https://doi.org/10.4269/AJTMH.16-0348.

Schmerse, F. *et al.* (2014) “In vivo visualization of uterine mast cells by two-photon microscopy,” *Reproduction (Cambridge, England)*, 147(6), pp. 781–788. Available at: https://doi.org/10.1530/REP-13-0570.

Schneider, L.A. *et al.* (2007) “Molecular mechanism of mast cell mediated innate defense against endothelin and snake venom sarafotoxin,” *The Journal of experimental medicine*, 204(11), pp. 2629–2639. Available at: https://doi.org/10.1084/JEM.20071262.

Schwartz, L.B. (1990) “Tryptase, a mediator of human mast cells,” *The Journal of Allergy and Clinical Immunology*, 86(4 PART 2), pp. 594–598. Available at: https://doi.org/10.1016/S0091-6749(05)80222-2.

Schwarzer, M. *et al.* (2019) “Germ-Free Mice Exhibit Mast Cells With Impaired Functionality and Gut Homing and Do Not Develop Food Allergy,” *Frontiers in immunology*, 10(FEB). Available at: https://doi.org/10.3389/FIMMU.2019.00205.

Serhan, N. *et al.* (2025) “Maternal stress triggers early-life eczema through fetal mast cell programming,” *Nature 2025 646:8083*, 646(8083), pp. 161–170. Available at: https://doi.org/10.1038/s41586-025-09419-8.

Shimokawa, C. *et al.* (2017) “Mast Cells Are Crucial for Induction of Group 2 Innate Lymphoid Cells and Clearance of Helminth Infections,” *Immunity*, 46(5), pp. 863-874.e4. Available at: https://doi.org/10.1016/J.IMMUNI.2017.04.017.

Smith, E.S.J. and Lewin, G.R. (2009) “Nociceptors: a phylogenetic view,” *Journal of comparative physiology. A, Neuroethology, sensory, neural, and behavioral physiology*, 195(12), pp. 1089–1106. Available at: https://doi.org/10.1007/S00359-009-0482-Z.

Sonoda, T. *et al.* (1984) “Proliferation of peritoneal mast cells in the skin of W/Wv mice that genetically lack mast cells,” *The Journal of experimental medicine*, 160(1), pp. 138–151. Available at: https://doi.org/10.1084/JEM.160.1.138.

Sonoda, T., Hayashi, C. and Kitamura’, Y. (1983) *Presence of Mast Cell Precursors in the Yolk Sac of Mice*, *DEVELOPMENTAL BIOLOGY*.

Stanworth, D.R. (1993) “The discovery of IgE,” *Allergy*, 48(2), pp. 67–71. Available at: https://doi.org/10.1111/J.1398-9995.1993.TB00687.X.

Starkl, P. *et al.* (2020) “IgE Effector Mechanisms, in Concert with Mast Cells, Contribute to Acquired Host Defense against Staphylococcusaureus,” *Immunity*, 53(4), pp. 793-804.e9. Available at: https://doi.org/10.1016/j.immuni.2020.08.002.

Starkl, P. *et al.* (2024) “Mast cell–derived BH4 and serotonin are critical mediators of postoperative pain,” *Science Immunology*, 9(98). Available at: https://doi.org/10.1126/SCIIMMUNOL.ADH0545;WEBSITE:WEBSITE:AAAS-SITE;WGROUP:STRING:PUBLICATION.

Stone, K.D., Prussin, C. and Metcalfe, D.D. (2010) “IgE, Mast Cells, Basophils, and Eosinophils,” *The Journal of allergy and clinical immunology*, 125(2 Suppl 2), p. S73. Available at: https://doi.org/10.1016/J.JACI.2009.11.017.

Suo, C. *et al.* (2022) “Mapping the developing human immune system across organs,” *Science (New York, N.Y.)*, 376(6597). Available at: https://doi.org/10.1126/SCIENCE.ABO0510.

Tatemoto, K. *et al.* (2006) “Immunoglobulin E-independent activation of mast cell is mediated by Mrg receptors,” *Biochemical and Biophysical Research Communications*, 349(4), pp. 1322–1328. Available at: https://doi.org/10.1016/j.bbrc.2006.08.177.

Tauber, M. *et al.* (2023) “Landscape of mast cell populations across organs in mice and humans,” *Journal of Experimental Medicine*, 220(10). Available at: https://doi.org/10.1084/jem.20230570.

Tojima, R. *et al.* (2024) “Roles of C/EBPα, GATA2, TGF-β-signaling, and epigenetic regulation in the expression of basophil-specific protease genes.” Available at: https://doi.org/10.1101/2024.02.24.581851.

Tu, L.L. *et al.* (2005) “Notch signaling is an important regulator of type 2 immunity,” *The Journal of Experimental Medicine*, 202(8), p. 1037. Available at: https://doi.org/10.1084/JEM.20050923.

Turner, H. and Kinet, J.P. (1999) “Signalling through the high-affinity IgE receptor FcεRI,” *Nature*, 402(6760 SUPPL. 1), pp. 24–30. Available at: https://doi.org/10.1038/35037021;KWRD=SCIENCE.

Tyagi, N. *et al.* (2015) “Comparisons of Allergenic and Metazoan Parasite Proteins: Allergy the Price of Immunity,” *PLoS Computational Biology*, 11(10). Available at: https://doi.org/10.1371/JOURNAL.PCBI.1004546,.

Vermillion, D.L. *et al.* (1988) “Antigen-induced contraction of jejunal smooth muscle in the sensitized rat,” *The American journal of physiology*, 255(6 Pt 1). Available at: https://doi.org/10.1152/AJPGI.1988.255.6.G701.

Waki, N. *et al.* (1990) *Intraperitoneally injected cultured mast cells suppress recruitment and differentiation of bone marrow-derived mast cell precursors in the peritoneal cavity of W/Wv mice - PubMed*, *Exp Hematol*. Available at: https://pubmed.ncbi.nlm.nih.gov/1968010/ (Accessed: December 27, 2025).

Wang, F., Yang, T.L.B. and Kim, B.S. (2020) “The Return of the Mast Cell: New Roles in Neuroimmune Itch Biology,” *Journal of Investigative Dermatology*, 140(5), pp. 945–951. Available at: https://doi.org/10.1016/J.JID.2019.12.011.

Wang, Z. *et al.* (2017) “Skin microbiome promotes mast cell maturation by triggering stem cell factor production in keratinocytes,” *Journal of Allergy and Clinical Immunology*, 139(4), pp. 1205-1216.e6. Available at: https://doi.org/10.1016/j.jaci.2016.09.019.

Waskow, C. *et al.* (2009) “Hematopoietic stem cell transplantation without irradiation,” *Nature Methods 2009 6:4*, 6(4), pp. 267–269. Available at: https://doi.org/10.1038/nmeth.1309.

Weitzmann, A. *et al.* (2020) “Mast Cells Occupy Stable Clonal Territories in Adult Steady-State Skin,” *Journal of Investigative Dermatology*, 140(12), pp. 2433-2441.e5. Available at: https://doi.org/10.1016/j.jid.2020.03.963.

Williams, C.M.M. and Galli, S.J. (2000) “The diverse potential effector and immunoregulatory roles of mast cells in allergic disease,” *Journal of Allergy and Clinical Immunology*, 105(5), pp. 847–859. Available at: https://doi.org/10.1067/MAI.2000.106485.

Wong, G.W. *et al.* (2014) “Ancient origin of mast cells,” *Biochemical and biophysical research communications*, 451(2), p. 314. Available at: https://doi.org/10.1016/J.BBRC.2014.07.124.

Wu, W.J. *et al.* (2021) “IL-4 and IL-13 Promote Proliferation of Mammary Epithelial Cells through STAT6 and IRS-1,” *International journal of molecular sciences*, 22(21). Available at: https://doi.org/10.3390/IJMS222112008.

Wulff, B.C. *et al.* (2012) “Mast Cells Contribute to Scar Formation during Fetal Wound Healing,” *Journal of Investigative Dermatology*, 132(2), pp. 458–465. Available at: https://doi.org/10.1038/JID.2011.324.

Xing, W. *et al.* (2011) “Protease phenotype of constitutive connective tissue and of induced mucosal mast cells in mice is regulated by the tissue,” *Proceedings of the National Academy of Sciences of the United States of America*, 108(34), pp. 14210–14215. Available at: https://doi.org/10.1073/PNAS.1111048108/-/DCSUPPLEMENTAL.

Yang, B. *et al.* (2013) “Food allergen-induced mast cell degranulation is dependent on PI3K-mediated reactive oxygen species production and upregulation of store-operated calcium

channel subunits," *Scandinavian Journal of Immunology*, 78(1), pp. 35–43. Available at: https://doi.org/10.1111/SJI.12062;REQUESTEDJOURNAL:JOURNAL:13653083.

Yang, L. *et al.* (2024) "Intraepithelial mast cells drive gasdermin C-mediated type 2 immunity," *Immunity*, 57(5), pp. 1056-1070.e5. Available at: https://doi.org/10.1016/j.immuni.2024.03.017.

Yoshimoto, M. *et al.* (2022) "Mast Cell Repopulating Ability Is Lost During the Transition From Pre-HSC to FL HSC," *Frontiers in Immunology*, 13. Available at: https://doi.org/10.3389/fimmu.2022.896396.

Zaiss, D. *et al.* (2013) "Amphiregulin enhances regulatory T cell-suppressive function via the epidermal growth factor receptor," *cell.comDMW Zaiss, J Van Loosdregt, A Gorlani, CPJ Bekker, A Gröne, M SibiliaImmunity, 2013•cell.com* [Preprint]. Available at: https://www.cell.com/immunity/fulltext/S1074-7613(13)00002-2?elq=be39f8235ac0487787b0bfec29dd628c&mobileUi=0 (Accessed: December 26, 2025).

Zaiss, D.M. *et al.* (no date) "Amphiregulin, a TH2 cytokine enhancing resistance to nematodes," *Science*, 314(5806), p. 1746. Available at: https://doi.org/10.1126/SCIENCE.1133715;ISSUE:ISSUE:DOI.

Zeisberg, M. and Kalluri, R. (2012) "Cellular Mechanisms of Tissue Fibrosis. 1. Common and organ-specific mechanisms associated with tissue fibrosis," *American Journal of Physiology - Cell Physiology*, 304(3), p. C216. Available at: https://doi.org/10.1152/AJPCELL.00328.2012.

Zhao, S., Umpierre, A.D. and Wu, L.J. (2024) "Tuning neural circuits and behaviors by microglia in the adult brain," *Trends in Neurosciences*, 47(3), pp. 181–194. Available at: https://doi.org/10.1016/J.TINS.2023.12.003.

Zhao, X.O. *et al.* (2022) "Mast cell chymase affects the functional properties of primary human airway fibroblasts: Implications for asthma," *Journal of Allergy and Clinical*

Immunology, 149(2), pp. 718–727. Available at: https://doi.org/10.1016/J.JACI.2021.07.020.

Chapter 1

Mast cells are not essential for pubertal mammary gland branching

This chapter has been published in the European Journal of Immunology

Eur J Immunol. 2025 Aug 17;55(8):e70036. doi: 10.1002/eji.70036

Note: Formatting changes incorporated (Methods and Materials, References added to end of chapter)

Introduction

Mast cells (MCs) are tissue-resident immune cells found throughout nearly all tissues in the body. While they are most recognised for their role in allergy and anaphylaxis, the tissue remodelling mechanisms that cause pathological damage in this context may play beneficial roles to support tissue development under homeostasis. The mammary gland undergoes extensive morphogenesis postnatally, and MCs present in the mammary gland have been proposed to contribute to its maintenance and development (Lilla and Werb, 2010). However, this work was based on the *Kit*-dependent MC deficiency model which affects multiple haematopoietic cell types (Keller et al., 1995; Sharma et al., 2007) as well as the mammary epithelium itself (Polat, 2007; Regan et al., 2012). Therefore, there is a need to re-assess the functions of MCs in mammary gland development. Here, we targeted MCs using complementary *Kit* independent MC deficiency models to identify the contribution of MCs to mammary gland branching at puberty.

Publication inserted pages

Mast cells are not essential for pubertal mammary gland branching

Authors and affiliations

Simran Kapoor[1], Clara M. Munz[1], Jimmy Marsden[1, 2], Cyril Carvalho[1], Holly Tinsley[1], Marlene Magalhaes Pinto[1], Bert Malengier-Devlies[1], Solvig Becker[1], Guillaume Seuzaret[1], Katelyn Patatsos[1, 3], Ramazan Akyol[6], Amy B Pederson[4], Gillian Wilson[5], Marc Dalod[6], Rebecca Gentek[1, #]

[1]Institute for Regeneration and Repair, Centre for Reproductive Health, Centre for Inflammation Research, University of Edinburgh, UK

[2]Currently: Institute of Medical Sciences, University of Aberdeen, UK & Research Institute for Environmental and Occupational Health, Université de Rennes I, France

[3]Currently: Murdoch Children's Research Institute, Royal Children's Hospital Victoria, Australia

[4]Institute of Ecology and Evolution, School of Biological Sciences, University of Edinburgh, UK

[5]Institute of Infection, Immunity and Inflammation, University of Glasgow, UK

[6]Aix-Marseille University, CNRS, INSERM, Centre d'Immunologie de Marseille-Luminy (CIML)

[#]Corresponding author

Correspondence should be addressed to:

Rebecca.Gentek@ed.ac.uk

The University of Edinburgh

Institute for Regeneration and Repair (IRR)

Centre for Reproductive Health (CRH)

4-6 Little France Drive

EH16 4UU Edinburgh

United Kingdom

Keywords

Mast cells, mammary gland, branching, puberty

Abbreviations

- TEBs: Terminal end buds
- TEDs: Duct ends

Abstract

Mast cells are long-lived, tissue-resident immune cells of the myeloid lineage with cardinal functions in allergy and atopic disease. They are now increasingly recognized also for protective roles e.g. against infections and venoms. Other functions originally assigned to mast cells in development and physiology, however, have been refuted, and for yet others, the true contribution of mast cells remains uncertain.

Mast cells have been implicated in promoting ductal branching in the pubertal mammary gland, the organ that produces and secretes milk in mammals, but these findings are based on mouse models that are not mast cell specific. In this study, we therefore re-addressed the impact of mast cells on mammary gland branching using several complementary genetic models, including a newly generated transgenic mouse line (*Ms4a2*$^{lsl\text{-}hDTR}$). We report that neither constitutive deficiency of mast cells, nor their conditional ablation induced at puberty affect mammary gland branching. Our results thus dispute that mast cells promote

this process in mice, at least in a unique and non-redundant manner. This study adds to a growing body of work clarifying the biological roles of mast cells and further expands the toolbox available to the field of mast cell research.

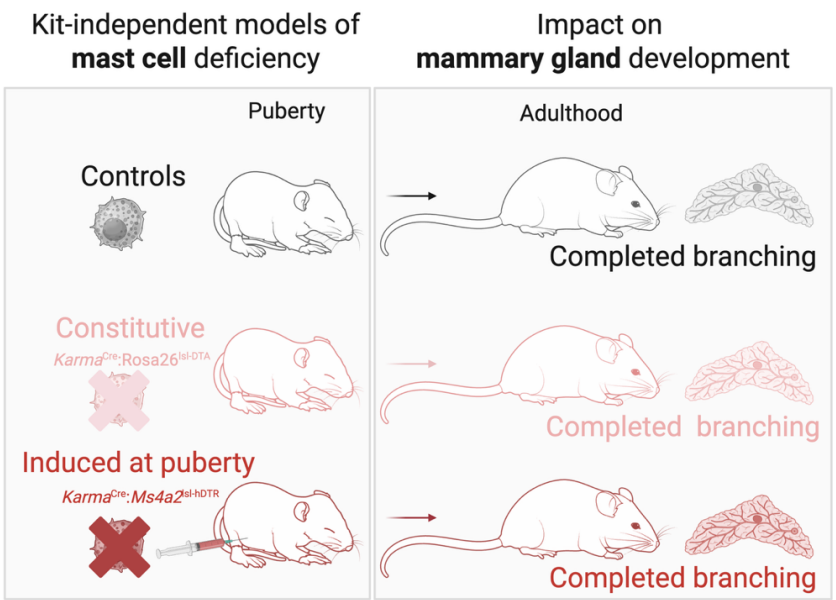

Abstract Figure. Mast cells are not essential for pubertal mammary gland branching.

Introduction

The mammary gland is an organ specific to the mammalian reproductive system, and its primary function is milk production and secretion. It consists of milk ducts that spread throughout an adipose tissue pad and end in terminal end ducts (TEDs) and terminal end buds (TEBs), which facilitate duct branching and elongation during development and pregnancy. The mammary gland is also rich in resident immune cells and is indeed also of immunological importance: transfer of immunoglobulin antibodies and immune cells through the milk can support offspring immunity (Atyeo and Alter, 2021), and the gland also provides an immunological barrier during suckling.

The mammary gland develops in a series of discrete steps ranging from embryonic to postnatal stages. In mice, mammary gland development is initiated at day 10.5-11 of embryonic development (E10.5-E11) with the formation of ectodermal disks that from E13.5 onwards invade the underlying mesenchyme and eventually form the nipples. The developing ductal epithelium then starts branching, resulting in a few rudimentary branches present at birth (Hinck and Silberstein, 2005; Macias and Hinck, 2012; Richert et al., 2000; Sternlicht et al., 2006; Watson and Khaled, 2008). These branches then remain largely quiescent and only grow allometrically until puberty, which marks the key period of mammary gland development. The start of ductal branching is often the first defining sign of puberty onset, and in humans is a developmental window of susceptibility to breast cancer (Goldberg et al., 2020; Krisanits et al., 2020). During puberty, the previously rudimentary ducts grow and TEBs are formed. Cells at the end of the TEBs then proliferate to invade the fat pad, and branches form through bifurcation of TEBs (Hinck and Silberstein, 2005). This process repeats until the ductal tree has invaded the entire fat pad. Throughout the reproductive cycle, the mammary gland undergoes further dynamic changes, enabling it to fulfil its physiological functions. With pregnancy, the secretory epithelium forms alveoli to prepare for lactation. Upon weaning, these alveoli undergo involution, and the gland returns to a state similar to that before pregnancy. Mammary gland remodeling is a carefully orchestrated process that relies on internal and external signals. Growth factors and hormones act on the mammary epithelium and stroma to facilitate branching and alveoli formation. Whilst fetal mammary gland development is independent of estrogen (Mallepell et al., 2006), it is suppressed by androgens in male mice. Testosterone exposure results in regression of mammary gland development (Durnberger and Kratochwii, 1980), and androgens cause mesenchymal cells to condense around the developing epithelium, preventing further gland development (Heuberger et al., 1982). On the contrary, pubertal

branching depends on estrogen receptor α expression in epithelial cells (Mallepell et al., 2006). During puberty, progesterone acts on stromal cells to promote branching (Brisken and O'Malley, 2010; Macias and Hinck, 2012). Finally, remodeling during pregnancy is induced by prolactin, which acts together with progesterone to promote alveolar growth. Local influences from stromal cells further contribute to remodeling. For example, fibroblasts in the mammary gland stroma communicate with the developing epithelium (Howard and Lu, 2014) by providing an extracellular matrix capable of maintaining the mammary glands (Thorne et al., 2015).

Another player in the morphogenesis of mammary gland ducts are immune cells: alveolarization during pregnancy is impaired in mice deficient in IL-4 and IL-13 (Khaled et al., 2007), and pubertal duct elongation and branching are reduced in mice lacking eosinophils and macrophages in the mammary gland (V Gouon-Evans et al., 2000) (Valérie Gouon-Evans et al., 2002; Lin et al., 2002; Rothenberg et al., 1997). This seems to also be true for mice deficient in mast cells, which show a reduction in the number of TEBs, as well as numbers and length of ducts during puberty (Lilla and Werb, 2010). Mast cells are potent myeloid effector cells best known as mediators of allergy and anaphylaxis and for their implications in atopic disease. They also have protective roles, for example against bacteria and venoms (Marichal et al., 2013; Starkl et al., 2022; Starkl et al., 2020b) and by promoting avoidance behavior towards food allergens (Plum et al., 2023b; Florsheim et al., 2023). However, their contribution to normal tissue functioning and development remain heavily debated (Rodewald and Feyerabend, 2012). This is at least in part due to limitations in the tools used to study mast cells. Their maturation and survival depend on stem cell factor, and inactivating mutations in its receptor Kit cause mast cell deficiencies. Traditionally, Kit-dependent mouse models have therefore been used to investigate mast cell functions (Reber et al., 2012). The usefulness of these models is limited, however, because Kit

mutations also affect other immune and non-immune cells, as evidenced by several defects in Kit mutant mice that are unrelated to mast cells (Reber et al., 2012). This is of particular importance to the mammary gland, since Kit is expressed by the breast epithelium (Polat, 2007) (Regan et al., 2012). Mast cells can be found near the ducts at the onset of puberty, and it has been suggested that they can directly interact with the ductal epithelium (Lilla and Werb, 2010). Pubertal branching is stunted in the absence of mast cells, a defect that is rescued by adulthood through an unknown compensatory mechanism (Lilla and Werb, 2010). However, these findings were made in mutant *Kit*^{Wsh} mice. It is currently unknown if mice with Kit-independent mast cell deficiency copy this phenotype, and hence, whether this defect is indeed attributable to the absence of mast cells.

In this study, we re-addressed the involvement of mast cells in pubertal mammary gland branching using Kit-independent genetic mouse models of mast cell deficiency, including a new Cre-responsive conditional transgenic line in which mast cell depletion can be induced by administration of Diphtheria toxin. Unexpectedly, we found no defects in mammary gland branching in the absence of mast cells. Our data therefore dispute a critical contribution of mast cells to this developmental process, at least in a unique and non-redundant manner.

Results

Mast cells are present in postnatal mammary glands and functional at puberty.

In principle, mast cells could regulate ductal branching via locally restricted mechanisms or through longer-range signaling, since granules can travel far upon release. The mammary gland consists of ductal epithelium and stromal cells, including adipocytes. Mast cells can be found associated with all these structures, i.e. near TEBs and embedded in the adipose

stroma (Figure 1A). Mast cells can also be detected close to the lymph node and major blood vessels (Figure S1A), as previously reported (Lilla and Werb, 2010). However, in both pubertal and adult glands, more than half (54% at puberty and 59% in adults) of mast cells are located within 100 µm of TEBs (Figure 1B).

Like other immune cells, mast cells are commonly studied by flow cytometry, and they can also be identified in single cell transcriptomics datasets of samples obtained by tissue dissociation (Tauber et al., 2023). Nonetheless, to our knowledge, this approach has not exhaustively been applied to mast cells in the mammary gland. Therefore, we initially characterized mast cells in mammary glands from pubertal (5.5 weeks) and adult (aged 8-15 weeks) virgin mice by flow cytometry. Mast cells were identified as hematopoietic ($CD45^+$) cells that lack markers for other myeloid lineages ($CD64^-$ and/or $F4/80^-$, $CD11b^{low}$) and express CD117 (Kit^+) and the IL33-receptor alpha ($ST2^+$) (Figure 1C and S1B; Note, a similar gating strategy was also used for peritoneal cavity as a reference tissue (Figure S1C)). A characteristic feature of mast cells is their intracellular granules. These are densely packed with potent effectors and differ in their composition between distinct classes of mast cells. Mammary gland mast cells are of the connective tissue type (Tauber et al., 2023) (Lilla and Werb, 2010). These types of mast cells feature heparin-containing intracellular granules, which can be stained for with Avidin (Tharp et al., 1985) (Bergstresser et al., 1984) (Kett et al., 2003). Indeed, most $CD117^+$ (Kit^+) $ST2^+$ mast cells also stained positive with fluorescently labelled Avidin in the mammary gland at puberty and in adulthood (Figure 1C). We thus used this as the primary gating strategy to identify mammary gland mast cells throughout this study. Compared to puberty, mast cells were approximately 6-fold more abundant in adult glands (Figure 1D). We also noted variation between individual mice. This was true both at puberty and in adult glands. In other organs of the reproductive system like the uterus, mast cell numbers vary with the estrus cycle (Woidacki et al., 2013b) (L Padilla 1,

1990). Indeed, in rats, mast cells are more abundant at diestrus (Ramirez et al., 2012). Moreover, histamine levels are higher in the murine gland at estrus (Maslinski C, 1993) (Wagner and Fogel, 2004). We therefore stratified pubertal animals by estrus stage. This showed that mast cell numbers are slightly elevated at estrus, but comparable otherwise (Figure 1E). Of note, we also obtained significantly less mast cells from abdominal fat pads of adult male mice compared to females (Figure S1D). Whilst sex-specific differences in mast cell numbers may exist in the adipose stroma, this could indicate that most of the mast cells we identify in females by flow cytometry are duct-associated, in keeping with our imaging analysis.

Since mast cells are thought to promote ductal branching during puberty, we next wanted to assess the activation status of the mast cells present at this stage. Mast cell activation results in granule release, which can be measured by surface staining for the tetraspanin CD63, a component of granule membranes that becomes externalized upon degranulation (Kraft et al., 2013a). To gauge if mast cells can be activated in the pubertal gland, we thus determined surface expression of CD63 alongside levels of intracellular heparin-containing granules on freshly isolated cells *ex vivo*, without experimental treatments to trigger degranulation (Figure 1F). Using this assay, most mast cells are either actively degranulating (Avidin^{high} CD63^{high}, on average 26.2%) or have recently been activated (Avidin^{low} CD63^{high}, 50.2%), whilst only minor fractions appear to be in a non-active (Avidin^{high} CD63^{low}, 17.8%) or immature or refractory stage (Avidin^{low} CD63^{low}; 5%), indicating that at puberty, mammary gland mast cells can degranulate. To further confirm their functionality, we performed an assay to investigate whether mast cells sorted from the pubertal mammary gland are able to degranulate upon stimulation. In this assay, we determined the extent of degranulation by measuring heparin-containing granules (identified by Avidin staining) on the cell surface released upon stimulation with Substance P. Mast cells from the mammary

gland were able to degranulate upon stimulation, indicated by increasing granule presence over the course of 30 minutes (Figure 1G, Figure S1E). As expected, macrophages sorted from the same glands could not be stimulated in this manner.

In summary, we confirmed that mast cells are present in the adult and pubertal mammary gland. Moreover, we provide evidence that mast cells are also functional in the pubertal gland.

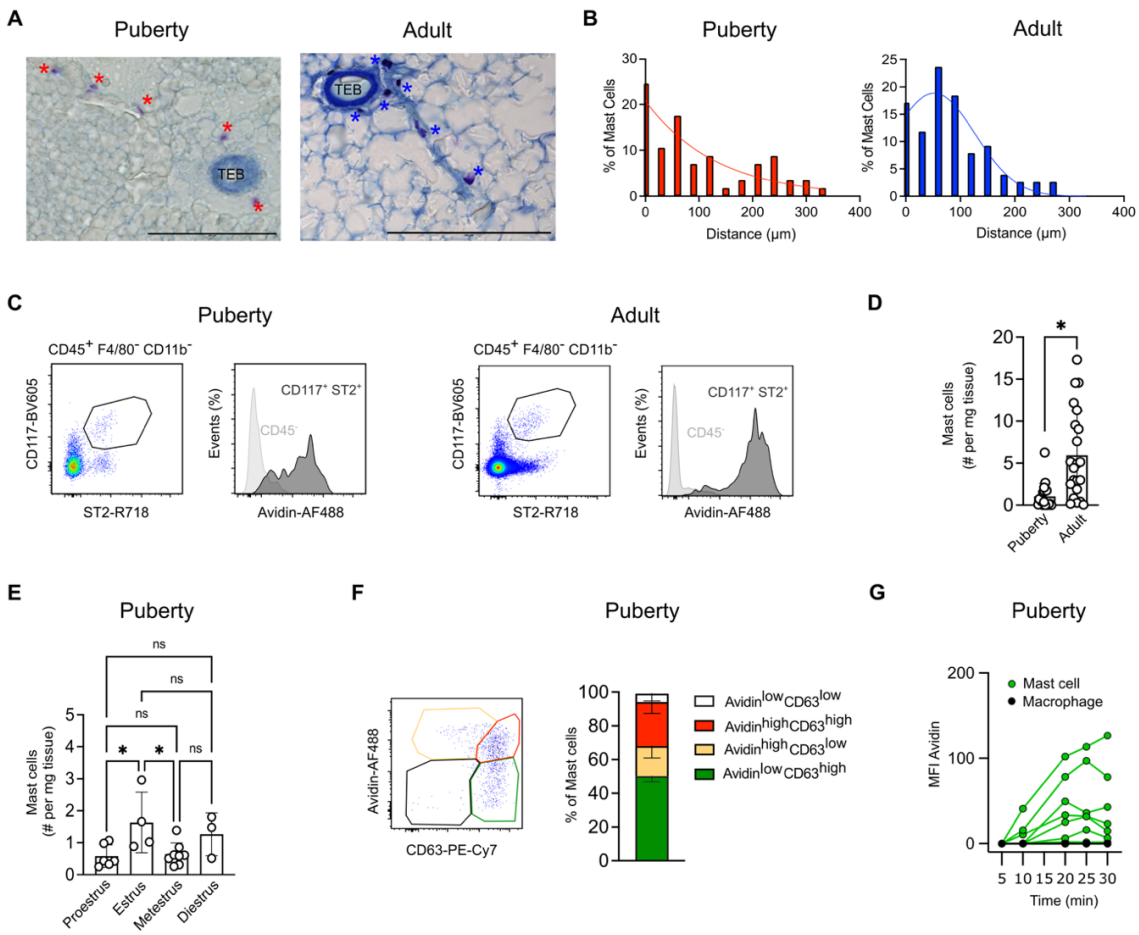

Chapter (1) Figure 1: Mast cells are present in the postnatal mammary gland and are activated at puberty.

(A, B) Histological analysis of mast cells in the mouse mammary gland. Pubertal (left) and adult (right) mammary glands were stained with Toluidine Blue, a metachromatic dye staining mast cell granules (purple). (A) Representative images. Scale bar = 200um. (B) Mast cell distribution. The frequency of mast cells within the indicated distances (in micrometers) from terminal end buds (TEBs) was quantified. Data are representative (A) and cumulative (B) of 4 individual mice per developmental time point. (C) Flow cytometry identification strategy for mast cells within the pubertal (5.5 weeks; left panels) and adult (8-15 weeks;

right panels) mammary gland. (D) Quantification of mast cells (CD117 (Kit^+) $Avidin^+$) in pubertal and adult mammary glands. Data in (C, D) are from at least 19 mice per age. Quantified data are shown as mean with error bars indicating the SD. *p< 0.05 as determined by Mann-Whitney test. ns = not significant. (E) Mast cell numbers ($CD117^+$ (Kit^+) $Avidin^+$) in pubertal mammary glands stratified by estrus stage. Data from minimally 3 mice per estrus stage. Quantified data are shown as mean with error bars indicating the SD. *p< 0.05 as determined by one way ANOVA test. ns = not significant. (F) Flow cytometric assessment of primary mammary gland mast cell activation states at puberty (5.5 weeks). Mast cells were gated as $CD117^+$ (Kit^+) $ST2^+$ as shown in (C). The levels of degranulation were estimated by intracellular Avidin staining for heparin containing granules and surface staining of CD63. Data are representative of (left) and quantified (right) for 6 individual mice. (G) Time course of mast cell degranulation upon stimulation with Substance P. Mast cells (green) were sorted from the pubertal (5.5 weeks) mammary gland and subjected to short term culture and longitudinal imaging for release of heparin containing granules. Macrophages (black) isolated from the same glands were analyzed as negative controls. *Figures D-E generated by Jimmy Marsden and Rebecca Gentek. Figures F-G jointly generated by Clara Munz and Simran Kapoor.*

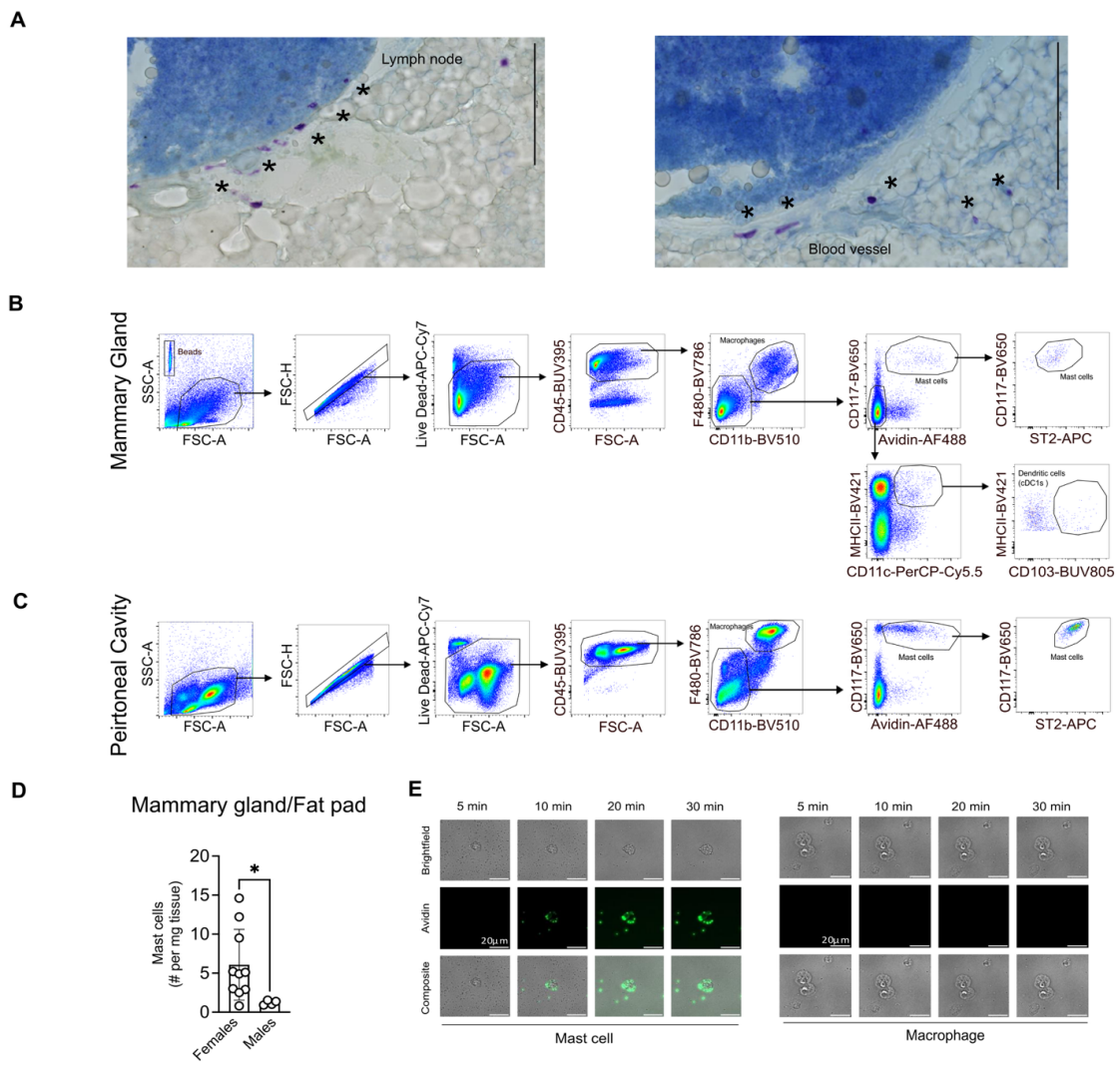

Chapter (1) Supplementary Figure S1 (related to Figure 1): Presence and functionality of mast cells in the mammary gland.

(A) Representative images for localization of mast cells (purple) near the lymph node and blood vessels in the pubertal mammary gland stained by Toluidine Blue. Scale bar = 200um. (B) Flow cytometry gating strategy used to identify mast cells (live single cells, $CD45^+$, $CD117^+$ (Kit^+) $Avidin^+$ $ST2^+$), macrophages (live single cells, $CD45^+$, $F4/80^+$ $CD11b^+$) and dendritic cells

(live single cells, $CD45^+$, $CD117^-$ (Kit^-) $Avidin^-$, $CD11c^+$ $MHCII^+$ $CD103^+$) in mammary glands. (C) Flow cytometry gating strategy for identification of mast cells (live single cells, $CD45^+$, $CD117^+$ (Kit^+) $Avidin^+$ $ST2^+$) in the peritoneal cavity. (D) Flow cytometric mast cell quantification in the male abdominal fat pad compared to the female mammary gland at adulthood. Data are cumulative of at least 4 individual mice per group from at least 2 independent experiments. Data are shown as mean with error bars indicating the SD. *$p<0.05$ as determined by Mann-Whitney test. (E) Representative images for time course of degranulation assay. Mast cells sorted from the pubertal mammary glands (pooled from 4 individual mice) were stimulated with Substance P. Avidin staining (green) for heparin containing granules. As negative control, macrophages from the same pubertal mammary glands were analysed the same way. Scale bar = 20mm. *Figure D generated by Jimmy Marsden and Rebecca Gentek. Figure E generated by Clara Munz.*

Mammary glands of $Karma^{Cre}$:$Rosa26^{lsl\text{-}DTA}$ mice are constitutively deficient in mast cells.

The data implicating mast cells in ductal branching in the mammary gland are primarily based on Kit^{Wsh} mice (Lilla and Werb, 2010). To investigate if the transient delay in branching observed in these mice is indeed attributable to mast cells, we sought to use mice in which mast cell-deficiency does not depend on mutations in *Kit*. First, we wanted to utilize the Cre loxP system to constitutively ablate mast cells. The *Karma* gene (also known as *Gpr141b*) encodes an orphan G-protein-coupled receptor. In $Karma^{Cre}$:$Rosa26^{lsl\text{-}DTA}$ mice, Cre activity results in removal of a stop cassette that otherwise prevents expression of the Diphtheria toxin alpha subunit (DTA), thereby inducing death specifically in cells expressing *Karma*, the gene driving Cre recombinase (Mattiuz et al., 2018a). $Karma^{Cre}$ targets connective tissue mast cells in the skin (Mattiuz et al., 2018a), and $Karma^{Cre/wt}$:$Rosa26^{lsl\text{-}DTA/wt}$ mice are

profoundly deficient in peritoneal cavity mast cells (Figure S2A). We thus assessed the level of mast cell depletion in the postnatal mammary gland of *Karma*^{Cre}:Rosa26$^{lsl\text{-}DTA}$ mice (Figure 2A). Considering our focus on pubertal maturation, we analyzed the window around puberty with higher granularity. Encouragingly, *Karma*^{Cre}:Rosa26$^{lsl\text{-}DTA}$-mediated virtually complete ablation of mast cells in the mammary gland at all stages analyzed, i.e. prior to puberty (3 weeks), at the onset (5 weeks), during (5.5 weeks) and at conclusion (6.5 weeks) of puberty, as well as in mature adults (8-12 weeks) (Figure 2B).

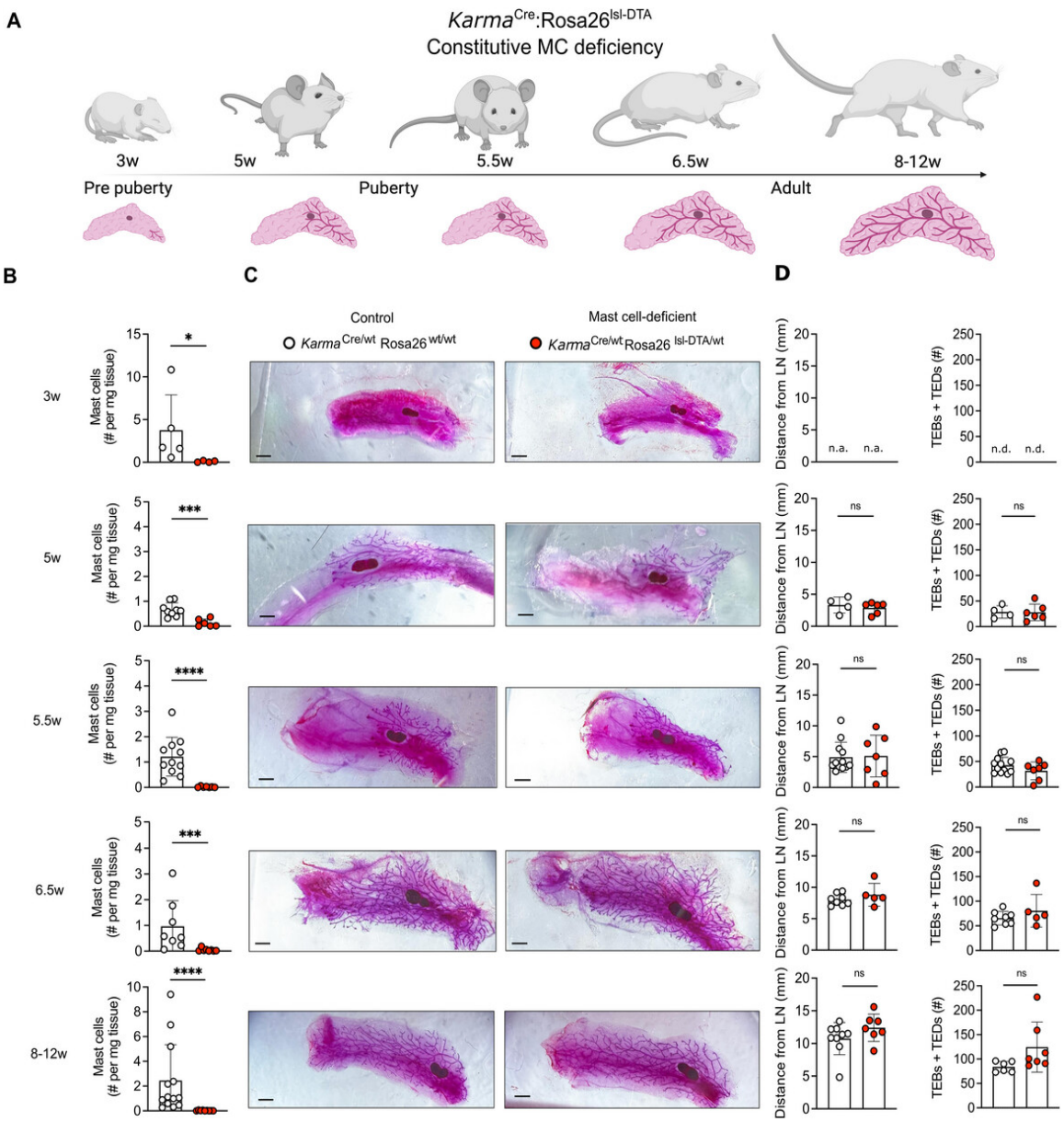

Chapter (1) Figure 2: Constitutive mast cell deficiency has no impact on mammary gland branching.

(A) Schematic illustrating experimental approach. *Karma*$^{Cre/wt}$:Rosa26$^{lsl-DTA}$ mice were analyzed at 3, 5, 5.5, 6.5 and 8-12 weeks (w) of age. (B) Time course analysis showing mast

cell numbers in *Karma*$^{Cre/wt}$:Rosa26$^{lsl\text{-}DTA/wt}$ mice (red) compared to mast cell-proficient littermate controls (*Karma*$^{Cre/wt}$:Rosa26$^{wt/wt}$ mice; white). Mast cells were quantified by flow cytometry at the indicated developmental time points. (C) Representative mammary glands of mast cell-deficient mice (*Karma*$^{Cre/wt}$:Rosa26$^{lsl\text{-}DTA/wt}$, right) and mast cell-proficient littermates (*Karma*$^{Cre/wt}$:Rosa26$^{wt/wt}$; left), analyzed for branching by Carmine staining at the indicated life stages. Scale bars = 1mm. (D) Analysis of postnatal mammary gland branching on Carmine-stained mammary glands of mast cell-deficient mice (*Karma*$^{Cre/wt}$:Rosa26$^{lsl\text{-}DTA/wt}$; red) and mast cell-proficient littermates (*Karma*$^{Cre/wt}$:Rosa26$^{wt/wt}$; white) across postnatal development. The distance of the branching front and the number of terminal end buds (TEBs) and end ducts (TEDs) past the middle of the lymph node were measured. Data are representative (C) and cumulative (B, D) of at least 5 individual mice per group from at least 2 independent experiments. Data in (B, D) are shown as mean with error bars indicating the SD. ****$p<0.0001$, ***$p<0.001$, *$p<0.05$ as determined by Mann-Whitney test. ns = not significant.

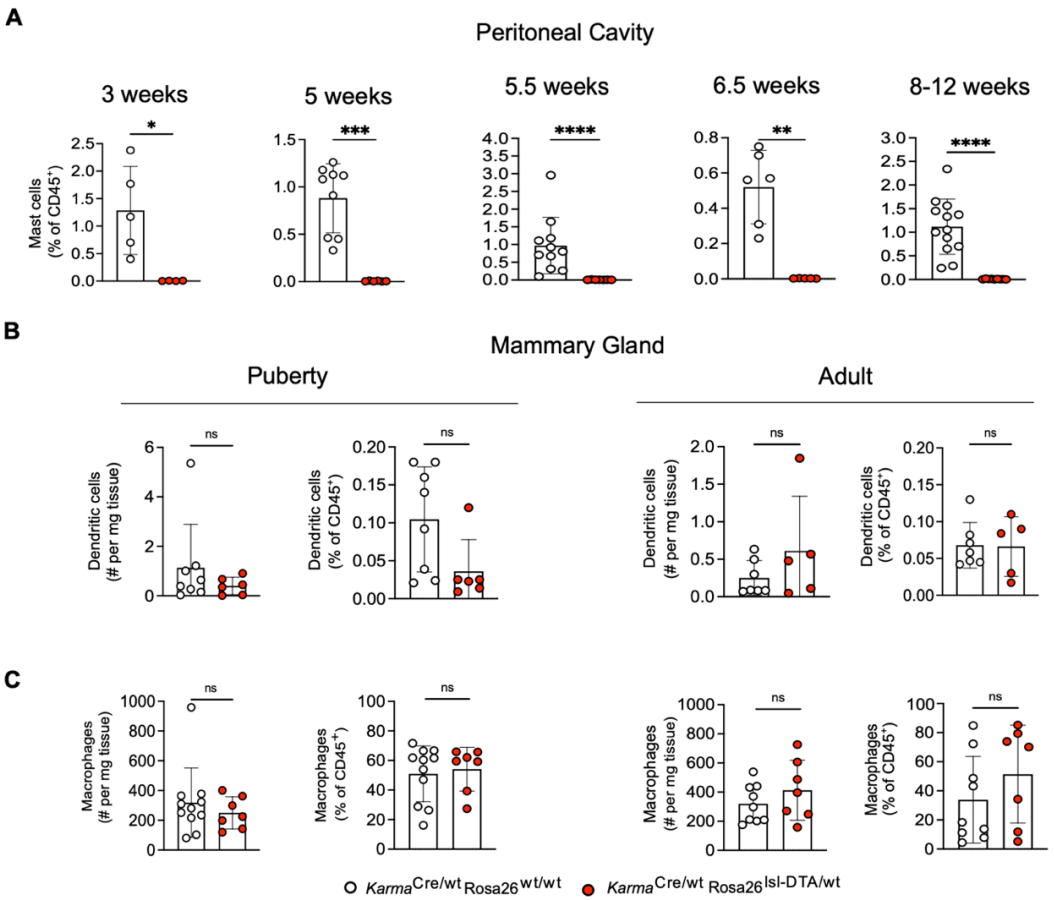

Chapter (1) Supplementary Figure S2 (related to Figure 2): Mast cells and dendritic cells in *Karma^{Cre}:Rosa26$^{lsl\text{-}DTA}$* mice.

(A) Mast cell numbers and/or relative abundance within hematopoietic compartment (% within CD45$^+$ cells) of the peritoneal cavity of Karma$^{Cre/wt}$:Rosa26$^{lsl\text{-}DTA/wt}$ (red) compared to mast-cell proficient littermate Karma$^{Cre/wt}$:Rosa26$^{wt/wt}$ controls (white) at the indicated ages, as measured by flow cytometry. (B,C) Dendritic cell (B) and macrophage (C) numbers and relative abundance within hematopoietic compartment (% within CD45$^+$ cells) and numbers in the mammary gland of Karma^{Cre}:Rosa26$^{lsl\text{-}DTA}$ mice at puberty (5.5 weeks; left) and

adulthood (8-12 weeks; right). Data are cumulative of at least 4 individual mice per group from at least 2 or more independent experiments. Data are presented as mean with error bars indicating the SD. Data are shown as mean with SD as error bars. ****p<0.0001, ***p<0.001, **p<0.01, *p<0.05 as determined by Mann- Whitney test. ns = not significant.

Constitutive mast cell deficiency in Karma^{Cre}:Rosa26$^{lsl\text{-}DTA}$ mice has no effect on mammary gland branching.

Having established *Karma*^{Cre}:Rosa26$^{lsl\text{-}DTA}$ mice as a tool for robust mast cell deficiency in mammary glands, we next performed Carmine staining to investigate if these mice show any branching defects. If mast cells did indeed promote pubertal branching, then these mice should exhibit impaired ductal branching like previously reported in *Kit*^{Wsh} mice (Lilla and Werb, 2010). Because any defect might be transient in nature and compensated by adulthood, as is the case in *Kit*^{Wsh} mice (Lilla and Werb, 2010), we performed a time course analysis. Prior to puberty, at 3 weeks of age, mammary glands only contain rudimentary ducts. These were indistinguishable in mast cell-deficient *Karma*$^{Cre/wt}$:Rosa26$^{lsl\text{-}DTA/wt}$ and *Karma*$^{Cre/wt}$:Rosa26$^{wt/wt}$ control mice (Figure 2C, 2D). In our hands, the onset of puberty occurs at around 5 weeks of age, as evidenced by ductal outgrowth beyond the lymph node and the first signs of branching. To our surprise, despite the absence of mast cells, *Karma*$^{Cre/wt}$:Rosa26$^{lsl\text{-}DTA/wt}$ mice did not show defects in branching at any stage of postnatal development (Figure 2C, 2D). Between 5.5 and 6.5 weeks of age, ducts spread out and branches multiply, and the process is fully concluded by 8-12 weeks, when the entire fat pad is covered in ducts. However, at neither of these time points did we observe differences between mast cell-deficient *Karma*$^{Cre/wt}$:Rosa26$^{lsl\text{-}DTA/wt}$ animals and mast cell-proficient controls (*Karma*$^{Cre/wt}$:Rosa26$^{wt/wt}$). This was true for the extent of branching, as determined by the distance of the branching front beyond the lymph node, as well as the number of

TEBs and TEDs. These data suggest that pubertal mammary gland branching occurs independently of mast cells, unlike currently thought.

Specific ablation of mast cells at the onset of puberty has no effect on mammary gland branching in Karma^{Cre}:Ms4a2$^{lsl\text{-}hDTR}$ mice.

A potential caveat of the *Karma*^{Cre}:Rosa26$^{lsl\text{-}DTA}$ model is that *Karma*^{Cre} also targets dendritic cells, specifically conventional (c)DC1 (Mattiuz et al., 2018a). DCs are present in the mammary gland, including subsets that resemble cDC1 (Betts et al., 2018) (Wilson et al., 2022). They have also been implicated in regulating ductal branching, albeit in an inhibitory manner. Indeed, it has been reported that CD11c^{+} cells, which encompass DCs and macrophages, inhibit branching via a mechanism that involves antigen presentation to T cells (Plaks et al., 2015). Moreover, cDC1 are reduced in *CD11c*^{Cre}:*Irf8*$^{fl/fl}$ mice, and they show a trend towards moderately increased branching at 6 weeks of age (Dawson et al., 2020). Whether these effects are due to targeting cDC1 has not been addressed. However, if branching was indeed promoted by mast cells and inhibited by cDC1s, then it is possible that simultaneous ablation of both has a net zero effect. Consequently, any effects of mast cell deficiency might be "masked" by concomitant absence of cDC1s. DCs are very sparse in the mammary gland at puberty (Wilson et al., 2022) and, in our hands, not significantly depleted in pubertal and adult *Karma*^{Cre}:Rosa26$^{lsl\text{-}DTA}$ mice (Figure S2B). In addition, the abundance of other immune cell populations like macrophages reassuringly also seemed unaffected in pubertal and adult *Karma*^{Cre}:Rosa26$^{lsl\text{-}DTA}$ mice (Figure S2C). Nonetheless, we wanted to exclude possible effects of deficiency of DCs and other lineages in the mammary gland on branching. To circumvent targeting DCs and other lineages, we therefore revised an alternative genetic strategy that exploits the efficacy of *Karma*^{Cre} to enable selective ablation of mast cells, but not cDC1s or other lineages. To do so, we crossed *Karma*^{Cre} mice to a new

transgenic line that we generated here. The latter is a derivation of the *Ms4a2*^{hDTR} model, also known as "Red mast cell and basophil" (RMB) mice (Dahdah et al., 2014) in which the human Diphtheria toxin receptor (hDTR) is expressed under control of the *Ms4a2* gene, which encodes the beta subunit of the IgE receptor. In these mice, mast cells and the closely related basophils are sensitive to Diphtheria toxin-mediated ablation, because they both express *Ms4a2* (Dahdah et al., 2014). Reassuringly, delivery of the toxin into the mammary fat pad of pre-pubertal *Ms4a2*$^{hDTR/wt}$ mice (Figure S3A) resulted in complete loss of mast cells in the mammary gland (Figure S3B). Despite local administration of Diphtheria toxin, we found that mast cells were also efficiently ablated in the peritoneal cavity (Figure S3C), indicating systemic action.

To further refine this approach, we rendered the *Ms4a2*^{hDTR} system conditional by introducing a loxP-flanked stop cassette in front of the sequence coding for hDTR (see Material and Methods). This approach restricts Diphtheria toxin-sensitivity to cells that have undergone Cre-mediated recombination and express *Ms4a2*. We refer to this new line here as *Ms4a2*$^{lsl\text{-}hDTR}$. Intercrossing *Karma*^{Cre} and *Ms4a2*$^{lsl\text{-}hDTR}$ mice results in a combined model in which only mast cells are susceptible to depletion by Diphtheria toxin, but not cDC1s or basophils, since these respectively lack expression of *Ms4a2* or *Karma*.

Indeed, administration of a single dose of 1µg Diphtheria toxin by subcutaneous injection into the mammary fat pad just prior to the onset of puberty at 4 weeks (Figure 3A, S3D) specifically resulted in the absence of mast cells in the mid-pubertal gland of *Karma*^{Cre}:*Ms4a2*$^{lsl\text{-}hDTR}$ mice at 5.5 weeks (Figure 3B), but not other lineages including cDC1s and macrophages (Figure S3E, S3F). We chose this time point because in our hands, most branching occurred between 5.5 and 6.5 weeks (Figure 2C). We then used this experimental strategy to determine if conditional ablation of mammary gland mast cells at the onset of

puberty affects ductal branching in this critical window. Like in the *Karma*^{Cre}:Rosa26$^{lsl\text{-}DTA}$ model, however, we found no difference in the extent of duct migration into the fat pad and branching between mast cell-deficient (*Karma*$^{Cre/wt}$:*Ms4a2*$^{wt/hDTR}$) and control mammary glands (*Karma*$^{Cre/wt}$:*Ms4a2*$^{wt/wt}$) (Figure 3C, D). Moreover, branching was fully completed in adult (8-12 weeks) glands treated at 4 weeks (Figure S3G, S3H), similar to *Karma*^{Cre}:Rosa26$^{lsl\text{-}DTA}$ mice. However, unlike peritoneal mast cells that remained absent in adult animals given Diphtheria toxin at 4 weeks (Figure S3I), mast cell numbers were indistinguishable from control animals in adult mammary glands injected at the onset of puberty (Figure S3J).

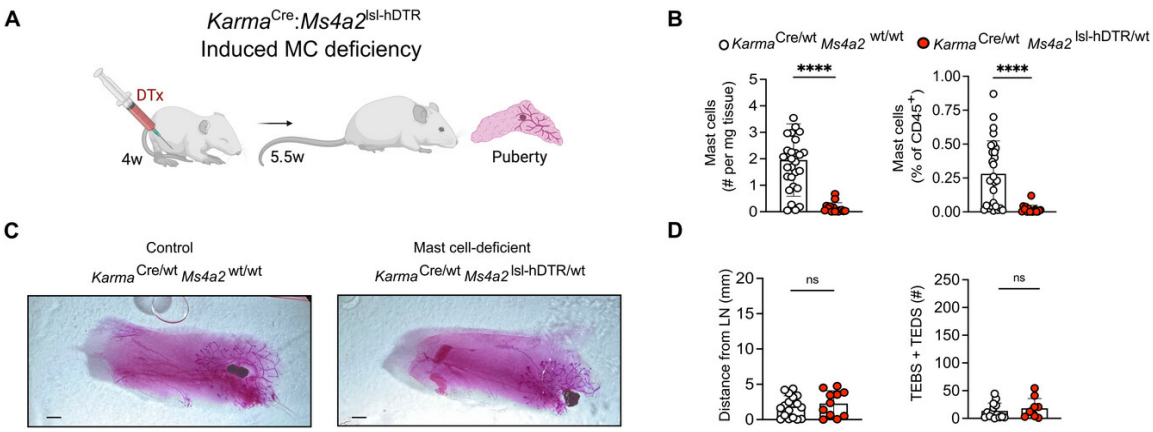

Chapter (1) Figure 3: Mast cell deficiency induced at puberty does not affect mammary gland branching.

(A) Diagram illustrating experimental approach. To induce mast cell ablation, Karma$^{Cre/wt}$:Ms4a2$^{lsl\text{-}hDTR/wt}$ mice were treated with 1mg Diphtheria toxin at 4 weeks (w) of age by subcutaneous injection into the mammary gland fat pad. Littermate control animals (Karma$^{Cre/wt}$:Ms4a2$^{wt/wt}$) were treated the same way. Animals were analyzed at puberty (5.5 weeks of age). (B) Mammary gland mast cell numbers and relative abundance within hematopoietic compartment (% within CD45^{+} cells) as determined by flow cytometry. (C, D) Branching as determined by Carmine staining of pubertal mammary glands from 5.5 weeks-

old mast cell-deficient (Karma$^{Cre/wt}$:Ms4a2$^{lsl\text{-}hDTR/wt}$; right/red) and mast cell-proficient mice (Karma$^{Cre/wt}$:Ms4a2$^{wt/wt}$ mice; left/white). (C) Representative photographs of Carmine-stained mammary glands. Scale bars = 1mm. (D) The extent of branching was measured as distance of branches and the number of terminal end buds (TEBs) and end ducts (TEDs) from the middle of the lymph node. Data are representative (C) and cumulative (B, D) of at least 10 individual mice per group from at least 4 independent experiments. Data in (B, D) are presented as mean with error bars indicating the SD. ****p<0.0001 as determined by Mann-Whitney test. ns = not significant.

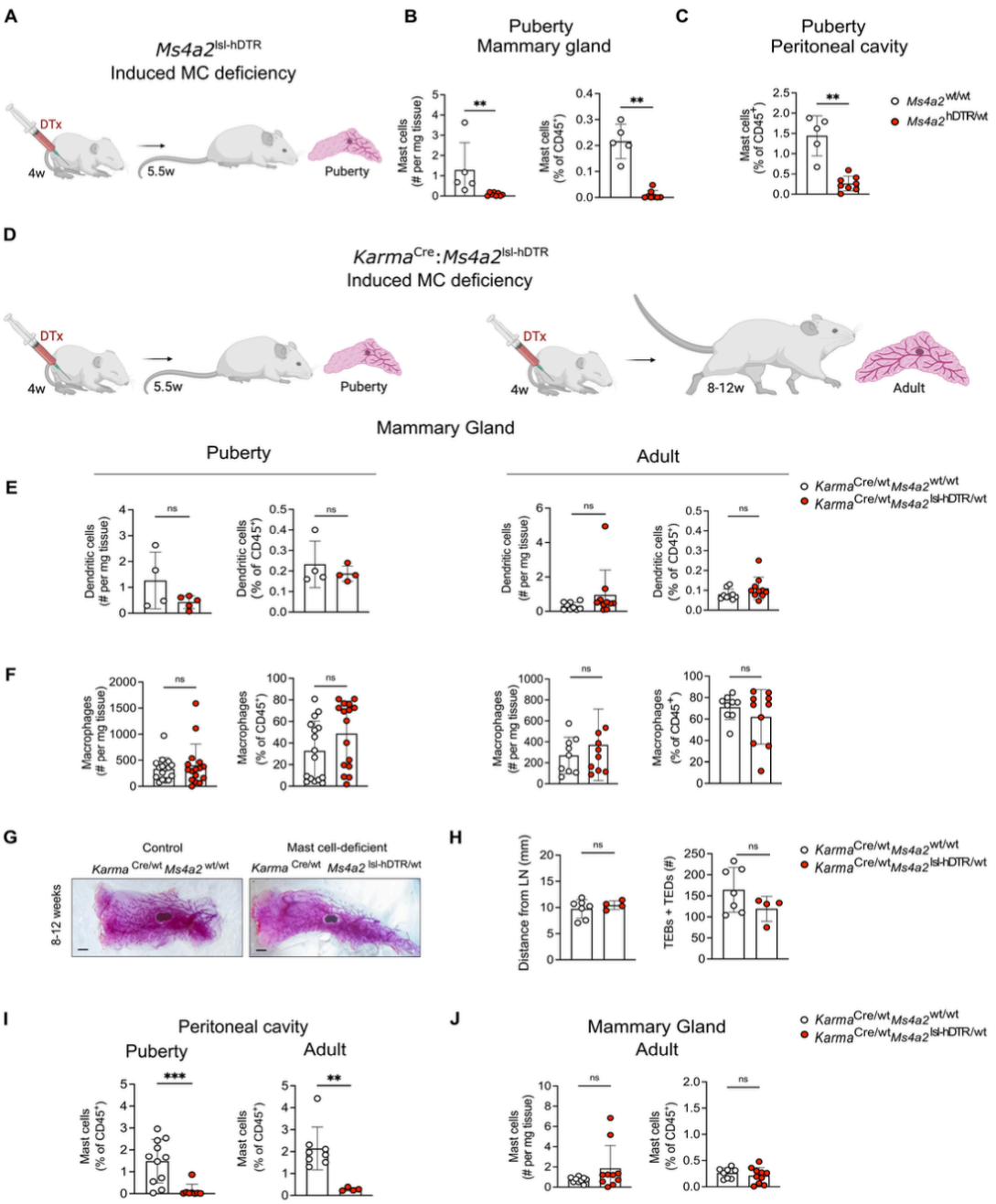
A
Ms4a2lsl-hDTR
Induced MC deficiency
DTx
4w
5.5w
Puberty
B
Puberty
Mammary gland
Mast cells (# per mg tissue)
Mast cells (% of CD45+)
**
C
Puberty
Peritoneal cavity
Mast cells (% of CD45+)
**
Ms4a2wt/wt
Ms4a2hDTR/wt
D
Karmacre:Ms4a2lsl-hDTR
Induced MC deficiency
DTx
4w
5.5w
Puberty
DTx
4w
8-12w
Adult
Mammary Gland
Puberty
Adult
E
Dendritic cells (# per mg tissue)
Dendritic cells (% of CD45+)
ns
Karmacre/wtMs4a2wt/wt
Karmacre/wtMs4a2lsl-hDTR/wt
F
Macrophages (# per mg tissue)
Macrophages (% of CD45+)
ns
G
Control
Karmacre/wtMs4a2wt/wt
Mast cell-deficient
Karmacre/wtMs4a2lsl-hDTR/wt
8-12 weeks
H
Distance from LN (mm)
TEBs + TEDs (#)
ns
Karmacre/wtMs4a2wt/wt
Karmacre/wtMs4a2lsl-hDTR/wt
I
Peritoneal cavity
Puberty
Adult
Mast cells (% of CD45+)
***
**
J
Mammary Gland
Adult
Mast cells (# per mg tissue)
Mast cells (% of CD45+)
ns
Karmacre/wtMs4a2wt/wt
Karmacre/wtMs4a2lsl-hDTR/wt

Chapter (1) Supplementary Figure S3 (related to Figure 3): Mast cells, dendritic cell and mammary gland branching in *Ms4a2^{hDTR}* and *Karma^{Cre}:Ms4a2$^{lsl\text{-}hDTR}$* mice.

To induce mast cell ablation, Ms4a2^{hDTR} (A-C) or Karma^{Cre}:Ms4a2$^{lsl\text{-}hDTR}$ mice (D-J) were treated with 1mg Diphtheria toxin at 4 weeks of age by subcutaneous injection into the mammary gland fat pad. Littermate control animals (Ms4a2$^{wt/wt}$ or Karma$^{Cre/wt}$:Ms4a2$^{wt/wt}$) were treated the same way. (A) Scheme depicting the use of the Ms4a2^{hDTR} model with depletion at 4 weeks and analysis at puberty. (B, C) Flow cytometry was used to determine mast cell numbers and relative abundance within hematopoietic compartment (% within CD45^{+} cells) in the mammary gland (B) and peritoneal cavity (C) at puberty (5.5 weeks). (D) Diagram showing the use of the Karma^{Cre}:Ms4a2$^{lsl\text{-}hDTR}$ model with depletion at 4 weeks and analysis at either puberty or in adulthood. (E) Dendritic cell and (F) macrophage cell numbers and relative abundance within hematopoietic compartment (% within CD45^{+} cells) in the pubertal mammary gland of Karma^{Cre}:Ms4a2$^{lsl\text{-}hDTR}$ mice following treatment with Diphtheria toxin at 4 weeks. Data were obtained using flow cytometry. (G-J) Effects of Diphtheria toxin administration to 4-weeks-old Karma^{Cre}:Ms4a2$^{lsl\text{-}hDTR}$ mice, determined at puberty or in adulthood. (G, H) Branching as determined by Carmine staining of pubertal mammary glands from adult mast cell-deficient (Karma$^{Cre/wt}$:Ms4a2$^{lsl\text{-}hDTR/wt}$ mice; right/red) and mast cell-proficient mice (Karma$^{Cre/wt}$:Ms4a2$^{wt/wt}$ mice; left/white). (G) Representative images of mammary glands stained with Carmine. Scale bars = 1mm. (H) Quantification of (G). The extent of branching was measured as distance of branches and the number of terminal end buds (TEBs) and end ducts (TEDs) from the middle of the lymph node. (I) Effects of Diphtheria toxin treatment on the number of mast cells were assessed in the peritoneal cavity. Flow cytometry was used to determine mast cell numbers and relative abundance within hematopoietic compartment (% within CD45^{+} cells) of the peritoneal cavity during puberty (5.5 weeks; left) and adulthood (8-12 weeks; right). (J) Adult mammary gland mast cell numbers and relative abundance within hematopoietic compartment (% within CD45^{+}

cells) assessed by flow cytometry. Data in (B, C, E, F, H, I, J) are cumulative of at least 4 individual mice per group from at least 2 or more independent experiments. Data in (B, C, E, F, H, I, J) are presented as mean with error bars indicating the SD. ***p<0.001, **p<0.01 as determined by Mann-Whitney test or unpaired t-test as applicable. ns = not significant.

Collectively, we obtained data in several complementary and *Kit*-independent models that challenge the notion that mast cells promote pubertal branching in the mammary gland, at least in an unique, essential manner.

Discussion

In this study, we investigated if mast cells promote ductal branching of the mammary gland during puberty, as previously reported in Kit^{Wsh} mice (Lilla and Werb, 2010). Using two complementary alternative genetic models for either constitutive or selective inducible ablation of mast cells, we found no evidence for an involvement of mast cells in this developmental process.

There are several possible explanations for the absence of a branching phenotype, which are not mutually exclusive. First, as introduced, expression of Kit is not restricted to mast cells, or even the immune system. This includes the epithelium of the mammary gland (Polat, 2007) (Regan et al., 2012). Indeed, many roles previously assigned to mast cells in *Kit* mutant mice have been refuted in Kit-independent models. For example, $Cpa3^{Cre}$ or "Cre master" mice lack mast cells due to Cre-mediated cytotoxicity, and unlike *Kit* mutant mice, these are susceptible to antibody-induced arthritis (Feyerabend et al., 2011a), autoimmune

encephalomyelitis (Feyerabend et al., 2011a) and diet-induced obesity [46].(Gutierrez et al., 2015). The latter has also been confirmed in *Mcpt5*^{Cre}:Rosa26$^{lsl\text{-}DTA}$ mice (Chmelař et al., 2016). In the mammary gland, Kit is expressed in epithelial cells, where it has been associated with growth and maintenance (Polat, 2007) (Lim et al., 2009) (Regan et al., 2012) (Talaiezadeh et al., 2012). Therefore, it is conceivable that direct effects on mammary epithelial cells, rather than mast cells, are at least partially responsible for the temporary branching defect reported in Kit-mutant mice. Our findings thus add to a growing body of work showcasing the limitations of Kit-based models for mast cell research, and for the first time, highlight these in a developmental context. Whilst the use of Kit-mutant versus Kit-independent mice could explain the discrepancy between our findings and the literature, we acknowledge that Lilla and Werb (Lilla and Werb, 2010) also observed stunted branching at puberty in mice treated with chromolyn sodium to prevent mast cell degranulation, as well as in mice deficient in Dipeptidyl peptidase I (DPPI) (Lilla and Werb, 2010). Chromolyn sodium is commonly used as mast cell stabilizing agent, but can also impact additional cell types, including other granulocytes, lymphocytes, and stromal cells like fibroblasts, endothelial and epithelial cells. Whilst some of these may be indirect, direct effects of chromolyn sodium on other cell types have also been reported *in vitro* and *in* vivo (Puzzovio et al., 2022) (Cimpean and Raica, 2016) (Heinke et al., 1995). Indeed, chromolyn can even suppress biological responses in the absence of mast cells (Oka et al., 2012), calling its use as a specific and efficient mast cell stabilizer into question. In a similar manner, DPPI is needed for the activation of mast cell proteases, notably chymases (Wolters et al., 2001). However, it also mediates activation of proteases in cytotoxic lymphocytes, monocytes and neutrophils (Chalmers et al., 2023).

Second, although we found no branching defects in either *Karma*^{Cre}:Rosa26$^{lsl\text{-}DTA}$ or *Karma*^{Cre}:*Ms4a2*$^{lsl\text{-}hDTR}$ mice, it remains possible that mast cells do contribute to the

regulation of gland remodeling. However, rather than having unique, non-redundant effects, they may normally do so in cooperation with other cell types. Alternatively, other cells may functionally compensate at least when (only) mast cells are absent, even if they physiologically are not the main drivers of the process. Such concerted action of mast cells with other cells has been described in the uterus. To facilitate increased blood flow to growing fetuses, uterine spiral arteries need to be transformed from thick-walled vessels to vessels with enlarged lumen during gestation. Fetal growth restriction occurs if this process is insufficient. This occurs in *Kit*^{Wsh} mice and can be rescued by reconstitution with wild-type mast cells (Woidacki et al., 2013b). On the contrary, *Cpa3*^{Cre} mice only show a mild spiral artery remodeling defect that does not cause fetal growth restriction (Meyer et al., 2018). Spiral artery remodeling however requires smooth muscle cells to become apoptotic, and this is mediated by *Mcpt5* (Meyer et al., 2017a). In the uterus, Mcpt5 is produced not only by mast cells, but also a subset of natural killer (NK) cells (Meyer et al., 2017a). Akin to *Cpa3*^{Cre} mice that lack only mast cells but not NK cells, those lacking just NK cells also only show a mild defect in spiral artery remodeling (Meyer et al., 2017a). Profoundly defective uterine vascular remodeling and fetal growth restriction are therefore only observed in mice with combined deficiency in both, mast cells and NK cells, achieved either genetically in *Mcpt5*^{Cre}:Rosa26$^{lsl\text{-}DTA}$ mice or via antibody-mediated depletion of NK cells in mast cell-deficient *Cpa3*^{Cre} mice (Meyer et al., 2017a). Moreover, numbers of uterine mast cells are increased in IL-15 knockout mice which are genetically deficient in NK cells, and conversely, uterine NK cell numbers are higher in *Kit*^{Wsh} mice compared to mast cell-proficient controls (Meyer et al., 2017b). This underscores that a compensatory increase in other immune cells can indeed occur in the absence of mast cells, and that this may mask defects. Given how vital spiral artery remodeling is to reproductive success, it is perhaps unsurprising that a complex regulatory system with several layers has evolved. In the mammary gland, such a scenario could explain why branching is unaffected in mice with selective mast cell

deficiency, i.e. *Karma*^{Cre}:*Ms4a2*$^{lsl\text{-}hDTR}$ (in which mammary gland DCs are unaffected), but is delayed at puberty in DPPI knockout mice or following treatment with chromolyn sodium (Lilla and Werb, 2010), which may also affect other cells, as discussed above. These considerations further underscore the complexity of choosing appropriate genetic models to study mast cell functions, even for Kit-independent approaches. As the example of the uterus illustrates, mast cell depletion can have different outcomes depending on the (trans)gene used.

Finally, it is also possible that diverse types of mast cells exist within the mammary gland, which may have distinct biological roles. Indeed, it is increasingly recognized that mast cells are heterogenous beyond the classic dichotomy of connective- and mucosal-type mast cells (Dwyer et al., 2021; Tauber et al., 2023). Mast cells also dynamically change across life stages (Derakhshan et al., 2021; Tauber et al., 2023; Gentek et al., 2018). One aspect in which mast cells differ is their developmental origin. At mucosal sites, mast cells are predominantly derived from hematopoietic stem cells (HSCs) (Tauber et al., 2023; Gentek et al., 2018; Z. Li et al., 2018; Yoshimoto et al., 2022). In many connective tissues, however, mast cells are long-lived and self-maintain largely independently of HSCs in the bone marrow (Tauber et al., 2023; Gentek et al., 2018; Z. Li et al., 2018). They also retain sizeable populations of the first mast cells that originate from yolk sac erythro-myeloid progenitors (Gentek et al., 2018; Z. Li et al., 2018). Mast cells from distinct sources also retain functional differences, at least upon immunological challenge e.g. by infections, or in dynamic settings like tissue remodeling during development (Chia et al., 2023). Any such heterogeneity has not yet been resolved for mammary gland mast cells, but it is conceivable that they comprise subpopulations which e.g. are more or less responsive to hormones, and may thereby differently impact branching, perhaps even in opposing ways. Since *Karma*^{Cre}:Rosa26$^{lsl\text{-}DTA}$

and *Karma*^{Cre}:*Ms4a2*$^{lsl\text{-}hDTR}$ mice lack all mast cells in the mammary gland, this is a possibility that we cannot account for here.

Data Limitations and Perspectives

One limitation is that we did not investigate other stages of mammary gland development. Mast cells colonize peripheral tissues in the fetus (Malcolm A. S. Moore, 1970; Y Kitamura et al., 1979; Sonoda et al., 1983b; Gentek et al., 2018; Liu et al., 2015). They might thus also already be present and functional in the fetal gland. We did not address this formally, however, the rudimentary, pre-pubertal tree was indistinguishable between *Karma*^{Cre}:Rosa26$^{lsl\text{-}DTA}$ mice and mast cell-proficient controls (Figure 2C). These mice are devoid of mammary mast cells at all stages tested, indicating that mast cells may also be dispensable for fetal gland morphogenesis. However, this would need to be investigated specifically at fetal stages. During pregnancy, ducts first undergo additional branching and later form milk-secreting alveoli (Macias and Hinck, 2012). The number of mammary gland mast cells increases in mid to late pregnancy, coinciding with alveolar remodeling (Iavnilovitch et al., 2006). Furthermore, lactation involves the plasminogen cascade of serine proteases (Leif R. Lund et al., 2000) and mast cell granules contain Plasma Kallikrein (PKa), an activator of the cascade (Lilla et al., 2009). Plasminogen and PKa are also needed for involution after weaning (Leif R. Lund et al., 2000) (Lilla et al., 2009). Mast cells may thus be involved in alveolarization and involution. This could in future work be addressed in an inducible model to avoid potential confounding effects of maternal (uterine) mast cell deficiency. Intriguingly, in *Karma*^{Cre}:*Ms4a2*$^{lsl\text{-}hDTR}$ mice, mammary gland (but not peritoneal) mast cells fully recovered by adulthood following depletion at puberty onset (Figure S3I, S3J), perhaps indicating requirements for mast cells in the post-pubertal gland. *Ms4a2*$^{lsl\text{-}DTR}$

will be a valuable tool to disentangle developmental roles for mast cells in the gland, and beyond.

Author Contributions

Study and experimental design: Simran Kapoor and Rebecca Gentek. Conduction, analysis, and/or interpretation of experiments and data: Simran Kapoor, Clara M. Munz, Jimmy Marsden, Cyril Carvalho, Holly Tinsley, Marlene Magalhaes Pinto, and Bert Malengier-Devlies. Provision of samples or tools: Ramazan Akyol and Marc Dalod. Technical assistance: Solvig Becker, Guillaume Seuzaret, and Katelyn Patatsos. Intellectual contribution: Gillian Wilson and Amy B. Pederson. Drafting and revising the manuscript: Simran Kapoor, Rebecca Gentek, and Clara M. Munz. Funding acquisition: Rebecca Gentek and Simran Kapoor.

Funding

This research was supported by a Chancellor's Fellowship from the University of Edinburgh, and work in the Gentek lab is further funded by a Senior Research Fellowship from the Kennedy Trust for Rheumatology Research (both awarded to Rebecca Gentek). The generation of the *Ms4a2*$^{lsl\text{-}hDTR}$ line was funded by Cancer Research UK. Simran Kapoor is supported by a Wellcome Trust Host Pathogen and Global Health PhD studentship. The funding bodies were not involved in the design, drafting, editing, or content of the manuscript.

Ethics Statement

All animal work was performed under project license (PPL) number PP1871024 in accordance with the Animals (Scientific Procedures) Act 1986 (ASPA).

Conflicts of Interest

The authors declare no conflicts of interest.

Data and material availability

All data related to this study are available either in the paper or in the Supplementary Materials. Raw data are available upon request.

Peer Review

The peer review history for this article is available at https://publons.com/publon/10.1002/eji.70036

Acknowledgements

We thank the University of Edinburgh Bioresearch & Veterinary Services for their invaluable services and experimental support, in particular Michael Dodds for outstanding animal husbandry and William Mungall for technical assistance. We further thank the IRR Flow Cytometry Facility and Calum Bain and Elaine Emmerson for invaluable support and scientific feedback.

Conclusion

Using multiple *Kit*-independent models of constitutive and inducible MC targeting, we showed that mammary gland branching at puberty proceeds normally even in the absence of MCs. Contrary to previous work (Lilla and Werb, 2010), our findings challenge the prevailing view that MCs are essential promoters of mammary gland branching at puberty. Instead, we suggest that this developmental process is likely compensated for, despite the absence of MCs. Our study provides further evidence to the need to study the functions of MCs in *Kit*-independent models, and we provide new genetic approaches to study MC functions *in vivo* across physiological contexts.

Materials and Methods

Mouse lines

Rosa26$^{lsl\text{-}DTA}$ ("DTA176") mice were purchased from The Jackson Laboratory (strain #010527). *Karma*^{Cre} mice (Mattiuz et al., 2018a) were gifted by Marc Dalod (Marseille, France), and the *Ms4a2*^{hDTR} line (also known as "red mast cell and basophil" or RMB mice (Dahdah et al., 2014), was obtained from Pierre Launay. *Ms4a2*$^{lsl\text{-}hDTR}$ mice (official name: C57BL/6NRj-*Ms4a2*^{tm2Ciphe}) are a new line we generated at the Centre d'immunophénomique (CIPHE) in Marseille (France). In these mice, the 3'-UTR of the *Ms4a2* gene encoding the FcεRI β chain includes a cassette composed of an internal ribosomal entry site, a sequence coding for the fluorescent protein tdTomato (tdT), a 2A cleavage sequence, and the human diphtheria toxin receptor (hDTR). In this line, expression of the hDTR and tdT transgenes is prevented by a stop codon that is flanked by loxP Cre recognition sites. This stop codon is removed upon Cre-mediated recombination, making these mice a Cre-inducible version of the *Ms4a2*^{hDTR} line. An overview of the transgene is shown in Figure S4.

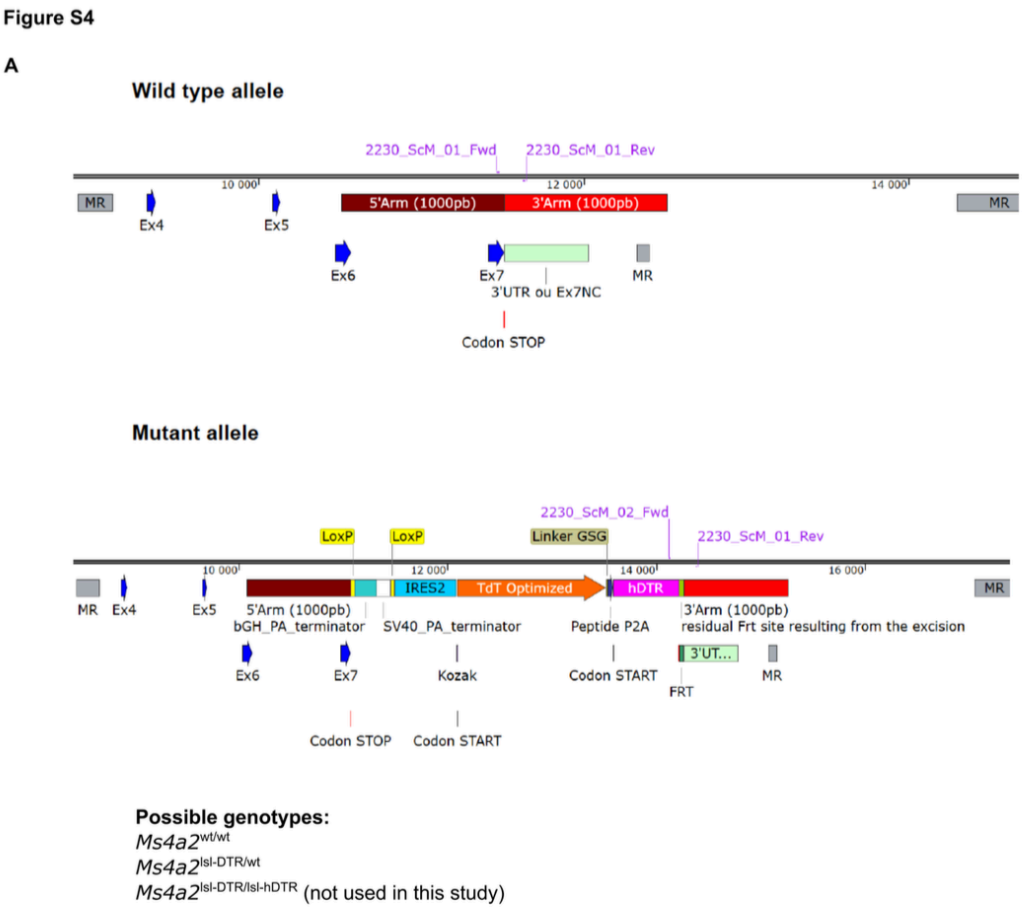

Chapter (1) Supplementary Figure S4 (related to Methods): Genetic modifications in *Ms4a2*$^{lsl\text{-}hDTR/wt}$ mice.

Schematic overview of genetic alterations. A knock-in of the Ms4a2 murine gene (Ensembl number ENSMUSG00000024680) was carried out by the insertion of an LSL_tdT_P2A_hDTR sequence in the 3'UTR of the Ms4a2 gene. A residual FRT element is present just after the LSL_tdT_P2A_hDTR sequence in the mutant allele, a result of the deletion of the NeoR cassette. This NeoR cassette provided neomycin resistance as a positive marker during the

selection of mutant mES cells. Ex: Exon, P2A: Peptide 2A, SV40: Simian Virus 40, hDTR: human Diphtheria toxin receptor. Possible genotypes are indicated.

Animal ethics and housing conditions

All animal work was performed under project license (PPL) number PP1871024 in accordance with the Animals (Scientific Procedures) Act 1986 (ASPA). Mice were bred and housed at the animal facility in the University of Edinburgh (Edinburgh, UK) under specific pathogen-free conditions at a controlled temperature of 22°C with a 12-hour light/dark cycle. Access to food (irradiated chow pellets) and water (reverse osmosis water) was available *ad libitum*.

Diphtheria toxin-mediated mast cell depletion

Diphtheria toxin (322326, Merck) was aliquoted in filtered PBS and stored at −80°C. *Ms4a2*^{hDTR} and *Karma*^{Cre}:*Ms4a2*$^{lsl\text{-}hDTR}$ mice were injected under general isoflurane anesthesia at 4 weeks of age with 1µg Diphtheria toxin through the nipple into the fat pad of the 4th mammary gland.

Mast cell degranulation assay

Mast cells were isolated from the mammary gland by flow cytometric cell sorting based on CD117 and ST2 expression. The sorted mast cells were then plated in Tyrode's buffer into µ-Slide 18 Well plates (iBidi) with polymer coated coverslip bottom, pre-coated with ibiTreat (iBidi) and incubated for 2 hours at 37°C, 5% CO2. The Tyrode's buffer was supplemented with 2mg/ml Avidin (ThermoFisher) to allow for staining and detection of mast cell heparin granules upon degranulation. Under controlled atmospheric conditions (37°C) in a chamber, the mast cells were stimulated to degranulate with 100 µM Substance P (Merck), or vehicle

(Tyrode's buffer) and fluorescence was recorded 30 minutes post stimulation using the Zeiss Observer Live microscope system. Mean fluorescence intensity (MFI) was quantified for each individual mast cell (defined by phase contrast) using Fiji software.

Mammary gland harvest

The 4th abdominal mammary gland fat pads were removed at the indicated ages for analysis by flow cytometry and/or imaging. The lymph node was excluded from the gland collected for cell suspension preparation and flow cytometry, and glands intended for imaging were left intact.

Estrus staging

Where assessed, estrus staging was performed by vaginal smear using 1x phosphate-buffered saline (PBS) onto Superfrost^{TM} Plus Adhesion Microscope Slides (Epredia). Vaginal smears were air-dried, and then fixed in ice-cold 100% methanol, followed by staining with haematoxylin and eosin.

Peritoneal lavage

Where done, peritoneal lavage was performed by injecting RPMI (supplemented with 2% FCS) into the abdominal cavity of mice immediately after cull, followed by gentle massaging to dislodge cells, and retrieval of the cell suspension using a syringe. The retrieved cell suspension was filtered through a 100µm filter membrane (John Stanair & Co) and stained for flow cytometry as detailed below.

Preparation of single cell suspensions and flow cytometry

The dissected abdominal mammary gland fat pads were collected in RPMI supplemented with 2% FCS. Samples were cut manually into small pieces, followed by digestion in

0.8mg/ml Dispase II (Merck), 5mM $CaCl_2$, 10mM HEPES (Merck), 0.1mg/ml DNaseI (Roche), 3mg/ml Collagenase D (Merck) in RPMI (supplemented with 2% FCS) at 37°C at 900rpm in a Thermo-Shaker (Grant-bio) for 20 minutes or until digested. Samples were filtered through a 100µm filter membrane (John Stanair & Co), and washed with FACS buffer (2% FCS, 2 mM EDTA in PBS) to obtain a homogenous cell suspension. Cells were transferred to a 96 well-plate and incubated with 1:800 Zombie Live/Dead NIR (ThermoFisher Scientific) in PBS for 20-30 minutes at room temperature in the dark. Cells were then washed with FACS buffer and centrifuged at 530g for 5 minutes at 4°C. The supernatant was removed, and cells were incubated with 0.5% anti-mouse CD16/32 Trustain Fx (Biolegend), 5% mouse serum (Invitrogen) and 5% rat serum (Merck) in FACS buffer for 20-30 minutes at 4°C. Cells were then washed with FACS buffer and centrifuged at 530g for 5 minutes at 4°C. Cells were then labelled with antibody mix diluted in FACS buffer and Brilliant Stain Buffer (BD) as detailed below for 20-30 minutes at 4°C.

Marker	Fluorophore	Supplier	Clone number	Dilution
CD45	BUV395	BD Biosciences	30-F11	1:800
CD117 (Kit)	BV650	Biolegend	2B8	1:300
CD117 (Kit)	BV605	Biolegend	ACK2	1:300
CD11b	BV510	Biolegend	M1/70	1:400
CD64	BV711	Biolegend	X54-5/71	1:300
F4/80	BV786	Biolegend	BM8	1:300
CD63	Pe/Cyanine7	Biolegend	NVG-2	1:200

ST2	APC	Biolegend	DIH9	1:200
ST2	R718	BD	U29-93	1:200
MHCII	BV421	Biolegend	107632	1:200
CD11c	PerCP-Cy5.5	Biolegend	117328	1:300
CD103	BUV805	BD	741948	1:300

Cells were then fixed in 4% paraformaldehyde solution (PFA) for 15 minutes at room temperature away from light. Fixed cells were subsequently stained intracellularly with 1:10000 Avidin-AF488 (ThermoFisher Scientific) diluted in immunohistochemistry (IHC) buffer (0.1M Tris at pH 7.4, constituted with 0.5% bovine serum albumin, 2% Triton X-100) and 0.05 g/ml milk powder) for 1 hour at room temperature or overnight at 4^{o}C in the dark. Cells were washed with FACS buffer and acquired in FACS buffer with counting beads (Invitrogen) (equivalent to 10 000 beads) added for quantification. Data was acquired using a 5L Fortessa (BD). Cells were pre-gated as live singlets. Mast cells were then defined as CD45^{+} CD11b^{low} F4/80^{-} and/or CD64^{-} CD117^{+} (Kit^{+}) ST2^{+} and/or Avidin^{+}. Dendritic cells were identified as CD45^{+} CD11b^{-} F4/80^{-} CD117^{-} (Kit^{-}) Avidin^{-} CD11c^{+} MHCII^{+} CD103^{+}. Macrophages were identified as CD45^{+} CD11b^{+} F4/80^{+}.

Mammary gland imaging and analysis

Dissected abdominal mammary gland fat pads were collected and spread onto Superfrost^{TM} Plus Adhesion Microscope Slides (Epredia) and fixed for 24 hours in Carnoy's buffer (75% ethanol, 25% glacial acetic acid).

To visualize mast cells within the mammary gland, fixed glands were first washed in PBS and then embedded in OCT matrix (CellPath). The tissue was then cryo-sectioned at a thickness

of 20µm onto Superfrost™ Plus Adhesion Microscope Slides (Epredia). The sections were first air dried, and then washed in PBS or distilled water to remove excess OCT. Each slide was stained for 2 minutes in Toluidine Blue (comprising 0.1% Toluidine blue O (Sigma) in 1% sodium chloride, pH 2.3-2.5) for metachromatic staining of mast cells, after which excess staining was removed by gently washing the slide in distilled water. The slides were mounted in aqueous Fluoromount G mounting media (ThermoFisher Scientific) and imaged. Images were acquired on the Zen Axioscan at 10x magnification and analyzed using Fiji software. A circular region of interest (ROI) with a fixed perimeter was drawn around two distinct TEBs of the gland. Two ROIs were used per gland to account for within-gland variation, and overlapping regions were avoided when drawing up the ROIs. Mast cells within the ROIs were identified by metachromatic staining (characteristic purple shade) and marked using the multi-point tool. The shortest distance of each mast cell from the TEB within the ROI was measured using the measure tool in Fiji, and the actual distance calibrated using the appropriate scale in micrometers.

To visualise branching of the mammary gland, fixed glands were stained in Alum Carmine staining solution (0.1% carmine dye (ThermoFisher Scientific), 0.25% aluminium potassium sulfate dodecahydrate (ThermoFisher Scientific) in distilled water) for 2-7 days or until fully stained. Excess staining was removed by transferring the glands to a destaining solution (70% ethanol, 0.072% HCl) for 30 minutes or until excess staining was sufficiently removed. Glands were then dehydrated in an alcohol series (75%, 80%, 95%, 100% ethanol) and finally cleared in xylene overnight or until the fat pad was cleared. The slides were mounted in pertex mounting media (HistoLab) and imaged. Images were acquired on a Leica Stereomicroscope at 0.8x magnification and analyzed using Fiji software. Branching parameters were measured from a line perpendicular to the length of the fat pad bisecting the lymph node. The distance covered by branches (in mm) was measured from the lymph

node to the longest branch terminating in a TEB. Numbers of TEBs and TEDs were counted in the direction of invading branching. Branching parameters were quantified by 2 independent parties blinded to experimental groups and/or genotypes.

Statistical analysis

Unless otherwise stated, mean values and SD as specified in the respective figure legends were calculated in Prism (GraphPad), parametric (one way ANOVA, unpaired t tests) and non-parametric t tests (Mann-Whitney) were used where applicable. p values of less than 0.05 were considered statistically significant.

References

Atyeo, C. and Alter, G. (2021) "The multifaceted roles of breast milk antibodies," *Cell*. Elsevier B.V., pp. 1486–1499. Available at: https://doi.org/10.1016/j.cell.2021.02.031.

Bergstresser, P.R., Tigelaar, R.E. and Tharp, M.D. (1984) "Conjugated avidin identifies cutaneous rodent and human mast cells," *Journal of Investigative Dermatology*, 83(3), pp. 214–218. Available at: https://doi.org/10.1111/1523-1747.ep12263584.

Betts, C.B. *et al.* (2018) "Mucosal Immunity in the Female Murine Mammary Gland," *The Journal of Immunology*, 201(2), pp. 734–746. Available at: https://doi.org/10.4049/jimmunol.1800023.

Brisken, C. and O'Malley, B. (2010) "Hormone action in the mammary gland.," *Cold Spring Harbor perspectives in biology*. Available at: https://doi.org/10.1101/cshperspect.a003178.

Chalmers, J.D., Kettritz, R. and Korkmaz, B. (2023) "Dipeptidyl peptidase 1 inhibition as a potential therapeutic approach in neutrophil-mediated inflammatory disease," *Frontiers in Immunology*. Frontiers Media SA. Available at: https://doi.org/10.3389/fimmu.2023.1239151.

Chia, S.L. *et al.* (2023) "Mast cell ontogeny: From fetal development to life-long health and disease," *Immunological Reviews*. John Wiley and Sons Inc, pp. 31–53. Available at: https://doi.org/10.1111/imr.13191.

Chmelař, J. *et al.* (2016) "No role for mast cells in obesity-related metabolic dysregulation," *Frontiers in Immunology*, 7(NOV). Available at: https://doi.org/10.3389/fimmu.2016.00524.

Cimpean, A.M. and Raica, M. (2016) "The Hidden Side of Disodium Cromolyn: from Mast Cell Stabilizer to an Angiogenic Factor and Antitumor Agent," *Archivum Immunologiae et Therapiae Experimentalis*, 64(6), pp. 515–522. Available at: https://doi.org/10.1007/s00005-016-0408-8.

Dahdah, A. *et al.* (2014) “Mast cells aggravate sepsis by inhibiting peritoneal macrophage phagocytosis,” *Journal of Clinical Investigation*, 124(10), pp. 4577–4589. Available at: https://doi.org/10.1172/JCI75212.

Dawson, C.A. *et al.* (2020) “Tissue-resident ductal macrophages survey the mammary epithelium and facilitate tissue remodelling,” *Nature Cell Biology*, 22(5), pp. 546–558. Available at: https://doi.org/10.1038/s41556-020-0505-0.

Derakhshan, T. *et al.* (2021) “Lineage-specific regulation of inducible and constitutive mast cells in allergic airway inflammation,” *Journal of Experimental Medicine*, 218(1). Available at: https://doi.org/10.1084/JEM.20200321.

Durnberger, H. and Kratochwii, K. (1980) *Specificity of Tissue Interaction and Origin of Mesenchymal Cells in the Androgen Response of the Embryonic Mammary Gland*, *Cell*.

Dwyer, D.F. *et al.* (2021) *Human airway mast cells proliferate and acquire distinct inflammation-driven phenotypes during type 2 inflammation*, *Sci. Immunol*. Available at: https://www.science.org.

Feyerabend, T.B. *et al.* (2011) “Cre-mediated cell ablation contests mast cell contribution in models of antibody- and T cell-mediated autoimmunity,” *Immunity*, 35(5), pp. 832–844. Available at: https://doi.org/10.1016/j.immuni.2011.09.015.

Florsheim, E.B. *et al.* (2023) “Immune sensing of food allergens promotes avoidance behaviour,” *Nature*, 620(7974), pp. 643–650. Available at: https://doi.org/10.1038/s41586-023-06362-4.

Gentek, R. *et al.* (2018) “Hemogenic Endothelial Fate Mapping Reveals Dual Developmental Origin of Mast Cells,” *Immunity*, 48(6), pp. 1160-1171.e5. Available at: https://doi.org/10.1016/j.immuni.2018.04.025.

Goldberg, M. *et al.* (2020) “Pubertal timing and breast cancer risk in the Sister Study cohort,” *Breast Cancer Research*, 22(1). Available at: https://doi.org/10.1186/s13058-020-01326-2.

v Gouon-Evans, M E Rothenberg and J W Pollard (2000) “Postnatal mammary gland development requires macrophages and eosinophils,” *Development* [Preprint].

Gutierrez, D.A. *et al.* (2015) “Hematopoietic Kit Deficiency, rather than Lack of Mast Cells, Protects Mice from Obesity and Insulin Resistance,” *Cell Metabolism*, 21(5), pp. 678–691. Available at: https://doi.org/10.1016/j.cmet.2015.04.013.

Heinke, S. *et al.* (1995) “Inhibition of volume-activated chloride currents in endothelial cells by chromones,” *British Journal of Pharmacology*, 115(8), pp. 1393–1398. Available at: https://doi.org/10.1111/j.1476-5381.1995.tb16629.x.

Heuberger, B. *et al.* (1982) *Induction of androgen receptor formation by epithelium-mesenchyme interaction in embryonic mouse mammary gland*, *Proc. Natd Acad. Sci. USA*.

Hinck, L. and Silberstein, G.B. (2005) “The mammary end bud as a motile organ,” *Breast Cancer Research*, pp. 245–251. Available at: https://doi.org/10.1186/bcr1331.

Howard, B.A. and Lu, P. (2014) “Stromal regulation of embryonic and postnatal mammary epithelial development and differentiation,” *Seminars in Cell and Developmental Biology*. Elsevier Ltd, pp. 43–51. Available at: https://doi.org/10.1016/j.semcdb.2014.01.004.

Iavnilovitch, E. *et al.* (2006) “Expression of a carboxy terminally truncated Stat5 with no transactivation domain in the mammary glands of transgenic mice inhibits cell proliferation during pregnancy, delays onset of milk secretion, and induces apoptosis upon involution,” *Molecular Reproduction and Development*, 73(7), pp. 841–849. Available at: https://doi.org/10.1002/mrd.20479.

Kett, W.C. *et al.* (2003) “Avidin is a heparin-binding protein. Affinity, specificity and structural analysis,” *Biochimica et Biophysica Acta - General Subjects*, 1620(1–3), pp. 225–234. Available at: https://doi.org/10.1016/S0304-4165(02)00539-1.

Khaled, W.T. *et al.* (2007) “The IL-4/IL-13/stat6 signalling pathway promotes luminal mammary epithelial cell development,” *Development*, 134(15), pp. 2739–2750. Available at: https://doi.org/10.1242/dev.003194.

Kitamura, Y., Shimada, M. and Go, S. (1979) *BRIEF NOTES Presence of Mast Cell Precursors in Fetal Liver of Mice*, *DEVELOPMENTAL BIOLOGY*.

Kraft, S. *et al.* (2013) "The Tetraspanin CD63 Is Required for Efficient IgE-Mediated Mast Cell Degranulation and Anaphylaxis," *The Journal of Immunology*, 191(6), pp. 2871–2878. Available at: https://doi.org/10.4049/jimmunol.1202323.

Krisanits, B. *et al.* (2020) "Pubertal mammary development as a 'susceptibility window' for breast cancer disparity," in *Advances in Cancer Research*. Academic Press Inc., pp. 57–82. Available at: https://doi.org/10.1016/bs.acr.2020.01.004.

L Padilla 1, K.R.H.M.F.V.H.A.M.C.M.I.R. (1990) "Histamine content and mast cells distribution in mouse uterus: the effect of sexual hormones, gestation and labor.," *Cell Mol Biol* [Preprint].

Leif R. Lund *et al.* (2000) "Lactational competence and involution of the mouse mammary gland require plasminogen," *Development* [Preprint].

Li, Z. *et al.* (2018) "Adult Connective Tissue-Resident Mast Cells Originate from Late Erythro-Myeloid Progenitors," *Immunity*, 49(4), pp. 640-653.e5. Available at: https://doi.org/10.1016/j.immuni.2018.09.023.

Lilla, J.N. *et al.* (2009) "Active plasma kallikrein localizes to mast cells and regulates epithelial cell apoptosis, adipocyte differentiation, and stromal remodeling during mammary gland involution," *Journal of Biological Chemistry*, 284(20), pp. 13792–13803. Available at: https://doi.org/10.1074/jbc.M900508200.

Lilla, J.N. and Werb, Z. (2010) "Mast cells contribute to the stromal microenvironment in mammary gland branching morphogenesis," *Developmental Biology*, 337(1), pp. 124–133. Available at: https://doi.org/10.1016/j.ydbio.2009.10.021.

Lim, E. *et al.* (2009) "Aberrant luminal progenitors as the candidate target population for basal tumor development in BRCA1 mutation carriers," *Nature Medicine*, 15(8), pp. 907–913. Available at: https://doi.org/10.1038/nm.2000.

Lin, E.Y. *et al.* (2002) *The Macrophage Growth Factor CSF-1 in Mammary Gland Development and Tumor Progression*, *Journal of Mammary Gland Biology and Neoplasia*.

Liu, J. *et al.* (2015) "Mast Cells Participate in Corneal Development in Mice," *Scientific Reports*, 5. Available at: https://doi.org/10.1038/srep17569.

Macias, H. and Hinck, L. (2012) "Mammary gland development," *Wiley Interdisciplinary Reviews: Developmental Biology*, pp. 533–557. Available at: https://doi.org/10.1002/wdev.35.

Malcolm A. S. Moore, D.M. (1970) "Ontogeny of the Haemopoietic System: Yolk Sac Origin of In Vivo and In Vitro Colony Forming Cells in the Developing Mouse Embryo*," *Br J Haematol* [Preprint].

Mallepell, S. *et al.* (2006) *Paracrine signaling through the epithelial estrogen receptor is required for proliferation and morphogenesis in the mammary gland*. Available at: www.pnas.orgcgidoi10.1073pnas.0510974103.

Marichal, T. *et al.* (2013) "A beneficial role for immunoglobulin E in host defense against honeybee venom," *Immunity*, 39(5), pp. 963–975. Available at: https://doi.org/10.1016/j.immuni.2013.10.005.

Maslinski C, K.D.F.W.K.A.P.P. (1993) "Histamine: its metabolism and localization in mammary gland.," *Comp Biochem Physiol C.* [Preprint].

Mattiuz, R. *et al.* (2018) "Novel Cre-Expressing Mouse Strains Permitting to Selectively Track and Edit Type 1 Conventional Dendritic Cells Facilitate Disentangling Their Complexity in vivo," *Frontiers in Immunology*, 9. Available at: https://doi.org/10.3389/fimmu.2018.02805.

Meyer, N., Woidacki, K., Knöfler, M., *et al.* (2017) "Chymase-producing cells of the innate immune system are required for decidual vascular remodeling and fetal growth," *Scientific Reports*, 7. Available at: https://doi.org/10.1038/srep45106.

Meyer, N., Woidacki, K., Maurer, M., *et al.* (2017) “Safeguarding of fetal growth by mast cells and natural killer cells: Deficiency of one is counterbalanced by the other,” *Frontiers in Immunology*, 8(JUN). Available at: https://doi.org/10.3389/fimmu.2017.00711.

Meyer, N., Schüler, T. and Zenclussen, A.C. (2018) “Simultaneous ablation of uterine natural killer cells and uterine mast cells in mice leads to poor vascularization and abnormal doppler measurements that compromise fetal well-being,” *Frontiers in Immunology*, 8(JAN). Available at: https://doi.org/10.3389/fimmu.2017.01913.

Oka, T. *et al.* (2012) “Evidence questioning cromolyns effectiveness and selectivity as a mast cell stabilizer in mice,” *Laboratory Investigation*, 92(10), pp. 1472–1482. Available at: https://doi.org/10.1038/labinvest.2012.116.

Plaks, V. *et al.* (2015) “Adaptive Immune Regulation of Mammary Postnatal Organogenesis,” *Developmental Cell*, 34(5), pp. 493–504. Available at: https://doi.org/10.1016/j.devcel.2015.07.015.

Plum, T. *et al.* (2023) “Mast cells link immune sensing to antigen-avoidance behaviour,” *Nature*, 620(7974), pp. 634–642. Available at: https://doi.org/10.1038/s41586-023-06188-0.

Polat, A. (2007) “c-KIT expression in columnar cell lesions of the breast accompanied by benign and malignant breast diseases,” *Pathology Research and Practice*, 203(11), pp. 765–769. Available at: https://doi.org/10.1016/j.prp.2007.08.010.

Puzzovio, P.G. *et al.* (2022) “Cromolyn Sodium differentially regulates human mast cell and mouse leukocyte responses to control allergic inflammation,” *Pharmacological Research*, 178. Available at: https://doi.org/10.1016/j.phrs.2022.106172.

Ramirez, R.A. *et al.* (2012) “Alterations in mast cell frequency and relationship to angiogenesis in the rat mammary gland during windows of physiologic tissue remodeling,” *Developmental Dynamics*, 241(5), pp. 890–900. Available at: https://doi.org/10.1002/dvdy.23778.

Regan, J.L. *et al.* (2012) “C-Kit is required for growth and survival of the cells of origin of Brca1-mutation-associated breast cancer,” *Oncogene*, 31(7), pp. 869–883. Available at: https://doi.org/10.1038/onc.2011.289.

Richert, M.M. *et al.* (2000) *An Atlas of Mouse Mammary Gland Development*, *Journal of Mammary Gland Biology and Neoplasia*.

Rodewald, H.R. and Feyerabend, T.B. (2012) “Widespread Immunological Functions of Mast Cells: Fact or Fiction?,” *Immunity*, pp. 13–24. Available at: https://doi.org/10.1016/j.immuni.2012.07.007.

Rothenberg, M.E. *et al.* (1997) *Targeted Disruption of the Chemokine Eotaxin Partially Reduces Antigen-induced Tissue Eosinophilia*, *J. Exp. Med*.

Sonoda, T., Hayashi, C. and Kitamura’, Y. (1983) *Presence of Mast Cell Precursors in the Yolk Sac of Mice*, *DEVELOPMENTAL BIOLOGY*.

Starkl, P. *et al.* (2020) “IgE Effector Mechanisms, in Concert with Mast Cells, Contribute to Acquired Host Defense against Staphylococcusaureus,” *Immunity*, 53(4), pp. 793-804.e9. Available at: https://doi.org/10.1016/j.immuni.2020.08.002.

Starkl, P. *et al.* (2022) “IgE antibodies increase honeybee venom responsiveness and detoxification efficiency of mast cells,” *Allergy: European Journal of Allergy and Clinical Immunology*, 77(2), pp. 499–512. Available at: https://doi.org/10.1111/all.14852.

Sternlicht, M.D. *et al.* (2006) “Hormonal and local control of mammary branching morphogenesis,” *Differentiation*, 74(7), pp. 365–381. Available at: https://doi.org/10.1111/j.1432-0436.2006.00105.x.

Talaiezadeh, A., Jazayeri, S.N. and Nateghi, J. (2012) “Expression of c-kit protein in cancer vs. normal breast tissue,” *Wspolczesna Onkologia*, 16(4), pp. 306–309. Available at: https://doi.org/10.5114/wo.2012.30058.

Tauber, M. *et al.* (2023) “Landscape of mast cell populations across organs in mice and humans,” *Journal of Experimental Medicine*, 220(10). Available at: https://doi.org/10.1084/jem.20230570.

Tharp, M.D. *et al.* (1985) *Conjugated Avidin Binds to Mast Cell Granules1*, *The Journal of Histochemistry and Cytochemistry Inc*.

Thorne, J.T. *et al.* (2015) “Dynamic reciprocity between cells and their microenvironment in reproduction,” *Biology of Reproduction*. Society for the Study of Reproduction. Available at: https://doi.org/10.1095/biolreprod.114.121368.

Valérie Gouon-Evans, Elaine Y Lin and Jeffrey W Pollard (2002) “Requirement of macrophages and eosinophils and their cytokines/chemokines for mammary gland development,” *Breast Cancer Res* [Preprint].

Wagner, W. and Fogel, W.A. (2004) “Mammary histidine decarboxylase vulnerability to enzyme antisense oligonucleotides: Histamine and polyamine systems cross-talk,” in *Amino Acids*. Springer Wien, pp. 311–316. Available at: https://doi.org/10.1007/s00726-004-0077-5.

Watson, C.J. and Khaled, W.T. (2008) “Mammary development in the embryo and adult: A journey of morphogenesis and commitment,” *Development*, pp. 995–1003. Available at: https://doi.org/10.1242/dev.005439.

Wilson, G.J. *et al.* (2022) “Diverse myeloid cells are recruited to the developing and inflamed mammary gland,” *Immunology*, 165(2), pp. 206–218. Available at: https://doi.org/10.1111/imm.13430.

Woidacki, K. *et al.* (2013) “Mast cells rescue implantation defects caused by c-kit Deficiency,” *Cell Death and Disease*, 4(1). Available at: https://doi.org/10.1038/cddis.2012.214.

Wolters, P.J. *et al.* (2001) “Dipeptidyl Peptidase I is Essential for Activation of Mast Cell Chymases, but Not Tryptases, in Mice,” *Journal of Biological Chemistry*, 276(21), pp. 18551–18556. Available at: https://doi.org/10.1074/jbc.M100223200.

Yoshimoto, M. *et al.* (2022) “Mast Cell Repopulating Ability Is Lost During the Transition From Pre-HSC to FL HSC,” *Frontiers in Immunology*, 13. Available at: https://doi.org/10.3389/fimmu.2022.896396.

Chapter 2

Development and specification of mast cells in barrier tissues during embryonic organogenesis

Introduction

Mast cells (MCs) are immune cells that reside in nearly all vascularised tissues throughout the body. They are particularly enriched in major barrier organs including the skin, respiratory tract and gastrointestinal tract (da Silva et al., 2014). Positioned within these barrier tissues, MCs are poised to act as sentinel immune cells where they are most known for their pathological role in allergic reactions (Galli and Tsai, 2012; Krystel-Whittemore et al., 2016). It is now increasingly recognised however, that MCs have a diverse range of important functions beyond allergy in host defence and tissue remodeling (da Silva et al., 2014; Krystel-Whittemore et al., 2016; Metcalfe et al., 1997; West and Bulfone-Paus, 2022).

MCs are typically classified into two distinct subsets depending on whether they reside in connective or mucosal tissues (Derakhshan et al., 2022; Tauber et al., 2023). Connective tissue MCs (CMCs) differ from mucosal tissue MCs (MMCs) in their structure, biochemistry and transcriptome, and are associated with distinct functions (see Literature Review). Local microenvironmental cues within different tissue types may therefore play a key role in shaping MC identity and functional plasticity in different contexts in tissues, contributing to MC heterogeneity. Increasing evidence suggests that differences in developmental timing of these distinct MC subtypes may dictate the state of the tissue microenvironment encountered during differentiation and maturation, thereby cumulatively shaping MC

identity. Delineating how MC identity is established and maintained across tissues under homeostasis is therefore essential to interpret how they determine immune responses in health and disease.

MMCs are only detected in tissues after birth (Tauber et al., 2023). Haematopoietic progenitors derived from the bone marrow traffic to mucosal tissues where they give rise to MMCs. Consequently, their development therefore occurs in a microenvironment shaped by postnatally arising cues. The microbiome is one such cue which emerges after birth and profoundly influences MMC emergence, as well as their functional maturation in homeostasis and allergic disease (Schwarzer et al., 2019; Tauber et al., 2023). Nonetheless, MMCs are generally sparse in the steady state, and they are more robustly induced by inflammatory stimuli triggered by insults encountered postnatally. MMCs were first prominently identified in mucosal tissues during worm infections (MacDonald et al., 1980;Abe, 1988; Mayrhofer, 1979; Ruitenberg & Elgersma, 1976; Arizono et al., 1996), as well as during allergic inflammatory conditions such as asthma (Reber et al., 2015) and food allergies (Hagel et al., 2013; Yang et al., 2013). Type 2 T-cell responses underpin both helminth and allergic inflammation (McSorley et al., 2018). Key mediators of this response, including Notch signalling as well as cytokines like Il-10 and Tgfb (McSorley et al., 2018; Tu et al., 2005), play a key role in generating an “MMC” type of signature. Bone marrow haematopoiesis generates MC progenitors (MCPs) that first commit to the MC lineage (Arinobu et al., 2005; Chen et al., 2005b; Dahlin and Hallgren, 2015) and migrate to the peripheral tissue where they mature (Bankova et al., 2015; Gurish et al., 2001). The type 2 signals MCps encounter in these peripheral tissues can then directly promote an increase in serine proteases like Mcpt1 and Mcpt2 and concomitantly repressing other proteases like Mcpt5 and cathepsin G (Derakhshan et al., 2021, 2025; Meurer et al., 2025; Nakano et al.,

2021), generating the core “MMC” signature. MMCs therefore acquire their identity depending on their local microenvironment during their emergence and differentiation.

The importance of microenvironmental cues in driving MC identity is further reflected by the plasticity of the MMC phenotype. MC identity can switch from strict MMC signatures and can also comprise of both CMC-like and MMC-like transcriptional profiles. For instance, MCs expressing varying combinations of Mcpt1, Mcpt2 and Mcpt5 have been detected in response to different stimuli encountered over the course of inflammation and resolution as they migrate and localise within different tissues along the gastrointestinal tract (Friend et al., 1998; Friend et al., 1996). Similarly in the respiratory tract, MCs in various locations along the lung and trachea broadly express proteases Mcpt1, Mcpt2 as well as Mcpt4, Mcpt7 and Cpa3 (Xing et al., 2011), going beyond the classical CMC/MMC dichotomy. These studies have profoundly demonstrated how the state of the tissue influences MC identity.

In contrast to mucosal tissues, most connective tissues are already seeded by MCs in embryonic and neonatal stages of development (Combs et al., 1965; Gentek et al., 2018; Li et al., 2018; Tauber et al., 2023). Bone marrow-derived progenitors do not contribute significantly to CMCs under steady state (Gentek et al., 2018a; Kitamura et al., 1983b; Li et al., 2018; Kitamura et al., 1977). Rather, embryonic waves of haematopoiesis give rise to MCs in connective tissues during organogenesis and maintain themselves independently of the bone marrow under steady state (Gentek et al., 2018a; Z. Li et al., 2018; Tauber et al., 2023). As early as embryonic day (E) 9.5, the first wave of haematopoiesis from the yolk sac generates erythro-myeloid progenitors (EMPs), followed by the emergence of definitive haematopoietic stem cells (HSCs) from the aorta-gonad-mesonephros region by E10.5 (Gentek et al., 2018a; Z. Li et al., 2018). These EMP and HSC progenitors sequentially colonise the fetal liver which give rise to immune cells, including MCs, that seed peripheral

tissues and mature during the course of embryogenesis. Because of their early prenatal development, CMCs are exposed to a markedly distinct set of microenvironmental cues compared to MMCs which may shape their identity.

In the case of other tissue-resident immune lineages such as macrophages, EMPs first commit to the core macrophage programme-expressing lineage prior to migrating and seeding tissues in the embryo, after which local tissue-specific microenvironmental cues direct transcriptional diversification (Mass et al., 2016). This raises the question of whether fetal MC progenitors (MCPs) similarly acquire and specify their identity during haematopoietic development in the embryo. Moreover, it is also unclear which transcriptional factors regulate fetal MC identity. Transcription factors like *Gata2* and *Mitf* regulate the commitment of adult MCPs to the MC lineage (Arinobu et al., 2005; Ohmori et al., 2015; Qi et al., 2013; Tojima et al., 2024), and it is unknown whether fetal MCPs follow a similar programme.

In fetal skin, MCP seeding begins as early as E11.5 and continues in a defined window until E14.5, with the first heparin-comprising granular MCs detectable by E16.5 (Gentek et al., 2018; Li et al., 2018; Tauber et al., 2023; Ma et al., 2025). By E18.5, MCs continue to mature but appear to be self-maintained rather than continually recruited (Li et al., 2018; Ma et al., 2025). Despite the apparent completion of skin seeding by E14.5, the presence of MCPs at E15.5 in the fetal liver (Ma et al., 2025) raises the possibility that fetal liver MCPs continue to contribute to MC seeding in other tissues whose developmental windows extend beyond that of the skin. This has important implications for understanding whether the developmental kinetics are conserved or vary between tissues during embryogenesis.

Unlike the skin which predominantly comprises connective tissues, the lung is a mixed mucosal/connective tissue organ, and in adults, comprises both CMCs and inducible MMCs (Xing et al., 2011; Tauber et al., 2023). However, MC development in the embryonic lung remains largely uncharacterised. Cells derived from fetal liver progenitors have been sparsely detected in the fetal lung by E14.5 (Ma et al., 2025), however their identity and maturation states have not been defined. One question that remains unknown is whether other peripheral tissues like the lung follow similar MC developmental kinetics to the skin or adopts a distinct trajectory.

A second, closely related question is understanding when MC heterogeneity is first established during development. Despite sharing a core transcriptomic signature, adult CMCs exhibit varying levels of transcriptional diversity across distinct sites such as the peritoneum, skin, tongue, trachea and oesophagus (Dwyer et al., 2016a). EMP-derived tissue resident macrophages are transcriptionally diverse in adult tissues (Blériot et al., 2020), and this heterogeneity is already specified during fetal development where their precursors acquire tissue-specific transcriptional programmes soon after seeding peripheral tissues (Mass et al., 2016). It remains unknown whether MCs follow a similar pattern where the core MC programme is integrated with tissue-specific signals to establish tissue-specific MC heterogeneity.

Transcriptomic analysis of embryonic haematopoietic compartment has revealed the presence of *Cpa3*$^{+}$ progenitors in fetal yolk sac and fetal liver that contribute to *Cpa3*$^{+}$ mast cell progenitors and mast cells in the fetal skin by E13.5 (Ma et al., 2025). This study will further characterise MC development at E15.5-E18.5 across fetal liver, skin and lung, using the previously generated dataset of (Ma et al., 2025) as a baseline reference for early MC development at E13.5. By performing a spatio-temporal analysis of MC development in

distinct tissues during early, mid, and late fetal development, this work shows that MC identity is established early during development as part of a core MC programme. Tissue-specific kinetics further determine MC maturation profiles, providing key insights into how tissue-specific MC identity and heterogeneity is established.

Results

Single cell profiling reveals the development of committed mast cells in the fetal liver by E15.5

MCPs have previously been transcriptionally defined in the fetal liver as early as E11.5 (Z. Li et al., 2018; Ma et al., 2025), representing early progenitor stages of fetal MC development. While these early MCPs contribute to peripheral MC populations (Ma et al., 2025), it remains unclear whether MC lineage commitment occurs only after peripheral tissue seeding or whether MCPs differentiate beyond their progenitor state at later stages.

Although fetal liver MCPs could also be detected at E15.5 using flow cytometry (Ma et al., 2025), their transcriptional state - and thus their degree of lineage commitment - has not been examined.

To define the progression of this lineage beyond E13.5, we isolated live, $CD45^+$ cells from the fetal liver at E15.5 and performed single cell RNA sequencing (Figure 1A). This allowed us to directly compare the E15.5 transcriptome to the published reference E13.5 transcriptome (Ma et al., 2025). After performing quality control to exclude doublets and dead cells, we recovered 2317 high quality $CD45^+$ cells (Figure S1A). Dimensional reduction and unsupervised clustering revealed 19 clusters (Figure 1B), assigned based on their top DEGs referenced to the previously published reference dataset (Ma et al., 2025) (Figure S1B). Being the major site of haematopoiesis at this stage, the fetal liver comprised of a

broad range of haematopoietic populations including haematopoietic stem and progenitor cells (c3_HSPC_1, c12_HSPC_2), B-cells (c0_Bcell_1 and c15_Bcell_2), NK cells (c14_NKcell), neutrophil progenitors (c1_NeuP) and neutrophils (c8_Neu), granulocyte-monocyte progenitors (c2_GMP) and monocyte-dendritic cell progenitors (c6_MDP), monocytes (c4_Mono), macrophage subpopulations (c5_Mac_1, c9_Mac_2) as well as liver-specific macrophages called Kupffer cells (c11_Kupffer_1, c18_Kupffer_2). In addition, the liver dataset also comprised of megakaryocyte-erythrocyte progenitors (c10_MEP) and a small proportion of erythrocytes (c13_Ery) and megakaryocytes (c17_Mk). *Cpa3*$^{+}$ MC-lineage populations (c16_MC and c7_Cpa3) were detected and analysed subsequently.

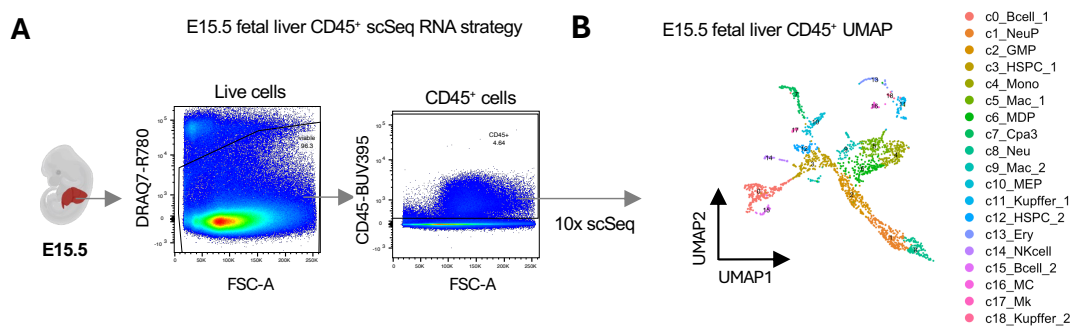

Chapter (2) Figure 1: Single cell transcriptomic profiling of fetal liver haematopoietic cells at E15.5.

(A) Schematic (left) showing experimental workflow of single cell RNA sequencing (scSeq). Live CD45^{+} haematopoietic cells were isolated from from fetal liver of E15.5 fetuses for 10x scSeq. (B) UMAP plot of the sequenced E15.5 fetal liver CD45^{+} cells (n=2317) following dimensional reduction and unsupervised clustering to reveal 19 distinct clusters.

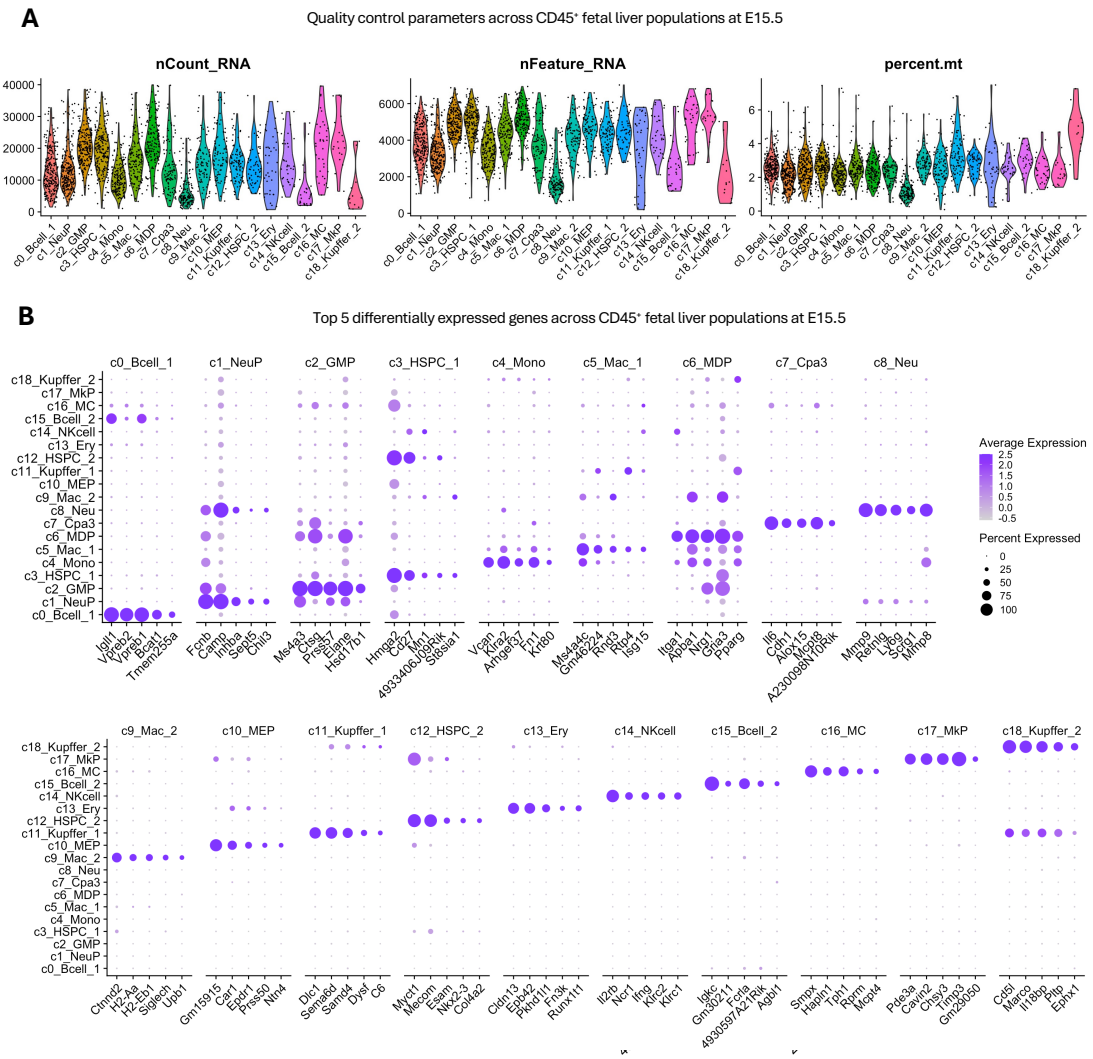

Chapter (2) Supplementary Figure S1: Single cell transcriptomic profiling of fetal liver haematopoietic cells at E15.5.

(A) Violin plots showing quality control metrics for E15.5 fetal liver CD45$^+$ cells across identified clusters, including total RNA counts (nCount_RNA), number of detected genes (nFeature_RNA) and percentage of mitochondrial genes (percent.mt). (B) Dot plot showing the expression of top 5 differentially expressed genes across clusters identified. Colour scale

indicates average expression of each gene. Dot sizes represent the percent of cells expressing each gene.

At E13.5, *Cpa3* expression was restricted to a single basophil-mast cell progenitor cluster (c4_BMCP) (Figure 2A). The c4_BMCP cluster was previously sub-clustered by (Ma et al., 2025), which revealed the presence of mast cell progenitors (MCP), basophil progenitors (BasoP), basophils (Baso) as well as an undefined progenitor population (udP) which resembled the bipotential progenitors in adult bone marrow (Dahlin et al., 2018) (Figure S2A). Due to lack of availability of the dimensions used to generate the published E13.5 liver UMAP, we performed re-clustering to ensure consistency of parameters with the remaining analysis and we used this UMAP as our E13.5 liver reference dataset (Figure 2B, S2A).

Comparison of *Cpa3* expression levels between the E13.5 and E15.5 transcriptomes revealed a clear developmental shift in MC populations. Although *Cpa3* expression was restricted to a single cluster (c4_BMCP), by E15.5 *Cpa3* expression could be detected within two transcriptionally distinct clusters: a mixed basophil-mast cell progenitor cluster and a discrete MC cluster (c16_MC) (Figure 2C).

Given the comparable *Cpa3* expression levels between E13.5 c4_BMCP and E15.5 c7_Cpa3 (Figure 2A), we sought to investigate whether any fetal liver MCPs with *Cpa3* expression levels similar to those detected at E13.5 would also reside within c7_Cpa3 at E15.5. To further resolve the progenitor populations within c7_Cpa3 cluster at E15.5, we next attempted to sub-cluster c7_Cpa3 cluster based on transcriptional relatedness to the sub-clusters of the *Cpa3*$^{+}$ sub-clusters identified at E13.5. Seurat mapping enabled projection of the E15.5 cells on top of the E13.5 reference cells based on similarity of transcriptional

profile. This analysis reliably detected baso-like and basoP-like cells in the fetal liver by E15.5, supported by high mapping prediction scores for these sub-populations (Figure 2D, S2B). However, almost no cells within the c7_Cpa3 cluster shared a similar transcriptome to the E13.5 MCPs (Figure 2D). A few udP-like cells were also detected, however they showed low prediction scores (Figure S2B) and increased expression of canonical MC-associated proteases (*Cma1, Tpsb2*) (Figure S2C), indicating divergence from the E13.5 udP transcriptional state towards MC differentiation.

A discrete population of cells expressing *Cpa3* highly could be detected within the c16_MC cluster (Figure 2C). Mapping cells from both the *Cpa3*$^{+}$ cells from the E15.5 liver (c16_MC and c7_Cpa3 clusters) to the E13.5 liver reference enabled identification of MCP-like cells with a high prediction score, in addition to the previously identified udP-, baso- and basoP-like cells (Figure 2E, S2D). These MCP-like cells exclusively derived from the discrete MC cluster (c16_MC), while the udP-, baso- and basoP-like cells exist in the c7_Cpa3 cluster (Figure S2E).

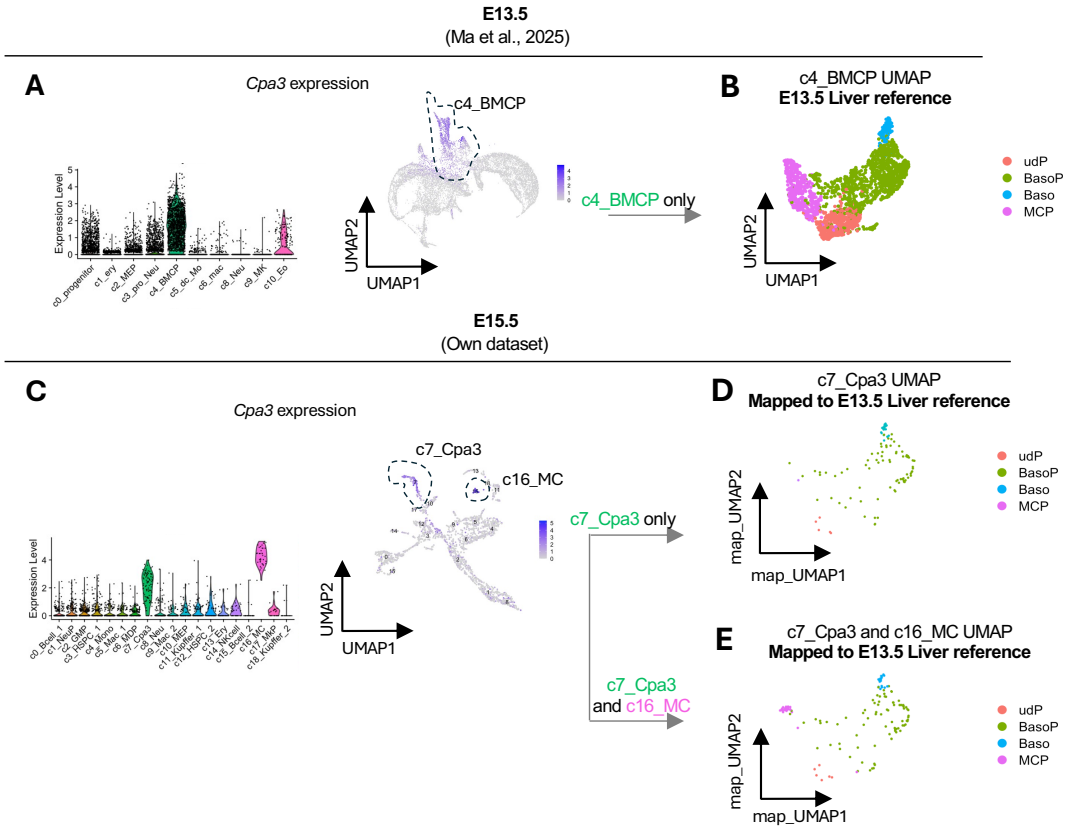

Chapter (2) Figure 2: Developmental diversification of *Cpa3*⁺ mast cell and basophil lineages in the fetal liver between E13.5 and E15.5.

(A) Violin plot and feature plot showing expression of Cpa3 among the clusters identified in the E13.5 fetal liver dataset generated by (Ma et al., 2025). (B) Reference UMAP plot of the re-clustered *Cpa3*⁺ (c4_BMCP) cells from the E13.5 fetal liver dataset, revealing four sub-clusters – undefined progenitors (udP), basophils (Baso), basophil progenitors (BasoP) and mast cell progenitors (MCP). (C) Violin plot and feature plot showing expression of Cpa3 among the clusters identified in the E15.5 fetal liver dataset generated in Figure 1B. (D) Projection of the c7_Cpa3 cluster onto the E13.5 fetal liver reference using Seurat mapping, with cells coloured by predicted E13.5 sub-cluster identity. (E) Projection of the c7_Cpa3 and

c16_MC clusters onto the E13.5 fetal liver reference using Seurat mapping, with cells coloured by predicted E13.5 sub-cluster identity.

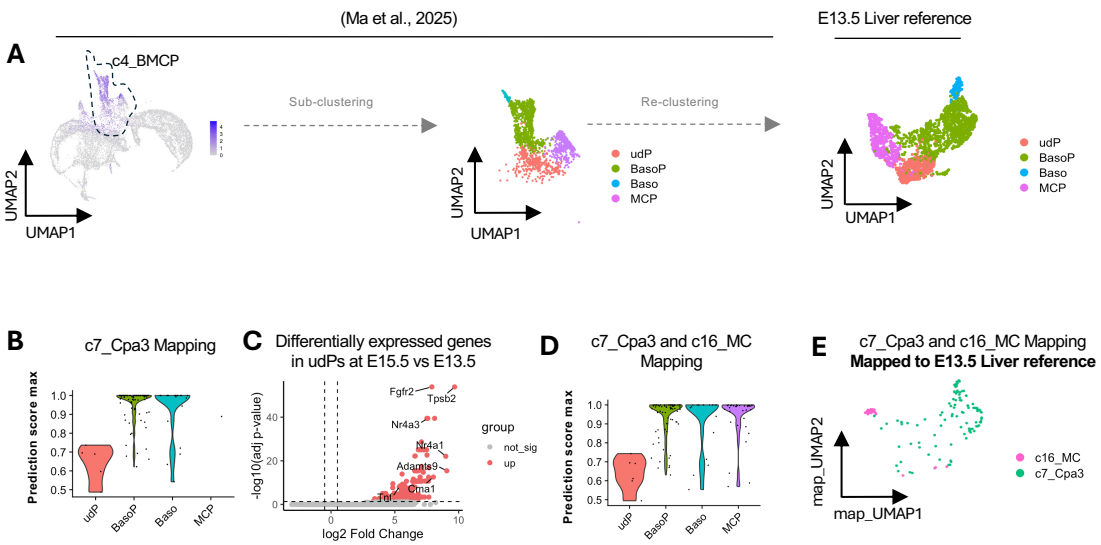

Chapter (2) Supplementary Figure S2: Generation of E13.5 fetal liver reference dataset.

E13.5 fetal liver transcriptomic dataset from (Ma et al., 2025) used to generate fetal liver reference for downstream analyses. (A) UMAP feature plot showing expression of *Cpa3* across the sequenced E13.5 fetal liver CD45^{+} cells, with expression localised within the c4_BMCP cluster. Sub-clusters of c4_BMCP previously annotated by (Ma et al., 2025) were shown alongside re-clustering of the c4_BMCP clusters using consistent parameters to generate the reference UMAP dataset used throughout the analyses. (B) Prediction scores generated from Seurat-based mapping of the E15.5 fetal liver c7_Cpa3 cluster onto the E13.5 fetal liver reference. Cells in the E15.5 fetal liver are assigned to and coloured by their predicted identity. (C) Volcano plot showing top DEGs in undefined progenitors (udPs) in the

fetal liver at E15.5 compared to E13.5 fetal liver udPs. Genes in red are significant ($p < 0.05$) and up-regulated based on average log2 fold change. Genes in grey are non-significant. (D) Prediction scores generated from Seurat-based mapping of the E15.5 fetal liver c7_Cpa3 and 16_MC cluster onto the E13.5 fetal liver reference. Cells in the E15.5 fetal liver are assigned to and coloured by their predicted identity. (E) UMAP showing overlay of the E15.5 fetal liver c7_Cpa3 and c16_MC clusters on top of the mapped E15.5 fetal liver, showing the distribution of E15.5 predicted cell states (Figure 2D-E) within each original (unmapped) E15.5 fetal liver cluster.

To assess how the mapped E15.5 *Cpa3*$^{+}$ progenitors have diverged from their progenitor counterparts at E13.5 in the fetal liver, we next investigated the changes in expression of the top differentially expressed genes across the sub-clusters that were previously identified in the E13.5 liver reference dataset (Ma et al., 2025). BasoP- and Baso-like cells at E15.5 showed relatively similar transcriptional signatures at E13.5 (Figure 3A), indicating that their developmental programme is largely conserved between timepoints. Consistent with the divergence of the udP state described above (Figure S2B-D), the udP-like cells at E15.5 showed partial upregulation of MC genes, however the MC signature was weaker than the MCP-like cells at this stage (Figure 3A). The MCP-like cells at E15.5 show a strong shift in increasing expression of canonical MC genes (*Kit, Serpinb1a*), associated with maturation, and a decrease in expression of canonical MCP genes (*Gzmb, Trbc1, Sox4, Itga4, Vamp5)* (Figure 3A).

Zbtb16 was another marker identified in MCPs (Ma et al., 2025) and by E15.5, the MCP-like cluster lost expression of *Zbtb16*, and increased expression of MC chymase (*Cma1)* and tryptase (*Tpsb2*) (Figure 3B, 3C). Together, these data indicate that by E15.5, the fetal liver

MCPs undergo a transcriptional shift and progress from a progenitor state towards a mature, lineage committed MC transcriptional programme.

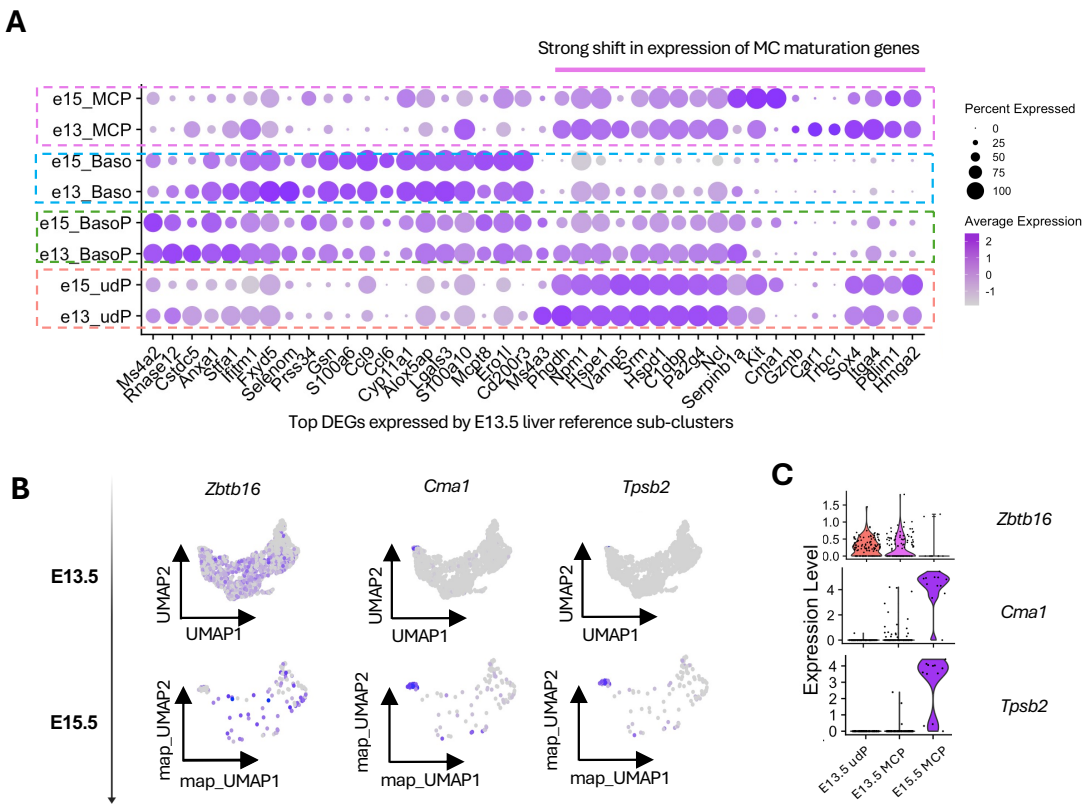

Chapter (2) Figure 3: Transcriptional changes in *Cpa3*⁺ mast cell and basophil lineages in the fetal liver between E13.5 and E15.5.

(A) Dot plot comparing the top 10 differentially expressed genes (DEGs) across the *Cpa3*⁺ sub-clusters identified in the E13.5 fetal liver dataset with the corresponding predicted *Cpa3*⁺ sub-clusters in the E15.5 fetal liver. Colour scale indicates average expression of each gene. Dot sizes represent the percent of cells expressing each gene. (B) Feature plots showing the expression of *Zbtb16, Cma1* and *Tpsb2* between E13.5 and E15.5 in the fetal

liver datasets. (C) Violin plots showing the expression levels of *Zbtb16, Cma1* and *Tpsb2* between the E13.5 udP, E13.5 MCP and E15.5 MCP clusters.

To determine how the development of E13.5 MCPs progresses by E15.5, we reconstructed the developmental trajectory between the two timepoints. Slingshot Pseudotime Trajectory analysis revealed a single continuous trajectory between the E13.5 udPs, progressing through the E13.5 MCPs and terminating in the E15.5 more mature MC population (Figure 4A). Cells segregated along pseudotime, with E13.5 udP, E13.5 MCP and E15.5 MC-like MCPs occupying progressively later positions in order of increasing pseudotime maturation (Figure 4B). This indicated that temporal maturation is likely the primary driver of transcriptional variation along the principal component axes.

In adult MC haematopoietic studies, bone marrow-derived bipotent basophil-mast cell progenitors (BMCPs) commit to the basophil/MC lineage by upregulating *Gata2* (Li et al., 2015), and subsequently commit to MCs by downregulating *Cebpa* and upregulating *Mitf* (Tshori and Nechushtan, 2012; Ohmori et al., 2015; Qi et al., 2013; Tojima et al., 2024). We next asked whether fetal MCPs commit to the MC lineage by following similar transcriptional changes. In line with these studies, we identified a similar transcriptional programme in MC development embryonically with progressive increase of *Gata2* and decrease of *Gata1* (Figure 4C). *Cebpa* was downregulated within the E13.5 MCP already, whereas *Mitf* upregulated only by E15.5 (Figure 4C, S3A, S3B) when other MC maturation genes appeared (Figure 3A-C), indicating that *Mitf* may mark commitment to the MC lineage. Of note, *Cebpa* expression was maintained in the Baso and BasoP lineages and was associated with increasing *Mcpt8* expression (Figure S3B-C), consistent with established basophil lineage

commitment programmes observed in adult haematopoiesis (Ohmori et al., 2015; Qi et al., 2013; Tojima et al., 2024).

Upregulation of *Gata2* and *Mitf* is associated with upregulation of several MC genes in adult haematopoietic studies on MC differentiation (Morii et al., 2004; Kitamura et al., 2002). Consistent with this, our Slingshot Trajectory analysis tracing fetal MC development could also identify a gradient of gene expression of MC receptors (*Kit, Il1rl1*), histamine synthase (*Hdc*), heparin synthase (*Hs3st1*) as well as MC proteases (*Cma1, Mcpt4, Tpsb2, Cpa3*) increasing over pseudotime axis (Figure 4D).

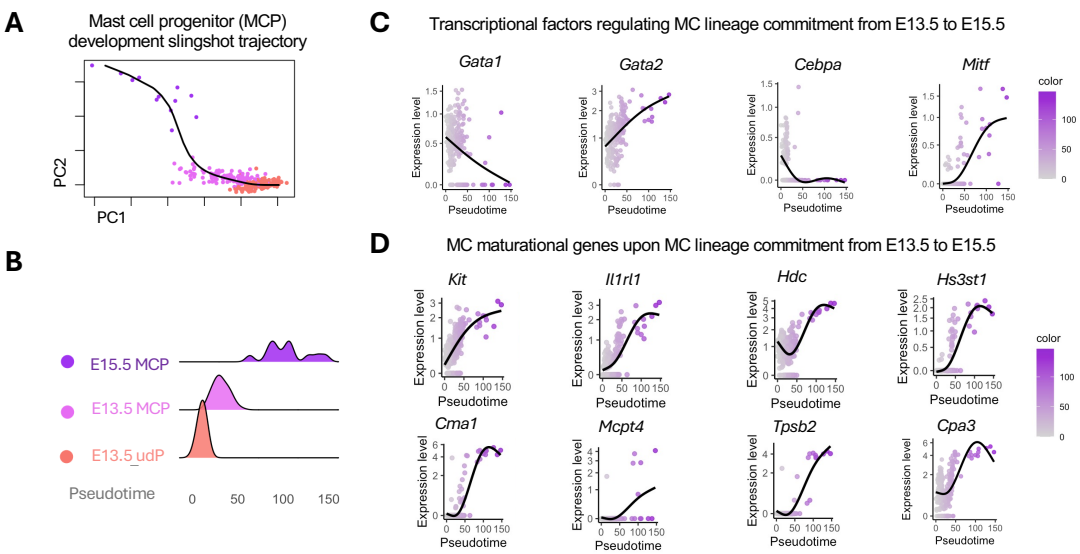

Chapter (2) Figure 4: Developmental trajectory and gene expression dynamics of mast cell differentiation between E13.5 and E15.5 fetal liver.

(A) Slingshot pseudotime trajectory inferred from E13.5 and E15.5 fetal liver Cpa3^{+} sub-clusters related to the mast cell lineage. Principal component analysis (PCA) plot showing the inferred pseudotime of E13.5 udP, E13.5 MCP and E15.5 MCP. Line indicates inferred

developmental trajectory. (B) Distribution of E13.5 udP, E13.5 MCP and E15.5 MCP along the inferred pseudotime axis, with 0 as the pseudotime origin. (C) Smoothed expression trends of mast cell commitment associated transcription factors along the pseudotime axis. (D) Smoothed expression trends of mast cell commitment associated effector genes (*Kit, Il1rl1, Hdc, Hs3st1, Cma1, Mcpt4, Tpsb2, Cpa3*) along the pseudotime axis. Colour scale indicates average expression of each gene across the cells.

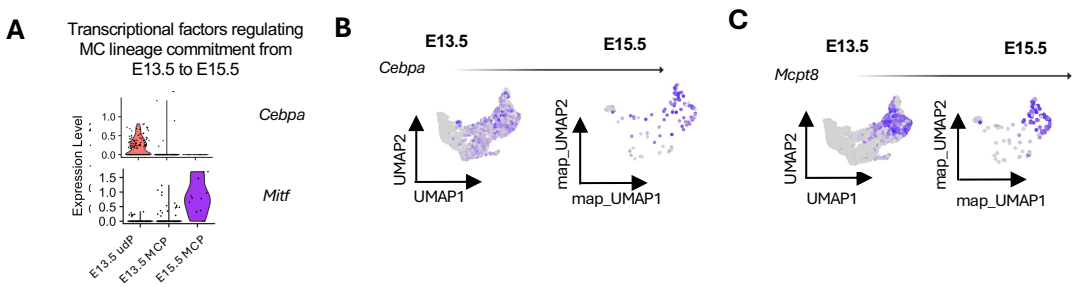

Chapter (2) Supplementary Figure S3: Transcriptional changes in *Cpa3*$^{+}$ mast cell and basophil lineages in the fetal liver between E13.5 and E15.5.

(A) Violin plots showing expression of transcription factors *Cebpa* and *Mitf* between the E13.5 udP, E13.5 MCP and E15.5 MCP clusters. (B) UMAP feature plot showing expression of *Cebpa* in the E13.5 fetal liver reference (left) and mapped E15.5 fetal liver cells (right). (C) UMAP feature plot showing expression of *Mcpt8* in the E13.5 fetal liver reference (left) and mapped E15.5 fetal liver cells (right).

Expression of integrin β7 (*Itgb7*) is associated with MCP trafficking in both adult (Bankova et al., 2015a; Gurish et al., 2001a) and embryonic MC development (Z. Li et al., 2018). In line with these studies, *Itgb7* expression was highest in the MCPs at E13.5, and remained detectable, albeit at reduced levels, in E15.5 MCs (Figure 5A). *Cx3cr1* expression was

identified in embryonic MCPs and MCs (Derakhshan et al., 2021; Gentek et al., 2018a; Z. Li et al., 2018) and may be important in chemokine signaling for MCP trafficking. We confirmed that *Cx3cr1* expression could be detected in the MCPs at E13.5 and was also retained in the maturing MCs by E15.5 (Figure 5B).

Together, these data indicate a developmental shift in the *Cpa3*-expressing population in the fetal liver, largely driven by the resolution of MCPs at E13.5 into a discrete committed MC identity by E15.5. At a transcriptomic level, this MC development programme is characterized by a loss of progenitor markers and induction of canonical MC lineage-associated transcription factors, effector genes and trafficking receptors. Nonetheless, we cannot exclude the possibility that limited cell yield may result in underrepresentation of cell populations expressing progenitor markers in the fetal liver at this stage.

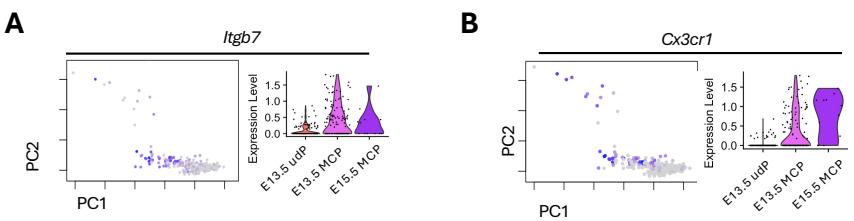

Chapter (2) Figure 5: Expression of mast cell progenitor trafficking markers during mast cell development in the fetal liver between E13.5 and E15.5.

(A) Feature plot embedded in principal component analysis (PCA) space (left) and corresponding violin plot (right) showing expression of *Itgb7* in E13.5 undefined progenitor (udP), E13.5 mast cell progenitor (MCP) and E15.5 MCP. (B) Feature plot embedded in PCA space (left) and corresponding violin plot (right) showing expression of *Cx3cr1* in E13.5 udP, E13.5 MCP and E15.5 MCP.

Mast cell progenitors seed fetal skin early but disappear after E15.5

Fetal liver MCPs seed developing skin (at least in the limbs) as early as E11.5, where they subsequently mature into MCs (Gentek et al., 2018a; Z. Li et al., 2018; Ma et al., 2025). Lineage tracing has further established that the seeding of fetal skin by liver MCPs occurs within a defined window until E14.5 (Ma et al., 2025). However, how MCPs seed tissues and differentiate across the skin MC developmental window (E13.5-E18.5) remains undefined at a single-cell resolution.

To address this, we used a similar sorting strategy to that used for the fetal liver to isolate live, $CD45^+$ cells (see M&M Figure 1) at E15.5 and E18.5, with additional enrichment for MCs at E18.5 (see M&M Figure 2). We performed sorting from fetal skin from pups separately at E15.5 and E18.5 (as two sequencing runs) and performed single cell sequencing (Figure 6A). Datasets from E15.5 and E18.5 were integrated to account for technical variation across the two sequencing runs (Figure 6A), and doublets and dead cells were removed (Figure S4A). We recovered 7775 $CD45^+$ cells and performed dimensional reduction and unsupervised clustering to reveal 17 clusters (Figure 6B), which were annotated based on their top DEGs using published fetal skin dataset references (Ma et al., 2025) (Figure S4B). The cellular composition shifted from E15.5 to E18.5, reflecting the haematopoietic developmental progression alongside ongoing fetal skin organogenesis (Figure 6C). Of these, *Cpa3*-expressing clusters identified across the two timepoints appeared transcriptionally distinct between E15.5 and E18.5 (Figure 6D, S4C), indicating marked developmental progression between MC lineages as they develop in the skin.

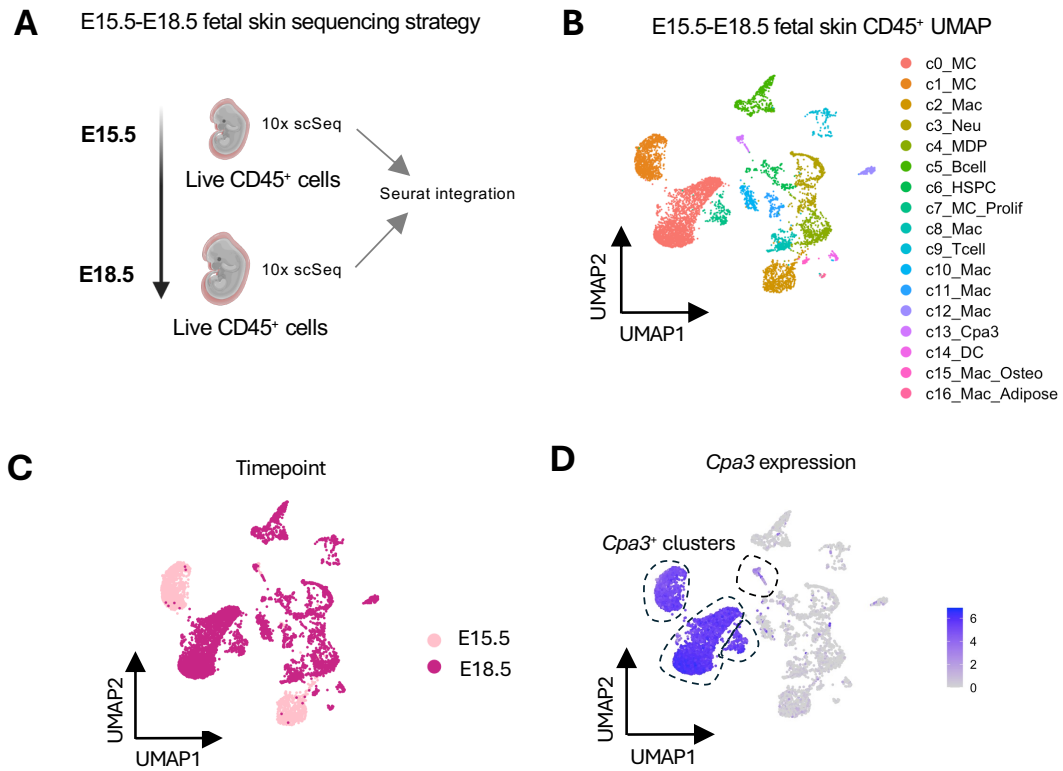

Chapter (2) Figure 6: Single cell transcriptomic profiling of E15.5 and E18.5 fetal skin haematopoietic cells.

(A) Schematic (left) showing experimental workflow of single cell RNA sequencing (scSeq). Live CD45$^+$ haematopoietic cells were isolated from from fetal skin of E15.5 and E18.5 fetuses for 10x scSeq. Samples from both sequencing runs were integrated using Seurat Integration. (B) UMAP plot of the sequenced and integrated dataset of E15.5 and E18.5 fetal skin CD45$^+$ cells merged (n=7775) together. Cells were dimensionally reduced followed by unsupervised clustering to reveal 17 distinct clusters. (C) UMAP visualisation showing the distribution of E15.5 and E18.5 fetal skin cells across identified clusters. (D) UMAP feature plot showing Cpa3 expression across fetal skin clusters at E15.5 and E18.5.

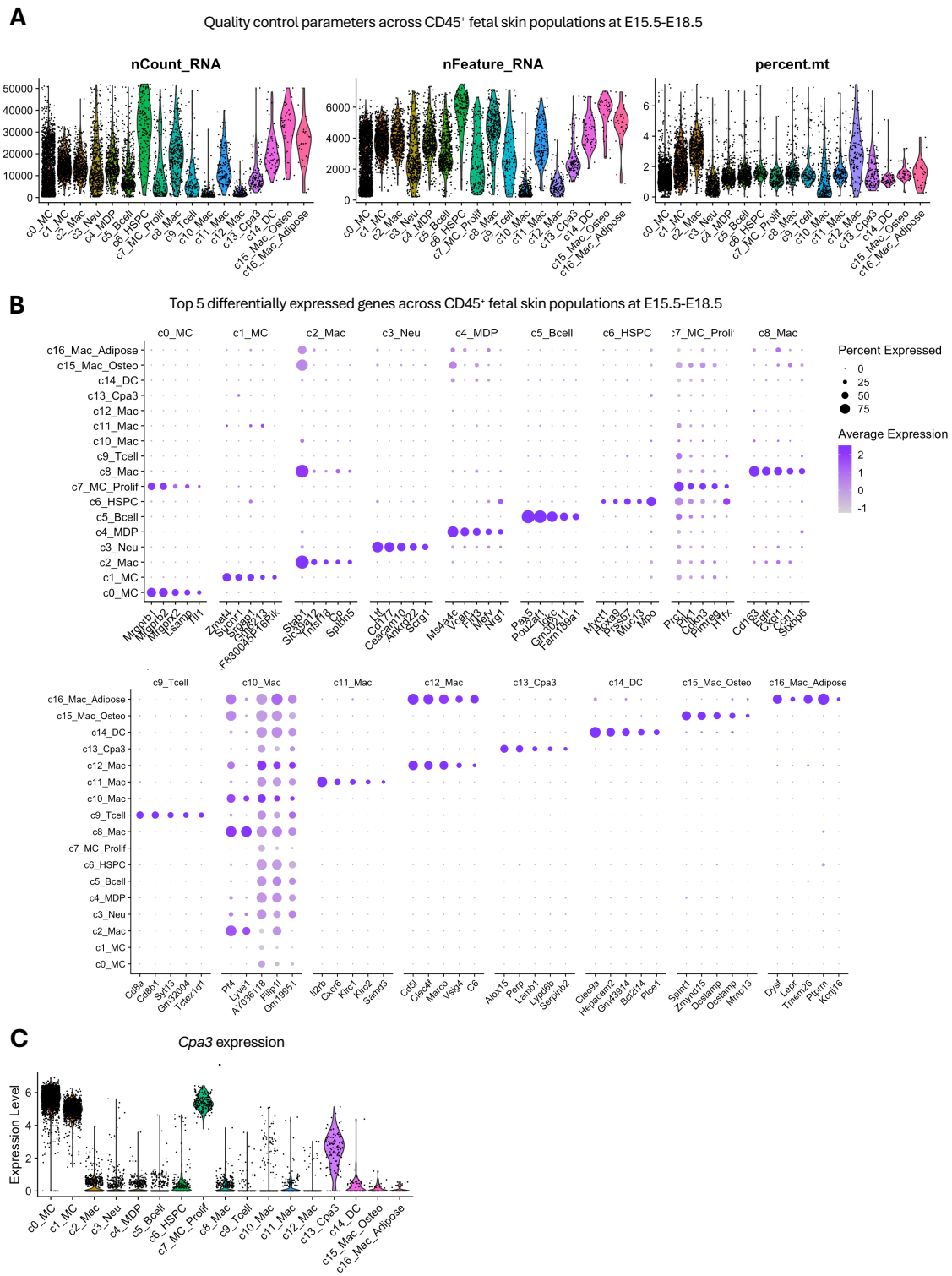
A
Quality control parameters across CD45⁺ fetal skin populations at E15.5-E18.5
nCount_RNA
nFeature_RNA
percent.mt
B
Top 5 differentially expressed genes across CD45⁺ fetal skin populations at E15.5-E18.5
Percent Expressed
Average Expression
C
Cpa3 expression
Expression Level

Chapter (2) Supplementary Figure S4: Single cell transcriptomic profiling of E15.5 and E18.5 fetal skin haematopoietic cells.

(A) Violin plots showing quality control metrics for E15.5 fetal liver CD45$^+$ cells across identified clusters, including total RNA counts (nCount_RNA), number of detected genes (nFeature_RNA) and percentage of mitochondrial genes (percent.mt). (B) Dot plot showing the expression of top 5 DEGs across clusters identified. Colour scale indicates average expression of each gene. Dot sizes represent the percent of cells expressing each gene. (C) Violin plot showing expression levels of *Cpa3* across identified clusters.

To characterise MC development in the fetal skin during this period, we first established an early developmental reference for skin MCs by E13.5, when both MCPs and MCs are already present (Ma et al., 2025). In the published E13.5 fetal skin dataset (Ma et al., 2025), *Cpa3*$^+$ cells were previously annotated as mast cells (MCs), proliferating MCs (Prolif_MCs) and basophils (Baso) (Figure S5A, S5B). However, these annotations did not distinguish between more progenitor-like and mature committed lineage states. Because our fetal liver analysis revealed that the fetal liver is the major source of progenitors at this stage, we resolved the developmental identity of these skin *Cpa3*$^+$ populations across the fetal liver *Cpa3*$^+$ developmental continuum. Mapping of the E13.5 fetal skin *Cpa3*$^+$ populations onto the E13.5 fetal liver reference UMAP (Figure S5B) revealed substantial heterogeneity within the skin MC clusters: rather than corresponding to a single committed MC state, cells within the E13.5 skin MC and Prolif_MC clusters were distributed across the continuum of E13.5 fetal liver MCPs and udPs (Figure S5C, S5D). This indicated the presence of progenitor-like cells alongside more differentiated MCs in fetal skin. Similarly, the E13.5 skin basophil cluster was also heterogeneous, with cells mapping to either E13.5 fetal liver progenitors (BasoP) or mature basophils (Baso) (Figure S5C, S5D).

Based on these findings, we generated a more developmentally refined E13.5 fetal skin reference by sub-clustering *Cpa3*$^{+}$ populations into progenitor-like and mature MC and basophil lineages, supported by high prediction scores (Figure S5E, S5F). We overlaid these sub-clusters on the original *Cpa3*$^{+}$ published fetal skin dataset (Figure S5G). In addition to these mapping analyses, we further confirmed the MC lineage commitment of the fetal skin MC subcluster at E13.5 based on downregulation of *Cebpa* (restricted to basophils), upregulation of MC-lineage associated *Mitf*, and downregulation of MCP-associated *Zbtb16* (Figure S5H). The resulting clusters (Figure S5G) were re-embedded using dimensionality reduction parameters to maintain consistency of our parameters with the rest of the analysis.

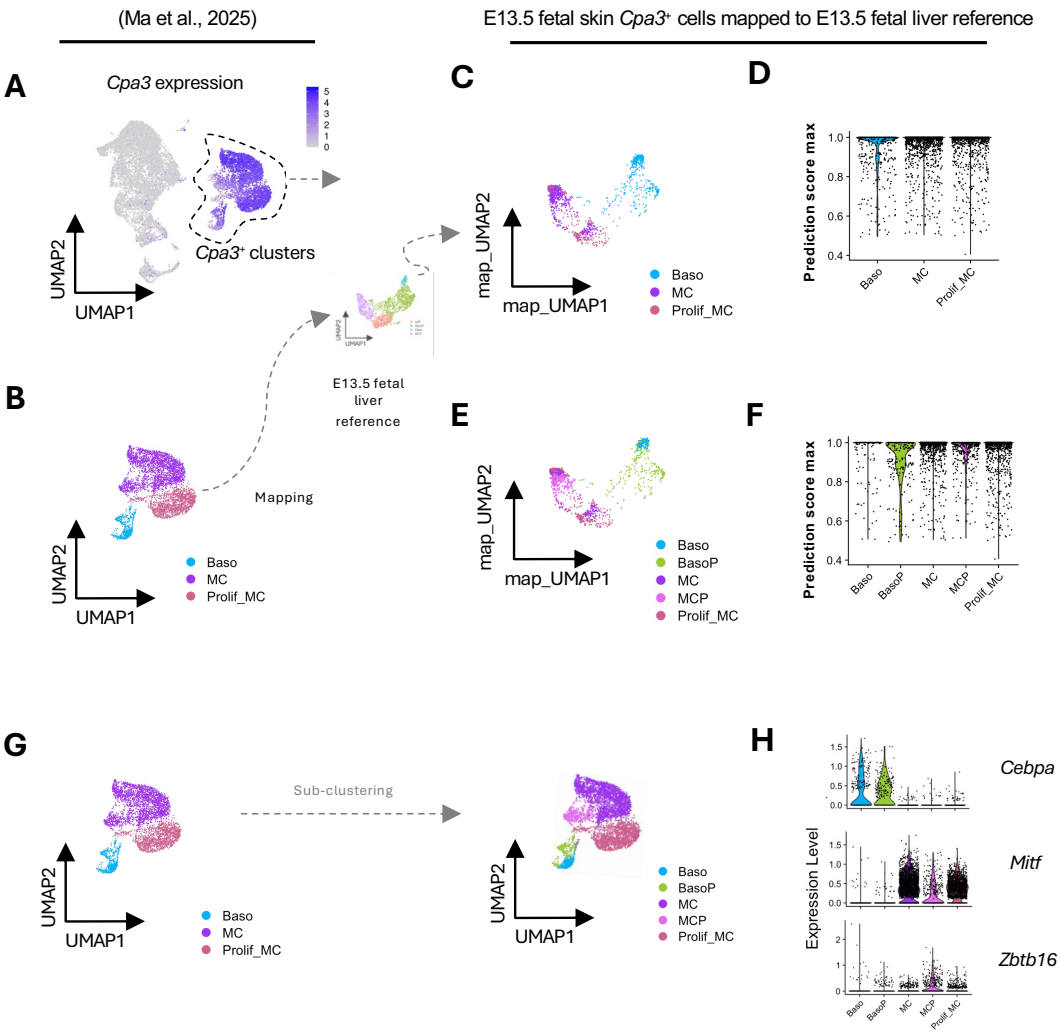

Chapter (2) Supplementary Figure S5: Generation of E13.5 fetal skin reference dataset.

E13.5 fetal skin transcriptomic dataset from (Ma et al., 2025) used to generate fetal skin reference for downstream analyses. (A) UMAP feature plot showing expression of *Cpa3* across the sequenced E13.5 fetal skin CD45$^+$ cells, with expression localised within the c4_BMCP cluster. (B) Sub-clusters of *Cpa3*$^+$ clusters previously annotated by (Ma et al., 2025) as basophils (Baso), (non-proliferating) mast cells (MC) and proliferating MCs (Prolif_MC). (C) Projection of the E13.5 fetal skin *Cpa3*$^+$ sub-clusters onto the E13.5 fetal liver reference

using Seurat mapping, with cells coloured by E13.5 skin sub-cluster identity. (D) Prediction scores generated from Seurat-based mapping of the E13.5 fetal skin Cpa3^{+} sub-clusters onto the E13.5 fetal liver reference. Cells in the E13.5 fetal liver are assigned to and coloured by their original annotations. (E) Further sub-clustering of E13.5 fetal skin *Cpa3*$^{+}$ sub-clusters annotated as basophils (Baso), basophil progenitors (BasoP), mast cell progenitors (MCP), (non-proliferating) mast cells (MC) and proliferating MCs (Prolif_MC). (F) Projection of the E13.5 fetal skin *Cpa3*$^{+}$ newly annotated sub-clusters onto the E13.5 fetal liver reference using Seurat mapping, with cells coloured by E13.5 skin new sub-cluster identity. (G) Prediction scores generated from Seurat-based mapping of the E13.5 fetal skin *Cpa3*$^{+}$ newly annotated sub-clusters onto the E13.5 fetal liver reference. Cells in the E13.5 fetal liver are assigned to and coloured by their new annotations. (H) Violin plots howing expression levels of *Cebpa, Mitf* and *Zbtb16* across identified E13.5 fetal skin sub-clusters.

This generated dataset was used as the E13.5 fetal skin reference dataset as a baseline for subsequent maturation analyses (Figure 7A, 7B). To track MC maturation in the skin as fetal development progresses, we extracted the *Cpa3*$^{+}$ clusters in E15.5 and E18.5 skin (Figure 6D), and mapped them onto E13.5 fetal skin reference dataset (Figure 7B). Within the MC lineage, mapping revealed that at E15.5, a small proportion of *Cpa3*$^{+}$ cells resembled the MCP population, although the majority already resembled the committed MC state (Figure 7C). By E18.5 however, *Cpa3*$^{+}$ cells mapped exclusively to the committed MC population (Figure 7D), indicating complete resolution of progenitor-like states into mature MCs.

To quantify the loss of fetal liver progenitor identity over time, we quantified the E13.5 fetal liver MCP signature across the developmental timepoints. Signature scorecard analysis revealed that highest fetal liver MCP signature score was detected within the MCP

subcluster at E13.5 and E15.5, but was absent at E18.5 (Figure 7E). In contrast, the MC subclusters consistently displayed low liver MCP signature scores at all stages (Figure 7D), indicating extinguishing of progenitor-associated transcriptional programmes upon MC commitment even at the earliest stages. This was further supported by loss of expression of the progenitor-associated gene *Zbtb16* in both MCs and proliferating MCs over time (Figure 7F). Consistent with these transcriptional changes, MCPs decreased substantially by E15.5 and were no longer detectable by E18.5 (Figure 7G). However, the proportion of committed MCs continued to increase substantially over time, ultimately comprising the majority of *Cpa3*$^{+}$ cells by E18.5 (Figure 7G). The proliferating MCs (Prolif_MCs) decreased over time, but a small proportion was still retained at E18.5 (Figure 7G). Notably, basophils and basophil progenitor populations comprised only a minor population that decreased over time (Figure 7G), indicating that the MC lineage is the dominant *Cpa3*$^{+}$ population in the developing fetal skin.

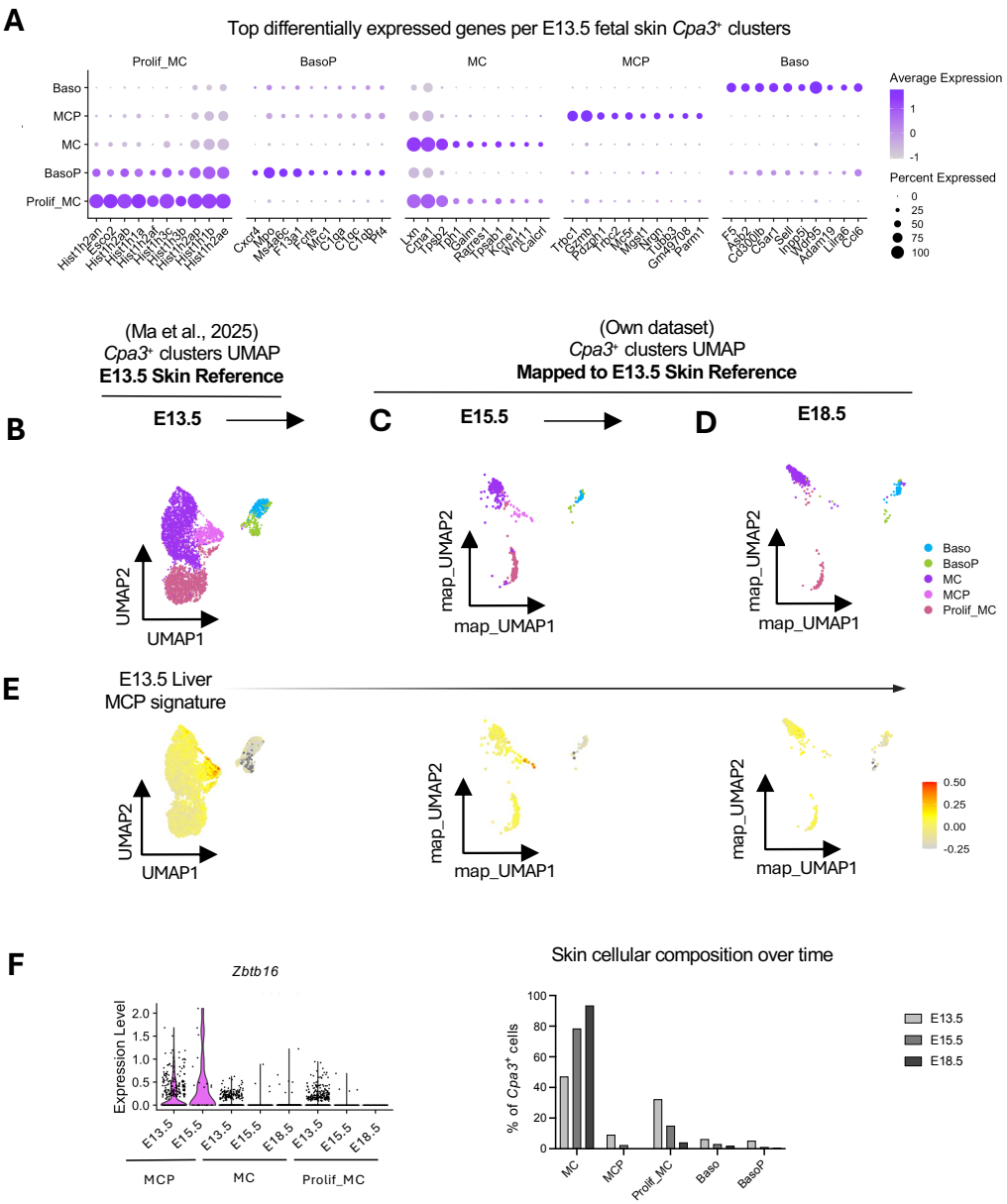

Chapter (2) Figure 7: Progressive developmental maturation of *Cpa3*⁺ mast cell and basophil lineages in the fetal skin between E15.5 and E18.5.

(A) Dot plot showing top 10 differentially expressed genes associated with basophils (Baso), basophil progenitors (BasoP), mast cell progenitors (MCP), (non-proliferating) mast cells (MC) and proliferating MCs (Prolif_MC) clusters at E13.5 in the fetal skin, used as a developmental baseline to define the populations. Colour scale indicates average expression of each gene. Dot sizes represent the percent of cells expressing each gene. (B) Reference UMAP plot of fetal skin dataset at E13.5, visualizing MC, Proli_MC, Baso, BasoP and udP clusters. (B) Projection of Cpa3^{+} cells from E15.5 fetal skin onto the E13.5 reference fetal skin dataset using Seurat mapping. (D) Projection of *Cpa3*$^{+}$ cells from E18.5 fetal skin onto the E13.5 reference fetal skin dataset using Seurat mapping. Cells in the E15.5 (C) and E18.5 (D) mapped datasets are coloured by predicted E13.5 sub-cluster identity. (E) Signature scorecard showing enrichment of E13.5 fetal liver mast cell progenitor (MCP) gene signature overlaid on UMAP of E13.5 (left), E15.5 (middle) and E18.5 (right) skin datasets. (F) Violin plot showing expression of *Zbtb16* across fetal skin *Cpa3*$^{+}$ populations at E13.5, E15.5 and E18.5. (G) Quantification of *Cpa3*$^{+}$ sub-populations (as a proportion of total *Cpa3*$^{+}$ cells) across developmental timepoints.

Fetal skin mast cell maturation occurs locally and progressively in situ

Having established that MCs become the dominant *Cpa3*$^{+}$ population by E18.5, we next evaluated how MCs mature in fetal skin. We first reconstructed the differentiation trajectory connecting these cells to their earlier developmental states. Slingshot Trajectory analysis revealed a continuous developmental trajectory from MCPs at E13.5 to MCs at E13.5, E15.5 and E18.5 (Figure 8A). E13.5 MCP were positioned at the origin of the pseudotime axis, consistent with their progenitor identity, whereas E13.5 MCs occupied slightly later, reflecting early commitment (Figure 8B). MCs at E15.5 and E18.5 shifted considerably along pseudotime (Figure 8B), marking a developmental transition.

Across increasing pseudotime, gene expression gradients revealed progressive maturation of MCs in fetal skin from E13.5 to E18.5. Expression of progenitor gene *Zbtb16* is lost along pseudotime (Figure 8C), indicating loss of progenitor state. Concomitant with this, MC proteases (*Cma1, Mcpt4, Tpsb2, Cpa3*) steadily increased over time (Figure 8C), consistent with the acquisition of a "CMC signature". Avidin, which binds to and stains heparin granules in MCs was detectable in fetal skin by E16.5, but not at earlier stages like E14.5 (Gentek et al., 2018a). Consistent with this, we found that heparin and histamine synthesis, marked by expression of enzymes involved in their synthesis (*Hs3st1* and *Hdc* respectively) was also upregulated by E15.5 (Figure 8C). These data suggest that MCs become granulated upon maturation by E15.5. However, not all MC genes increase progressively over time in fetal skin MCs. Expression of *Tph1,* the enzyme that is involved in serotonin production in MCs, increased in E15.5 skin MCs but was lost by E18.5 (Figure 8C), indicating potential functional changes in skin MCs over the course of development.

Notably, E18.5 MCs displayed a bimodal pseudotime distribution, with one population occupying intermediate pseudotime state and the other occupying the terminal pseudotime state (Figure 8B). In adults, MCs in connective tissues like the skin express *Mrgprb2,* which increases with increasing maturation (Tauber et al., 2023). We therefore asked whether the "E18_early" MCs differed from "E18_late" MCs. Both populations represented distinct clusters of E18.5 MCs (Figure S6A), yet they generally expressed similar median levels of *Mrgprb2* at this stage (figure S6B, S6C). Notably however, a smaller fraction of MCs in the "E18_early" MCs upregulate *Mrgprb2* expression highly while "E18_late" MCs exhibit more uniform expression of *Mgrprb2* (Figure S8B, S8C). The top DEGs associated with the "E18_late" subset were associated with activation related genes (*Nr4a3, Pde4d, Nfat5, Gab2, Tgfbr2*) (Figure S6D).

Taken together, these data indicating that by E18.5, skin MCs mature and acquire the canonical mature CMC signature marked by *Mrgprb2* expression, but heterogeneity over pseudotime primarily reflects differences in activation state.

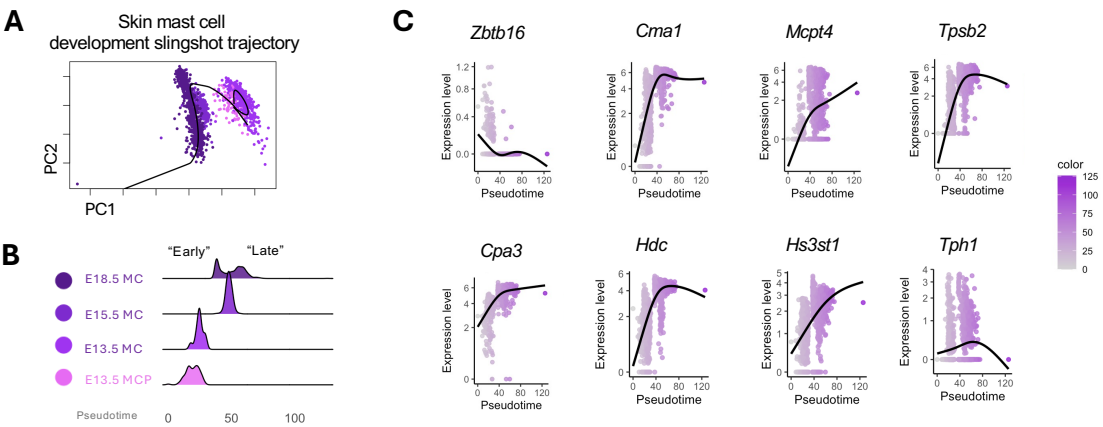

Chapter (2) Figure 8: Developmental trajectory and gene expression dynamics of mast cell differentiation in fetal skin.

(A) Slingshot pseudotime trajectory inferred from E13.5, E15.5 and E18.5 fetal skin *Cpa3*$^{+}$ sub-clusters related to the mast cell lineage. Principal component analysis (PCA) plot showing the inferred pseudotime of E13.5 MCP and MCs between E13.5, E15.5 and E18.5 timepoints. Line indicates inferred developmental trajectory. (B) Distribution of E13.5 MCP and MCs between E13.5, E15.5 and E18.5 along the inferred pseudotime axis, with 0 as the pseudotime origin. E18 "Early" and "Late" mast cell populations mark the bimodal distribution of mast cells along pseudotime. (C) Smoothed expression trends of mast cell progenitor gene (*Zbtb16*), mast cell associated effector genes (*Cma1, Mcpt4, Tpsb2, Cpa3, Hdc, Hs3st1, Tph1*) along the pseudotime axis. Colour scale indicates average expression of each gene across the cells.

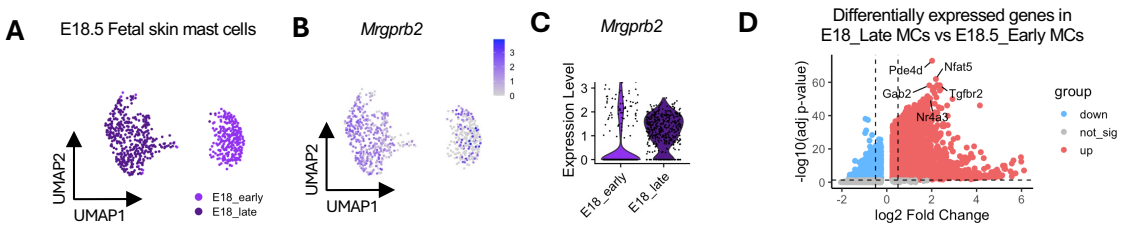

Chapter (2) Supplementary Figure S6: Heterogeneity of mast cell maturation states at E18.5 in fetal skin.

(A) UMAP visualisation of E18.5 fetal skin mast cells showing separation of cells occupying earlier (E18_early) and later (E18_late) pseudotime states (as described in Figure 8B). (B) UMAP feature plot showing expression of *Mrgprb2* across E18.5 fetal skin mast cells. (D) Volcano plot showing top DEGs in E18_late MCs compared to E18_early MCs in fetal skin. Genes in red are significant ($p < 0.05$) and up-regulated based on average log2 fold change, whereas genes in blue are significant ($p < 0.05$) and down-regulated based on average log2 fold change. Genes in grey are non-significant.

We next examined expression of progenitor-associated migration and trafficking genes across pseudotime. Early in pseudotime at E13.5-E15.5, MCPs and MCs expressed progenitor migration-associated genes *Itgb7* and *Cx3cr1,* which were progressively extinguished by E18.5 (Figure 9A-B). This pattern is consistent with a model in which MCPs migrate to the fetal skin at these early stages, followed by local expansion and subsequent maturation. We therefore examined cell cycling in actively proliferating and non-proliferating MC subsets.

At each developmental stage, the proliferating MC populations comprised a distinct cluster from quiescent MCs. Other fetal immune cell populations like Langerhans cells and

epidermal T-cells follow a hierarchical self-renewal pattern via proliferation of cells that are more immature and progenitor-like (Gentek et al., 2018b; Ghigo et al., 2013). We therefore wondered if these proliferating fetal skin MCs followed a similar pattern of maintenance and maturation. However, proliferating MC clusters lost progenitor-associated migration markers (Figure 9A-B) and underwent transcriptional maturation (Figure 9C) similarly to the other MCs at the same developmental stage, indicating that these proliferating MCs were more likely a subset of MCs that undergo active cycling. Since the proliferating MC clusters declined over time (Figure 7H), we hypothesised that proliferating MC populations likely contribute to the expanding MC pool early in development, whereas by E18.5 most MCs are terminally mature and quiescent, and may not require substantial turnover. In support of this, E13.5 MCs had the highest number of MCs actively in S/G2M phase, consistent with recent proliferative activity, which declined by E15.5 (Figure 9D). By E18.5, most MCs were in the G1 phase (Figure 9D), indicative of quiescence. Interestingly, the E18.5 MCs that appeared early in pseudotime had a modest increase in S/G2M cell cycling score relative to the E18.5 MCs that appeared later (Figure 9D), suggesting recent proliferative activity in the less mature MCs.

Taken together, these data may support a model in which MCPs seed fetal skin early and differentiate into MCs, a subset of which undergo local proliferation that contributes to MC expansion which subsequently mature in situ into a large, terminally differentiated population with limited late progenitor input (Figure 9E).

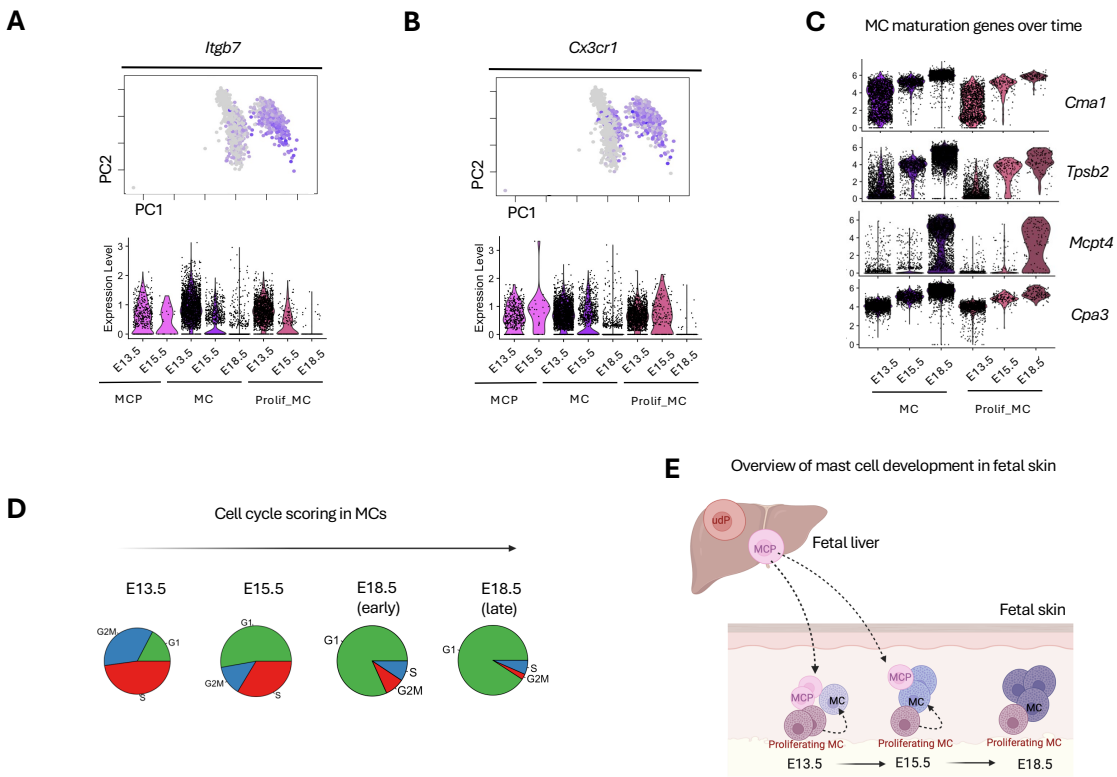

Chapter (2) Figure 9: Local developmental dynamics of mast cells in fetal skin.

(A) Feature plot embedded in principal component analysis (PCA) space (top) and corresponding violin plot (bottom) showing expression of *Itgb7* across *Cpa3*$^{+}$ populations at E13.5, E15.5 and E18.5. (B) Feature plot embedded in PCA space (top) and corresponding violin plot (bottom) showing expression of *Cx3cr1* across *Cpa3*$^{+}$ populations at E13.5, E15.5 and E18.5. (C) Violin plot showing expression of mast cell associated effector genes (*Cma1, Tpsb2, Mcpt4, Cpa3*) in mast cells (MC) and proliferating MCs (Prolif_MC) between E13.5, E15.5 and E18.5. (D) Cell cycle phase assignment of mast cells from E13.5, E15.5 and E18.5 (early and late). (E) Schematic summarising the temporal progression of mast cell progenitors and mast cells in fetal skin across developmental timepoints.

Fetal lung mast cells follow delayed developmental kinetics

Previous work has identified MCs in the fetal lung by E18.5 arising from embryonic progenitors (Z. Li et al., 2018), however it remains unknown whether MC development in other such peripheral tissues follows a similar pattern as observed in fetal skin. *Cpa3*$^{+}$ progenitor-derived cells have been detected in the fetal lung as early as E14.5, albeit sparsely (Ma et al., 2025), but the identity and developmental phenotype of these cells remain undefined. We therefore asked whether we could identify MCs and their progenitors in the fetal lung by E15.5.

We performed single cell sequencing on live CD45^{+} cells isolated from E15.5 and E18.5 fetal lungs, as described previously (Figure 10A, see M&M Figure 1-2). After integrating the two sequencing runs, we ran quality control checks to exclude doublets and dead cells, followed by dimensional reduction and unsupervised clustering on remaining 3513 cells, which revealed the presence of 16 clusters defined by their top DEGs which we annotated using published fetal lung references (Ma et al., 2025) (Figure 10B, S7A-B). These included haematopoietic stem cell progenitors and granulocyte-monocyte progenitors (c3_HSPC_GMP), monocyte-dendritic cell progenitors (c2_MDP), neutrophils (c8_Neu), macrophages (c0_Mac_1, c9_Mac_2), dendritic cells (c14_DC), B-cells (c11_Bcell), NK cells (c12_NKcell) as well as developing T-cell subpopulations (c1_Lymphoid_Prog, c6_Tcell_DP_1, c5_Tcell_DP_2, c4_Tcell_Tox). As observed in the skin, fetal lungs also comprised of some megakaryocytes (c15_Mk) and erythrocytes (c13_Ery) along with their progenitors (c10_MEP_Cpa3). As observed in the fetal skin dataset, the cellular composition of the fetal lung changed over time between E15.5-E18.5 (Figure 10C), reflecting ongoing development.

We next examined *Cpa3* expression to identify MC and basophil lineage populations within the fetal lung. *Cpa3* expression was detected primarily within two clusters – c7 which expressed Cpa3 most highly, followed by the c10 cluster (Figure 10D, S7C). Cluster c7 expressed canonical MC markers (*Tpsb2, Tph1, Tpsb2, Mrgprb2)*, so we annotated it as c7_MC (Figure S10A). However, c10 expressed DEGs representing both megakaryocyte-erythrocyte progenitors as well as basophil/MC lineage markers indicating heterogeneity within this cluster (Figure S7B). To resolve which clusters within the fetal lung belong to the MC/basophil lineage, we combined the *Cpa3*$^{+}$ clusters (c7_MC and c10_MEP_Cpa3) (Figure 10E) and sub-clustered it to reveal the presence of MCs, basophils (Baso), undefined progenitors (udPs) similar to the adult bone marrow bipotent MC-basophil progenitors (Dahlin et al., 2018) as well as megakaryocyte progenitors (MkP), and erythrocyte progenitors (EryP) (Figure 10E, S8A). Of these, *Cpa3* expression was the highest in the MCs, followed by modest expression in the udP and Baso clusters (Figure S8B). These clusters could be detected at E15.5 and shifted in composition by E18.5 (Figure S8C), indicating developmental shifts over time.

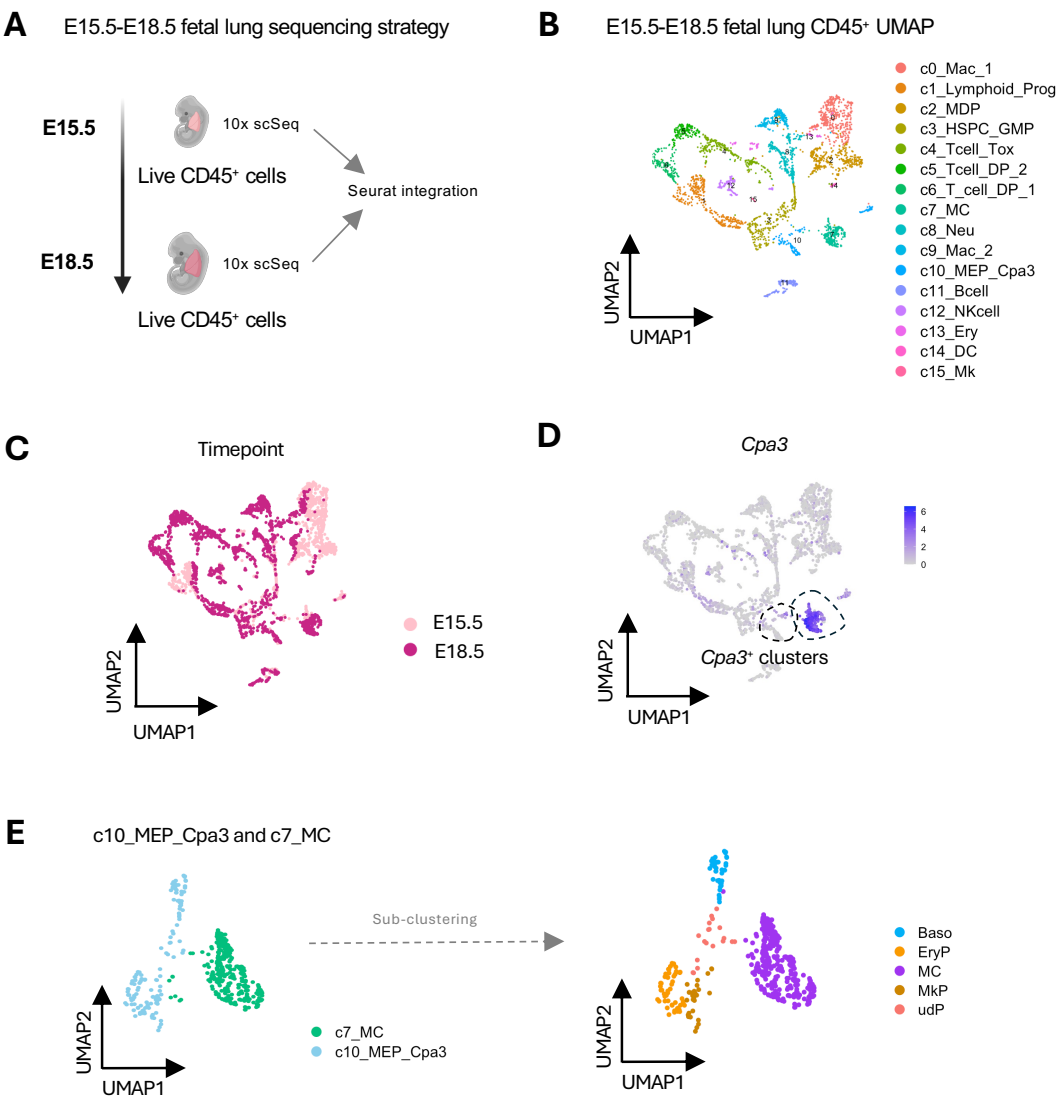

Chapter (2) Figure 10: Single cell transcriptomic profiling of E15.5 and E18.5 fetal lung haematopoietic cells.

(A) Schematic (left) showing experimental workflow of single cell RNA sequencing (scSeq). Live CD45+ haematopoietic cells were isolated from fetal lung of E15.5 and E18.5 fetuses for

10x scSeq. Samples from both sequencing runs were integrated using Seurat Integration. (B) UMAP plot of the sequenced and integrated dataset of E15.5 and E18.5 fetal lung $CD45^+$ cells merged (n=3513) together. Cells were dimensionally reduced followed by unsupervised clustering to reveal 16 distinct clusters. (C) UMAP visualisation showing the distribution of E15.5 and E18.5 fetal lung cells across identified clusters. (D) UMAP feature plot showing *Cpa3* expression across fetal lung clusters at E15.5 and E18.5. (E) UMAP of combined *Cpa3*$^+$ clusters (c7_MC, c10_MEP_Cpa3) following sub-clustering to reveal sub-clusters including mast cells (MC), basophils (Baso), undefined progenitors (udP), megakaryocyte progenitors (MkP) and erythrocyte progenitors (EryP).

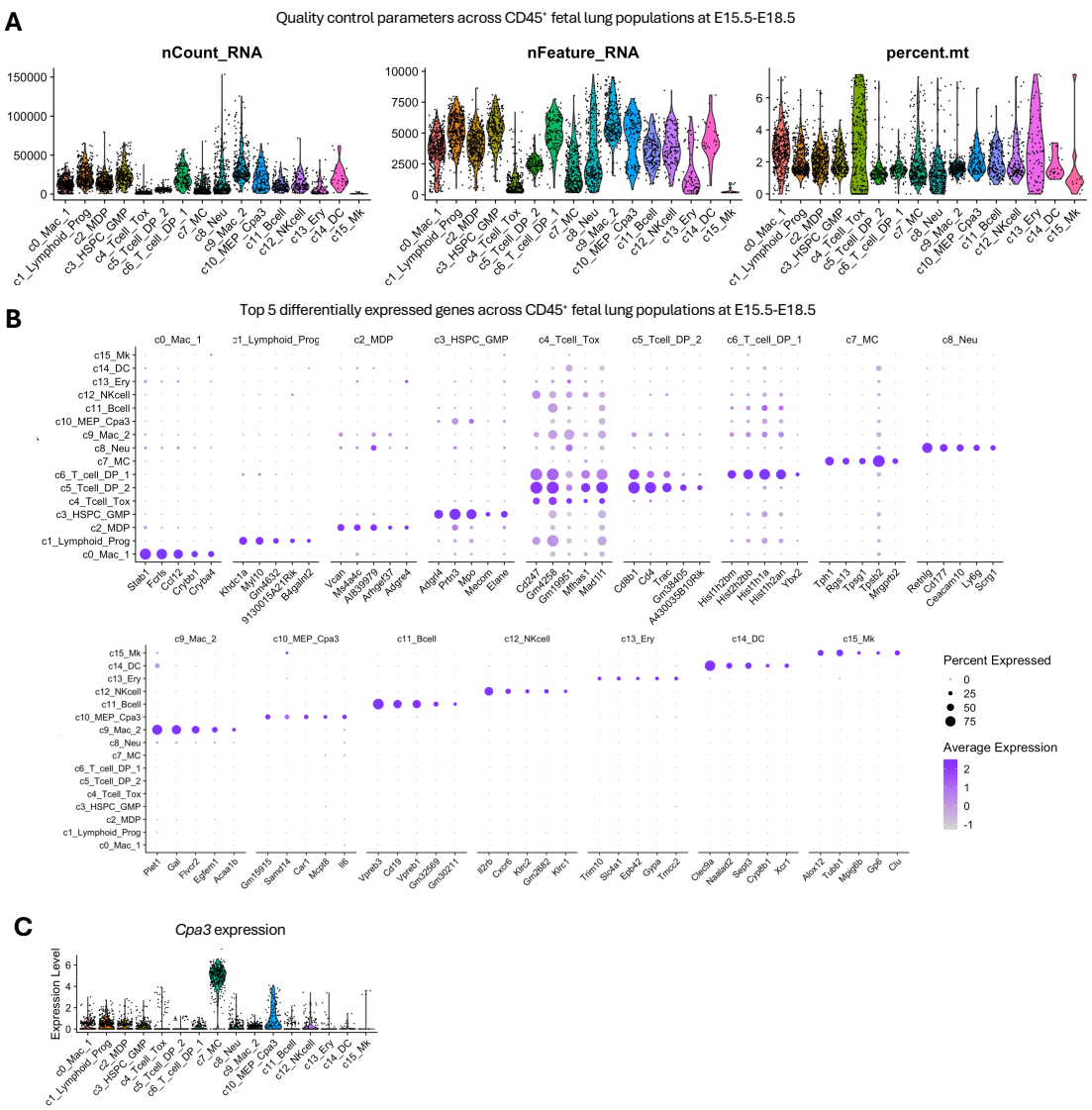

Chapter (2) Supplementary Figure S7: Single cell transcriptomic profiling of E15.5 and E18.5 fetal lung haematopoietic cells.

(A) Violin plots showing quality control metrics for E15.5 fetal liver CD45⁺ cells across identified clusters, including total RNA counts (nCount_RNA), number of detected genes (nFeature_RNA) and percentage of mitochondrial genes (percent.mt). (B) Dot plot showing

the expression of top 5 differentially expressed across clusters identified. Colour scale indicates average expression of each gene. Dot sizes represent the percent of cells expressing each gene. (C) Violin plot showing expression levels of *Cpa3* across identified clusters.

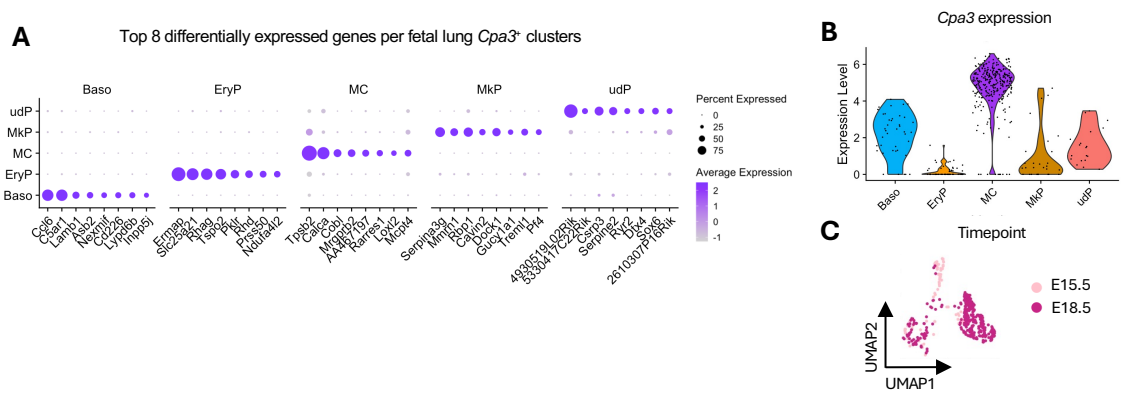

Chapter (2) Supplementary Figure S8: Sub-clustering of *Cpa3*⁺ clusters in the E15.5 and E18.5 fetal lung.

Heterogeneity within the c10_MEP_Cpa3 cluster and c7_MC cluster were resolved by sub-clustering to reveal mast cells (MC), basophils (Baso), undefined progenitors (udP), megakaryocyte progenitors (MkP) and erythrocyte progenitors (EryP) (as shown in Figure 10E). (A) Dot plot showing expression of top 8 differentially expressed genes across *Cpa3*⁺ sub-clusters identified. (B) Violin plot showing expression of *Cpa3* across *Cpa3*⁺ sub-clusters identified. (C) UMAP visualisation showing the distribution of E15.5 and E18.5 fetal lung cells across identified sub-clusters.

Since we were interested in tracing MC development within the fetal lung, we focused our subsequent analysis on cells from the MC, Baso and udP clusters where *Cpa3* expression was detectable (Figure 11A-B, S8B). The MC, Baso and udP clusters at E15.5 were used as a baseline for maturational analysis based on their top DEGs (Figure 11B). Between E15.5 and E18.5, we observed a dramatic shift in development of these *Cpa3*$^{+}$ clusters in the fetal lung, with MCs expanding and becoming the dominant population by E18.5 (Figure 11C, 11D). This was accompanied by a reciprocal decrease in basophils (Figure 11C, 11D).

To determine how these populations in the fetal lung relate to the fetal liver progenitors at E13.5, we compared expression of the E13.5 fetal liver MCP signature in the *Cpa3*$^{+}$ populations from the E15.5 and E18.5 fetal lungs. Signature scorecard analysis revealed that the lung MCs at E15.5 had a stronger fetal liver MCP signature than the fetal skin MCs at the same timepoint (Figure 11E, 7D), indicating that lung MCs retained progenitor-like features at this stage. In line with this, progenitor-associated *Zbtb16* expression was detected within the E15.5 lung MCs not in skin MCs at the same stage (Figure 11F).

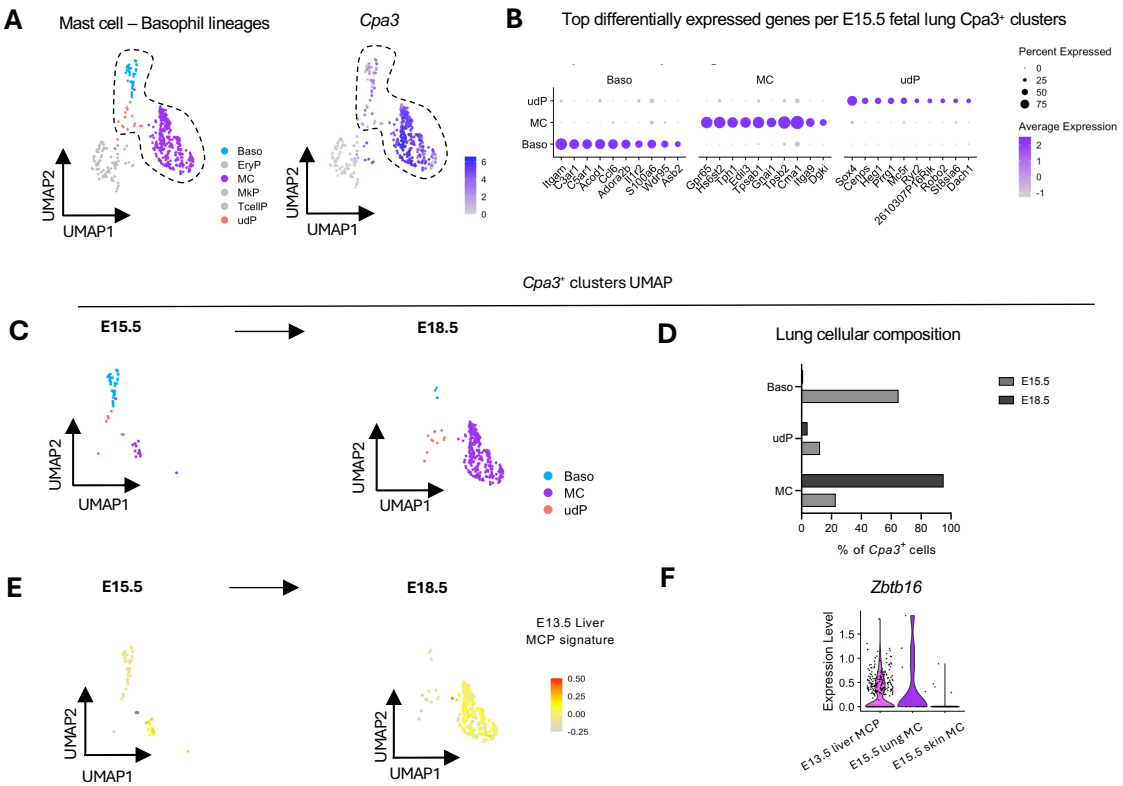

Chapter (2) Figure 11: Progressive developmental maturation of *Cpa3*⁺ mast cell and basophil lineages in the lung between E15.5 and E18.5.

(A) UMAP (left) and feature plot (right) showing high *Cpa3* expression in mast cell (MC), basophil (Baso) and undefined progenitor (udP) sub-clusters among the *Cpa3*⁺ clusters defined in Figure 10E. (B) Dot plot showing top 10 differentially expressed genes associated with MC, Baso and udP clusters at E15.5 in the fetal lung, used as a reference for comparison across developmental stages. Colour scale indicates average expression of each gene. Dot sizes represent the percent of cells expressing each gene. (C) UMAP showing fetal lung MC, Baso and udP sub-clusters at E15.5 (left) and E18.5 (right). (D) Quantification of fetal lung MC, Baso and udP sub-clusters (as a proportion of total *Cpa3*⁺ cells) across developmental

timepoints. (E) Signature scorecard showing enrichment of E13.5 fetal liver mast cell progenitor (MCP) gene signature overlaid on UMAP of E15.5 (left) and E18.5 (right) lung datasets. (F) Violin plot showing expression of *Zbtb16* of fetal lung mast cell (MC) at E15.5 compared to fetal liver mast cell progenitors (MCP) at E13.5 and fetal skin mast cells (MC) at E15.5.

We hypothesised if the fetal lung MCs may be developmentally delayed relative to the fetal skin MCs at E15.5. To further assess the maturational state of lung MCs at this stage, we investigated expression of MC commitment and maturation markers. However, despite persistence of *Zbtb16* expression, E15.5 lung MCs lacked expression of *Cebpa* and instead expressed high levels of *Gata2 and Mitf* at levels comparable to the skin MCs at E15.5 (Figure S9A), indicating MC lineage commitment. This was accompanied by functional maturation of lung MCs exhibiting increased expression of MC proteases (*Cma1, Tpsb2, Cpa3*), albeit at lower levels than skin MCs at the same developmental stage (Figure S9B). This may reflect developmental delay in maturation of the committed fetal lung MCs at E15.5, or alternatively, distinct transcriptional profiles in different tissues.

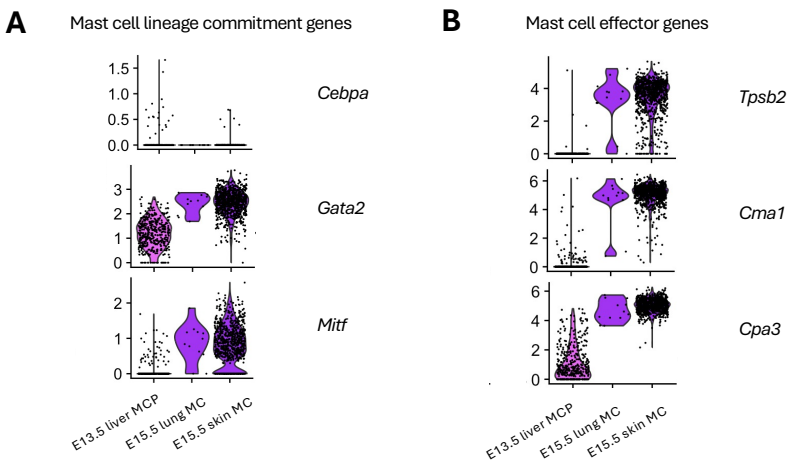

Chapter (2) Supplementary Figure S9: Expression of committed mast cell programme in fetal lung mast cells by E15.5.

(A) Violin plot showing expression of transcription factors *Cebpa*, *Gata2* and *Mitf* across *Cpa3*$^{+}$ sub-clusters identified. (B) Violin plot showing expression of mast cell effector genes *Tpsb2, Cma1* and *Cpa3* across *Cpa3*$^{+}$ sub-clusters identified.

Fetal lung MC maturation is asynchronous with distinct subtypes emerging by E18.5

To place fetal lung MCs along a developmental continuum, we constructed a pseudotime trajectory which revealed a single continuous path originating from the udPs at E15.5 progressing through MCs from E15.5 to E18.5 (Figure 12A). The udPs lay at the origin of the pseudotime reflecting their progenitor state, with E15.5 and E18.5 MCs progressively shifting forward (Figure 12B), reflecting developmental progression.

Across increasing pseudotime, gene expression gradients revealed progressive commitment of MCs in fetal lung from E15.5 to E18.5 (Figure 12C). Expression of progenitor gene *Zbtb16*

is lost along pseudotime (Figure 12C), indicating gradual exit from a progenitor-like state. Histidine carboxylase (*Hdc)* transcripts upregulated in fetal lung MCs over time. However, unlike the fetal skin MCs, fetal lung MCs do not show uniform, progressive increase in canonical connective tissue type MC proteases (*Cma1, Mcpt4, Tpsb2, Cpa3*) over time (Figure 12C). This was also the case for serotonin (*Tph1*) as well as histamine (*Hs3st1*) expression.

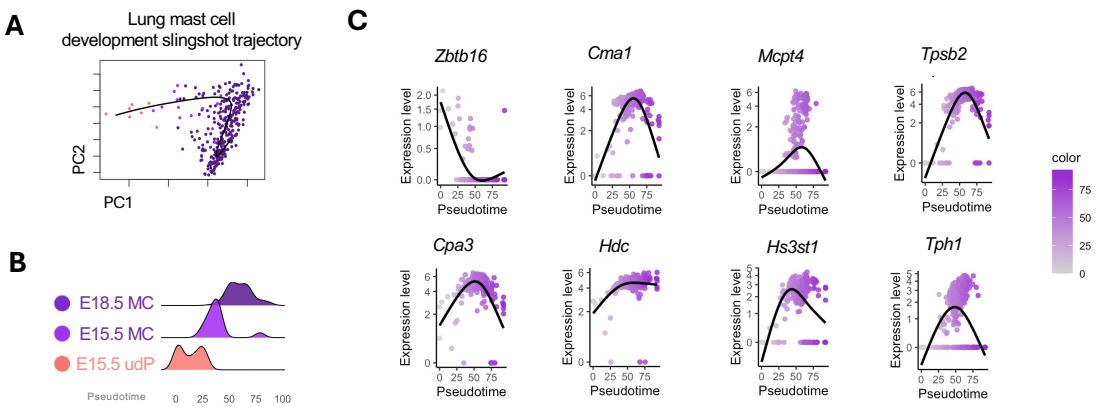

Chapter (2) Figure 12: Developmental trajectory and gene expression dynamics of mast cell differentiation in fetal lung.

(A) Slingshot pseudotime trajectory inferred from E15.5 and E18.5 fetal lung *Cpa3*$^{+}$ sub-clusters related to the mast cell lineage. PCA plot showing the inferred pseudotime of E15.5 udP and MCs between E15.5 and E18.5 timepoints. Line indicates inferred developmental trajectory. (B) Distribution of E15.5 udP and MCs between E15.5 and E18.5 along the inferred pseudotime axis, with 0 as the pseudotime origin. (C) Smoothed expression trends of mast cell progenitor gene (*Zbtb16*), mast cell associated effector genes (*Cma1, Mcpt4, Tpsb2, Cpa3, Hdc, Hs3st1, Tph1*) along the pseudotime axis. Colour scale indicates average expression of each gene across the cells.

To further investigate how lung MCs expand and mature between E15.5 and E18.5, we subclustered the lung MC population, which revealed the presence of two MC subtypes (MC_1, MC_2) in addition to the basophils and udP cells (Figure 13A). MC_1 cells were the dominant MC population at E15.5 and E18.5; however, by E18.5, a second MC population, MC_2, also emerged (Figure 13B). Overlay of the distinct MC subsets onto this trajectory demonstrated that fetal lung MC maturation is asynchronously maturing by E18.5, with distinct subsets occupying different positions along the developmental axis (Figure 13C). Cells within cluster MC_1 shifted forward along the pseudotime between E15.5 and E18.5, indicating progressive maturation over time (Figure 13C), whereas MC_2 occupied the terminal position of pseudotime (Figure 13C).

Despite their proximity along pseudotime, MC_1 and MC_2 populations in the fetal lung at E18.5 expressed distinct transcriptional profiles (Figure 13E). From E15.5 to E18.5, MC_1 progressively upregulated expression of MC proteases (*Cma1, Mcpt4, Tpsb2,* Cpa3) as well as *Hdc* and *Hs3st1.* In contrast, the MC_2 population showed reduced expression of these genes at E18.5, which may contribute to the non-uniform gene expression pattern observed at late pseudotime. Notably, both fetal lung MC populations MC_1 and MC_2 expressed *Mrgprb2* at comparable levels by E18.5, similar to skin MCs at this stage. This indicates that acquisition of the mature connective tissue MC marker *Mrgprb2* (Tauber et al., 2023) occurred in both skin and lung MCs by E18.5, despite other transcriptional heterogeneity that may reflect tissue-specific programmes.

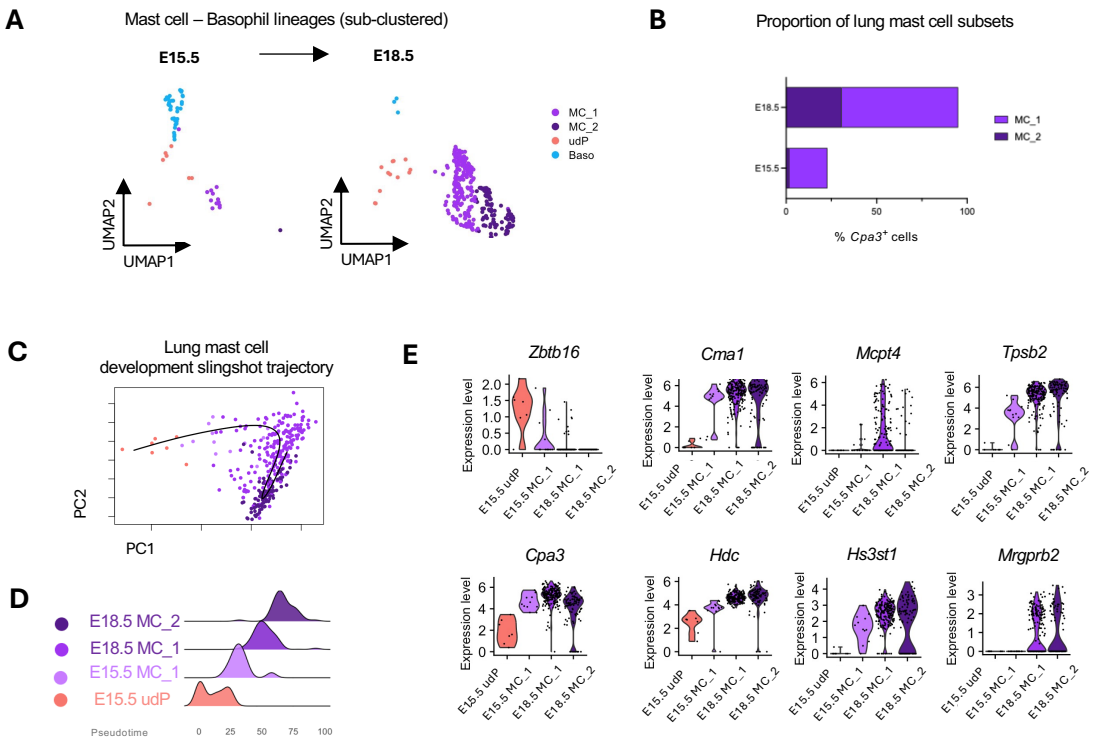

Chapter (2) Figure 13: Heterogeneity and asynchronous maturation of mast cells in the fetal lung between E15.5 and E18.5.

(A) UMAP showing sub-clustered *Cpa3*$^{+}$ mast cell-basophil lineage populations in the fetal lung at E15.5 (left) and E18.5 (right), revealing sub-clusters of mast cells (MC_1 and MC_2), basophils (Baso) and undefined progenitors (udP). (B) Quantification of fetal lung MC sub-populations MC_1 and MC_2 (as a proportion of total *Cpa3*$^{+}$ cells) across developmental timepoints. (C) Overlay of the MC subsets on the inferred Slingshot pseudotime trajectory inferred from E15.5 and E18.5 fetal lung *Cpa3*$^{+}$ sub-clusters related to the mast cell lineage. (D) Distribution of E15.5 udP and MCs (MC_1 and MC_2) between E15.5 and E18.5 along the inferred pseudotime axis, with 0 as the pseudotime origin. (E) Violin plots showing expression of mast cell progenitor gene (*Zbtb16*), mast cell associated effector genes (*Cma1,*

Mcpt4, Tpsb2, Cpa3, Hdc, Hs3st1) as well as the connective tissue marker Mrg receptor (*Mrgprb2*) between E15.5 udP and E15.5 and E18.5 MCs (MC_1 and MC_2).

To provide insights into whether fetal lung MCs rely on recruitment or mature locally in situ like fetal skin, we next examined expression of progenitor-associated migration and trafficking genes across fetal lung MC populations. Like in the fetal skin, MCs (MC_1) in the fetal lung at E15.5 expressed progenitor migration-associated genes *Cx3cr1* and *Itgb7* (Figure 14A, 14B). However, in contrast to fetal skin where MCs uniformly lost expression of these migration genes by E18.5, only the MC_1 population in the fetal lung retained expression of *Cx3cr1* and *Itgb7* at E18.5 (Figure 14A). In contrast, the MC_2 population in the fetal lung lost expression of both *Cx3cr1* and *Itgb7* at E18.5 (Figure 14A-B), consistent with their advanced position in pseudotime analysis.

Nonetheless, MCs appeared to expand by E18.5, yet we could not detect the absence of clearly identifiable MCP clusters in the fetal lung. We therefore examined whether MCs retain proliferative capacity to support expansion during development. E15.5 MCs (MC_1) had the highest proportion of cells in S/G2M phase (Figure 14C), indicating active cycling at this stage with the potential to contribute to the expanding MC pool. MC_1 retained proliferative capacity at E18.5, however an increasing proportion of these cells transitioned into G1 (Figure 14C), consistent with gradual acquisition of quiescence. Notably, MC_2 also retained some proliferative capacity (Figure 14C).

Taken together, these analyses support a model in which lineage committed MCs are present in the lung by E15.5 and retain progenitor features and proliferative capacity. By E18.5, lung MCs undergo maturation but do so asynchronously by giving rise to transcriptionally distinct

populations that differ in their expression of progenitor trafficking genes, effector gene programmes and proliferative state (Figure 14D).

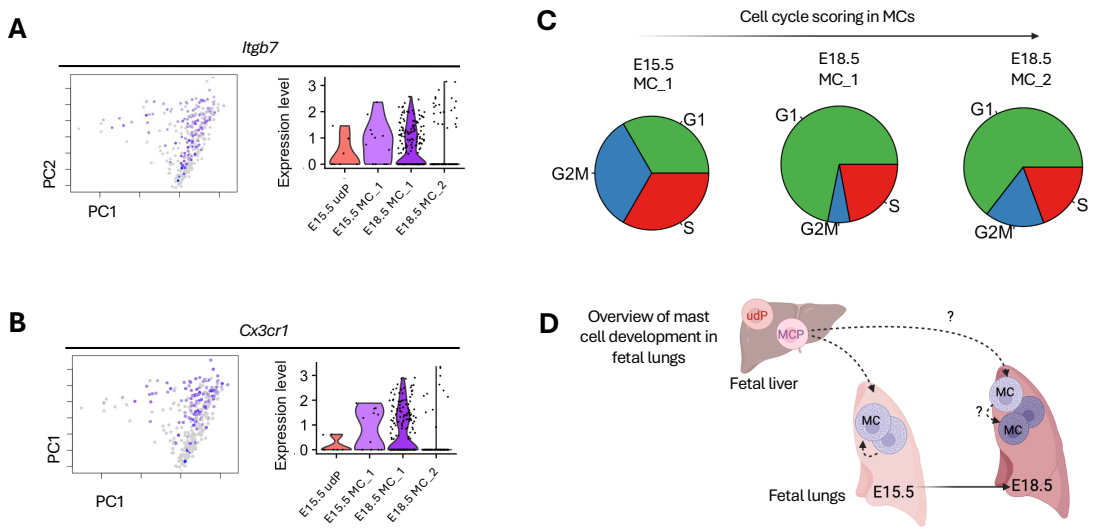

Chapter (2) Figure 14: Asynchronous developmental dynamics of mast cells in fetal lung.

(A) Feature plot embedded in PCA space (top) and corresponding violin plot (bottom) showing expression of *Itgb7* across *Cpa3*$^{+}$ populations at E15.5 and E18.5. (B) Feature plot embedded in PCA space (top) and corresponding violin plot (bottom) showing expression of *Cx3cr1* across *Cpa3*$^{+}$ populations at E15.5 and E18.5. (C) Cell cycle phase assignment of lung mast cells from E15.5 and E18.5 (D) Schematic summarising the temporal progression of mast cell progenitors and mast cells in fetal lung across developmental timepoints.

A core temporal programme underlies mast cell development but proceeds with tissue-specific kinetics

Our analyses so far revealed distinct developmental kinetics of MCs in fetal skin and lung, however they do not address whether these differences are driven by spatial tissue-specific divergence of core developmental programmes, or from differential progression along a core temporally driven developmental programme. To distinguish whether MCs diverge based on developmental stage or tissue context, we performed a principal component analysis (PCA) on MCs from fetal skin and lung at E15.5 and E18.5. Group-averaged PCA revealed that MCs at E15.5 cluster closer together than at E18.5, irrespective of tissue of residence (Figure 15A). Quantitatively, the primary axis of variation PC1 accounted for 28.8% of the total transcriptional variance, strongly separating the MCs by developmental time rather than by tissue. This suggested that developmental time explains a larger proportion of variance than tissue context at these stages and is consistent with a model in which MC development is likely governed primarily by a conserved, temporally directed transcriptional programme.

We previously described the transcriptional changes that accompanied the fetal liver MCp-to-MC differentiation between E13.5 and E15.5. To investigate if MCs followed a shared developmental programme in distinct peripheral tissues, we identified genes that were significantly upregulated (“CoreUp”) and downregulated (“CoreDown”) in the transition from E13.5 MCP to MC commitment (Figure 15B). By E15.5, MCs in both fetal skin and lung robustly increased expression of “CoreUp” genes associated with MC commitment, and this expression was maintained through E18.5 in all tissues examined (Figure 15B). In parallel, expression of MCp-associated “CoreDown” genes progressively decreased in MCs over time (Figure 15B). Representative CoreDown genes including *Gata1, Sox4, Trbc1, Gzmb, Zbtb16* were already reduced in E15.5 MCs in both the skin and lung, relative to the E13.5 liver

MCps (Figure 15C). This was accompanied by a sustained expression of CoreUp genes including *Gata2*, *Mitf, Hdc, Cma1, Tpsb2 and Cpa3* which was maintained across committed MCs from E15.5 to E18.5 (Figure 15C). Expression of *Mrgprb2*, a marker of mature CMCs in adult connective tissues (Tauber et al., 2023), was detected in both fetal skin and lung MCs but only by E18.5 (Figure 15C).

Together, these findings indicated that a shared core transcriptional programming underlying MC lineage commitment is acquired early and maintained over developmental time across tissues, while a shift towards maturational profile emerges by E18.5. Notably however, lung MCs at E15.5 retained expression of the CoreDown genes slightly more than the skin MCs at the same timepoint (Figure 15B, 15C), despite MC commitment. This indicated that tissue-specific kinetics drive differential resolution of progenitor-associated programmes and maturation, rather than divergent lineage specification.

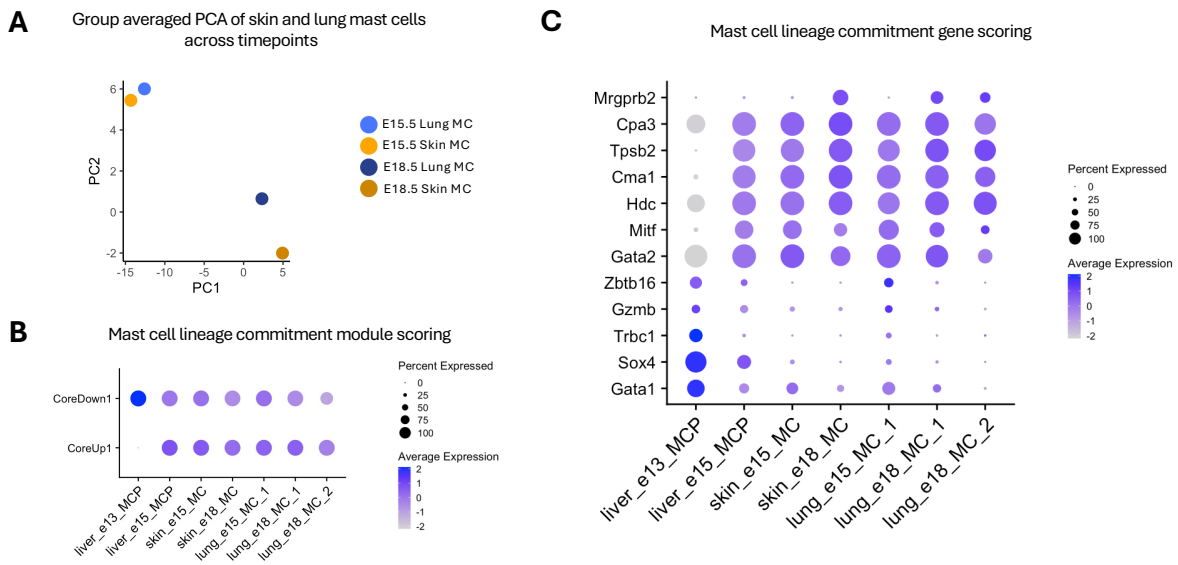

Chapter (2) Figure 15: Acquisition of a conserved mast cell lineage commitment programme across peripheral fetal tissues.

(A) Principal component analysis (PCA) of mast cells from fetal skin and lung at E15.5 and E18.5, with each dot representing the grouped average of the PCA profile of each sample. (B) Dot plot showing expression of the DEGs that are upregulated ("CoreUp") or downregulated ("CoreDown") during the transition from E13.5 fetal liver mast cell progenitors to committed mast cells, displayed across mast cell populations in the fetal liver, skin and lung at progressive developmental stages. Genes were considered significant based on adjusted p value < 0.01, and classified as upregulated or downregulated based on average log2 fold-change > 0.5 or < -0.5, respectively. (C) Expression of representative CoreDown and CoreUp genes visualised across mast cell populations in the fetal liver, skin and lung at progressive developmental stages.

Late fetal mast cells exhibit tissue-specific transcriptional imprinting

Adult CMCs exhibit transcriptional diversity across distinct sites such as the peritoneum, skin, tongue, trachea and oesophagus (Dwyer et al., 2016). We therefore asked when during development does this tissue-specific heterogeneity arise. Although we already established that MCs follow a temporal programme of development, our PCA analysis also revealed more subtle separation of MCs between fetal skin and lung MCs by E18.5 (Figure 16A). This suggested that MCs may begin to diverge in identity and exhibit subtle transcriptional differences at late developmental stages by E18.5. To investigate whether such differences extend across organs, we extended our analysis to include MCs from a third fetal tissue, the meninges, to assess if MC transcriptional identity by E18.5 could be driven by the local tissue microenvironment.

To identify MCs in the meninges, we performed single cell sequencing of the $CD45^+$ haematopoietic compartment of E18.5 meninges (as established for fetal skin and lung previously). Following quality control and unsupervised clustering, we annotated 14 clusters and identified *Cpa3*$^+$ clusters including c12_Cpa3 representing the basophil/mast cell progenitor lineage and c4_MCs (Figure S10A-D, S11A). We sub-clustered these further to reveal MCs, proliferating MC and basophil clusters at this stage (Figure S11B-C).

We then subsetted MCs we identified at E18.5 from meninges, lung, and skin tissue from our analyses so far and performed Seurat integration (Figure 16A) to account for technical variation over different sequencing runs. *Mrgprb2* was expressed in E18.5 MCs from all three organs, indicating that the upregulation of this mature CMC marker is part of the temporally defined conserved developmental programme (Figure 16B).

To address tissue-associated transcriptional differences at this stage, we performed PCA analysis on the MCs from these three tissues and averaged each group. This analysis revealed that MCs in the meninges and lung clustered closer together in PCA space than the skin MCs (Figure 16C). To further define the transcriptional features underlying the tissue-associated separation of MCs at E18.5, we next performed differential gene expression analysis between MCs in these three tissues (Figure 16D). Meningeal MCs exhibited an enrichment of genes associated with inflammatory and metabolic pathways (*Fabp7, S100a8, S100a9, Txnip, Apoe).* Lung MCs preferentially expressed genes development-associated genes (*Tph1, Igf2, Igf1r, H19)* as well as migration associated genes (*Itgb3, Cx3cr1).* Interestingly, lung and meningeal MCs share expression of metabolic genes like *Alox5ap and Alox5*. In contrast, skin MCs exhibited a canonical CMC profile, highly expressing proteases like *Mcpt4,* various cytokines (*Il6, Ccl2, Il13)* and neuropeptide substance P precursor (*Tac1).*

Together, these data indicate that although MCs acquire a shared mature identity during development, tissue-associated transcriptional diversification starts to become evident by E18.5. This late-stage diversification potentially reflects adaptation to local tissue environments and may provide an early foundation for tissue-specific heterogeneity in identity observed in adult CMCs.

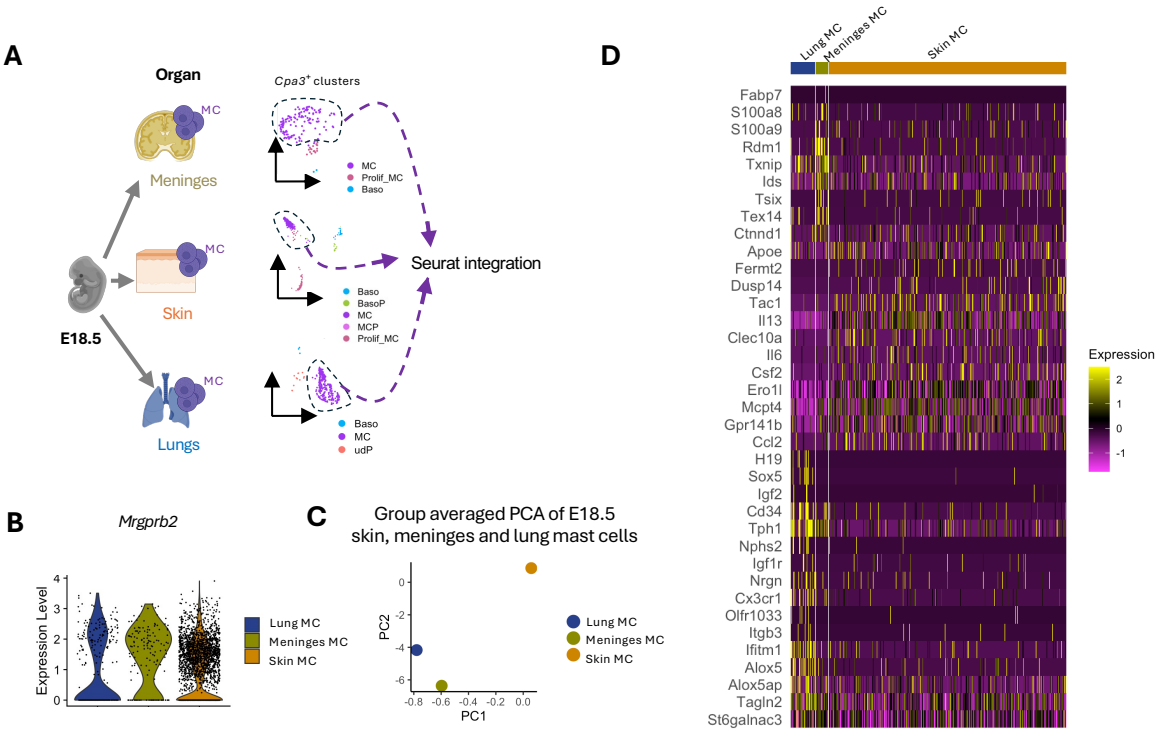

Chapter (2) Figure 16: Effects of local tissue microenvironment imprinting on mast cell identity in late fetal development.

(A) Schematic overview of workflow to assess the transcriptomic identities of mast cells at E18.5 across three fetal organs – the skin (orange), meninges (yellow) and lungs (blue). *Cpa3*$^{+}$ mast cell-basophil lineages were sub-clustered per organ, and mast cell populations from each organ were further extracted. Mast cells from each organ were then integrated together into a Seurat object using Seurat Integration. (B) Violin plot showing expression of mature connective tissue mast cell marker *Mrgprb2* across E18.5 mast cells from meninges, lung and skin. (C) PCA of E18.5 mast cells from meninges, lung and skin each dot representing the grouped average of the PCA profile of each sample. (D) Heatmap showing

top 15 differentially expressed genes between E18.5 mast cells from meninges, lung and skin.

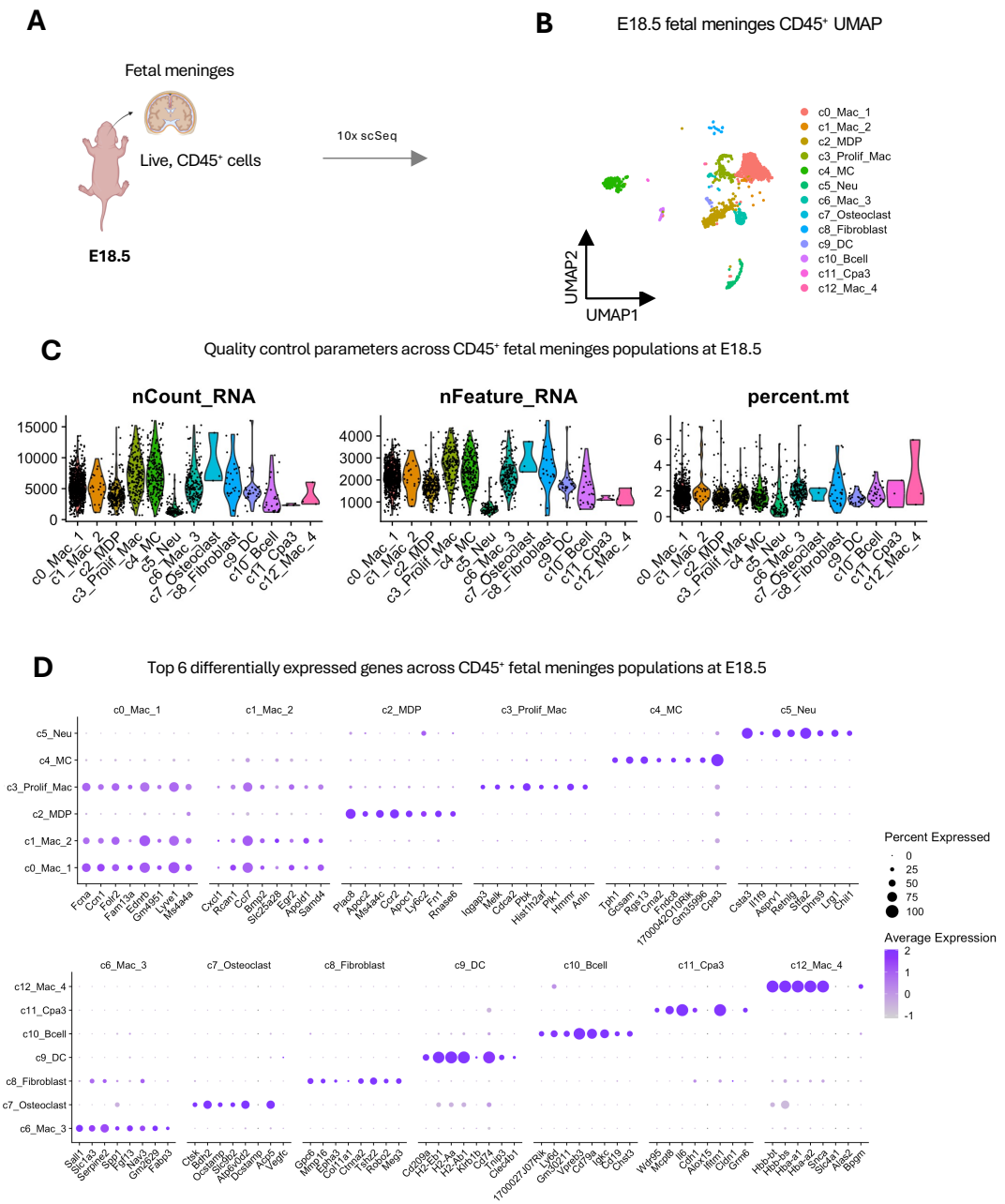

Chapter (2) Supplementary Figure S10: Single cell transcriptomic profiling of haematopoietic cells in E18.5 fetal meninges.

(A) Schematic (left) showing experimental workflow of single cell RNA sequencing (scSeq). Live CD45$^+$ haematopoietic cells were isolated from from fetal meninges of E18.5 fetuses for 10x scSeq. (B) UMAP plot of the sequenced and integrated dataset of E18.5 fetal meningeal CD45$^+$ cells (n=1883) together. Cells were dimensionally reduced followed by unsupervised clustering to reveal 13 distinct clusters. (C) Violin plots showing quality control metrics for E18.5 fetal meninges CD45$^+$ cells across identified clusters, including total RNA counts (nCount_RNA), number of detected genes (nFeature_RNA) and percentage of mitochondrial genes (percent.mt). (D) Dot plot showing the expression of top 8 differentially expressed genes across clusters identified. Colour scale indicates average expression of each gene. Dot sizes represent the percent of cells expressing each gene.

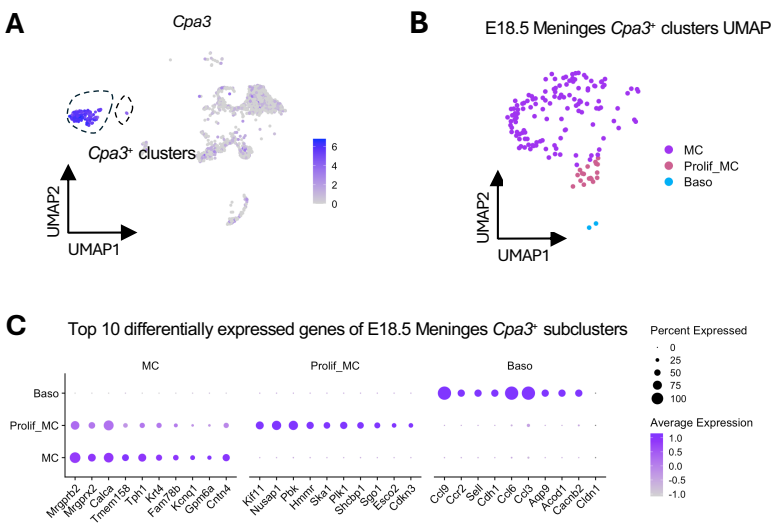

Chapter (2) Supplementary Figure S11: Meningeal *Cpa3*$^+$ mast cell-basophil populations at E18.5.

(A) UMAP feature plot showing *Cpa3* expression across fetal meningeal clusters at E18.5. (B) UMAP plot showing sub-clusters of *Cpa3*$^{+}$ clusters in E18.5 fetal meninges annotated as mast cells (MC), basophils (Baso) and proliferating MCs (Prolif_MC). (C) Dot plot showing the expression of top 10 differentially expressed genes across *Cpa3*$^{+}$ sub-clusters identified. Colour scale indicates average expression of each gene. Dot sizes represent the percent of cells expressing each gene.

Discussion

It is well established that MCs first arise within tissues during fetal haematopoiesis (Combs et al., 1965; Gentek et al., 2018a; Z. Li et al., 2018; Tauber et al., 2023). During this developmental period, other fetal immune cells like macrophages arise and establish long term tissue residency by first acquiring a core programme of macrophage identity and subsequently getting imprinted by the tissue they colonise (Mass et al., 2016). In this way, the heterogeneity of macrophages is established by the tissues they colonise, which enables them to play an integral role in organogenesis. However, it remains largely unknown how MC identity is established during embryogenesis. In this study, my findings comprehensively support a model in which MC identity is driven by a conserved, temporally ordered core transcriptional programme that is initiated in fetal liver progenitors and subsequently executed within peripheral tissues as they undergo maturation. Tissue context during these embryonic stages tunes the kinetics of progenitor programme resolution and shapes tissue-specific transcriptional imprinting as they emerge during maturation.

Previously, MCPs with immature MC phenotypes were previously detected in the fetal liver and circulation as early as E11.5 (Guiraldelli et al., 2013; Z. Li et al., 2018; Ma et al., 2025). Although hypogranular, they already begin to transcriptionally express certain MC proteases

at this stage (Guiraldelli et al., 2013; Z. Li et al., 2018; Ma et al., 2025). Fate mapping revealed that these fetal liver MCPs directly contribute to MCs seeding embryonic tissue (Ma et al., 2025). While flow cytometric analyses showed the continued presence of these MCPs in the fetal liver by E15.5, it remained unknown whether these MCPs retained their progenitor potential at this stage. Intriguingly, MC-like precursors could be detected in fetal circulation at E15.5 that appeared partially differentiated (Rodewald et al., 1996), which may reflect the shift in MC programme at this stage. Here, we show at a transcriptional single cell resolution, that fetal liver MCps undergo a substantial shift in their identity between E13.5 and E15.5 as they lose their progenitor-associated transcriptional features and acquire characteristics of MC commitment.

The transition of MCPs towards the MC lineage is marked by an upregulation of the lineage defining transcription factors *Gata2* and *Mitf*. Previous *in vitro* and *in vivo* work in adult mice has revealed that these transcription factors promote MC commitment by repressing *Cebpa*-driven basophil differentiation (Ohmori et al., 2015; Qi et al., 2013; Tojima et al., 2024), and concomitantly activating *Cpa3*, *Mcpt4, Cma1 (Mcpt5*), *Mcpt6, Mcpt7,* histidine decarboxylase (*Hdc*) (Zon et al., 1991; Kitamura et al., 2002). The earliest committed MCs already begin to express serine proteases like *Mcpt5* in embryonic tissue (Combs et al., 1965). Consistent with this, we observe upregulation of these MC genes in MCs by E15.5, indicating that the same regulatory programmes underpin MC commitment during embryogenesis. Moreover, we note that this programme is shared across MCs in fetal skin as well as fetal lung, suggesting that MC identity is established in a conserved manner across tissues. Taken together, MCs may therefore also follow a similar model to fetal macrophages (Mass et al., 2016), whereby MCPs may already establish lineage commitment prior to tissue colonisation and undergo terminal maturation in peripheral tissues.

Despite shared execution of a core MC programme, we observe marked tissue-specific differences in the rate at which progenitor-associated features are extinguished, likely driven by tissue-specific kinetics of MC development. MCPs seed fetal skin early and differentiate into MCs (Gentek et al., 2018; Li et al., 2018; Ma et al., 2025). Fate mapping revealed that MCPs only contribute to MC development within a defined window until E14.5/E15.5 (Ma et al., 2025). The expansion of MCs between E15.5 to E18.5 is therefore indicative of local MC development in this period. In line with this, we show the presence of a defined population that resembles fetal liver MCPs in the skin at E13.5, which rapidly decreases by E15.5 and are no longer detectable by E18.5.

EMP-derived macrophages migrate to peripheral tissues in the embryo using the *Cx3cr1/Cx3cl1* chemokine axis within a defined window from E8.5-E12.5 (Stremmel et al., 2018). We and others (Derakhshan et al., 2021; Gentek et al., 2018a; Z. Li et al., 2018) have shown that fetal liver MCPs also express *Cx3cr1*, suggesting that fetal MCs may also rely on this signaling axis. Moreover, the migration of MCPs into fetal skin may also be restricted to a limited window. For instance, we showed that fetal skin MCs retain expression of *Cx3cr1* at E13.5 and E15.5*,* but this is lost by E18.5. *Cx3cr1* knockout models will be needed to address the role of this signaling axis in MCP trafficking and MC development in the fetal tissues.

In addition, MCPs in fetus also likely rely on integrin signaling. Adult bone marrow-derived MCPs express integrin *Itgb7*, and is required for trafficking to peripheral gut and lung tissues (Abonia et al., 2006; Gurish et al., 2001). *Itgb7* is also expressed by fetal MCPs as early as E11.5 and give rise to MCs detectable in the skin and peritoneal cavity by E18.5 (Gentek et al., 2018a; Z. Li et al., 2018). However, phenotypically similar progenitors in the fetal liver that lack *Itgb7* do not give rise to MCs (Z. Li et al., 2018), indicating that MCPs

characteristically express *Itgb7*. It remains to be seen whether *Itgb7* is functionally required for MCPs to seed tissue and differentiate into MCs. However, *Itgb7* is also required for homing of other immune cells including T-cells, B-cells and innate lymphoid cells (Cimbro et al., 2012; Gorfu et al., 2010; Klose et al., 2014; Zhang et al., 2016), and is therefore thought to be a homing marker across immune cell populations. Use of conditional knockouts of *Itgb7* under MCP specific genes will be needed to elucidate whether fetal MCPs rely on integrin to migrate and differentiate into MCs peripherally.

The loss of MCP migration markers in fetal skin MCs by E18.5 suggests a transition from progenitor recruitment towards local maintenance mechanisms to support MC expansion and maturation. Consistent with this, our dataset revealed a subset of MCs which retain proliferative capacity even at E18.5, suggesting that they may contribute to maintenance and self-renewal of MCs in this period. Clonal tracing revealed that proliferating MCs that establish MC territories in adult skin are mature MCs themselves and express maturational effector MC genes like *Mcpt5* (Weitzmann et al., 2020). Here, we showed that the MCs maintain themselves similarly in fetal skin. Proliferating and quiescent fetal skin MCs displayed similarity in their transcriptional profiles at each stage of development, supporting a model in which fetal skin MCs undergo maturation and are maintained through local proliferation rather than through hierarchical proliferating progenitors. This model differs from other fetal-derived immune cells in the skin such as Langerhans cells and epidermal T-cells which self-renew through proliferation of immature progenitor cells (Gentek et al., 2018b; Ghigo et al., 2013).

In contrast to fetal skin, MC development in the lung appears delayed. At E15.5, fetal lung MCs are much sparser, and although they acquire the core MC programme, they retain certain MCP features including expression of *Zbtb16*. Fate-mapping needs to be performed

to resolve whether the retention of progenitor features in fetal lung MCs at this stage reflects recent recruitment or developmental plasticity. Moreover, by E18.5, fetal lung MC development does not follow a uniform maturation programme, as seen in the fetal skin. Instead, they diverge into two subsets distinguished over pseudotime analyses as a *Cx3cr1*$^{+}$*/Itgb7*$^{+}$ (MC_1) and *Cx3cr1*$^{-}$*/Itgb7*$^{-}$ (MC_2). While the *Cx3cr1*$^{+}$*/Itgb7*$^{+}$ (MC_1) subpopulation retained expression of canonical CMC proteases like *Mcpt4*, the *Cx3cr1*$^{-}$*/Itgb7*$^{-}$ (MC_2) subset exhibited a distinct transcriptional profile with a reduction in *Cpa3* expression. In adult lungs, *Itgb7*$^{+}$ MCs are associated with recent recruitment from bone marrow MCPs and subsequently develop an "MMC signature", similarly characterized by reduced *Cpa3* (Derakhshan et al., 2021). Although none of the subpopulations expressed canonical MMC proteases, it remains possible that the divergence in subpopulations reflects a subset of MCs that may become MMC-like after birth upon experiencing postnatal cues. Alternatively, the developmental plasticity in these subpopulations may serve distinct functions within the fetal lung itself.

A closely related question is whether tissue-specific differences in MC developmental kinetics are associated with tissue imprinting. To address this, I assessed whether fetal lung, meningeal and skin MCs already acquire site-specific differences in identity upon maturation by E18.5. By E18.5, skin MCs lose expression of certain genes like serotonin precursor *Tph1,* and instead acquire canonical protease expression associated with CMCs, including *Mcpt4*. Interestingly, at this stage they also upregulate expression of substance P precursor (*Tac1*), priming MCs for neuro-immune interactions early in life (Serhan et al., 2025). In contrast, MCs in the meninges preferentially expressed different markers like *S100a8, S100a9, Alox5ap.* These markers also define meningeal MC identity and functions in adult stages (Mamuladze et al., 2025), suggesting early and stable imprinting of meningeal MC identity. Interestingly, lung MCs retain expression of *Tph1,* a marker that is downregulated in skin

MCs by E18.5. This retention of markers may reflect differences in developmental kinetics if lung MCs spend less time in tissue compared to skin MCs which seed early and may progressively lose expression of these “early” effectors. Alternatively, serotonin signaling is an important driver of fetal lung development (Archambault and Delaney, 2023), and one may speculate that the retention of *Tph1* may be driven by developmental functions imposed on lung MCs at this stage.

An open area of research that remains is how the tissue microenvironment drives MC identity during development. Fibroblasts play an important role in regulating MC development in adult skin and *in vitro* cultures (Kitamura and Fujita, 1989; Kurashima et al., 2014; Levi-Schaffer et al., 1991) reflecting the importance of stromal cells in dictating MC identity. Stromal cells pay an important role in fetal tissue development (Morioka et al., 2025; Yin et al., 2024), and may therefore also influence MC development during embryogenesis.

Notably, one limitation of this study is the inability to stratify the developing MC populations by whether they derive from fetal EMP- or HSC- haematopoietic progenitors. One unanswered question is whether EMP-derived MCPs can directly seed fetal tissues like macrophages do, or whether the MCPs require a fetal liver intermediate. MC precursors could be detected in the yolk sac as early as E8.5/E9 and were found in higher numbers in the embryo proper, specifically the tail region of the developing liver, rather than in the blood, reflecting that they are preferentially homed to the fetal liver (Palis et al., 1999). Terminally differentiated, granulated MCs may appear after macrophages (Gentek et al., 2018a), which together may indicate that EMPs first pass through the fetal liver. Consistent with this, fetal liver progenitors show MC potential from E11.5 onwards (Li et al., 2018; Yoshimoto et al., 2022).

Nonetheless, other observations provide support of a more direct contribution of yolk sac EMP-derived progenitors to fetal tissue MCs. Precursors from the fetal yolk sac show MC potential until E13.5 before fetal liver haematopoiesis becomes dominant, and in fact are more efficient in generating MCs at E11.5 compared to fetal liver progenitors (Sonoda et al., 1983). Moreover, EMP-derived MCPs can already be detected in circulation and peripheral tissues at E11.5 (Z. Li et al., 2018). Further, EMP-derived MCPs in the fetal liver and peripheral skin tissue in the limbs are transcriptionally similar at E11.5 (Z. Li et al., 2018). However, they do show some transcriptional differences which suggests that they either already begin differentiating in the tissue, or alternatively, they have been recruited earlier and/or from elsewhere (possibly earlier from the yolk sac directly). All comparisons in our analyses however, are only made to fetal liver MCPs, and therefore there may still be some MCP populations which may have different features to the fetal liver MCPs. It remains possible that progenitors from yolk sac and fetal liver may contribute to MCPs and MCs with different features. Transcriptomic differences in developing MCPs and MCs across the fetal tissues analysed may reflect differences in progenitor contributions – a possibility we could not account for in our analyses. Definitively resolving whether EMP-derived MCPs can directly seed tissues or via a fetal liver intermediate will require cross-compartment comparisons of MCPs and MCs from the yolk sac, fetal liver and peripheral tissues across early and late developmental stages. Such analyses will require use of temporally controlled fate mapping approaches to trace yolk sac EMP or fetal liver HSC contributions (Gentek et al., 2018a; Z. Li et al., 2018).

A second unanswered question is whether ontogeny affects MC identity in fetal stages. At a transcriptional level at least, HSC-derived MCs in postnatal tissue were previously shown to express immunological response-associated genes, whereas EMP-derived MCs in embryonic

tissue expressed more development-associated genes (Gentek et al., 2018a; Z. Li et al., 2018). Extending fate mapping approaches to fetal development will allow comparisons of how ontogeny may affect transcriptional profiles and heterogeneity of developing MCs. Despite these apparent differences however, fate mapping previously revealed that in postnatal tissues, MCs still share a core MC programme irrespective of developmental origin (Gentek et al., 2018a; Z. Li et al., 2018).

Here we showed that even in fetal tissues, MCs appear to converge upon a shared programme of MC identity specification across all developmental stages, irrespective of origin. This suggests that origin may instead be more important in indicating tissue kinetics rather than directly impose a specific identity to the MCs. Although this needs to be further demonstrated by fate mapping, such a model would be in line with that of fetal macrophage development (Mass et al., 2016) In this case, immune cells like macrophages arise through temporally distinct "layered" haematopoietic waves to match the demands of the developing tissue, and be co-opted to facilitate and support development of the tissue it resides in (Mass and Gentek, 2021). Interestingly, MCs in fetal skin at E16.5 differ significantly from MCs in adult skin, where adult skin MCs express predominantly immune-related genes while fetal skin MCs express developmental genes (Gentek et al., 2018a). While fetal skin MCs at this stage are predominantly yolk sac derived while adult skin MCs are of a different origin and typically replaced with definitive progenitors (Gentek et al., 2018a; Z. Li et al., 2018), these differences may also reflect how embryonic tissue environment drives differences in the MCs.

Although the functions of MCs across embryonic tissues remain largely unknown in fetal development, MCs may also follow a demand-driven pattern of tissue seeding and identity imprinting following the acquisition of their core transcriptional programme. Further

research is needed to identify whether MCs may play critical developmental roles in tissue development during embryogenesis (addressed in Chapter 3).

Additional (author) contributions

Animal work: Simran Kapoor, Clara Munz and Rebecca Gentek

Technical assistance (genotyping): Solvig Becker

Preparation of sample cell suspensions and libraries: Simran Kapoor, Clara Munz and Rebecca Gentek

Single cell sorting for 10x sequencing: Clara Munz

Library generation for 10x sequencing: Meryam Beniazza

Materials and Methods

Mouse lines

Rosa26$^{lsl\text{-}DTA176}$ ("DTA176") mice (Wu et al., 2006) in this study were purchased from The Jackson Laboratory (strain #010527). In these mice, a transgene encodes for an attenuated form of Diphtheria toxin (DTA-176), with a LoxP-flanked transcriptional stop cassette upstream of the gene. Original *Cpa3*^{Cre} *Mcl-1*$^{fl/fl}$ mice were originally generated (Lilla et al., 2011) by crossing *Mcl*$^{+/fl}$ mice to *Cpa3*^{Cre} mice (generated by microinjecting the *Cpa3-Cre* transgene into embryonic stem cells in the C57BL/6J background) at Stanford University. *Cpa3*^{Cre} *Mcl-1*$^{fl/fl}$ mice in this study were obtained from Dr Phillip Starkl, MUW (Vienna, Austria), and bred to remove the *Mcl-1*$^{fl/fl}$ allele to generate the *Cpa3*-Cre mice where Cre expression is regulated under the control of the *Cpa3* promoter.

Cpa3^{Cre} *Rosa26*$^{lsl\text{-}DTA176}$ mice are a new line we generated in this study by crossing *Rosa26*$^{lsl\text{-}DTA176}$ mice to *Cpa3*-Cre mice. Upon Cre-mediated recombination under the *Cpa3* promoter, LoxP-stop-LoxP site specific recombination occurs, and the STOP codon is removed, enabling transcription of Diphtheria toxin.

Animal ethics and housing conditions

All animal work was performed under project license (PPL) number PP1871024 in accordance with the Animals (Scientific Procedures) Act 1986 (ASPA). Mice were bred and housed at the animal facility (BVS Chancellor's Building Animal Facility) in the University of Edinburgh (Edinburgh, UK) under specific pathogen-free conditions at a controlled temperature of 22^{o}C with a 12-hour light/dark cycle. Access to food (irradiated chow pellets) and water (reverse osmosis water) was available *ad libitum*.

Timed pregnancy and C-section

Rosa26$^{lsl\text{-}DTA176}$ mice were set up with *Cpa3*^{Cre} mice for timed matings. Matings were set up in either orientation (*Cpa3*$^{Cre/wt}$ x *Rosa26*$^{lsl\text{-}DTA176/\ lsl\text{-}DTA176}$ or *Cpa3*-Cre$^{Cre/Cre}$ x *Rosa26*$^{lsl\text{-}DTA176/wt}$).

Successful mating was confirmed by the presence of a vaginal plug the following morning, recorded as 0.5 days post-conception (E0.5). Plugged females were subsequently monitored and weighed at E12 to confirm pregnancy. Pregnant females (dams) were culled by cervical dislocation at chosen developmental timepoints (E15.5 or E18.5) and fetuses/newborn pups were delivered by C-section. Genotyping was performed using DNA isolated from the tail of the fetuses. Offspring were obtained at the expected Mendelian ratio, yielding approximately 50% *Cpa3* ^{Cre} targeted (*Cpa3*$^{Cre/wt}$ *Rosa26*$^{lsl\text{-}DTA176/wt}$) pups and 50% *Cpa3* ^{Cre} proficient littermate control pups lacking either the *Cpa3*^{Cre} allele (*Cpa3*$^{wt/wt}$ *Rosa26*$^{lsl\text{-}DTA176/wt}$) or the *Rosa26*$^{lsl\text{-}DTA176}$ allele (*Cpa3*$^{Cre/wt}$ *Rosa26*$^{wt/wt}$).

In case of one-hour observation analyses, each of the pups were individually placed in a 12-well plate on a heating pad to maintain temperature. Pups were monitored for up to 60 minutes, and subsequently culled by decapitation.

Preparation of sample cell suspensions and libraries

Organs were dissected from the fetuses/pups under a Leica stereomicroscope (10x magnification) and washed in phosphate buffered saline (PBS) (Life Technologies). Each sample (organ) was first mechanically cut into smaller pieces using scissors, followed by enzymatic digestion in in 0.8mg/ml Dispase II (Merck), 5mM $CaCl_2$, 10mM HEPES (Merck), 0.1mg/ml DNaseI (Roche), 3mg/ml Collagenase D (Merck) in RPMI (supplemented with 2% FCS) at 37^{o}C at 900rpm in a Thermo-Shaker (Grant-bio) for 15 minutes or until digested. The cell suspension obtained from each sample was then filtered through a 100 μm filter and

washed in FACS buffer (2% FCS, 2 mM EDTA in PBS) to stop digestion. Cell suspensions were then centrifuged at 500g for 2-5 minutes, resuspended in FACS buffer and transferred to a 98-well v-bottom plate (Corning). Samples were blocked with 0.5% anti-mouse CD16/32 Trustain Fx (Biolegend), 5% mouse serum (Invitrogen) and 5% rat serum (Merck) in FACS buffer for 20-30 minutes at 4°C. Cells were then washed with FACS buffer and centrifuged at 530g for 5 minutes at 4°C. Cells were then labelled with antibody mix diluted in FACS buffer and Brilliant Stain Buffer (BD) as detailed below for 20-30 minutes at 4°C.

Marker	**Fluorophore**	**Supplier**	**Clone number**	**Dilution**
CD45	BUV395	BD Biosciences	30-F11	1:800
CD117 (Kit)	BV650	Biolegend	2B8	1:300
CD11b	BV510	Biolegend	M1/70	1:400
F4/80	eF450	ThermoFisher Scientific	BM8	1:300
CD63	Pe/Cyanine7	Biolegend	NVG-2	1:200
ST2	APC	Biolegend	DIH9	1:200

Cells were washed with FACS buffer and acquired in FACS buffer using the FACSAria Cell Sorter (BD). DRAQ7 dye (ThermoFisher) was used in accordance to Manufacturer protocol prior to acquisition to exclude non-viable cells. Cells were pregated as live singlets and were subsequently sorted, followed by processing for multiplexing and library construction for E15.5 and E18.5 time points (see below).

E15.5 sequencing strategy

Following C-section at E15.5, fetuses were categorized as *Cpa3*^{Cre} proficient or *Cpa3*^{Cre} targeted by genotyping. Cells were FACS sorted as CD45^{+} (hematopoietic) cells from the lungs, liver and skin of fetuses from each of the two groups, as detailed in the gating strategy (M&M Figure 1). Cells were then counted using Luna FX7 to give input cell number 9k.

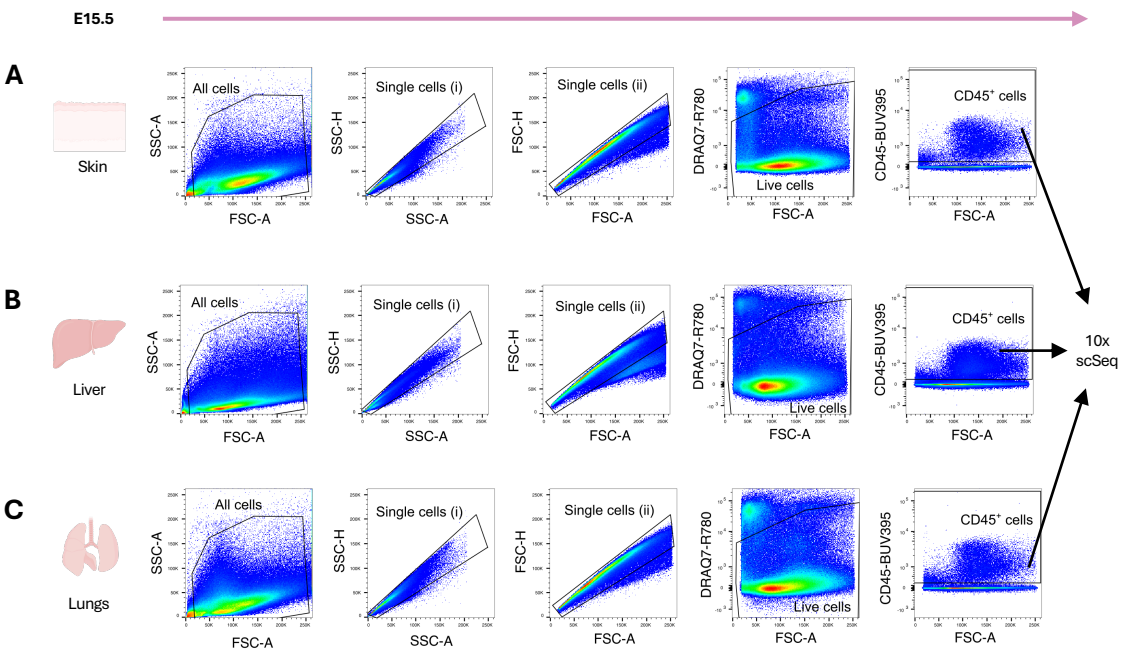

Chapter (2) M&M Figure 1: Gating strategy for sorting CD45^{+} cells in the skin, liver and lung at E15.5.

(A) Skin (B) Liver and (C) Lung tissue at E15.5 were prepared for sorting. Representative flow panels (from proficient mice) showing gating strategy for single cell sequencing. Gating was performed sequentially from left to right. Live, single cells were first selected, followed by

CD45$^+$ cells, which were subsequently sorted for 10x single cell sequencing (10x scSeq) downstream preparation.

FACS-sorted cells from different samples were multiplexed using the 10x Genomics Cell Multiplexing Oligos (CMOs), allowing multiplexing of multiple samples belonging to a specified group in a single run. Cells were first tagged by a unique CMO, and then pooled together within a library.

Two libraries (A–B) were generated as follows:
Library A: *Cpa3*^{Cre} proficient pups (pooled) lung (CD45$^+$ cells), liver (CD45$^+$ cells) and skin (CD45$^+$ cells) multiplexed together.
Library B: *Cpa3*^{Cre} targeted pups (pooled) lung (CD45$^+$ cells), liver (CD45$^+$ cells) and skin (CD45$^+$ cells) multiplexed together.

The two libraries (A-B) were prepared using the kits according to manufacturers protocol (10x Genomics) for 10x Genomics scRNA-seq 10X Genomics scRNA-seq 3' V3.1 at Edinburgh University Single Cell Facility (IRR North). Samples were sequenced at depth. Sequencing was performed using platform on sequencer (10x Genomics).

E18.5 sequencing strategy

Following C-section at E18.5, pups were monitored for one hour post-delivery. Cells were sorted from littermate pups categorized as *Cpa3*^{Cre} proficient or *Cpa3*^{Cre} targeted (stratified further as alive or dead in the one-hour observation period). From lung and skin tissue, cells were FACS sorted as CD45$^+$ (hematopoietic) cells from pups with enrichment for MCs gated

as CD45^{+} CD11b^{-} F4/80^{-} CD117^{+} (Kit^{+}) ST2^{+}, detailed in the gating strategy (M&M Figure 2). Cells were then counted using Luna FX7 to give input cell number 9k.

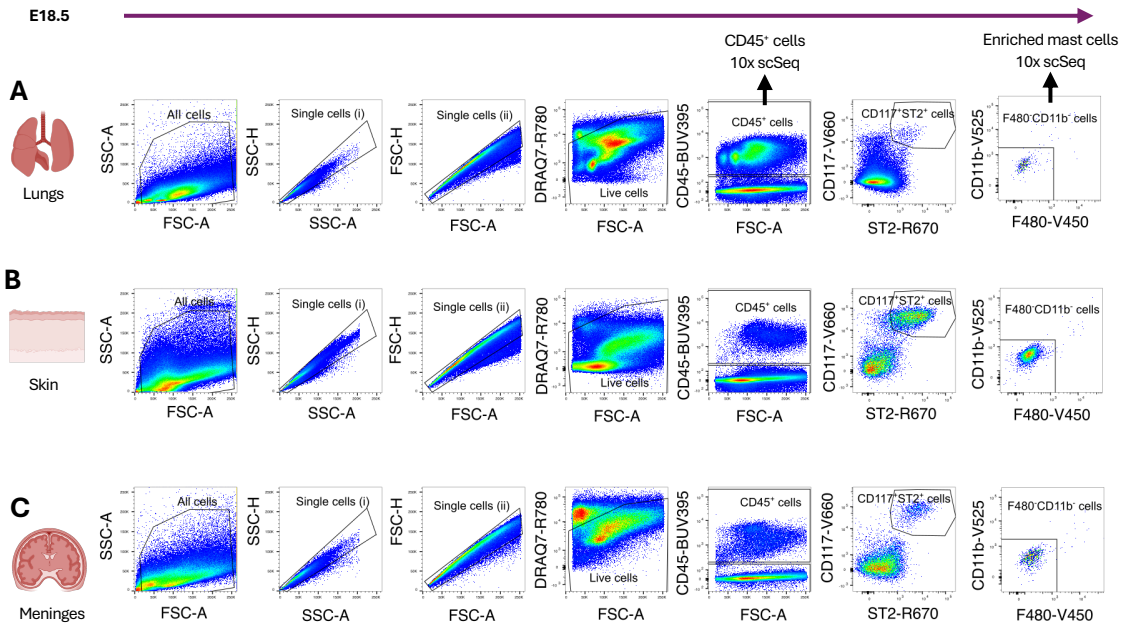

Chapter (2) M&M Figure 2: Gating strategy for sorting CD45^{+} cells, with enrichment of mast cells in the lung, skin and meninges at E18.5.

(A) Lung (B) Skin and (C) Meningeal tissues were prepared for sorting. Representative flow panels (from proficient mice) showing gating strategy for single cell sequencing. Gating was performed sequentially from left to right. Live, single cells were first selected, followed by CD45^{+} cells, which were subsequently sorted for 10x single cell sequencing (10x scSeq) downstream preparation. In addition, mast cells were enriched for during sorting by further gating of CD45^{+} cells as CD117^{+} ST2^{+} cells, and macrophages were excluded from this population by gating for F480^{-}CD11b^{-} mast cells.

For lung and skin tissue, FACS-sorted cells from different samples were multiplexed using the 10x Genomics chip preloaded with color-coded, uniquely barcoded gel beads, allowing multiplexing of multiple samples belonging to a specified group in a single run. Cells were loaded into separate wells, with each sample tagged by a unique barcode.
Four libraries (A–D) were generated as follows:
Library A: *Cpa3*^{Cre} proficient live group lung (CD45^{+} and MC) and skin (CD45^{+} and MC) samples multiplexed together.
Library B: *Cpa3*^{Cre} targeted live pup lung (CD45^{+} and MC) and skin (CD45^{+} and MC) samples multiplexed together.
Library C: *Cpa3*^{Cre} targeted dead pup lung (CD45^{+} and MC) and skin (CD45^{+} and MC) samples multiplexed together.

The libraries (A-C) were prepared using the kits according to manufacturers protocol (10x Genomics) for 10x Genomics scRNA-seq GEM-X Universal 3' v4 4 plex at Edinburgh University Single Cell Facility (IRR North). Libraries were purified using SPRIselect beads. Samples were sequenced at depth. Sequencing was performed using platform on sequencer (10x Genomics).

Meninges were sequenced as part of a different sequencing run performed earlier using a different multiplexing strategy. For meningeal tissue, FACS-sorted cells from different samples were multiplexed using the 10x Genomics Cell Multiplexing Oligos (CMOs), allowing multiplexing of multiple samples belonging to a specified group in a single run. Cells were first tagged by a unique CMO, and then pooled together within a library.

Two libraries (A–B) were generated as follows:

Library A: *Cpa3*^{Cre} proficient pups (pooled) meninges (CD45^{+} cells and enriched MCs), multiplexed together.
Library B: *Cpa3*^{Cre} targeted (live and dead) pups (pooled) meninges (CD45^{+} cells and enriched MCs), multiplexed together.

The two libraries (A-B) were prepared using the kits according to manufacturers protocol (10x Genomics) for 10x Genomics scRNA-seq 10X Genomics scRNA-seq 3' V3.1 at Edinburgh University Single Cell Facility (IRR North). Samples were sequenced at depth.

In all analyses presented in this chapter, only *Cpa3*^{Cre} proficient littermate control pups were used to establish the baseline transcriptional states in "normal" fetal development in the absence of targeting. Comparative analyses including the *Cpa3*^{Cre} targeted pups are presented in the following chapter (see Chapter 3).

Single cell sequencing (scSeq) workflow

scSeq alignment and quality control processing

Sequencing files were demultiplexed and converted to FASTQ files using CellRanger mkfastq pipelines (10x Genomics, v9.01). Reference genome was created using CellRanger mkref pipeline (10x Genomics, v9.01) by combining reference genome (GRCm38) with corresponding genomic sequence of Cre and *Rosa26*$^{lsl\text{-}DTA176}$ transgenes. Sequences were aligned to the reference genome using CellRanger (10x Genomics, v9.01). The raw reads, i.e., the Unique Molecular Identifiers (UMIs) from each library were aligned to the reference genome using CellRanger (10x Genomics, v9.01). Specifically, CellRanger multi-pipline (10x Genomics, v9.01) was used to handle multiplexing and create the raw gene-barcode matrix, comprising the number of UMIs for a specific gene associated with each valid cell barcode from each GEM multiplexed in the library (including background noise from non-true cells

like empty GEM droplets). To incorporate data from multiple GEM wells (each representing a library), CellRanger aggr pipeline (10x Genomics, v9.01) was used to create an aggregated matrix.

Downstream analysis was carried out in R (Version 2025.05.1+513) using the Seurat package (v5). First, we performed quality control of the aggregated matrix. The filtered feature-barcode matrix was filtered to remove noise and dead cells with mitochondrial gene levels >7.0 percent were removed. Gene expression was then log-normalised using the NormaliseData(), with the scale factor set to 10000. Dimensional reduction was then performed on this aggregated dataset. Highly variable features were identified via FindVariableFeatures() function selecting the top 3,000 variable genes. Scaling was performed on all genes using ScaleData() function to centre expression of each gene and standardise variance. Finally, we carried out a principal component analysis via RunPCA() function using highly variable features. The inflection point (elbow) in the elbow curve generated was used to determine the number of meaningful PCs to retain (PCs 1:35). The distribution of samples for obvious batch effects was assessed by visualising the distribution of the samples across the space of the first two PCs (PC1 vs PC2). Doublets were removed by firsti identifying maximum thresholds for total UMI counts (nCount_RNA) and genes (nFeature_RNA), where the threshold was defined as the mean plus three standard deviations of each metric across all cells. These thresholds were rounded to the nearest hundred and cells exceeding either threshold were excluded from downstream analyses. Additional suspected doublets were removed using the DoubletFinder pipeline to retain only single cells.

scSeq Seurat integration and dimensional reduction

In cases where multiple sequencing runs were combined, integration was performed using layer-based canonical correlation analysis (CCA) to account for technical variation between samples. The RNA assay was first split into layers corresponding to each individual sequencing run using the split() function. Each layer was then processed using the workflow described above, including NormalizeData(), FindVariableFeatures(), ScaleData() and RunPCA(). The embeddings were then integrated using IntegrateLayers() function by specifying the CCAIntegration method. The integrated CCA reduction was used for downstream visualisation and clustering to minimize between-group variation while preserving shared biological structure.

scSeq clustering

After quality control, each tissue was subsetted, re-normalised, and subjected to a second round of identification of highly variable features, scaling and PCA to ensure tissue-specific dimensionality reduction. To identify transcriptionally distinct clusters of cells within each tissue, a shared nearest neighbour graph was generated using the FindNeighbours() function on the basis of the biologically meaningful PCs identified (PCs 1:35). Clustering was then performed using the FindClusters() function on the basis of the Louvain clustering algorithm. Resolution for the FindClusters() function was specified on the basis of most biologically meaningful clusters. Resolution values to define the clustering granularity are specified in respective figure legends. Clusters were visualised using UMAP run via the RunUMAP() function using the top 35 PCs (PCs 1:35).

scSeq mapping

To compare cell clusters across organs and developmental stages, reference-based mapping was performed. Anchors were identified between the reference and query dataset using the FindTransferAnchors() function based on the PCA embedding of the reference. Cluster

annotations from the reference dataset were transferred to the query dataset using the TransferData() function to generate predicted cluster labels for the query cells. Predicted identities were compared with previously generated unsupervised cluster assignments to assess concordance. The query dataset was then mapped (projected) onto the reference dataset using the MapQuery() function which transferred reference annotations and projected the query cells onto the reference dataset UMAP and PCA space. This allowed for visualisation of both reference and query datasets in a shared low-dimensional space and enabled direct comparison of transcriptionally corresponding clusters while preserving the structure of the reference dataset.

scSeq differential gene expression analysis

Differential gene expression between clusters was identified using the FindMarkers() function. Marker genes were identified using a Wilcoxon rank-sum test, with p-values adjusted for multiple testing using the Bonferroni method. Genes were required to be expressed in at least 10% of cells in either of the two groups compared (min.pct = 0.1). Top differentially expressed genes were used to annotate each cluster. Where top differentially expressed genes were compared between two clusters, p-value and log2-fold change values used were denoted in legends.

Signature scorecard analysis

Gene signatures were quantified using the AddModuleScore() function, which calculates averaged expression scores for predefined gene sets while controlling for background expression. Gene signature scores were used for downstream visualisation of gene signatures across clusters.

Cell cycle scoring

Cell cycle phase assignment was performed using the CellCycleScoring() function with the updated 2019 canonical cell cycle gene sets (cc.genes.updated.2019). S-phase and G2/M phase gene lists were assigned using cc.genes.updated.2019$s.genes and cc.genes.updated.2019$g2m.genes, respectively. Cell cycle scores were calculated for each cell and cells were subsequently classified into G1, S or G2/M phases based on their relative S and G2/M scores. Cell cycle scores were used for downstream visualisation of cell-cycle variation across clusters.

scSeq trajectory analysis

Trajectory inference and pseudotime analysis were conducted in R using the Slingshot algorithm. Slingshot was applied to the PCA embedding on extracted Seurat object comprising of the Seurat clusters of interest, to infer the cellular differentiation trajectory between the clusters. Pseudotime values were computed for individual cells along the inferred lineages and visualised for each cluster along pseudotime.

To examine gene expression dynamics across pseudotime, gene-wise expression values were obtained from the Seurat object using the GetAssayData() function corresponding to log-normalised gene expression values. These gene-expression values were subsequently plotted against pseudotime for selected marker genes. Gene expression trends were estimated using a generalised additive model (GAM), fitted as y ~ s(x) to capture smooth, non-linear changes along the inferred trajectory.

Visualisation

UMAPs were visualised using the DimPlot() function. Feature plots were generated using the FeaturePlot() function. Violin plots were generated using the VlnPlot() function. Dot plots were generated using the DotPlot() function. Volcano plots were generated using the

ggplot2() function. Heatmaps were generated using pheatmap() function. Multi-plot panels were assembled using the patchwork package. Other plots generated were made using base R functions.

References

Abe, T. (1988) “Worm expulsion and mucosal mast cell response induced by repetitive IL-3 administration in Strongyloides ratti-infected nude mice,” *Immunology*, 63, pp. 181–185.

Abonia, J.P. *et al.* (2006) “Alpha-4 integrins and VCAM-1, but not MAdCAM-1, are essential for recruitment of mast cell progenitors to the inflamed lung,” *Blood*, 108(5), pp. 1588–1594. Available at: https://doi.org/10.1182/BLOOD-2005-12-012781.

Archambault, J.L. and Delaney, C.A. (2023) “A Review of Serotonin in the Developing Lung and Neonatal Pulmonary Hypertension,” *Biomedicines 2023, Vol. 11, Page 3049*, 11(11), p. 3049. Available at: https://doi.org/10.3390/BIOMEDICINES11113049.

Arinobu, Y. *et al.* (2005) “Developmental checkpoints of the basophil/mast cell lineages in adult murine hematopoiesis,” *Proceedings of the National Academy of Sciences of the United States of America*, 102(50), pp. 18105–18110. Available at: https://doi.org/10.1073/PNAS.0509148102;PAGEGROUP:STRING:PUBLICATION.

Arizono, N. *et al.* (1996) “Lung granulomatous response induced by infection with the intestinal nematode Nippostrongylusbrasiliensis is suppressed in mast cell-deficient Ws/Ws rats,” *Clinical and Experimental Immunology*, 106(1), p. 55. Available at: https://doi.org/10.1046/J.1365-2249.1996.D01-803.X.

Bankova, L.G. *et al.* (2015) “Maturation of mast cell progenitors to mucosal mast cells during allergic pulmonary inflammation in mice,” *Mucosal Immunology*, 8(3), pp. 596–606. Available at: https://doi.org/10.1038/mi.2014.91.

Blériot, C., Chakarov, S. and Ginhoux, F. (2020) “Determinants of Resident Tissue Macrophage Identity and Function,” *Immunity*, 52(6), pp. 957–970. Available at: https://doi.org/10.1016/J.IMMUNI.2020.05.014.

Chen, C.C. *et al.* (2005) “Identification of mast cell progenitors in adult mice,” *Proceedings of the National Academy of Sciences*, 102(32), pp. 11408–11413. Available at: https://doi.org/10.1073/PNAS.0504197102.

Cimbro, R. *et al.* (2012) “IL-7 induces expression and activation of integrin α4β7 promoting naive T-cell homing to the intestinal mucosa,” *Blood*, 120(13), pp. 2610–2619. Available at: https://doi.org/10.1182/BLOOD-2012-06-434779.

Combs, J.W., Lagunoff, D. and Benditt, E.P. (1965) “DIFFERENTIATION AND PROLIFERATION OF EMBRYONIC MAST CELLS OF THE RAT,” *The Journal of Cell Biology*, 25(3), p. 577. Available at: https://doi.org/10.1083/JCB.25.3.577.

Dahlin, J.S. and Hallgren, J. (2015) “Mast cell progenitors: Origin, development and migration to tissues,” *Molecular Immunology*, 63(1), pp. 9–17. Available at: https://doi.org/10.1016/J.MOLIMM.2014.01.018.

Derakhshan, T. *et al.* (2021) “Lineage-specific regulation of inducible and constitutive mast cells in allergic airway inflammation,” *Journal of Experimental Medicine*, 218(1). Available at: https://doi.org/10.1084/JEM.20200321.

Derakhshan, T. *et al.* (2025) “Human intraepithelial mast cell differentiation and effector function are directed by TGF-β signaling,” *The Journal of Clinical Investigation*, 135(1). Available at: https://doi.org/10.1172/JCI174981.

Derakhshan, T., Boyce, J.A. and Dwyer, D.F. (2022) “Defining mast cell differentiation and heterogeneity through single cell transcriptomics analysis,” *The Journal of allergy and clinical immunology*, 150(4), p. 739. Available at: https://doi.org/10.1016/J.JACI.2022.08.011.

Dwyer, D.F. *et al.* (2016) “Expression profiling of constitutive mast cells reveals a unique identity within the immune system,” *Nature Immunology*, 17(7), pp. 878–887. Available at: https://doi.org/10.1038/ni.3445.

Friend, D.S. *et al.* (1996) “Mast cells that reside at different locations in the jejunum of mice infected with Trichinella spiralis exhibit sequential changes in their granule ultrastructure and chymase phenotype,” *Journal of Cell Biology*, 135(1), pp. 279–290. Available at: https://doi.org/10.1083/jcb.135.1.279.

Friend, D.S. *et al.* (1998) “Reversible Expression of Tryptases and Chymases in the Jejunal Mast Cells of Mice Infected with Trichinella spiralis,” *The Journal of Immunology*, 160(11), pp. 5537–5545. Available at: https://doi.org/10.4049/JIMMUNOL.160.11.5537.

Galli, S.J. and Tsai, M. (2012) “IgE and mast cells in allergic disease,” *Nature medicine*, 18(5), p. 693. Available at: https://doi.org/10.1038/NM.2755.

Gentek, R. *et al.* (2018) “Hemogenic Endothelial Fate Mapping Reveals Dual Developmental Origin of Mast Cells,” *Immunity*, 48(6), pp. 1160-1171.e5. Available at: https://doi.org/10.1016/j.immuni.2018.04.025.

Gorfu, G. *et al.* (2010) “Beta7 integrin deficiency suppresses B cell homing and attenuates chronic ileitis in SAMP1/YitFc mice,” *Journal of immunology (Baltimore, Md. : 1950)*, 185(9), pp. 5561–5568. Available at: https://doi.org/10.4049/JIMMUNOL.0903938.

Guiraldelli, M.F. *et al.* (2013) “Rat Embryonic Mast Cells Originate in the AGM,” *PLOS ONE*, 8(3), p. e57862. Available at: https://doi.org/10.1371/JOURNAL.PONE.0057862.

Gurish, M.F. *et al.* (2001a) “Intestinal mast cell progenitors require CD49dbeta7 (alpha4beta7 integrin) for tissue-specific homing,” *The Journal of experimental medicine*, 194(9), pp. 1243–1252. Available at: https://doi.org/10.1084/JEM.194.9.1243.

Gurish, M.F. *et al.* (2001b) “Intestinal Mast Cell Progenitors Require CD49dβ7 (α4β7 Integrin) for Tissue-specific Homing,” *The Journal of Experimental Medicine*, 194(9), p. 1243. Available at: https://doi.org/10.1084/JEM.194.9.1243.

Hagel, A.F. *et al.* (2013) “Mast cell tryptase levels in gut mucosa in patients with gastrointestinal symptoms caused by food allergy,” *International archives of allergy and immunology*, 160(4), pp. 350–355. Available at: https://doi.org/10.1159/000341634.

Kitamura, Y. *et al.* (1977) “Development of mast cells from grafted bone marrow cells in irradiated mice,” *Nature*, 268(5619), pp. 442–443. Available at: https://doi.org/10.1038/268442A0.

Kitamura, Y. *et al.* (1983) “Different Radiosensitivities of Mast-Cell Precursors in the Bone Marrow and Skin of Mice,” *Radiation Research*, 93(1), pp. 147–156. Available at: https://doi.org/10.2307/3575950.

Kitamura, Y. *et al.* (2002) “Regulation of Mast Cell Phenotype by MITF,” *International Archives of Allergy and Immunology*, 127(2), pp. 106–109. Available at: https://doi.org/10.1159/000048178.

Kitamura, Y. and Fujita, J. (1989) “Regulation of M a s t Cell Differentiation,” 10(6). Available at: https://doi.org/10.1002/bies.950100604.

Klose, C.S.N. *et al.* (2014) “Differentiation of type 1 ILCs from a common progenitor to all helper-like innate lymphoid cell lineages,” *Cell*, 157(2), pp. 340–356. Available at: https://doi.org/10.1016/j.cell.2014.03.030.

Krystel-Whittemore, M., Dileepan, K.N. and Wood, J.G. (2016) “Mast cell: A multi-functional master cell,” *Frontiers in Immunology*. Frontiers Media S.A. Available at: https://doi.org/10.3389/fimmu.2015.00620.

Kurashima, Y. *et al.* (2014) “The Enzyme Cyp26b1 Mediates Inhibition of Mast Cell Activation by Fibroblasts to Maintain Skin-Barrier Homeostasis,” *Immunity*, 40(4), pp. 530–541. Available at: https://doi.org/10.1016/J.IMMUNI.2014.01.014.

Levi-Schaffer, F., Segal, V. and Shalit, M. (1991) “Effects of interleukins on connective tissue type mast cells co-cultured with fibroblasts,” *Immunology*, 72(2), p. 174. Available at: https://pmc.ncbi.nlm.nih.gov/articles/PMC1384480/ (Accessed: December 17, 2025).

Li, Z. *et al.* (2018) “Adult Connective Tissue-Resident Mast Cells Originate from Late Erythro-Myeloid Progenitors,” *Immunity*, 49(4), pp. 640-653.e5. Available at: https://doi.org/10.1016/j.immuni.2018.09.023.

Ma, W. *et al.* (2025) “Embryonic mast cells arise from the Cpa3-expressing precursors but not granulocyte-monocyte progenitors,” *Science China Life Sciences* [Preprint]. Available at: https://doi.org/10.1007/s11427-024-2891-1.

MacDonald, T.T., Murray, M. and Ferguson, A. (1980) “Nippostrongylus brasiliensis: Mast cell kinetics at small intestinal sites in infected rats,” *Experimental Parasitology*, 49(1), pp. 9–14. Available at: https://doi.org/10.1016/0014-4894(80)90050-8.

Mamuladze, T. *et al.* (2025) “Mast cells regulate the brain-dura interface and CSF dynamics,” *Cell*, 188(20), pp. 5487-5498.e16. Available at: https://doi.org/10.1016/j.cell.2025.06.046.

Mass, E. *et al.* (2016) “Specification of tissue-resident macrophages during organogenesis,” *Science*, 353(6304). Available at: https://doi.org/10.1126/SCIENCE.AAF4238/SUPPL_FILE/MASS.SM.PDF.

Mass, E. and Gentek, R. (2021) “Fetal-Derived Immune Cells at the Roots of Lifelong Pathophysiology,” *Frontiers in Cell and Developmental Biology*, 9, p. 648313. Available at: https://doi.org/10.3389/FCELL.2021.648313/FULL.

Mayrhofer, G. (1979) “The nature of the thymus dependency of mucosal mast cells: I. An adaptive secondary response to challenge with Nippostrongylus brasiliensis,” *Cellular Immunology*, 47(2), pp. 304–311. Available at: https://doi.org/10.1016/0008-8749(79)90340-X.

McSorley, H.J., Chayé, M.A.M. and Smits, H.H. (2018) “Worms: Pernicious parasites or allies against allergies?,” *Parasite Immunology*, 41(6), p. e12574. Available at: https://doi.org/10.1111/PIM.12574.

Metcalfe, D.D., Baram, D. and Mekori, Y.A. (1997) “Mast cells,” *Physiological reviews*, 77(4), pp. 1033–1079. Available at: https://doi.org/10.1152/PHYSREV.1997.77.4.1033.

Meurer, S.K. *et al.* (2025) “TGF-β1 Induces Mucosal Mast Cell Genes and is Negatively Regulated by the IL-3/ERK1/2 Axis,” *Cell Communication and Signaling : CCS*, 23(1), p. 76. Available at: https://doi.org/10.1186/S12964-025-02048-8.

Morioka, N., Ganier, C. and Watt, F.M. (2025) “Fetal Fibroblast Heterogeneity Defines Dermal Architecture during Human Embryonic Skin Development,” *Journal of Investigative*

Dermatology, 145(5), pp. 1081-1091.e7. Available at: https://doi.org/10.1016/J.JID.2024.12.027.

Nakano, N. *et al.* (2021) "Mucosal Mast Cell–Specific Gene Expression Is Promoted by Interdependent Action of Notch and TGF-β Signaling," *The Journal of Immunology*, 207(12), pp. 3098–3106. Available at: https://doi.org/10.4049/JIMMUNOL.2100112.

Ohmori, S.N.Y. *et al.* (2015) "GATA2 is critical for the maintenance of cellular identity in differentiated mast cells derived from mouse bone marrow," *Blood*, 125(21), pp. 3306–3315. Available at: https://doi.org/10.1182/BLOOD-2014-11-612465.

Palis, J. *et al.* (1999) "Development of erythroid and myeloid progenitors in the yolk sac and embryo proper of the mouse," *Development (Cambridge, England)*, 126(22), pp. 5073–5084. Available at: https://doi.org/10.1242/DEV.126.22.5073.

Qi, X. *et al.* (2013) "Antagonistic regulation by the transcription factors C/EBPα and MITF specifies basophil and mast cell fates," *Immunity*, 39(1), p. 97. Available at: https://doi.org/10.1016/J.IMMUNI.2013.06.012.

Reber, L.L. *et al.* (2015) "Potential effector and immunoregulatory functions of mast cells in mucosal immunity," *Mucosal Immunology*, 8(3), pp. 444–463. Available at: https://doi.org/10.1038/MI.2014.131.

Rodewald, H.R. *et al.* (1996) "Identification of a committed precursor for the mast cell lineage," *Science*, 271(5250), pp. 818–822. Available at: https://doi.org/10.1126/SCIENCE.271.5250.818.

Ruitenberg, E.J. and Elgersma, A. (1976) "Absence of intestinal mast cell response in congenitally athymic mice during Trichinella spiralis infection," *Nature*, 264(5583), pp. 258–260. Available at: https://doi.org/10.1038/264258A0.

Schwarzer, M. *et al.* (2019) "Germ-Free Mice Exhibit Mast Cells With Impaired Functionality and Gut Homing and Do Not Develop Food Allergy," *Frontiers in immunology*, 10(FEB). Available at: https://doi.org/10.3389/FIMMU.2019.00205.

da Silva, E.Z.M., Jamur, M.C. and Oliver, C. (2014) “Mast Cell Function: A New Vision of an Old Cell,” *Journal of Histochemistry and Cytochemistry*, 62(10), p. 698. Available at: https://doi.org/10.1369/0022155414545334.

Sonoda, T., Hayashi, C. and Kitamura’, Y. (1983) *Presence of Mast Cell Precursors in the Yolk Sac of Mice*, *DEVELOPMENTAL BIOLOGY*.

Stremmel, C. *et al.* (2018) “Yolk sac macrophage progenitors traffic to the embryo during defined stages of development,” *Nature communications*, 9(1). Available at: https://doi.org/10.1038/S41467-017-02492-2.

Tauber, M. *et al.* (2023) “Landscape of mast cell populations across organs in mice and humans,” *Journal of Experimental Medicine*, 220(10). Available at: https://doi.org/10.1084/jem.20230570.

Tojima, R. *et al.* (2024) “Roles of C/EBPα, GATA2, TGF-β-signaling, and epigenetic regulation in the expression of basophil-specific protease genes.” Available at: https://doi.org/10.1101/2024.02.24.581851.

Tu, L.L. *et al.* (2005) “Notch signaling is an important regulator of type 2 immunity,” *The Journal of Experimental Medicine*, 202(8), p. 1037. Available at: https://doi.org/10.1084/JEM.20050923.

West, P.W. and Bulfone-Paus, S. (2022) “Mast cell tissue heterogeneity and specificity of immune cell recruitment,” *Frontiers in Immunology*, 13, p. 932090. Available at: https://doi.org/10.3389/FIMMU.2022.932090/FULL.

Xing, W. *et al.* (2011) “Protease phenotype of constitutive connective tissue and of induced mucosal mast cells in mice is regulated by the tissue,” *Proceedings of the National Academy of Sciences of the United States of America*, 108(34), pp. 14210–14215. Available at: https://doi.org/10.1073/PNAS.1111048108/-/DCSUPPLEMENTAL.

Yang, B. *et al.* (2013) “Food allergen-induced mast cell degranulation is dependent on PI3K-mediated reactive oxygen species production and upregulation of store-operated calcium

channel subunits," *Scandinavian Journal of Immunology*, 78(1), pp. 35–43. Available at: https://doi.org/10.1111/SJI.12062;REQUESTEDJOURNAL:JOURNAL:13653083.

Yin, Y. *et al.* (2024) "Identification of a myofibroblast differentiation program during neonatal lung development," *Development (Cambridge)*, 151(9). Available at: https://doi.org/10.1242/DEV.202659/347303.

Yoshimoto, M. *et al.* (2022) "Mast Cell Repopulating Ability Is Lost During the Transition From Pre-HSC to FL HSC," *Frontiers in Immunology*, 13. Available at: https://doi.org/10.3389/fimmu.2022.896396.

Zhang, H.L. *et al.* (2016) "Regulatory T-cell depletion in the gut caused by integrin β 7 deficiency exacerbates DSS colitis by evoking aberrant innate immunity," *Mucosal Immunology*, 9(2), pp. 391–400. Available at: https://doi.org/10.1038/mi.2015.68.

Zon, L.I. *et al.* (1991) "GATA-binding transcription factors in mast cells regulate the promoter of the mast cell carboxypeptidase A gene.," *Journal of Biological Chemistry*, 266(34), pp. 22948–22953. Available at: https://doi.org/10.1016/S0021-9258(18)54446-X.

Chapter 3

Targeting Cpa3-expressing cells impairs embryonal development and leads to neonatal lethality

Introduction

The immune system is classically known for its role in protection against infections. In addition to directly eliminating pathogens, immune cells can orchestrate tissue remodelling processes that can contribute to tissue regeneration. However, tissue remodelling functions of immune cells are frequently associated with fibrotic pathogenesis in the context of chronic and dysregulated inflammation (Arinda et al., 2022). This has been well established in immune cells such as macrophages, whose functional identity depends on the stimulatory cues encountered during their development (Park et al., 2022). In inflammatory contexts, macrophages can adopt disease-associated functions that may drive pathology (Park et al., 2022); however, macrophages also constitutively reside within tissues under homeostatic conditions, where they play an important role in various developmental processes (Guan et al., 2025; Mosser et al., 2020; Nobs and Kopf, 2021; Park et al., 2022). Tissue residency of macrophages first emerges during the early haematopoeitic waves in embryonic development (Ginhoux and Guilliams, 2016). These haematopoietic waves also give rise to erythrocytes (Baron et al., 2013; Palis and Segel, 1998), as well as megakaryocytes (Palis et al., 2004). These cells play a critical role in maintaining vasculature and oxygenation to support embryonic development and therefore develop from the earliest haematopoietic wave during embryogenesis (McGrath et al., 2003). Following the initial establishment of the circulatory system, organogenesis proceeds in a highly spatial and temporally regulated

manner to develop organ systems in preparation for birth and postnatal survival, and defects in development of these tissues often manifest as neonatal lethality (Turgeon and Meloche, 2009). As such, developmental programmes that support organogenesis are subject to strong evolutionary selective pressure (Chow and Bentley, 2025; Coall et al., 2015).

Organogenesis requires coordinated functions of vascular, neural, epithelial and stromal cells during embryonic development (Daniel and Cleaver, 2019). Increasing evidence indicates that fetal-derived immune cells arising during this embryonic period are not generated solely in anticipation for postnatal functions. The identity of most tissue resident macrophages is specified by the organs that they reside in during development, suggesting that they may be integral to organogenesis (Mass et al., 2016). As such, the origin of immune cells early in fetal haematopoiesis may be "demand driven" to support development of fetal tissues as they emerge (Feyaerts et al., 2022; Mass and Gentek, 2021). For instance, microglia are the earliest macrophage populations to arise during fetal development and play an essential role in facilitating structural morphogenesis and synaptic pruning to shape the nervous system at these stages (Cabirol et al., 2022; Lawrence et al., 2024).

Mast cells (MCs) are another type of tissue resident immune cell whose embryonic origins are now well established (Gentek et al., 2018a; Z. Li et al., 2018). MCs also arise from the first wave of haematopoiesis in the yolk sac, following which they are replenished by fetal liver-derived precursors with tissue-specific kinetics (Gentek et al., 2018a; Z. Li et al., 2018). Unlike macrophages however, the physiological role of MCs in fetal tissues remains unknown. Their role has been predominantly described in the context of allergy and helminth infections in adult tissues, where they are mediators of a type 2 immune response (Amin, 2012; Pennock and Grencis, 2006b). MCs in neonates may already be responsive

to maternal IgE, sensitising and priming them to mediate allergic reactions postnatally (Msallam et al., 2020). Although dysregulated type 2 immune responses result in pathological tissue remodelling, it may be important for tissue regeneration in physiological conditions (Gieseck et al., 2018). Within tissues, MCs have been shown to interact with nerves, fibroblasts and blood vessels (Cairns, 1998; Krystel-Whittemore et al., 2016b), which may be beneficial in developmental contexts such as organogenesis. Since MCs arise during fetal development when active organogenesis is ongoing, it is therefore tempting to speculate whether MCs play physiologically relevant tissue development roles.

Notably, overt congenital defects associated with mast cell deficiency have not been clinically reported (Rodewald & Feyerabend, 2012). This raises the possibility that the absence of mast cells may be inconspicuous in the absence of a phenotype. An alternative plausible hypothesis is that a total absence of mast cells results in defective embryonic development and neonatal lethality, and is therefore masked in the surviving adult population. Although this possibility has been less explored, two reasons may support this hypothesis. First, MCs are already established and mature within fetal tissues between E15.5 and E18.5 - a critical window of organogenesis - positioning them to influence development of tissues that are required for survival at birth. Secondly, MCs and their effector mechanisms are strongly conserved across vertebrates and even non-vertebrates, where they have been implicated in facilitating processes associated with wound repair and tissue remodelling, suggesting an evolutionary constraint on these functions in MCs (St. John et al., 2023).

Although commonly used genetic mouse models employed so far have not revealed such a role for MCs, it is important to note that these models are inherently confounded. The most common genetic model used to target MCs are based on targeting c*Kit* signaling, which is

critical in regulating MC development (Tsai et al., 2022). c*Kit*-based MC targeting has revealed that MCs may play a role in promoting innervation and vascularisation in neonatal cornea (Liu et al., 2015). Deficiency in c*Kit* receptor (Kitamura et al., 1978) directly impairs development of both MC precursors and mature MCs. However, these models also impair c*Kit* signaling in haematopoietic stem cells (HSCs) and have notable off-target effects on other lineages including erythrocytes (Sharma et al., 2007; Waskow et al., 2004). Consequently, mice with homozygous *cKit* mutations are severely anaemic and die shortly after birth (Waskow et al., 2004). However, these defects were unlikely to be due to the absence of MCs, as these mice could be rescued by erythropoietin (Waskow et al., 2004). Moreover, *cKit*-deficient mice do not completely target MCs during embryonic development, as residual MCs are still detected early after birth (Kitamura et al., 1978). Moreover, c*Kit* signaling has been shown to be dispensable for early MC development, at least *in vitro* (Dahlin et al., 2017).

Alternative approaches to c*Kit*-based targeting have been developed recently. *Cpa3* is a protease that is constitutively expressed in most MC subsets, unlike *Karma* and *Mcpt5* which are largely restricted to mature connective tissue type MCs (Atiakshin et al., 2022; Dwyer et al., 2016; Mattiuz et al., 2018). Moreover, *Cpa3* expression has also been identified in MC precursors in the yolk sac and fetal liver (Ma et al., 2025) (See Chapter 2). As such, *Cpa3* may represent an attractive candidate marker for targeting MCs early in development.

However, currently used *Cpa3*-based genetic targeting models have several limitations. One such system is the "Hello Kitty" *Cpa3*^{Cre} *Mcl-1*$^{fl/fl}$ model which conditionally deletes the anti-apoptotic regulator *Mcl-1* in *Cpa3*-expressing MCs, exploiting their sensitivity to apoptosis in the absence of *Mcl-1* (Lilla et al., 2011), However, the system relies on floxing out the *Mcl-1* gene to achieve efficient conditional knockouts. Yet, different cells have different

sensitivity to *Mcl-1* (Chin and Fu, 2021), and it remains unknown whether fetal MCs and their precursors are also sensitive to this method of targeting.

An alternative is the "Cre-Master" *Cpa3*$^{Cre/Cre}$ model, which uses Cre-based genotoxicity to target cells depending on the extent of *Cpa3* expression (Feyerabend et al., 2011). Although the model efficiently targets mature MCs in postnatal tissues, basophil-MC precursors which express lower levels of *Cpa3* are incompletely targeted in adults (Feyerabend et al., 2011). However, *Cpa3* expression may vary in embryonic stages as well, where fetal MC precursors and subtypes in tissues may also express lower *Cpa3* levels that may not be sufficient to induce Cre toxicity (See Chapter 2). Therefore the "Cre-Master" model may be less reliable to constitutively target MC developmental programmes.

Here, we re-visit the paradigm of MC roles in development and investigate whether genetically targeting *Cpa3*-expressing lineages may reveal previously undescribed roles of MCs in embryonic development. By combining *Cpa3* Cre-based targeting with diphtheria toxin, we developed a novel genetic model – *Cpa3*^{Cre} *Rosa26*$^{lsl\text{-}DTA}$ to attempt to target MCs and their precursors broadly across embryonic tissues. Given the universal sensitivity of cells to diphtheria toxin, this system may overcome the limitations of previous models by increasing the sensitivity of cells expressing even low levels of *Cpa3* (Li et al., 2021). Strikingly, we discovered that *Cpa3*^{Cre} targeted mice in this genetic model die of neonatal lethality shortly after birth, accompanied by signs of respiratory distress and evidence of impaired lung development. However, we found that *Cpa3* targeting did not result in a complete ablation of MCs during fetal development, and remaining MCs appeared to have proliferative activity and reduced degranulation *in situ*. In addition, we also unexpectedly observed a reduction of platelets in *Cpa3*^{Cre} targeted neonates. This overlap raises the possibility that these lineages may share developmental trajectories during fetal

haematopoiesis, and perturbation of a *Cpa3*-expressing developmental branch may result in impaired tissue development during embryogenesis.

Results

Cpa3 is expressed early in fetal mast cell development

To establish the MC targeting model, we first evaluated which available Cre driver genes would be most suitable to target MC development early and across tissues during embryogenesis. Using the transcriptomic datasets generated in Chapter 2, we identified MC clusters and examined the expression of MC Cre driver genes available in our lab – including *Cpa3, Karma (Gpr141b)* and *Mcpt5 (Cma1)*.

We first looked at gene expression within MCs developing in peripheral tissues, specifically the skin and lung as they represent two distinct niches: the skin is rich in connective tissue, whereas the lung comprises a mixed connective/mucosal tissue environment. To capture key stages of fetal MC maturation, we assessed how gene expression levels shift between E15.5 and E18.5 to capture the period of MC maturation during normal fetal development in *Cpa3*^{Cre} proficient (untargeted) mice. Following unsupervised clustering on the CD45^{+} compartment, we detected MC clusters in both fetal skin and lung transcriptomic datasets (Figure S1A, S1B), based on expression of MC-specific differential gene expression (See Chapter 2). Within the MC cluster, *Cpa3* and *Mcpt5* were expressed consistently and robustly at E15.5, with expression increasing further by E18.5 in both tissues (Figure 1A, 1B). In contrast, *Karma* expression was temporally delayed, with low expression at E15.5 increasing only later by E18.5, and this was more prominent in the skin than in the lung (Figure 1C). These data suggested that *Cpa3* and *Mcpt5* genes are expressed strongly in MCs

even early in fetal development across tissues, whereas *Karma* expression emerges later and in a more restricted manner.

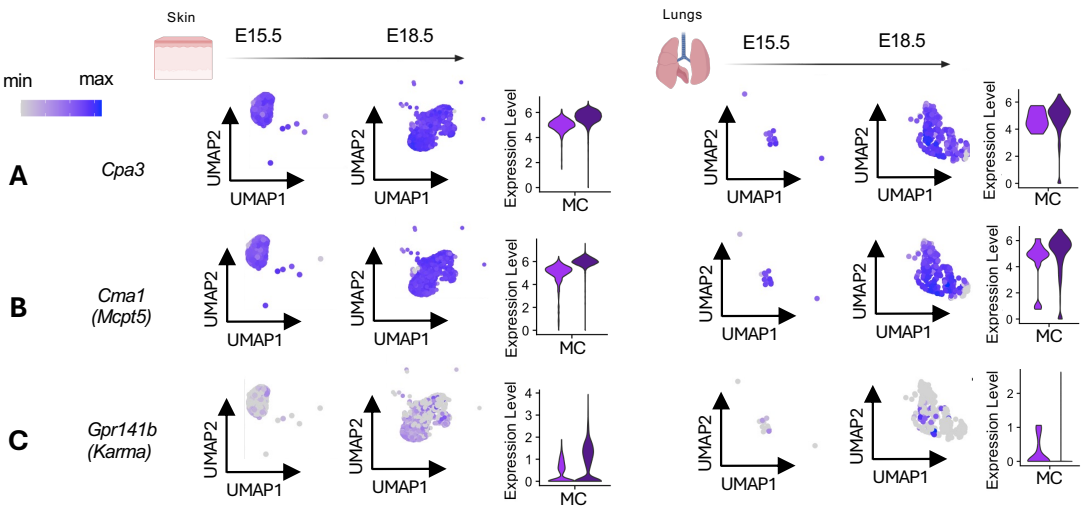

Chapter (3) Figure 1: Gene expression dynamics of developing mast cells in fetal tissues.

Single cell transcriptomic analysis of CD45^{+} mast cell (MC) clusters (shown in Figure S1A, S1B) from fetal skin (left) and lung (right) at E15.5 and E18.5. Feature plots and violin plots showing expression levels of (A) *Cpa3* (B) *Cma1 (Mcpt5)* (C) *Gpr141b (Karma)* in the MC clusters identified in fetal skin and fetal lung.

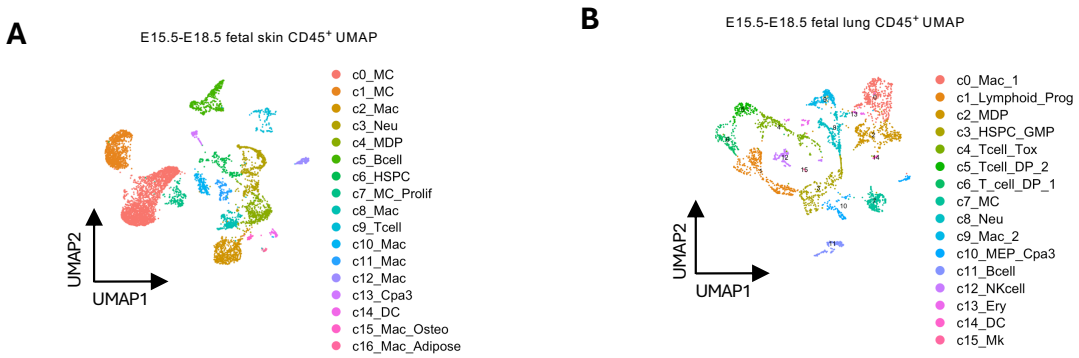

Chapter (3) Supplementary Figure S1: Identification of mast cell populations in fetal skin and lung.

(A) Clusters identified in the proficient fetal skin dataset merged between E15.5 and E18.5, including mast cell clusters c0_MC, c1_MC and c7_MC_Prolif. (B) Clusters identified in the proficient fetal lung dataset merged between E15.5 and E18.5, including mast cell clusters c7_MC. Differentially expressed genes used to identify and annotate the clusters described in Chapter 2.

Given that MCs express both *Mcpt5* and *Cpa3* throughout development in the peripheral tissues examined, we next examined whether their precursors in the fetal liver show similar gene expression patterns earlier in development. Fetal liver progenitors contribute to MC seeding in peripheral tissues (Gentek et al., 2018a; Z. Li et al., 2018; Ma et al., 2025) (Figure 2A), and previous transcriptomic analysis by Ma et al. (2025) led to the identification of *Cpa3*$^{+}$ progenitors in the fetal liver which contribute to MC development in peripheral tissues as early as E13.5. Their *Cpa3*$^{+}$ fetal liver progenitor dataset revealed subpopulations of basophils (Baso), basophil progenitors (BasoP), mast cell progenitors (MCP) and MCs at

E13.5 (Figure 2B, S2A, S2B). At E13.5, we found that MCPs already begin to express *Cpa3*, but not *Mcpt5* nor *Karma* (Figure 2C), suggesting that *Cpa3* expression in MCPs precedes MC maturation. These findings indicate that among the Cre driver genes assessed, *Cpa3* is expressed the earliest during fetal MC development.

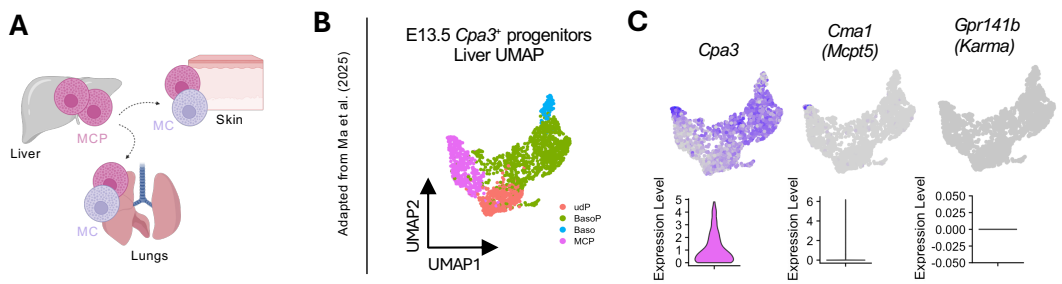

Chapter (3) Figure 2: Gene expression dynamics in mast cell-basophil progenitors in fetal liver at E13.5.

(A) Schematic illustrating the contribution of fetal liver progenitors to mast cells (MCs) in peripheral tissues, including skin and lung, during development. In the fetal liver, progenitors commit to the mast cell lineage and become mast cell progenitors (MCP), following which they seed peripheral tissues like skin and lung, where they differentiate into MCs (See Chapter 2). (B) UMAP plot of the *Cpa3*$^{+}$ sub-clustered fetal liver dataset at E13.5 generated in Chapter 2, adapted from (Ma et al., 2025). UMAP shows basophils (Baso), basophil progenitors (BasoP), mast cell progenitors (MCP) and mast cells (MCs). (C) Feature plots (top) and violin plots (bottom) showing expression level of *Cpa3, Cma1 (Mcpt5)* and *Gpr141b (Karma)* across the *Cpa3*$^{+}$ fetal liver sub-populations.

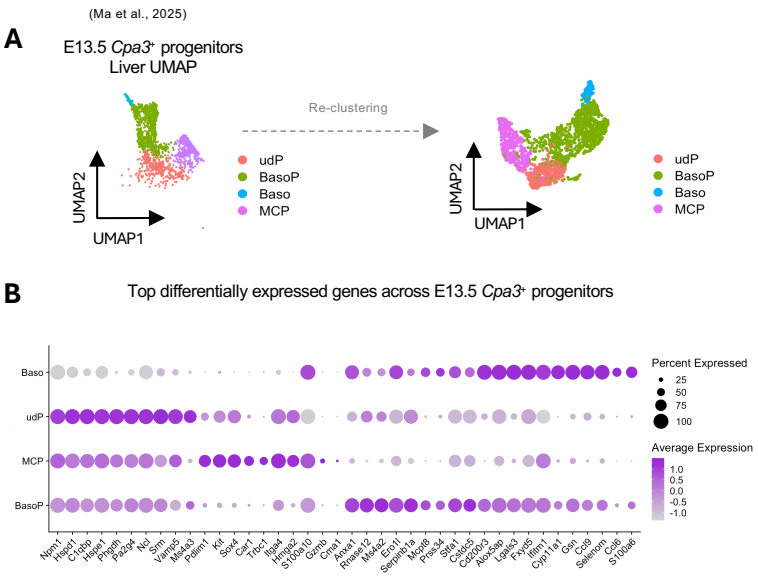

Chapter (3) Supplementary Figure S2: Identification of *Cpa3*$^{+}$ fetal liver progenitors.

(A) Original UMAP plot (left) of *Cpa3*$^{+}$ fetal liver sub-populations from Ma et al. (2025), re-clustered using known dimensional parameters to maintain consistency across analyses to generate adapted UMAP plot (right). (B) Top differentially expressed genes identified across *Cpa3*$^{+}$ fetal liver sub-populations including basophils (Baso), basophil progenitors (BasoP), mast cell progenitors (MCP) and mast cells (MCs). Differential gene expression list derived from (Ma et al., 2025). Colour scale indicates average expression of each gene. Dot sizes represent the percent of cells expressing each gene.

Cpa3^{Cre} *recombination occurs early and broadly compared to Mcpt5*^{Cre} *and Karma*^{Cre} *drivers*

To trace Cre-recombination in MCs under the assessed Cre driver genes, *Cpa3*^{Cre}, *Mcpt5*^{Cre} and *Karma*^{Cre} mice were crossed with *Rosa26*$^{lsl\text{-}tdT}$ reporter mice (Figure 3A), resulting in tdTomato (tdT) labelling following Cre-mediated recombination in the cell (Figure 3B). This

approach allowed us to identify cumulative history of Cre activity in MCs across different developmental stages. Using flow cytometry to identify cells within fetal lung and skin, we quantified the proportion of MCs (gated as $CD45^+$ $F4/80^-$ $CD11b^-$ $CD117^+$ (Kit^+) $ST2^+$) expressing tdT and compared this to another myeloid (non-MC) lineage, ie., macrophages (gated as $CD45^+$ $F4/80^+$ $CD11b^+$) as well as all remaining $CD45^+$ cells as controls (Figure 3C, Figure S3A, S3B).

The frequency of tdT^+ cells was compared across the three Cre-based reporter lines and visualised using a heatmap (Figure 3D). The highest proportion of tdT^+ cells at the early E15.5 stage in both skin and lung was driven by recombination under *Cpa3*^{Cre} labelling, followed by *Mcpt5*^{Cre} labelling. However, tissue-specific differences were notable. In the skin, frequency of *Cpa3*^{Cre} recombination increased dramatically within the MC population by E18.5, followed by *Mcpt5*^{Cre}. In the lung however, frequency of *Cpa3*^{Cre} recombination increased modestly by E18.5 but was still lower in *Mcpt5*^{Cre} reporter mice. *Karma*^{Cre} based recombination, and labelling at E15.5 was only detectable in fetal skin MCs but not in fetal lung MCs. Recombination under *Karma*^{Cre} increased by E18.5 in the fetal lung, but not as highly as in the skin MCs at this stage.

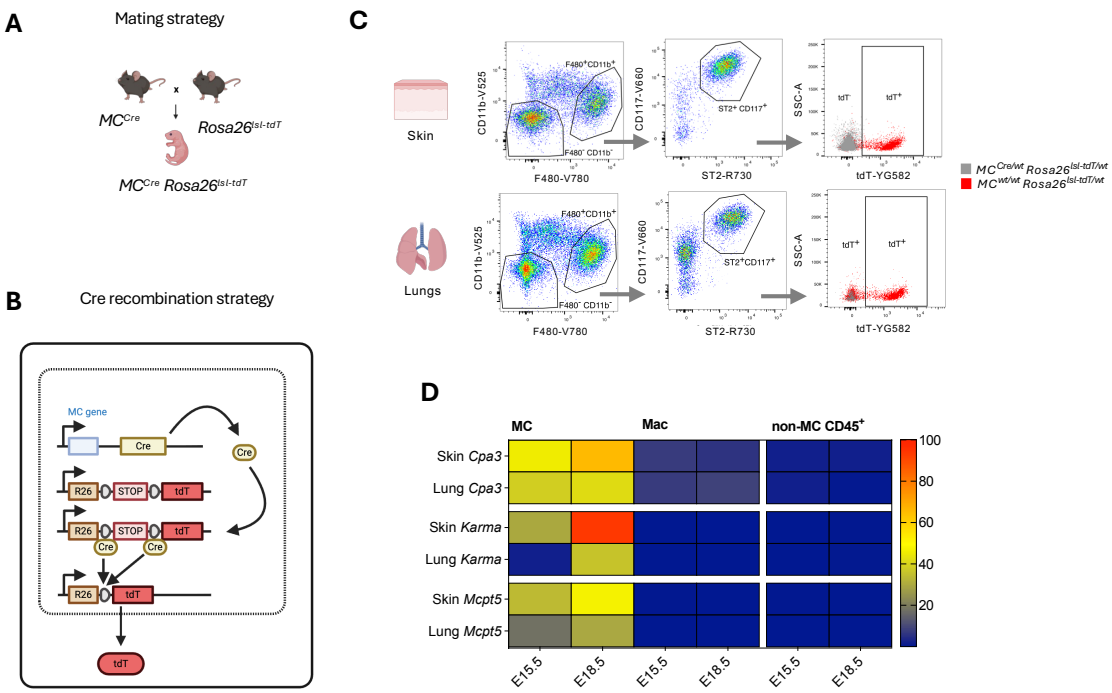

Chapter (3) Figure 3: Cre-mediated recombination in fetal mast cells under Cpa3, Mcpt5 and Karma gene drivers.

(A) Schematic illustrating mating strategy of *MC*^{Cre} *(*where *MC*^{Cre} refers to either *Cpa3*^{Cre}*, Mcpt5*^{Cre} and *Karma*^{Cre} mice) with *Rosa26*$^{lsl\text{-}tdT}$ reporter mice to enable tdTomato (tdT) expression following Cre-mediated recombination. (B) Cre-recombination strategy within each cell expressing the Cre driver and *Rosa26*$^{lsl\text{-}tdT}$ (tdT transgene) in the Rosa26 (R26) locus. Under the control of the chosen MC gene in the mouse model, Cre-mediated recombination occurs, following which the STOP codon is excised and tdT transgene is expressed in the cell. (C) Representative flow cytometry plots showing tdT expression in fetal skin (top) and lung (bottom) from *MC* ^{Cre} *(Cpa3*^{Cre}*) Rosa26*$^{lsl\text{-}tdT}$ reporter mice. Flow plots shown are from representative E15.5 tissues (full gating strategy for E15.5 and E18.5 shown in Figure S3A, S3B). Mast cells (MCs) were gated as CD45^{+} F4/80^{-} CD11b^{-} CD117^{+} (Kit^{+}) ST2^{+} cells, and subsequently tdT^{+} cells were gated as tdT^{+} MCs (red). Similar strategy was applied for

macrophages gated as CD45$^+$ F4/80$^+$ CD11b$^+$ cells and remaining CD45$^+$ cells. tdT$^-$ cells were determined using unlabeled control mice that lack Cre-mediated tdT expression (grey). (D) Heatmap showing the proportion of tdT$^+$ cells within mast cell (MC), macrophage (Mac) and remaining CD45$^+$ populations in fetal skin and lung at E15.5 and E18.5. Data in (D) is cumulative of at least 4 mice per group. *Data in D collectively generated by Simran Kapoor, Shin Li Chia and Clara Munz.*

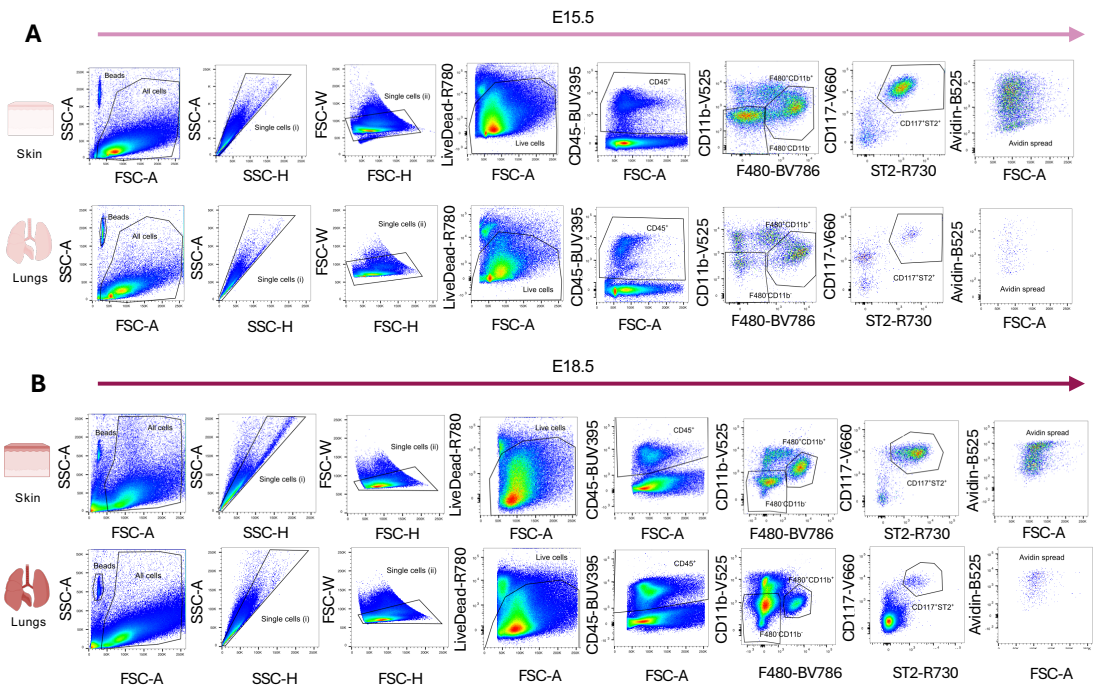

Chapter (3) Supplementary Figure S3: Flow cytometry gating strategy.

Representative flow cytometric panels (from proficient mice) showing gating strategy used for fetal skin (top) and lungs (bottom) at (A) E15.5 and (B) E18.5. Gating was performed sequentially from left to right. Population gated as beads represent counting beads used for quantification. Live, single cells were first selected, followed by CD45$^+$ cells. Subsequently,

F4/80 and CD11b were used to distinguish macrophages (F4/80^{+} CD11b^{+}) and mast cells (F4/80^{-} CD11b^{-}). Mast cells were further gated as CD117^{+} (Kit^{+}) ST2^{+} , with detectable spread of avidin staining (indicating variable heparin granular content within mast cell population). Representative data from *Cpa3*^{Cre} proficient mice.

These findings highlight distinct temporal and tissue-specific activation patterns of available mast cell Cre lines, with *Cpa3*^{Cre} recombination occurring the earliest in MCs across the examined fetal tissues.

Mice targeted in the Cpa3^{Cre} *Rosa26*$^{lsl\text{-}DTA}$ *model exhibit perinatal lethality*

Given the early Cre activity in MCs across fetal tissues in *Cpa3*^{Cre} *Rosa26*$^{lsl\text{-}tdT}$ mice, we next sought to leverage this driver to target *Cpa3*-expressing MCs and their precursors using a diphtheria toxin–based ablation approach. We crossed the *Cpa3*^{Cre} mice to the *Rosa26*$^{lsl\text{-}DTA}$ line (Figure 4A) to generate a mouse model in which diphtheria toxin A (DTA) expression is induced specifically in cells where Cre-mediated recombination occurs under control of the *Cpa3* promoter (Figure 4B). Due to the universal sensitivity of cells to DTA (Li et al., 2021), we reasoned that the *Cpa3*^{Cre} *Rosa26*$^{lsl\text{-}DTA}$ model should allow for more comprehensive depletion of *Cpa3*-expressing cells, including both *Cpa3*^{high} MCs and *Cpa3*^{low} MCPs across developing stages.

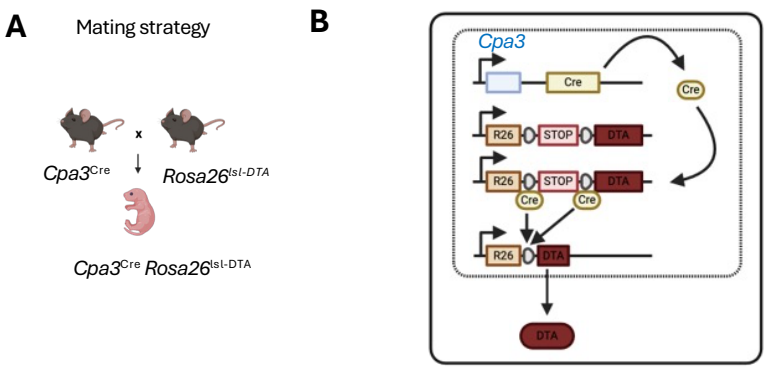

Chapter (3) Figure 4: Generation of novel mouse line *Cpa3^{Cre} Rosa26$^{lsl\text{-}DTA}$*.

(A) Schematic illustrating mating strategy of *Cpa3^{Cre}* mice with *Rosa26$^{lsl\text{-}DTA}$* mice to generate *Cpa3^{Cre} Rosa26$^{lsl\text{-}DTA}$* mice. (B) Cre-recombination strategy within each cell expressing the *Cpa3*^{Cre} and *Rosa26$^{lsl\text{-}DTA}$* (DTA) transgenes. Under the control of the *Cpa3* gene in the mouse model, Cre-mediated recombination occurs, following which the STOP codon is excised and diptheria toxin (DTA) transgene is expressed in the cell leading to cell death by apoptosis.

Strikingly, mice heterozygous for both *Cpa3^{Cre}* and *Rosa176$^{lsl\text{-}DTA}$* transgenes (hereafter referred to as "*Cpa3^{Cre}* targeted") were absent at adulthood, with no animals surviving beyond P2 (Figure 5A). Using a similar strategy described in Figure 4, we also crossed *Karma^{Cre}* and *Mcpt5^{Cre}* lines to *Rosa176$^{lsl\text{-}DTA}$*, but by contrast, both *Mcpt5^{Cre} Rosa176$^{lsl\text{-}DTA}$* (Figure S4A) and *Karma^{Cre} Rosa176$^{lsl\text{-}DTA}$* (Figure S4B) mice survived to adulthood.

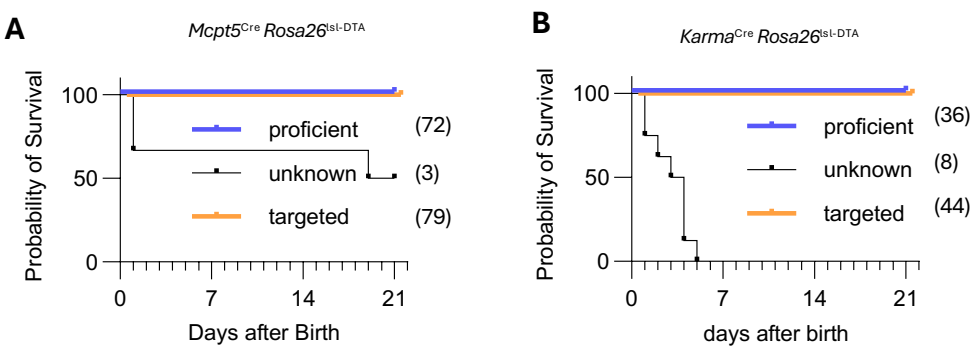

Chapter (3) Supplementary Figure S4: Survival curves for *Mcpt5^{Cre} Rosa26$^{lsl\text{-}DTA}$* and *Karma^{Cre} Rosa26$^{lsl\text{-}DTA}$* mice.

Kaplein-Meir curves showing survival distribution of offspring from (A) *Mcpt5^{Cre} Rosa26$^{lsl\text{-}DTA}$* mice and (B) *Karma^{Cre} Rosa26$^{lsl\text{-}DTA}$* mice following natural delivery, stratified by genotype (where proficient mice lack either the *MC^{Cre}* or *Rosa26$^{lsl\text{-}DTA}$* transgene, targeted mice are heterozygous for both *MC^{Cre}* or *Rosa26$^{lsl\text{-}DTA}$* transgene, or "unknown" mice whose genotype is unaccounted for). Numbers in brackets indicate number of mice per group. *Data in A-B collectively generated by Simran Kapoor and Clara Munz.*

Natural delivery poses challenges to characterising the nature of the lethality phenotype. Since we could not monitor natural birth, it resulted in the incomplete recovery of some carcasses due to maternal cannibalism (Capas-Peneda et al., 2021), and occasionally tissues were too decomposed for genotyping. As such, litter assessments were only partial in some cases due to unaccounted genotypes ("unknown" in Figure 5A). Performing caesarean sections (c-sections) circumvented these issues by allowing for consistent genotyping of all pups and intact collection of carcasses without the risk of decomposition.

To determine the onset of lethality, we therefore performed c-sections to recover all the neonate pups from the pregnant dam (Figure 5B). Following C-section at E18.5, the developmental stage immediately preceding natural birth, we could recover proficient and targeted pups at the expected 1:1 mendelian ratio (χ^2 test against a 1:1 ratio) (Figure 5C), indicating that the lethality was unlikely to arise embryonically. There was also no significant deviation from the expected genotype distribution at E17.5, an even earlier developmental stage (Figure 5C). These findings reinforced that the absence of surviving adult targeted mice in the model is unlikely due to increased lethality during late gestation stages *in utero*. In contrast, proficient and targeted pup ratios skewed significantly from the Mendelian ratio when assessed at P0 and P1 after birth (Figure 5C), indicating that lethality manifests postnatally, shortly after birth.

The cause of neonatal lethality can indicate the nature of the defect in organogenesis during fetal development (Turgeon and Meloche, 2009). To interpret the underlying cause of lethality in the targeted pups, we performed a one-hour long observation following C-section delivery at E18.5. This allowed us to precisely define the critical window of perinatal lethality to provide insights into the underlying cause. All pups took a first breath after delivery and showed basic movements (Data not shown), indicating that they were alive at birth. However, within one hour, approximately 50% of *Cpa3*^{Cre} targeted pups died (Figure 5D), with no sex biases observed (Figure S5A). *Cpa3*^{Cre} targeted pups appeared morphologically normal at birth with no gross abnormalities, however, they exhibited mild growth retardation compared to their proficient littermates (Figure 5E). Notably, *Cpa3*^{Cre} targeted pups that survived or died within the one-hour observation period did not show significant differences in birth weight (Figure 5E), indicating that growth retardation was a shared defect in *Cpa3*^{Cre} targeted pups and not indicative of survival outcome. Of note, a small proportion of *Cpa3*^{Cre} proficient pups died shortly after birth; however, these were

always markedly significantly smaller than the surviving proficient pups as well as the targeted pups (Figure S5B), consistent with sporadic intrauterine growth restriction (Kaur et al., 2022) rather than a genotype-specific defect.

Within the observation period, *Cpa3*^{Cre} targeted pups started showing signs of severe respiratory distress and appeared cyanotic, unlike their proficient littermates (Figure 5F). They showed limited movement and responsiveness to stimuli. Lungs dissected from the dead *Cpa3*^{Cre} targeted pups failed to float in solution, and appeared uninflated under the microscope (Figure 5G), indicating failed inflation. Lungs from the remaining 50% *Cpa3*^{Cre} targeted pups that survived the immediate one-hour monitoring period however did float in solution, suggesting sufficient aeration (Figure S5C). However, these pups took longer to acquire the characteristic pink skin coloration that is normally developed upon oxygenation when compared to proficient littermates (Figure 5H). Taken together, these findings indicate that *Cpa3*^{Cre} targeted pups that remain alive within the initial observation period may still have an intermediate respiratory defect that is compensated for and results in sufficient aeration. This is further reflected from analysis of the ductus arteriosus (DA), which normally undergoes remodeling-based closure upon transitioning from *in utero* placental oxygenation to lung-dependent circulation (Yarboro et al., 2021). This process occurs following sufficient oxygenation, and within the observation period, the *Cpa3*^{Cre} targeted dead pups tend to have an opened DA, while most *Cpa3*^{Cre} targeted live and proficient pups manage to close their DA (Figure S5D), potentially indicating differences in immediate ability to oxygenate and survive.

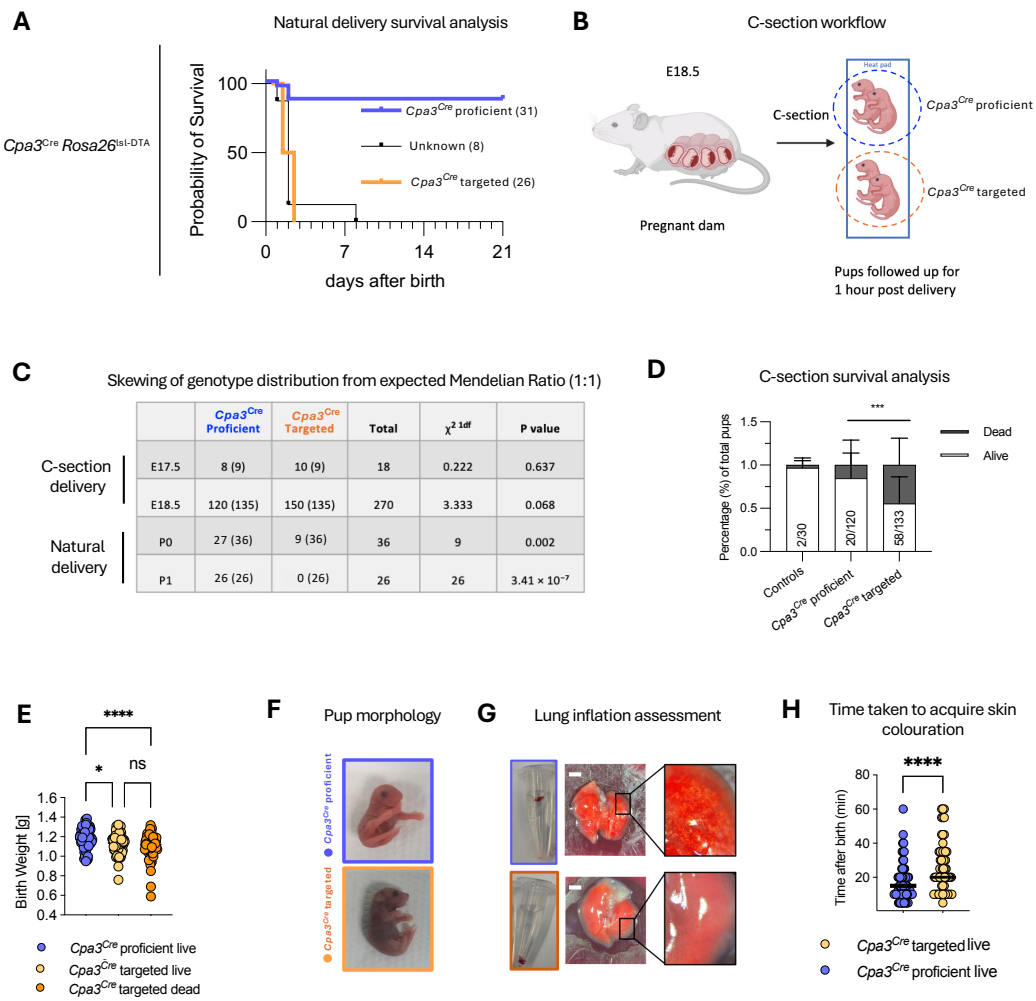

Chapter (3) Figure 5: Perinatal lethality and respiratory defects in *Cpa3^{Cre} Rosa26$^{lsl\text{-}DTA}$* targeted mice.

(A) Kaplein-Meir curve showing survival distribution of offspring from *Cpa3-Cre Rosa176-DTA* mice assessed following natural delivery, stratified by genotype (proficient, targeted or unaccounted for "unknown" mice). Numbers in brackets indicate number of mice per group. (B) Experimental schematic illustrating C-section delivery at E18.5 and postnatal monitoring of newborn neonate pups on heatpad for one hour. (C) Genotype distribution of *Cpa3^{Cre}*

proficient and *Cpa3*^{Cre} targeted offspring recovered at various timepoints by C-section *in utero* (E17.5, E18.5) and post natural delivery (P0, P1). Deviation from Mendelian 1:1 ratio was assessed using a Chi-square goodness-of-fit test (χ^2 test against a 1:1 ratio), with associated p-value indicated. P-values < 0.05 were considered significant. (D) Survival of littermate proficient and targeted pups, stratified by survival outcome (dead or alive) after one hour of observation following C-section delivery. Unrelated control pups from other litters delivered by C-section are shown for comparison. (E) Birth weight of *Cpa3*^{Cre} proficient and targeted pups, stratified by survival outcome. Weights measured directly after C-section. (F-G) Representative images of proficient (top) and targeted (bottom) pups showing (F) overall appearance and (G) lung floatation assay with morphology of lungs under dissection microscope (0.8x) at the end of the observation period following C-section delivery. Scale bar = 10mm. (H) Time-dependent acquisition of skin colouration associated with oxygenation in proficient and targeted pups during the observation period. Statistical significance is indicated where applicable (P-values were defined as **** < 0.0001, * < 0.05, ns = not significant). Data in (E) is cumulative of at least 57 mice per group. Data in (H) is cumulative of at least 61 mice per group. *Data in A-H generated by Simran Kapoor and Clara Munz.*

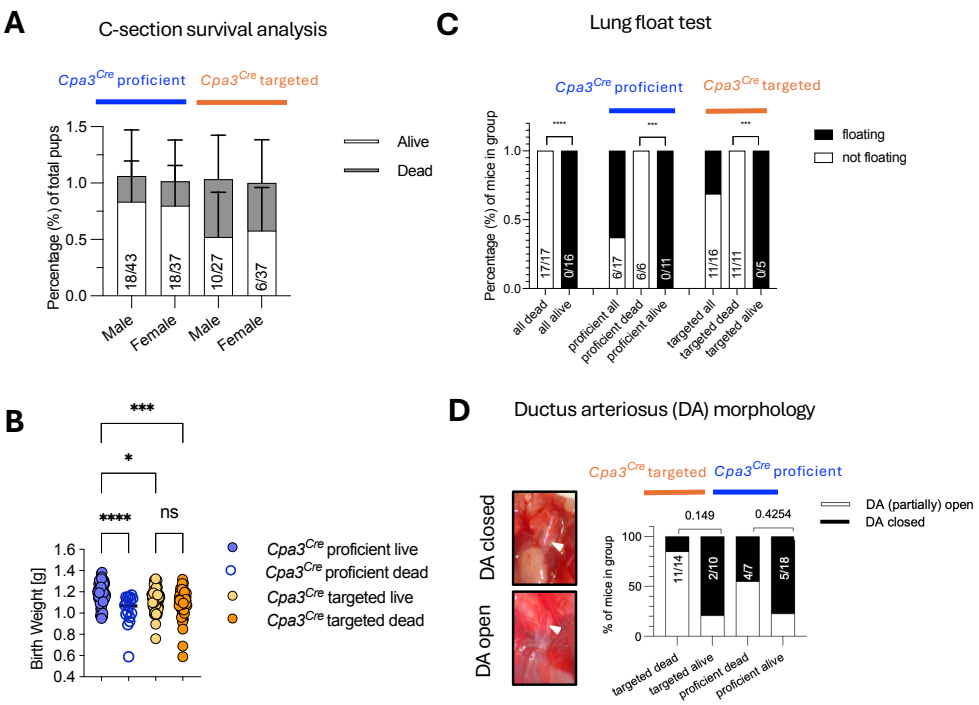

Chapter (3) Supplementary Figure S5: Perinatal lethality and respiratory defects in *Cpa3*^{Cre} targeted mice.

(A) Survival of littermate *Cpa3*^{Cre} proficient and targeted pups, stratified by sex (male "m" or female "f") and survival outcome (dead or alive) after one hour of observation following C-section delivery. (B) Birth weight of proficient and targeted pups, stratified by survival outcome. Weights measured directly after C-section. (C) Lung floatation assay performed on lungs isolated from *Cpa3*^{Cre} proficient and targeted pups stratified by their survival outcome following the observation period, showing the proportion of freshly dissected lungs based on whether they floated or failed to float in phosphate buffered saline solution (PBS). (D) Representative images (left) of ductus arteriosus (DA) morphology (arrow marking tissue remodelling-induced closure of the DA restricting blood flow through the vessel, or

failure thereof). Quantification (right) of the DA closure status in *Cpa3*^{Cre} proficient or targeted pups following the observation period, shown as percentage of pups with an open or closed DA. Statistical significance is indicated where applicable (P-values were defined as **** < 0.0001, *** < 0.001, * < 0.05, ns = not significant). Data shown in B are cumulative of at least 16 mice per group. *Data in A-D generated by Simran Kapoor and Clara Munz.*

Respiratory distress in Cpa3^{Cre} *targeted mice is driven by abnormal lung development*

We next sought to investigate whether developmental defects in the lungs of *Cpa3*^{Cre} targeted mice contributed to their respiratory distress. Lungs from *Cpa3*^{Cre} targeted pups appeared morphologically normal, with all four lobes present (Figure 5G), and lung wet weight did not significantly differ from proficient littermates (Figure 6A). However, histological analysis of haematoxylin-eosin-stained lung sections from mice at E18.5 (Figure 6B) revealed visible structural abnormalities in the lung architecture. Mean linear intercept, which reflects average saccule sizes, as well as the total fraction of airspace within the saccular areas was unchanged in targeted mice (Figure 6C-D). However, the lungs of *Cpa3*^{Cre} targeted pups displayed a trend towards increased inter-saccular thickness (Figure 6E). Notably, neither of these parameters were altered at E17.5 (Figure S6A-C), indicating the late-stage nature of this structural lung defect.

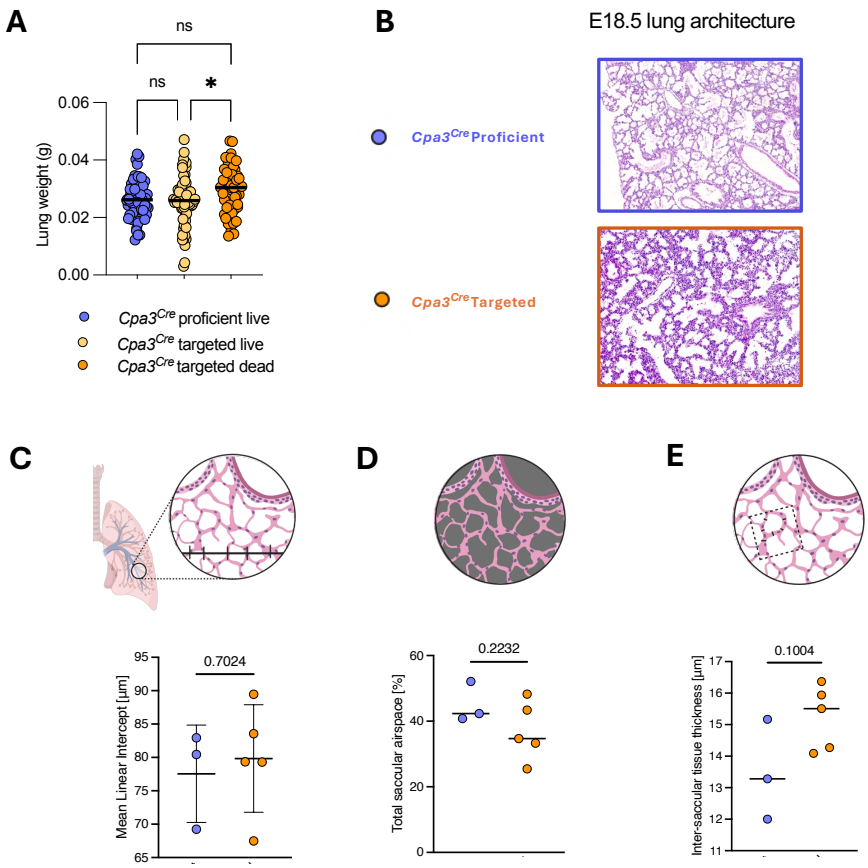

Chapter (3) Figure 6: Structural abnormalities in the lung architecture of *Cpa3^{Cre}* targeted mice at E18.5.

(A) Lung wet weight of proficient and targeted pups at E18.5. (B) Representative haematoxylin and eosin-stained lung sections from proficient and targeted pups at E18.5. (C-E) Schematic of how lung architecture parameters were analysed (top) and quantification (bottom) of (C) mean linear intercept (D) total fraction of airspace within saccular regions (E) inter-saccular septal thickness in fetal lungs from proficient and targeted pups at E18.5. Lungs were assessed prior to taking a first breath to avoid inflation related artifacts. Statistical significance is indicated where applicable (P-values were defined as * < 0.05, ns =

not significant). Data in (A) is cumulative of at least 50 mice per group. Data in (C-E) is cumulative of at least 3 mice per group. *Data in A generated by Simran Kapoor and Clara Munz. Data in B-E generated by Theresa Eulgem.*

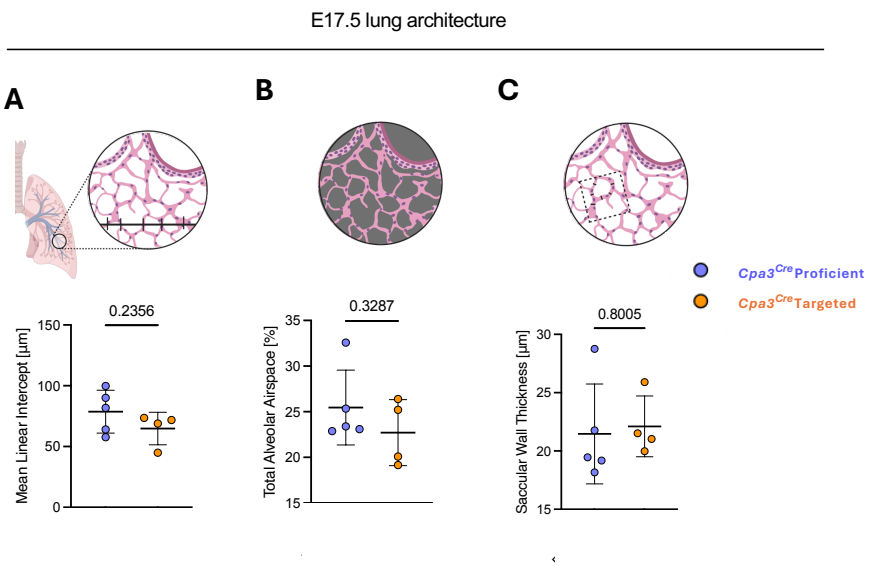

Chapter (3) Supplementary Figure S6: Structural abnormalities in the lung architecture of in the lungs of *Cpa3*^{Cre} targeted mice at E17.5.

Schematics (top) show parameter measured for quantification (bottom) of (A) mean linear intercept (B) total fraction of airspace within saccular regions (C) inter-saccular septal thickness in fetal lungs from proficient and targeted pups at E17.5. Lungs were assessed in fetuses culled at C-section prior to taking a first breath to avoid inflation related artifacts. Statistical significance is indicated where applicable. Data shown in (A-C) are cumulative of at least 4 mice per group. *Data in A-C generated by Solvig Becker and Simran Kapoor.*

In light of the above findings, we next examined the whole lung proteome of these mice to identify molecular pathways underlying the defective maturation. Principal component analysis (PCA) revealed that the lungs of all *Cpa3*^{Cre} targeted pups – whether dead or alive within the one-hour observation window - completely overlapped in a separate PCA analysis (Figure 7A). This indicated that the lung proteome is similar within the targeted group, irrespective of immediate survival ability. Moreover, the *Cpa3*^{Cre} targeted lungs clustered separately from the lungs of proficient littermates in the PCA space (Figure 7B), suggesting genotype-dependent differences in the lung proteome.

Consistent with this, we could not identify any significantly differentially expressed proteins (log2FC cutoff 0.1; p value cutoff 0.05) between targeted pups that remained alive versus those that died within one hour (Figure S7A), further reinforcing that the lung proteome of *Cpa3*^{Cre} targeted pups is similar, and the differences in the *Cpa3*^{Cre} proficient versus targeted pups in the PCA space (Figure 7A) are likely driven by genotype, rather than survival status. We found 19 significantly differentially expressed proteins (log2FC cutoff 0.1; p value cutoff 0.05) in the total *Cpa3*^{Cre} targeted lungs relative to the proficient lungs (Figure 7C). Of these 2 proteins (Plxnd1, Rfc5) were upregulated, while the remaining 17 proteins, including Tgfb1 and several platelet activation proteins, were downregulated in the *Cpa3*^{Cre} targeted lungs.

Given the established role of Tgfb signaling in lung development and dysplasia (Calthorpe et al., 2023), we further investigated the expression of Tgfb signaling proteins across the lungs of *Cpa3*^{Cre} targeted and proficient littermates (Figure 7D). Notably, many proteins could be detected at intermediate levels in the lungs of *Cpa3*^{Cre} targeted live pups compared to targeted dead and proficient littermates. To identify the nature of the strongest defect, i.e. lung defect that led to respiratory distress shortly after birth, we therefore performed statistical comparisons between the lungs of *Cpa3*^{Cre} targeted dead and proficient pups.

Scaled expression across the three groups revealed a significant reduction of Tgfb1 in the lungs of *Cpa3*^{Cre} targeted dead pups relative to proficient littermates. In contrast, Tgfb2 protein expression followed an opposite pattern and was significantly upregulated in the lungs of *Cpa3*^{Cre} targeted dead pups. Smad2, a protein downstream of Tgfb signaling pathways (Calthorpe et al., 2023) was also significantly upregulated in the lungs of *Cpa3*^{Cre} targeted dead pups, suggestive of abnormal Tgfb signaling.

Since lung development is characterised by extensive extra-cellular matrix (ECM) remodelling (Calthorpe et al., 2023; Willis and Borok, 2007), we then investigated the expression of various important ECM components and associated ECM remodelling enzymes (Mmp9, Mmp2, Timp3, Timp2, Fn1, Eln, Elane, Serpine1, Serpinb1a, Col4a1, Col4a2, Col4a3, Col1a1, Col1a2, Col2a1, Lama5) (Figure 7D). Lungs of *Cpa3*^{Cre} targeted dead pups had lower expression of matrix metalloprotease 9 (Mmp9) and its inhibitor Timp3. A similar pattern was observed for ECM remodeling proteins including elastin (Eln), proteases like neutrophil elastase (Elane), plasminogen activator inhibitor-1 (Serpine1), as well as protease inhibitor Seprineb1 (Serpineb1a). Collagens (type I-IV) and laminin proteins generally trended towards reduced expression in the lungs of *Cpa3*^{Cre} targeted dead pups, indicating mesenchymal defects. In addition, airway epithelial products including pulmonary surfactant proteins (type II epithelial function) and podoplanin (type I epithelial function) were reduced in the lungs of *Cpa3*^{Cre} targeted dead group, indicating defects in the epithelial compartment as well. Smooth muscle protein (Actg2) was also slightly increased in *Cpa3*^{Cre} targeted lungs relative to the proficient littermate lungs.

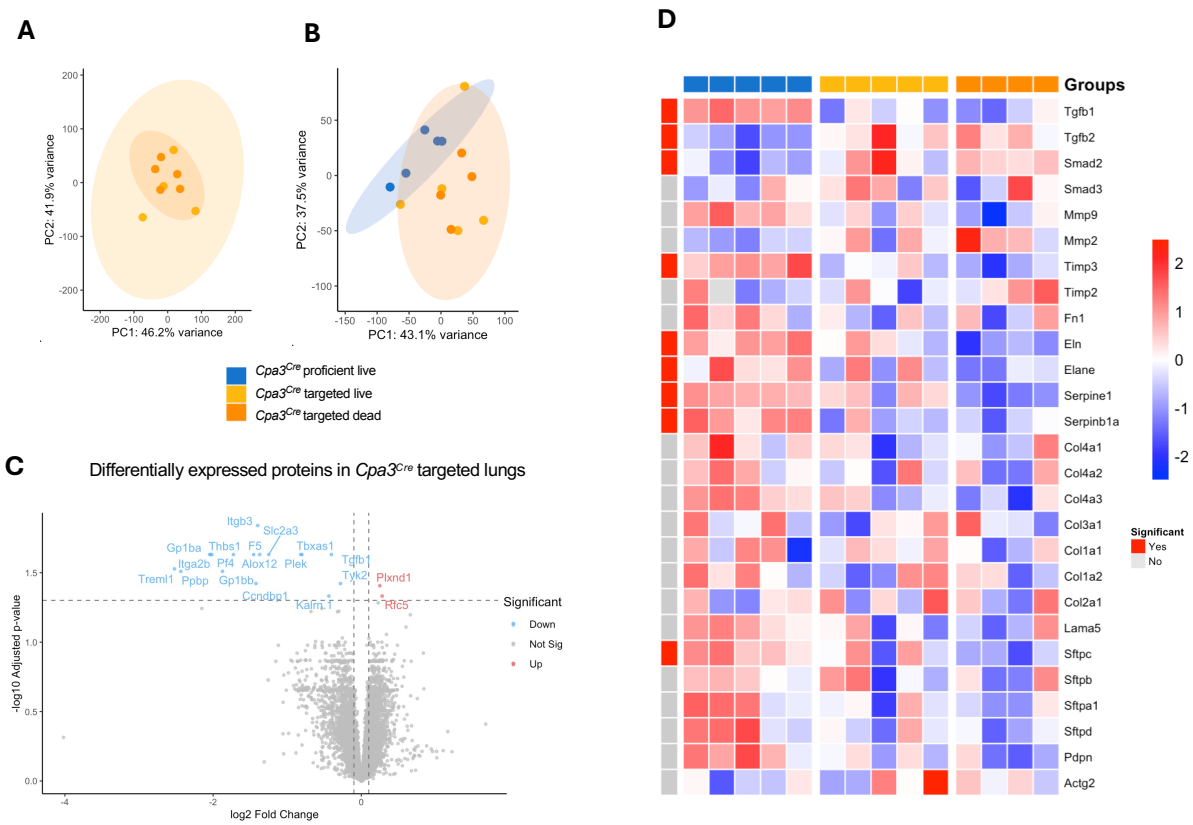

Chapter (3) Figure 7: Proteomic alterations in the lungs of *Cpa3*^{Cre} targeted mice at E18.5.

(A) Principal component analysis (PCA) of whole-lung proteomes from targeted pups that survived or died within the one-hour postnatal observation period. (B) PCA of whole-lung proteomes from proficient (n=5) and targeted live (n=5) and dead (n=4) pups. (C) Volcano plot showing differentially expressed proteins in lungs from targeted pups compared with proficient pups. The log2FC cutoff was 0.1, and p-value cutoff was 0.05 to determine significance and upregulation (red) or downregulation (blue) of protein expression. (D) Heatmap showing scaled expression of selected proteins in Tgfb signaling (Tgfb1, Tgfb2, Smad2, Smad3), extracellular matrix organisation (Mmp9, Mmp2, Timp3, Timp2, Fn1, Eln, Elane, Serpine1, Serpinb1a, Col4a1, Col4a2, Col4a3, Col1a1, Col1a2, Col2a1, Lama5),

epithelial function (Sftpc, Sftpb, Sftpa1, Sftpd, Pdpn), and smooth muscle (Actg) across proficient, targeted live, and targeted dead lung samples. Proteins significantly different between proficient and targeted dead group marked in red. P-value were considered significant at < 0.05.

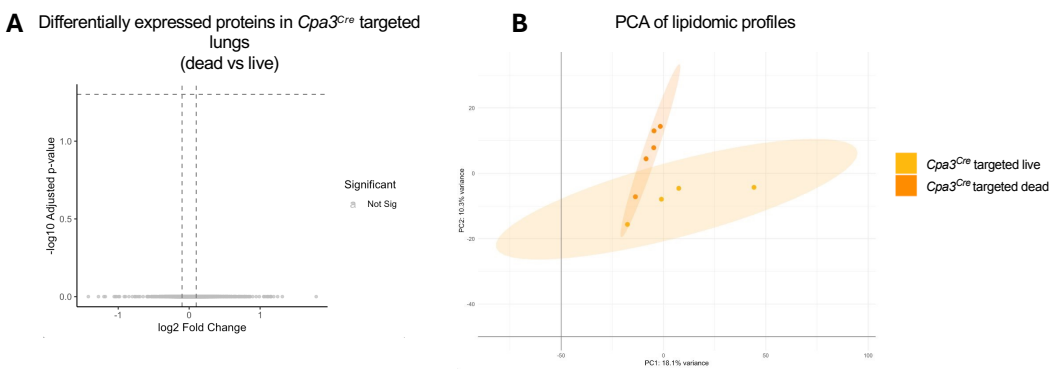

Chapter (3) Supplementary Figure S7: Proteomic and lipidomic alterations in the lungs of *Cpa3^{Cre}* targeted mice at E18.5.

(A) Volcano plot showing differentially expressed proteins in lungs from E18.5 *Cpa3^{Cre}* targeted pups that died in the one-hour postnatal observation window compared with the targeted pups that survived the period. Genes were considered significant at p-value cutoff < 0.05. (B) Principal component analysis (PCA) of lipidomes from the fetal lungs of E18.5 *Cpa3^{Cre}* targeted pups that survived or died within a one-hour postnatal observation period.

To determine whether differences in metabolic lipid pathways accompanied the phenotype, we also performed whole tissue lipidomics from the same lungs taken from *Cpa3^{Cre}* targeted and proficient pups. However, unlike the proteome, lipid composition of the groups separated by survival outcome rather than by genotype in the PCA space (Figure S7B). This

suggested that the lipid dysregulation observed in the groups is likely a secondary effect of death, rather than a driver of the lung phenotype in the *Cpa3*^{Cre} targeted pups.

Together these findings suggest that *Cpa3*^{Cre} targeted pups had impaired lung development during the terminal saccular maturation window, which was accompanied by dysregulated Tgfb signaling and a defective ECM.

Dysregulated epithelial-to-mesenchymal signaling in the lungs of Cpa3^{Cre} *targeted mice*

Dysregulated Tgfb signaling is a key driver for lung fibrosis in adults as well as neonates (Calthorpe et al., 2023; Willis and Borok, 2007), and proceeds by inducing epithelial-to-mesenchymal transition (EMT). Given the aberrant Tgfb and ECM signatures we identified in the lungs of targeted pups, we next investigated whether impaired EMT-like mechanisms may underlie the abnormal lung structure observed in *Cpa3*^{Cre} targeted pups.

Using single cell RNA sequencing, we isolated live, CD45^{-} cells from the lungs of *Cpa3*^{Cre} targeted pups and their proficient littermates after C-section delivery (E18.5) to assess the stromal compartment of the lungs (Figure 8A). Cell samples from *Cpa3*^{Cre} targeted and proficient pups were pooled and sequenced together as a single library in the same run, with samples from each genotype loaded into distinct chip positions (see Methods and Materials). Following quality control processing of the dataset to eliminate dead cells and doublets resulting in 7745 cells on which we performed Seurat integration to control for any technical variation introduced (Figure S8A. Subsequent dimensional reduction and unsupervised clustering on the cells led us to identify clusters which were visualized by Uniform Manifold Approximation and Projection (UMAP) (See Methods and Materials) (Figure 8B). We identified 21 clusters based on differential gene expression (DEGs) of key

markers – including fibroblasts (c0, c3, c7, c8, c12, c14, c17), mesothelial cells (c11) epithelial cells (c5, c13), endothelial cells (c1). In addition, we could also detect erythrocytes (c2, c6, c16), and a small population of megakaryocytes (c9) (Figure 8B, Figure S8A-B).

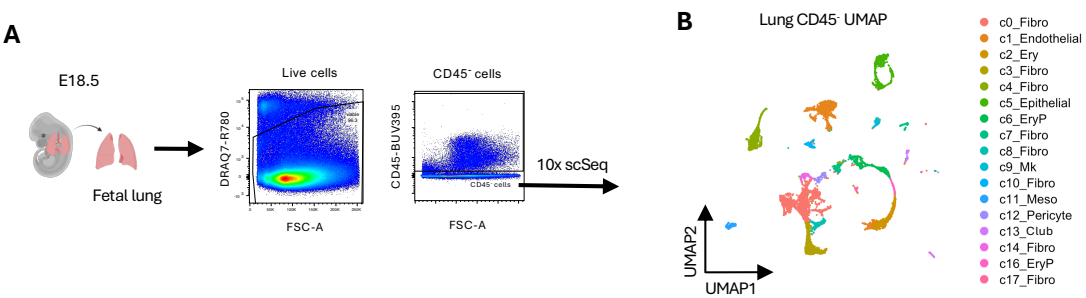

Chapter (3) Figure 8: Single cell transcriptomic profiling of the fetal lung stromal compartment at E18.5.

(A) Schematic showing experimental workflow of isolating live, singlet CD45^{-} cells from E18.5 fetal lungs from *Cpa3*^{Cre} targeted and proficient pups (following C-section delivery) for 10x single cell RNA sequencing (10x scSeq). (B) UMAP plot of sequenced fetal lung CD45^{-} cells at E18.5 (n=7745) following dimensional reduction and unsupervised clustering to reveal 21 clusters.

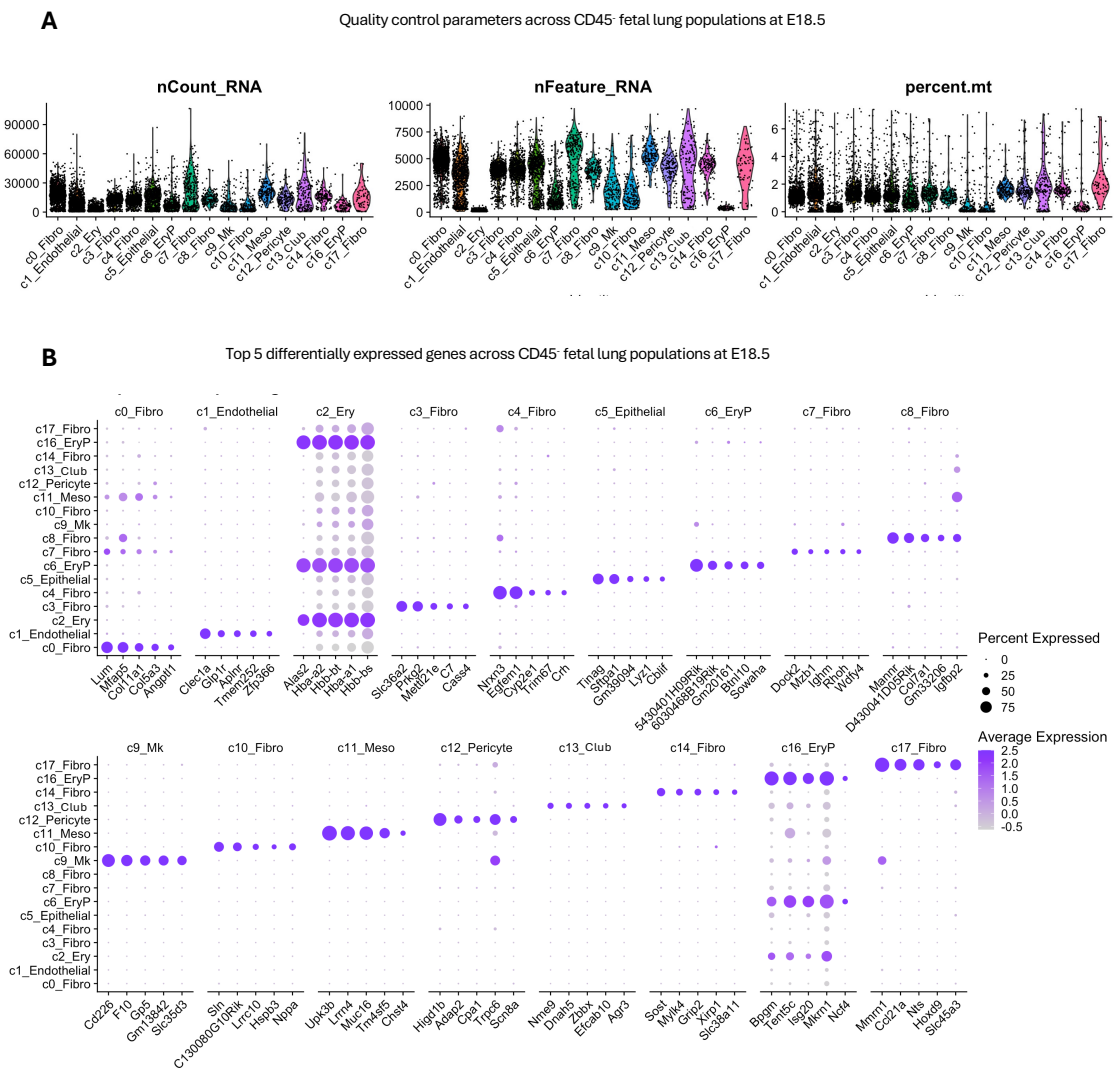

Chapter (3) Supplementary Figure S8: Single cell transcriptomic profiling of the fetal lung stromal compartment at E18.5 in *Cpa3*^{Cre} *Rosa26*$^{lsl\text{-}DTA}$ mice.

(A) Violin plots showing quality control metrics for E18.5 fetal lung CD45$^-$ stromal cells across identified clusters, including total RNA counts (nCount_RNA), number of detected genes (nFeature_RNA) and percentage of mitochondrial genes (percent.mt). (B) Top 5 differentially expressed genes in the CD45$^-$ clusters identified in the fetal lung at E18.5. Colour scale

indicates average expression of each gene. Dot sizes represent the percent of cells expressing each gene.

To further characterise the epithelial compartment, we then sub-clustered all lung epithelial cells on the basis of E-cadherin (*Cdh1*) expression to identify distinct epithelial cell subsets within the lung stroma (Figure 9A). This included airway type I (AT1) and type II (AT2) cells, biosynthetically active transitional cells, ciliated cells, Club cells, as well as a distinct population of mesenchymal-like epithelial cells (Figure 9B, Figure S9A).

The mesenchymal-like cells expressed EMT-associated transcription factors like *Zeb2*, *Snai1* alongside mesenchymal features like N-cadherin (*Cdh2*), actin smooth muscle (*Acta2*), vimentin (*Vim*) and platelet derived growth factor receptor alpha (*Pdgfra*) (Figure 9C). Strikingly, we found that mesenchymal cells were markedly increased in the lungs of $Cpa3^{Cre}$ targeted pups (Figure 9D), indicating an increase in epithelial plasticity and EMT transformation. $Cpa3^{Cre}$ targeted lungs also had increased proportion of AT1 cells relative to proficient mice (Figure 9D).

Among the epithelial cell populations, AT2 cells had the highest transcriptional perturbation, with 97 DEGs in the $Cpa3^{Cre}$ targeted group (67 upregulated, 30 downregulated) (Figure 9E). These included an upregulation of several ER stress genes (*Ubc, Hspa1b, Hspa1a*), as well as AP-1 signaling genes (*Fos/Jun*) (Figure 9F). While ER stress genes were consistently upregulated in all the epithelial cells in the $Cpa3^{Cre}$ targeted group indicative of global epithelial stress response within the $Cpa3^{Cre}$ targeted lung (Figure S9B), AP-1 activation was specifically higher within the AT2 cells (Figure 9G). Given that AP-1 signaling drive AT2-to-AT1 differentiation (Lynch et al., 2025), these data suggest that the observed increase in AT1 cells in the targeted lungs may reflect the increased AP-1-mediated AT2 cell activation. Tgfb2

signaling has been shown to be critical for AT1 cell function during lung development (Callaway et al., 2024). In line with this, we found that AT1 and the EMT-like cells expressed *Tgfb2* (Figure 9H), but not *Tgfb1* (Figure S9C), in the lung. Because both AT1 and EMT-like cells were expanded in the targeted lungs, these cells represent a plausible source of increased Tgfb2 expression observed in the bulk lung tissue proteome (Figure 7D).

These data suggest a model in which lung maturation of *Cpa3*^{Cre} targeted pups is impaired due to a combination of aberrant AT2-to-AT1 transition caused by exacerbated AP1-signaling and an increase in epithelial cells undergoing EMT (Figure 9I).

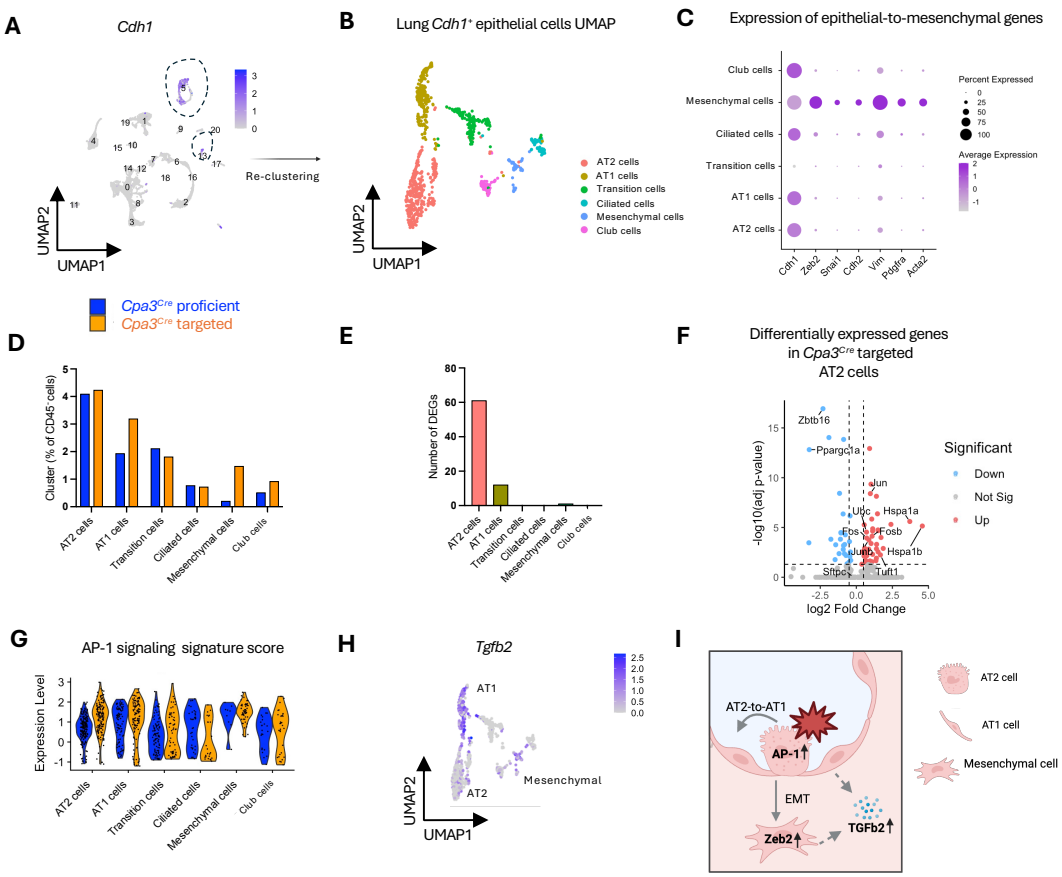

Chapter (3) Figure 9: Dysregulated epithelial-to-mesenchymal signaling in the lungs of *Cpa3*^{Cre} targeted mice at E18.5.

(A) UMAP feature plot showing *Cdh1* expression to define and subcluster epithelial cells within the E18.5 fetal lung CD45^{-} compartment. (B) UMAP plot showing *Cdh1*$^{+}$ epithelial sub-clusters following re-clustering analysis at an increased resolution, revealing presence of airway type 1 (AT1) and type 2 (AT2) cells, transitional cells, ciliated cells, Club cells and mesenchymal-like epithelial cells. (C) Dot plot showing expression of canonical epithelial and mesenchymal marker genes across epithelial sub-clusters. Colour scale indicates

average expression of each gene. Dot sizes represent the percent of cells expressing each gene. (D) Quantification of epithelial sub-clusters (as a proportion of $CD45^-$ cells) in proficient and targeted lungs. (E) Number of differentially expressed genes (DEGs) identified in each epithelial sub-cluster when comparing targeted and proficient lungs. DEGs identified used p-value cutoff of 0.05 and an absolute log2 fold-change cutoff of 0.5. (F) Volcano plot showing DEGs (p-value < 0.05; $\log_2$FC > 0.5) that are significantly upregulated (red) or downregulated (blue) in AT2 cells from targeted lungs relative to proficient lungs. (G) Violin plots showing AP-1 signalling signature scores (based on *Fos, Jun* signalling module expression) across epithelial sub-clusters in proficient and targeted lungs. (H) Feature plot showing *Tgfb2* expression across epithelial sub-clusters. (I) Schematic summarising proposed epithelial alterations in targeted lungs, including enhanced AT2-to-AT1 transition and increased epithelial-to-mesenchymal (EMT)-like state.

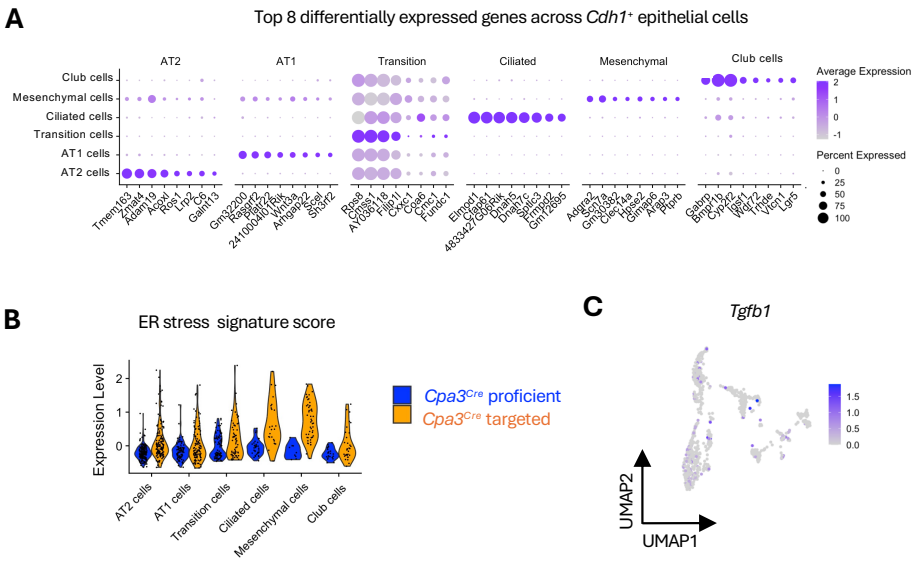

Chapter (3) Supplementary Figure S9: Dysregulated epithelial-to-mesenchymal signaling in the lungs of *Cpa3^{Cre}* targeted mice at E18.5.

(A) Top 8 differentially expressed genes across *Cdh1^{+}* epithelial cell sub-clusters in the fetal lung CD45^{-} cells at E18.5. Colour scale indicates average expression of each gene. Dot sizes represent the percent of cells expressing each gene. (B) Violin plots showing endoplasmic reticulum (ER) stress genes (*Hspa1a, Hspa1b, Dnaja1)* as a signature score across epithelial sub-clusters in *Cpa3*^{Cre} proficient and *Cpa3*^{Cre} targeted lungs at E18.5. (C) UMAP feature plot showing expression levels of *Tgfb1* expression across fetal lung epithelial cell sub-clusters at E18.5.

Cpa3^{Cre} targeted lungs exhibit dysfunctional fibroblast-extracellular matrix landscape

It has been well established that the interactions between epithelial cells and fibroblasts promote abnormal lung ECM remodeling in fibrosis (Sakai and Tager, 2013). We therefore

sought to investigate whether the epithelial dysfunction we observed in the targeted lungs also drive aberrant lung fibroblast development. Using the same stromal single cell sequencing dataset (as described in Figure 8A, 8B), we identified fibroblasts based on *Pdgfra/Pdgfrb* expression within the lung stroma (Figure 10A) and subsequently re-clustered them to resolve distinct fibroblast sub-clusters based on top DEGs (Figure 10B, Figure S10A). These included pericytes, matrix fibroblasts (Matrix_Fibro), adventitial fibroblasts (Adv_Fibro), Lgr5+ peribronchial fibroblasts (Peribronchi_Fibro), myofibroblasts (Myo_Fibro) and their precursors (Pre_Myo_Fibro), as well as actively proliferating fibroblasts (Prolif_Fibro). In addition, we captured some actin smooth muscle cells (ASM) and precursors (Pre_ASM). We could also detect chondrocytes and *Tbx20*$^{+}$ cardiac reprogramming-specific fibroblasts (Cardiac_Fibro), likely from contamination from adjacent heart muscle.

Myofibroblasts are known for their critical role in septal formation in the lung (R. Li et al., 2018; Lindahl et al., 1997). While the relative abundance of the Myo_Fibro cluster remained preserved in the *Cpa3*^{Cre} targeted condition (Figure 10C, 10D), they exhibited the most altered transcriptional profile (195 downregulated, 265 upregulated) (Figure 10E). Specifically, the *Cpa3*^{Cre} targeted Myo_Fibro cluster showed an increase in EMT-associated TFs like *Zeb2* and *Snai1* (Figure 10F, 10G). In contrast, the healthy lungs of proficient pups had high expression of *Cepbp*, an EMT-repressing TF critical to maintenance of the myofibroblast phenotype (Hu et al., 2012) (Figure 10F, 10G). Strikingly, the *Cpa3*^{Cre} targeted "EMT-like" Myo_Fibro cluster showed reduced expression of key ECM genes including collagens, laminins and elastin (Eln) (Figure 10F, 10G), which mirrors their reduced expression at a protein level (Figure 7D). Myofibroblast precursors – the Pre_Myo_Fibro cluster - were reduced in the *Cpa3*^{Cre} targeted lung (Figure 10D) and displayed

transcriptional changes (Figure 10E), indicative of defects within the myofibroblast development trajectory.

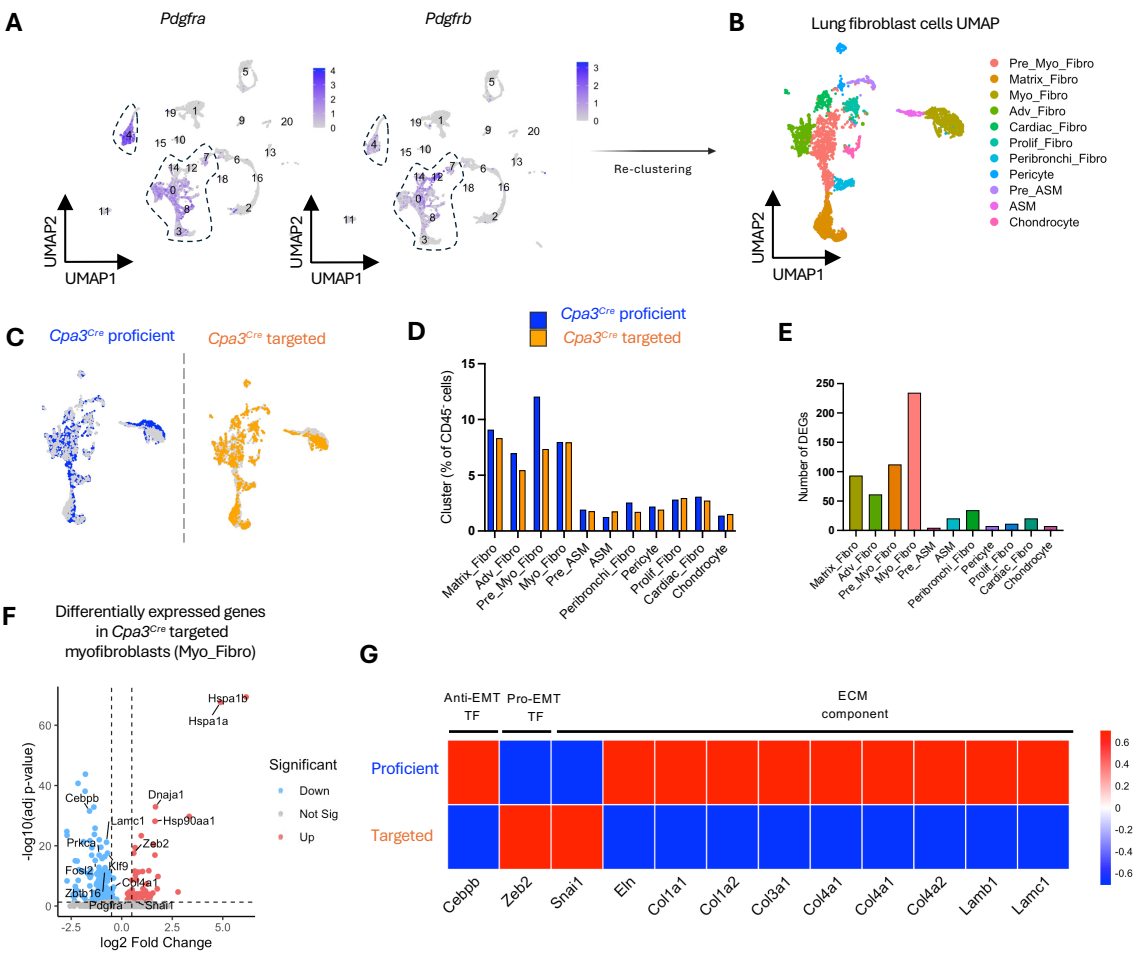

Chapter (3) Figure 10: *Cpa3*^{Cre} targeted lungs exhibit dysfunctional fibroblast-extracellular matrix landscape at E18.5.

(A) UMAP feature plots showing expression of *Pdgfrb* (left) and *Pdgfrb* (right) used to identify fibroblasts within the E18.5 fetal lung $CD45^-$ compartment. (B) UMAP plot of re-clustered fibroblast populations, including pericytes, matrix fibroblasts (Matrix_Fibro), adventitial fibroblasts (Adv_Fibro), *Lgr5*$^+$ peribronchial fibroblasts (Peribronchi_Fibro), myofibroblasts (Myo_Fibro) and their precursors (Pre_Myo_Fibro), as well as actively proliferating fibroblasts (Prolif_Fibro). In addition, we captured some actin smooth muscle cells (ASM) and precursors (Pre_ASM). (C) UMAP plots visualising differences in fibroblast populations between proficient (left) and targeted (right) lungs. (D) Quantification of fibroblast populations (as a proportion of $CD45^-$ cells) in proficient and targeted lungs. (E) Number of differentially expressed genes (DEGs) identified in each fibroblast population when comparing targeted and proficient lungs. DEGs identified used p-value cutoff of 0.05 and an absolute log2 fold-change cutoff of 0.5. (F) Volcano plot showing DEGs that are significantly upregulated (red) or downregulated (blue) in Myo-Fibro cells from targeted lungs relative to proficient lungs. (G) Heatmap showing scaled gene expression of selected epithelial-to-mesenchymal (EMT)-associated transcription factors and extracellular matrix (ECM) genes in proficient and targeted Myo-Fibro cells in the fetal lung.

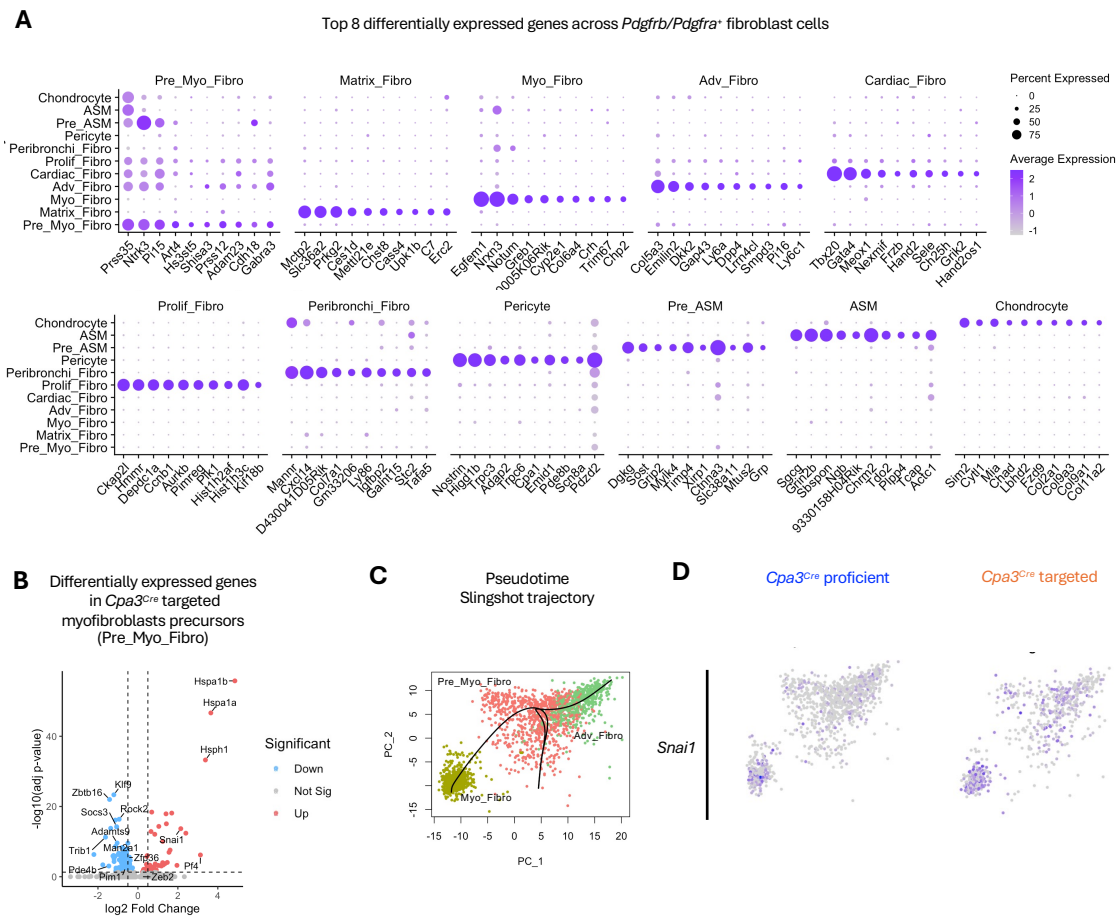

Chapter (3) Supplementary Figure S10: *Cpa3*^{Cre} targeted lungs exhibit dysfunctional fibroblast-extracellular matrix landscape at E18.5.

(A) Top 8 differentially expressed genes across *Pdgfra/Pdgfrb*$^{+}$ fibroblast sub-clusters in the fetal lung CD45^{-} cells at E18.5. Colour scale indicates average expression of each gene. Dot sizes represent the percent of cells expressing each gene. (B) Volcano plot showing differential gene expression analysis of fetal lung myofibroblast precursor cluster (Pre_Myo_Fibro) between *Cpa3*^{Cre} targeted and *Cpa3*^{Cre} proficient pups at E18.5. Genes were considered significant at p-value cutoff < 0.05 and minimum absolute $\log_2$ fold change

of 0.5 was used to identify upregulation (red) or downregulation (blue) of gene expression. (C) Slingshot trajectory analysis of fibroblast populations showing the inferred developmental trajectory linking myofibroblast precursor cluster (Pre_Myo_Fibro) and myofibroblast cluster (Myo_Fibro), following a distinct trajectory from other fibroblast lineages (Adv_Fibro cluster shown here). (D) UMAP feature plots showing expression of *Snai1* across fetal lung fibroblast populations in *Cpa3*^{Cre} targeted and *Cpa3*^{Cre} proficient pups at E18.5.

The Pre_Myo_Fibro cluster in the *Cpa3*^{Cre} targeted group showed significantly reduced expressed of key myofibroblast differentiation and maturation genes including *Trib1, Man2a1, Socs3, Rock2, Pde4b and Pim1* (Figure S10B), and had upregulated EMT transcription factors *Zeb2* and *Snai1* (Figure S10B), suggesting impaired myo-fibroblast development. Trajectory inference using Slingshot revealed a distinct developmental trajectory between Pre_Myo_Fibro cluster and the Myo_Fibro cluster, separate from other fibroblast clusters like the Adv_Fibro (Figure S10C). Moreover, increase in *Snai1* expression within the myofibroblast cluster and their precursor along this trajectory (Figure S10D) indicate an impaired development of myofibroblasts in the *Cpa3*^{Cre} targeted lungs. The reduction and transcriptional changes within the pre-myofibroblasts therefore represent a plausible source of mesenchymal perturbation that may contribute to the impaired myofibroblast compartment.

Taken together, the data suggested that the myofibroblasts and their precursors were most affected by *Cpa3*^{Cre} targeting in this model; their EMT-like phenotype results in a dysfunctional ECM state in the targeted lungs which may contribute to impaired lung development and structure.

Effect of Cpa3^{Cre} targeting on the mast cell compartment in fetal lungs

To determine whether the impaired lung development we observed in *Cpa3^{Cre}* targeted pups is due to the absence of mast cells, we first quantified MC abundance in the fetal lung using flow cytometry. MCs were gated as previously described (Figure S2A-B). Surprisingly, MCs were not reduced within the CD45^{+} compartment in fetal lungs at E15.5 (Figure 11A) and only a modest reduction could be detected by E18.5 (Figure 11B). The frequency of MCs in the fetal lung did not differ between *Cpa3^{Cre}* targeted pups that survived or died within the observation window. Notably, we did not identify a reduction in macrophages in these stages (Figure S11A-B), indicating that the perturbation did not broadly impact the myeloid compartment during fetal lung development.

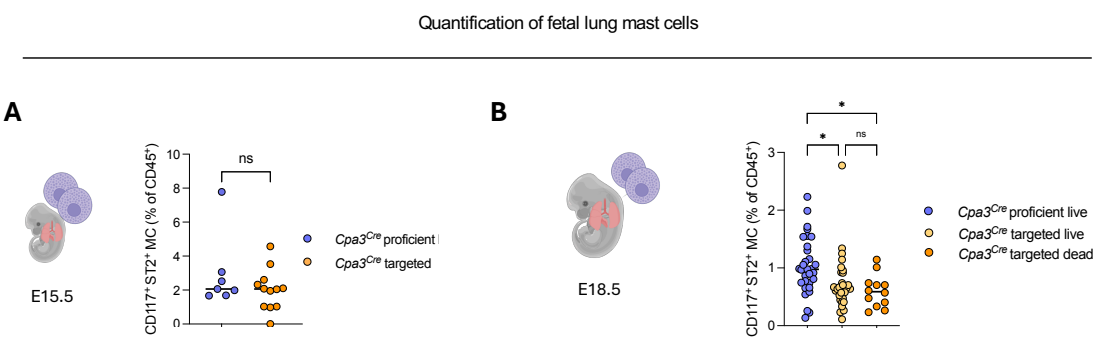

Chapter (3) Figure 11: Mast cell abundance in the fetal lung of *Cpa3^{Cre}* targeted mice.

Flow cytometric quantification of mast cells within the CD45^{+} compartment of fetal lungs in proficient and targeted pups at (A) E15.5 and (B) E18.5. *Cpa3^{Cre}* targeted pups are stratified by survival outcome during the one-hour observation period following C-section delivery at E18.5. Statistical significance is indicated where applicable (P-values were defined as * <

0.05, ns = not significant). Data from (A-B) are cumulative of at least 12 mice per group. *Data in A and B generated by Simran Kapoor and Clara Munz.*

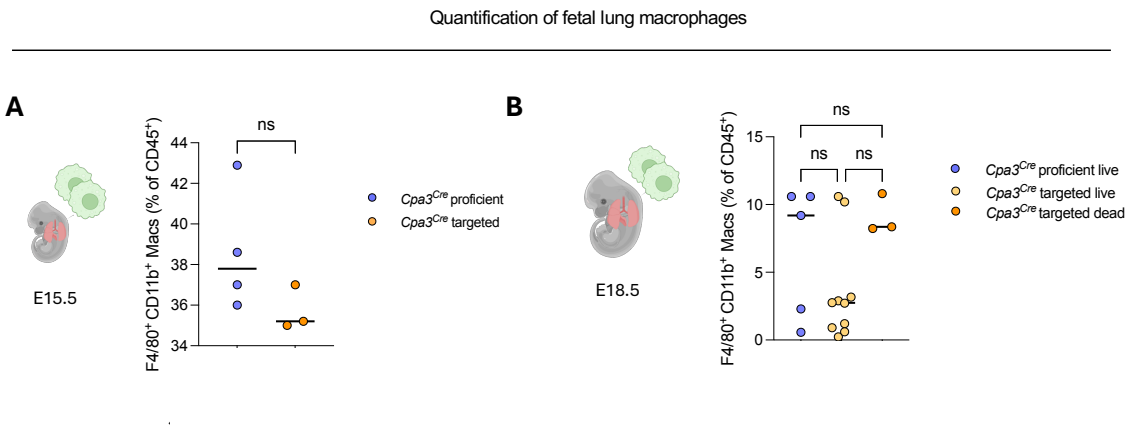

Chapter (3) Supplementary Figure S11: Macrophage abundance in the fetal lung of *Cpa3*^{Cre} targeted mice.

Quantification of macrophages (gated as CD45$^+$ CD11b$^+$ F4/80$^+$cells) as a proportion of CD45$^+$ cells in the fetal lung of *Cpa3*^{Cre} targeted and *Cpa3*^{Cre} proficient pups at (A) E15.5 and (B) E18.5. Data shown in (A) and (B) are cumulative of at least 3 mice per group. Statistical significance is indicated where applicable (P-values were defined as ns = not significant).

The fetal lung MC compartment is very heterogeneous during development, and changes drastically between E15.5 and E18.5, as previously described in Chapter 2. Given the limited reduction in the fetal MC compartment, we next asked whether *Cpa3*^{Cre} targeting affected specific MC subsets. Single cell RNA sequencing was therefore performed on the CD45$^+$ cells from the lungs of *Cpa3*^{Cre} targeted and proficient pups at E15.5 and E18.5, enriching for MCs at E18.5 (see M&M Figure 1). After performing Seurat integration to account for technical differences driven by the different experimental runs (Figure 12A, 12B), we performed

quality control to eliminate doublets and dead cells and were left with 17446 cells on which we performed dimensional reductional and unsupervised clustering. This revealed 16 distinct CD45⁺ cell populations based on top DEGs (Figure 12B, S12A-B). MCs (c7_MC) were identified on the basis of key MC genes including *Cpa3, Kit* and *Cma1* (Figure 12C).

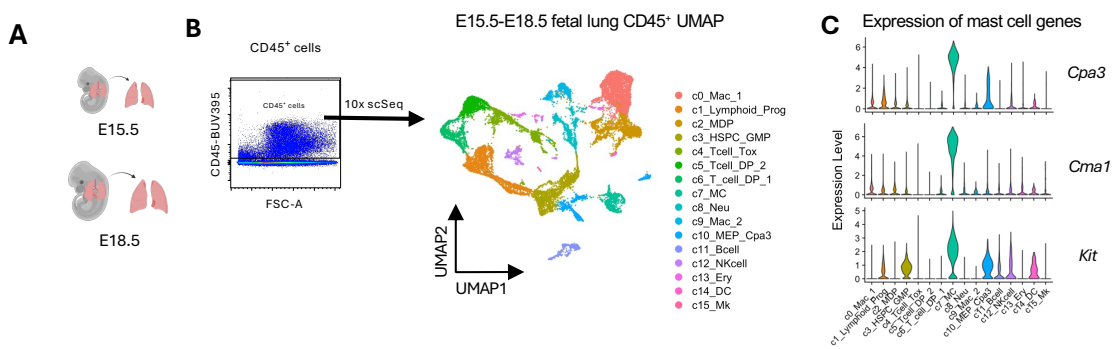

Chapter (3) Figure 12: Single cell transcriptomic profiling of E15.5 and E18.5 fetal lung haematopoietic cells.

(A) Schematic (left) showing experimental workflow of single cell RNA sequencing (scSeq). Live CD45⁺ haematopoietic cells were isolated from from fetal lung of E15.5 and E18.5 fetuses for 10x single cell sequencing (10x scSeq). Samples from both sequencing runs were integrated using Seurat Integration. (B) UMAP plot of the sequenced and integrated dataset of fetal lung CD45⁺ cells merged across E15.5 and E18.5 timepoints. Cells (n=17446) were dimensionally reduced followed by unsupervised clustering to reveal 16 distinct clusters. (C) Violin plots showing expression of mast cell genes *Cpa3, Cma1* and *Cpa3.*

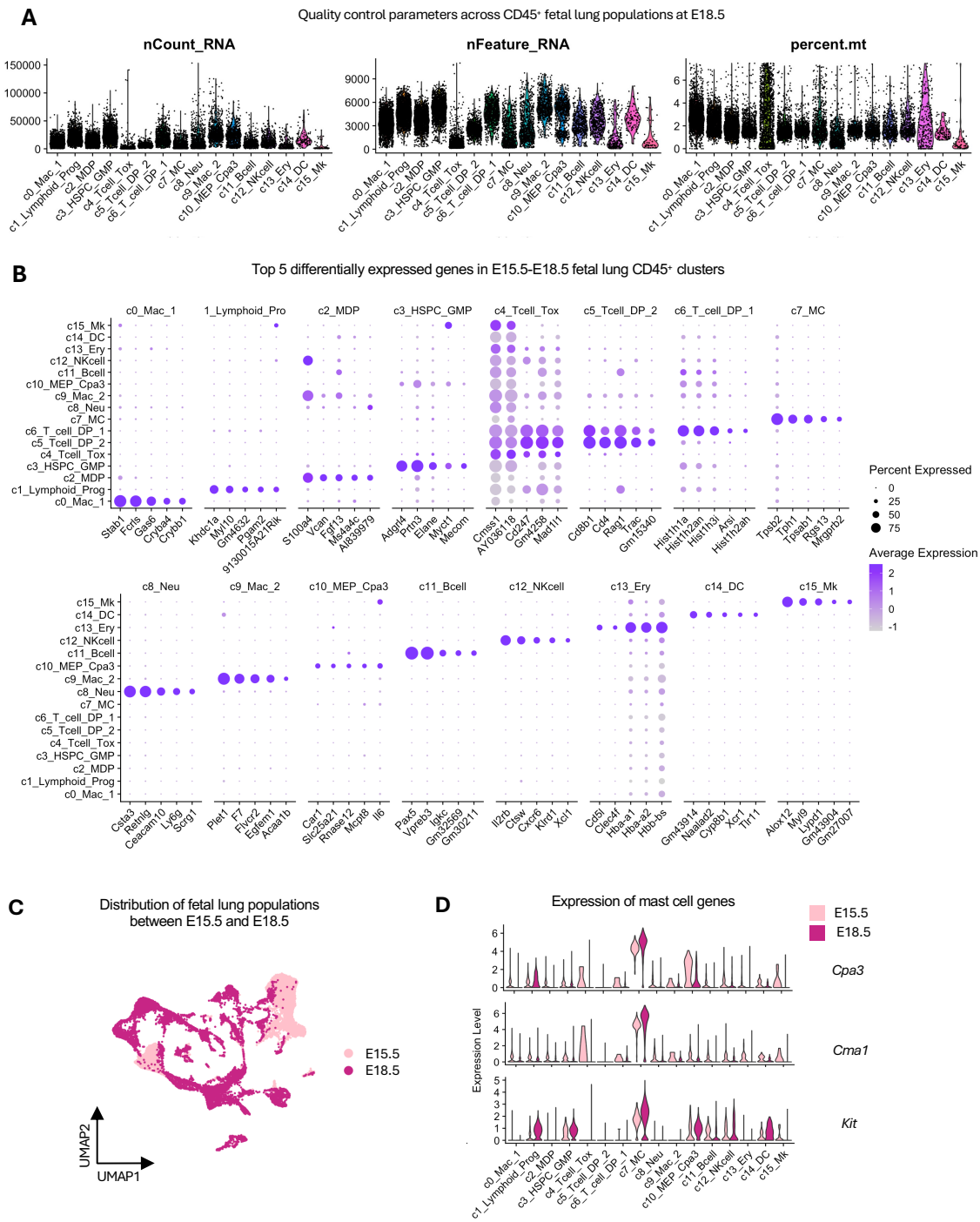
A
Quality control parameters across CD45+ fetal lung populations at E18.5
nCount_RNA
nFeature_RNA
percent.mt
B
Top 5 differentially expressed genes in E15.5-E18.5 fetal lung CD45+ clusters
Percent Expressed
Average Expression
C
Distribution of fetal lung populations between E15.5 and E18.5
E15.5
E18.5
UMAP2
UMAP1
D
Expression of mast cell genes
Expression Level
Cpa3
Cma1
Kit

Chapter (3) Supplementary Figure S12: Single cell transcriptomic profiling of CD45$^+$ cells in the fetal lung at E15.5 and E18.5 in *Cpa3^{Cre} Rosa26$^{lsl\text{-}DTA}$* mice.

(A) Violin plots showing quality control metrics for E15.5 and E18.5 fetal lung CD45$^+$ cells across identified clusters, including total RNA counts (nCount_RNA), number of detected genes (nFeature_RNA) and percentage of mitochondrial genes (percent.mt). (B) Top 5 differentially expressed genes in the CD45$^+$ clusters identified in the fetal lung at E15.5 and E18.5. Colour scale indicates average expression of each gene. Dot sizes represent the percent of cells expressing each gene. (C) Distribution of fetal lung CD45$^+$ clusters at E15.5 and E18.5. (D) Violin plot showing expression levels of *Cpa3* at E15.5 and E18.5 per fetal lung CD45$^+$ cluster.

Previous analysis (see Chapter 2) revealed that one subset of MCs was detected early at E15.5 (MC_1) while the second subset emerges later by E18.5 (MC_2) (Figure 13A, 13B, S13A). Within the *Cpa3*$^+$ compartment, we found that at E15.5, *Cpa3^{Cre}* targeted pups had a proportional increase in the MC_1 population compared to proficient littermates (Figure 13A). By E18.5, no differences could be detected in the MC_1 subset but the recently arising MC_2 population was increased in the *Cpa3^{Cre}* targeted pups (Figure 13B). Given the high levels of *Cpa3* in MCs as well as their precursors (Figure 1A-B, 2A-B), it is unlikely that lack of *Cpa3* expression and/or Cre activity (Figure 3D) could contribute to poor depletion efficacy of MCs in the fetal lung at these stages. We therefore wanted to assess whether MCs were being replenished within this compartment. Indeed, cell cycle scoring revealed that these subsets had a marked increase in proliferation in *Cpa3^{Cre}* targeted lungs relative to the proficient littermates (Figure 13C). This increase in proliferation may therefore contribute to the replenishment of the MC compartment despite our attempts to genetically target MCs in the fetal lung.

Although MC populations appeared to recover in the fetal lungs despite in *Cpa3*^{Cre} targeting, it remained possible that there may transcriptional differences in these repopulating MCs. To identify whether the remaining MCs in the fetal lung were functionally different, we performed differential gene expression analysis. We did not identify any significantly DEGs (at significance p-value cutoff at < 0.05) between targeted and proficient MCs at E15.5, indicating that the MCs were unlikely to be intrinsically different in the targeted group at this stage (Figure S13B). However by E18.5, differential gene expression analysis revealed that MCs in the targeted group significantly downregulated expression of some genes. This included serotonin transporter *Slc6a4,* as well as *Gab2* a scaffold protein that is essential for MC activation and degranulation in allergic responses (Gu et al., 2001). CD63 is used as an indicator for MC degranulation (Kraft et al., 2013b) (Figure 13D), and flow cytometric analysis revealed that CD63 expression was significantly lower in targeted MCs compared to proficient MCs at E18.5 (Figure 13E). Taken together, these results indicated that MCs show reduced activation and/or degranulation within the lung upon *Cpa3*^{Cre} targeting. Notably, avidin expression remained unchanged in targeted lung MCs (Figure 13E), indicating preservation of granule content despite altered activation dynamics.

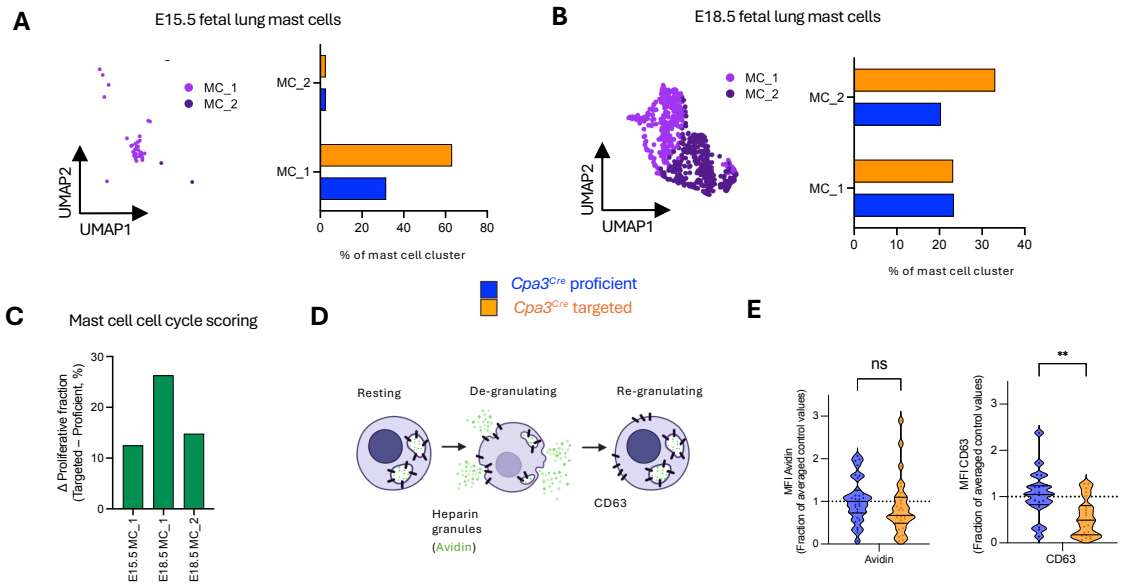

Chapter (3) Figure 13: Fetal lung mast cells persist and show altered proliferation and activation profiles despite *Cpa3*^{Cre} targeting.

(A-B) UMAP plot of mast cell populations (MC_1 and MC_2) (left) and quantification (right) of each mast cell population as a proportion of the mast cell cluster at (A) E15.5 and (B) E18.5. (C) Cell cycle scoring of fetal lung mast cells, showing the difference in the fraction of proliferating cells (cells in S/G2M phase) between targeted and proficient pups at E15.5 and E18.5. (D) Schematic illustrating mast cell degranulation and re-granulation dynamics, highlighting heparin granular content (marked by avidin) and CD63 surface expression associated with degranulation. (E) Flow cytometric quantification of intracellular expression of avidin (left) and surface expression of CD63 (right) on fetal lung mast cells at E18.5, shown as mean fluorescence intensity (MFI) normalised to averaged proficient lung MC control values. Statistical significance is indicated where applicable (P-values were defined as ** <

0.005, ns = not significant). Data in (E) are cumulative of at least 19 mice per group. *Data in E generated by Simran Kapoor and Clara Munz.*

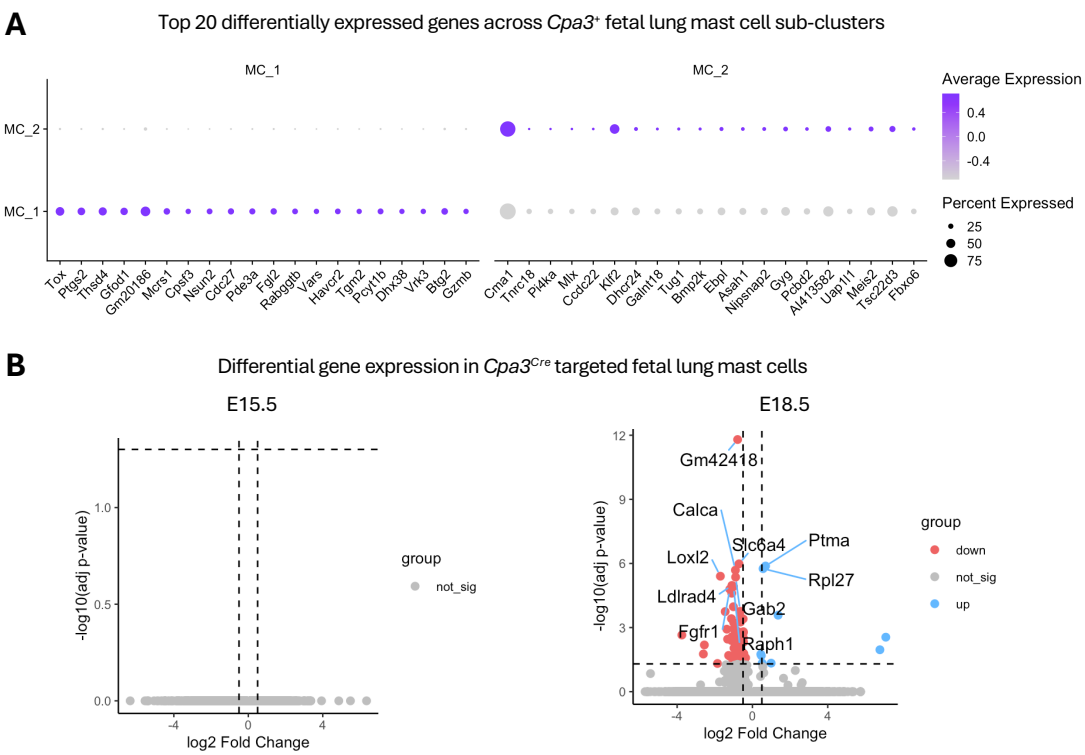

Chapter (3) Supplementary Figure S13: Effect of *Cpa3*^{Cre} targeting on fetal lung mast cells at E15.5 and E18.5.

(A) Top 20 differentially expressed genes in the two fetal lung mast cell subclusters MC_1 and MC_2 identified at E15.5 and E18.5. Colour scale indicates average expression of each gene. Dot sizes represent the percent of cells expressing each gene. (B) Volcano plot showing differential gene expression analysis of fetal lung mast cells between *Cpa3*^{Cre} targeted and *Cpa3*^{Cre} proficient pups at E15.5 (left) and E18.5 (right). Differences in gene expression were

considered significant at p-value cutoff < 0.05 and minimum absolute log_2 fold change of 0.5 was used to identify relative upregulation (blue) or downregulation (red) of gene expression.

Cpa3^{Cre} targeting causes additional hematological defects

Analysis of the lung proteome revealed that *Cpa3^{Cre}* targeted lungs expressing much lower levels of platelet-associated proteins (Figure 14A). To evaluate whether platelets were systemically affected upon *Cpa3^{Cre}* targeting, we also quantified platelets in the blood of *Cpa3^{Cre}* targeted pups and found that they had significantly lower platelet counts than proficient littermates (Figure 14B). Importantly, in other MC-targeting models such as *Mcpt5^{Cre} Rosa26$^{lsl\text{-}DTA}$* mice, the fetal lung still retains MCs, with only a modest reduction of the compartment (Figure S14A). However, these mice do not exhibit platelet reduction (Figure S14B), suggesting that *Mcpt5^{Cre}* targeting of MCs does not necessarily result in a direct reduction of platelets. Rather the impact on platelets and MCs in the *Cpa3^{Cre} Rosa26$^{lsl\text{-}DTA}$* model may be a result of targeting of other *Cpa3*-expressing lineages.

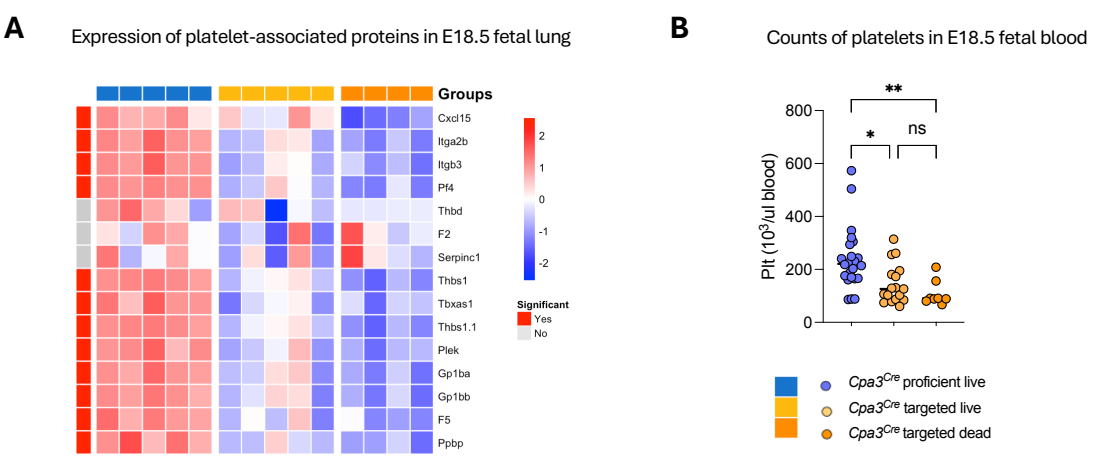

Chapter (3) Figure 14: Platelet-associated alterations in *Cpa3^{Cre}* targeted mice at E18.5.

(A) Heatmap showing scaled expression of selected platelet-associated proteins across proficient (n=5), targeted live (n=5), and targeted dead (n=4) lung samples. Proteins significantly different between proficient and targeted dead group marked in red. (B) Peripheral blood platelet counts in proficient and targeted live, and targeted dead pups. Data in (B) are cumulative of at least 7 mice per group. Statistical significance is indicated where applicable (P-values were defined as ** < 0.05, * < 0.05, ns = not significant). *Data in B generated by Clara Munz.*

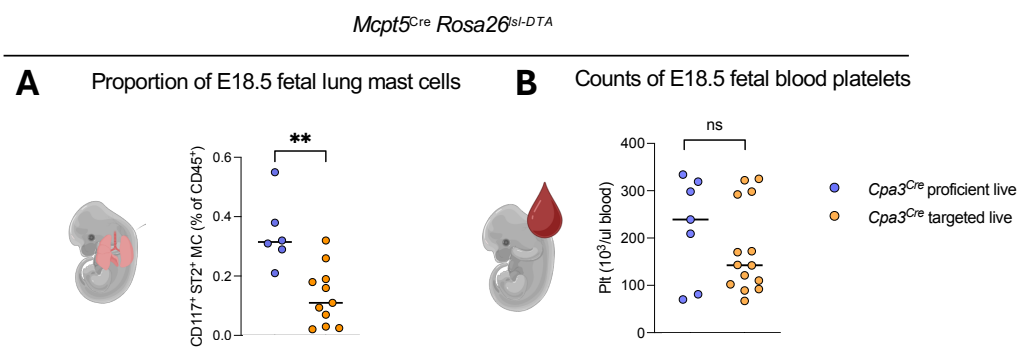

Chapter (3) Supplementary Figure S14: Effect of *Mcpt5*^{Cre} targeting on haematopoietic lineages at E18.5.

(A) Quantification of mast cells (gated as CD45$^+$ CD11b$^-$ F4/80$^-$ CD117$^+$ (Kit$^+$) ST2$^+$) as a proportion of the CD45$^+$ cells in the fetal lung; and (B) Quantification of platelets (10^3/uL of blood) in peripheral fetal blood in *Mcpt5*^{Cre} proficient and *Mcpt5*^{Cre} targeted pups at E18.5. Data shown in (A) and (B) are cumulative of at least 7 mice per group. Statistical significance is indicated where applicable (P-values were defined as ** < 0.005, ns = not significant). *Data in A-B generated by Simran Kapoor and Clara Munz.*

Platelets derive from megakaryocytes, and *Cpa3*-expressing progenitors early in fetal haematopoiesis have been shown to contribute to megakaryocyte development (Ma et al., 2025). This raises the possibility that our *Cpa3*^{Cre} driver may inadvertently also target progenitors upstream of platelet production.

To explore whether the *Cpa3*^{Cre} *Rosa26*$^{lsl\text{-}DTA}$ model may target other *Cpa3*-expressing lineages, we next investigated whether other populations were affected in our fetal lung transcriptomic dataset. Notably, we found that megakaryocyte-erythrocyte progenitors (MEPs) closely clustered with the basophil/MC lineage in the UMAP space (Figure 12B), and additional sub-clustering revealed the presence of megakaryocyte progenitors (MkP), erythrocyte progenitors (EryP), basophils (Baso), mast cells (MC) and undifferentiated progenitors (udPs) (Figure 15A, S15A). *Cpa3* expression was lowest in EryP cells (Figure 15B). Unlike the observed reduction in fetal blood platelets, we did not find any defects in erythropoiesis parameters in the *Cpa3*^{Cre} targeted pups (Figure S15C), suggesting that the erythroid compartment may be unaffected in this model.

Although the highest *Cpa3* expression was detected in MCs, lower levels of *Cpa3* expression could be detected in the Baso and udP clusters, with a small proportion of MkP also expressing *Cpa3* across stages (Figure 15B, S15B). Unlike EryP, MkPs additionally shared expression of *Gata2* (Figure 15C) which also defined MC lineages (Li et al., 2015; Ohmori et al., 2015; Tojima et al., 2024). To determine whether overlap between MkP and mast cell-basophil lineages in terms of gene expression profile was also associated with changes in population abundance, we next quantified the fetal lung CD45^{+} compartment at E15.5, an early developmental stage. Within the CD45^{+} compartment of the fetal lung, a modest reduction in the relative abundance of Baso, MC, udP as well as MkP could be detected in

Cpa3^{Cre} targeted pups already by E15.5 (Figure 15D), prior to the onset of lung development saccular stage.

Taken together, these data suggest that fetal lung MkP and circulating platelets are also reduced in the *Cpa3*^{Cre} *Rosa26*$^{lsl\text{-}DTA176}$ mice. However, these defects are unlikely to be driven by direct targeting of MkP given the lack of *Cpa3* expression, at least at E13.5 (Ma et al., 2025). Nonetheless, shared features between the developemental programmes of MkP and MCs may suggest shared upstream progenitors and future work will need to delineate how *Cpa3*-expressing progenitors contribute to these lineages in fetal development.

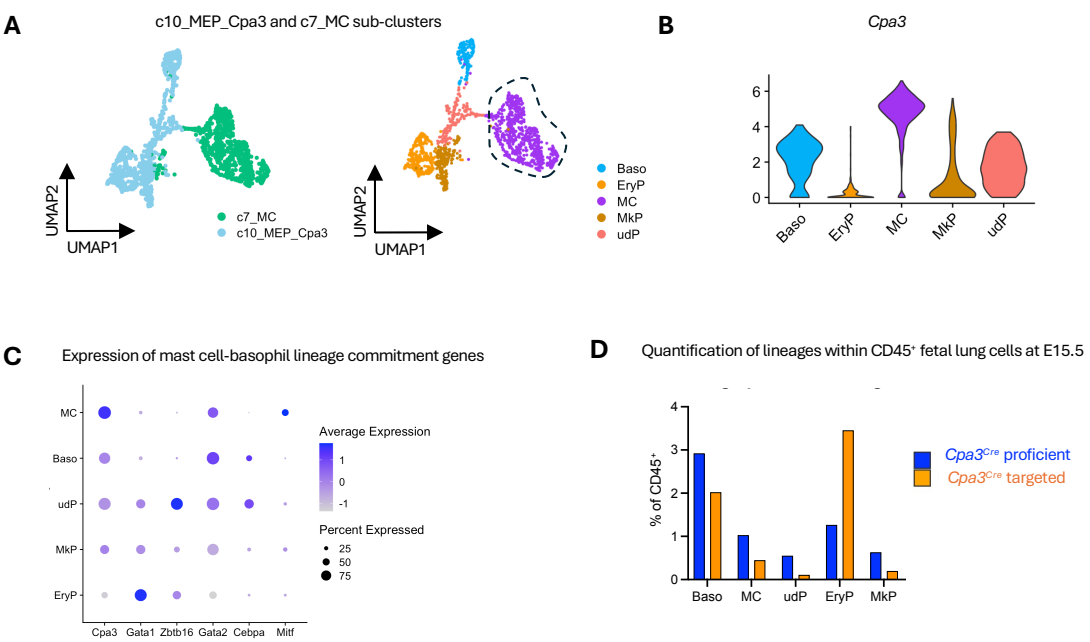

Chapter (3) Figure 15: Identification of additional Cpa3-expressing lineages in the fetal lung.

(A) UMAP plot of sub-clustered *Cpa3*$^{+}$ cells within the fetal lung including megakaryocyte progenitors (MkP), erythrocyte progenitors (EryP), basophils (Baso), mast cells (MC) and undifferentiated progenitors (udPs). (B) Violin plot showing *Cpa3* expression levels across the indicated sub-populations. (C) Dot plot showing expression of mast cell-basophil lineage commitment genes across the indicated sub-populations. Colour scale indicates average expression of each gene. Dot sizes represent the percent of cells expressing each gene. (D) Quantification of megakaryocyte progenitors (MkP), erythrocyte progenitors (EryP), basophils (Baso), mast cells (MC) and undifferentiated progenitors (udPs) as a proportion of sequenced CD45^{+} cells in the fetal lung at E15.5.

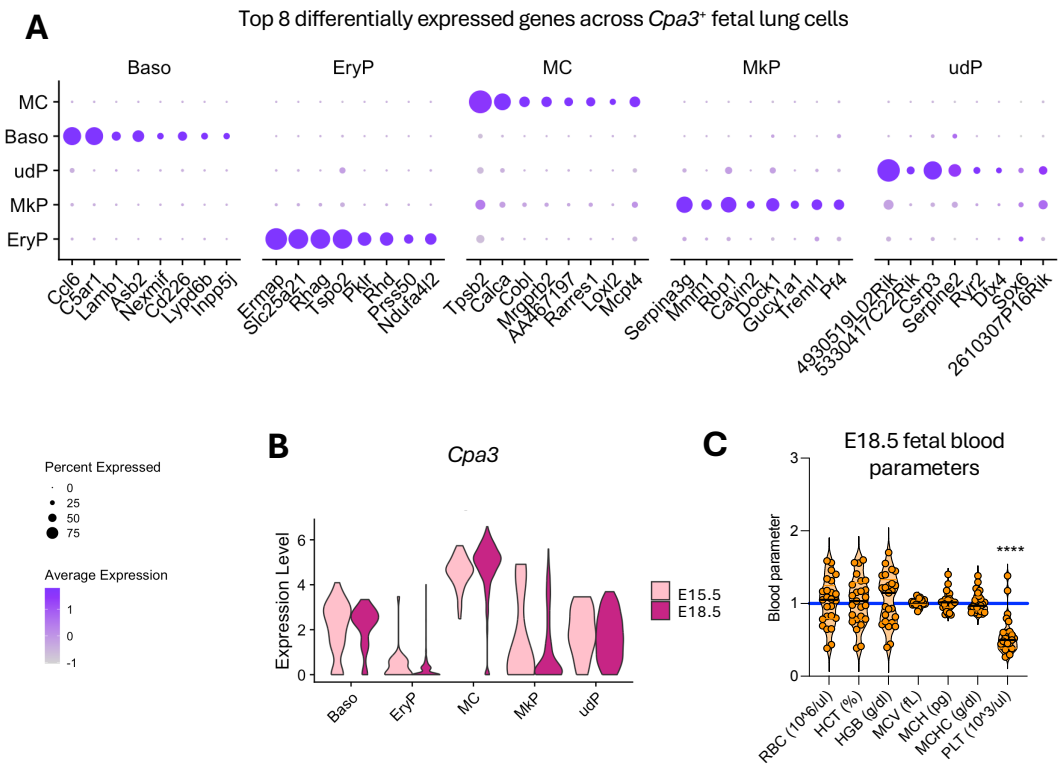

Chapter (3) Supplementary Figure S15: Effects of *Cpa3*^{Cre} targeting other fetal haematopoietic lineages.

(A-B) Single cell sequencing data of the sub-clustered *Cpa3*$^{+}$ populations within the CD45^{+} compartment of fetal lungs at E15.5 and E18.5. (A) Top 8 differentially expressed genes across the *Cpa3*$^{+}$ sub-clusters megakaryocyte progenitors (MkP), erythrocyte progenitors (EryP), basophils (Baso), mast cells (MC) and undifferentiated progenitors (udPs) (described in Figure 15A). Colour scale indicates average expression of each gene. Dot sizes represent the percent of cells expressing each gene. (B) Violin plot showing expression of *Cpa3* across *Cpa3*$^{+}$ sub-clusters at both E15.5 and E18.5. (C) Violin plot showing blood counts of *Cpa3*^{Cre} targeted pups at E18.5. Parameters evaluated include erythrocytes/red blood cells (RBC) and hematocrit (HCT), as well as functional parameters of RBCs including hemoglobin (HGB),

mean corpuscular volume (MCV), mean corpuscular hemoglobin (MCH) and mean corpuscular hemoglobin concentration (MCHC). Platelets (PLT) shown alongside for comparison. All values shown are normalized to average values in *Cpa3*^{Cre} proficient pups as controls. Data shown in (C) are cumulative of at least 25 mice per group. Statistical significance is indicated where applicable (P-values were defined as **** < 0.0001). *Data in C generated by Simran Kapoor and Clara Munz.*

Discussion

Conventionally used MC deficiency models fail to reveal overt developmental defects in embryonic stages, despite the early emergence of these immune cells during fetal haematopoiesis. One exception to this is the c*Kit* deficiency model, which revealed corneal innervation and vascularisation defects in the absence of MCs (Liu et al., 2015). However, *cKit* signalling is not specific to MCs (Gutierrez et al., 2015; Keller et al., 1995; Waskow et al., 2004), necessitating the re-evaluation of the role of MCs in fetal development. Using the *Karma*^{Cre}*-Rosa26*$^{lsl\text{-}DTA}$ model which target MCs independently of *Kit* (Mattiuz et al., 2018), we previously showed that MCs do not play an essential role in mammary gland development (Kapoor et al., 2025), contrary to findings from c*Kit* deficiency models (Lilla and Werb, 2010). However, *Karma (Gpr141b)* is not expressed throughout early stages of embryonic MC development (See Chapter 2), limiting its utility in investigating MC functions during this developmental window. The utility of other models like *Mcpt5*^{Cre}*-Rosa26*$^{lsl\text{-}DTA}$ is also limited in early MC developmental contexts, as *Mcpt5 (Cma1)* is expressed early upon MC differentiation but not in MC precursors (See Chapter 2).

In this study, we set out to investigate whether MCs may play a role in embryonic development using a novel approach. *Cpa3* is also expressed early in embryonic fetal yolk

sac and liver precursors that seed MCs in peripheral tissues (Ma et al., 2025), reflecting its importance in MC developmental programmes. However, current *Cpa3*-based MC targeting models rely on Cre genotoxicity and sensitivity to targeting is therefore dependent on the level of *Cpa3* expression and do not target basophil and mast cell progenitors in adults (Feyerabend et al., 2011b). We confirmed that the *Cpa3* transcript is expressed throughout the MC lineage during embryonic development. Moreover, we showed that MC precursors also express *Cpa3*, albeit at lower levels than committed mature MCs. By pairing *Cpa3-Cre* with Diphtheria toxin, we aimed to increase the sensitivity of targeting cells expressing *Cpa3* in order to extend our ability to target MC development in these early developmental stages. However, we found that this approach did not completely ablate MCs and the remaining MCs instead showed increased proliferative capacity. Yet, $Cpa3^{Cre}$ based targeting in mice resulted in impaired embryonic development, causing respiratory distress and lethality shortly after birth.

Respiratory distress driven by impaired lung saccular development

Lung development is a highly complex, temporally regulated process commencing at E9.5 following the emergence of the lung bud in the mesoderm germ layer (Herriges & Morrisey, 2014; Schittny, 2017). During the pseudoglandular stage (E12.5-E16.5), the lung buds undergo regulated branching morphogenesis to generate the respiratory network, followed by the canalicular phase (E16.5-E17.5) which involves the differentiation of these branches into alveoli precursor saccules lined with airway type I (AT1) and type II (AT2) epithelial cells. These saccules eventually develop into alveoli during the saccular phase (E18.5-P5).

Saccular thinning depends on appropriate vascularisation to facilitate the thinning of air-blood barriers in the saccules (Caldeira et al., 2021; Vu et al., 2003). Starting in the canalicular phase, developing capillary networks are separated from the airway septa by

mesenchymal cells, and saccular thinning is driven by coordinated apoptosis and condensation of the mesenchyme (Schittny, 2017; Paramore et al., 2024). We observed that the lungs of *Cpa3*^{Cre} targeted pups appeared morphologically altered, including a trend towards increased intrasaccular thickness. These findings suggest that lungs in these targeted pups have impaired saccular maturation, a defect which is frequently associated with respiratory failure upon birth (Tremblay et al., 2007; Wigglesworth & Desai, 1982). Although this difference did not reach statistical significance, the current sample size limits statistical power and additional cohorts of neonatal lungs will be required to confirm this effect. It also remains possible that the phenotype is only beginning to emerge at E18.5 resulting in the subtle nature of the defect at this stage. Consistent with the late-stage nature of the defect observed, the fetal lungs in targeted pups appeared normal at E17.5, reflecting that impaired saccular thinning is a late-stage developmental process in gestation (Schittny, 2017). In further support of this, our survival analyses revealed that only 50% of pups die within one hour when C-sections are performed at E18.5, whereas following natural delivery (P0), all targeted pups ultimately die within 1-3 days after birth. However, irrespective of survival, all pups within the targeted group share a similar proteome that is distinct from proficient lungs. Taken together, these findings reflect that the incomplete penetrance of the lethality phenotype at E18.5 may be consistent with a developmental defect that progressively worsens later during the end stages of sacculation.

Single cell sequencing of the stroma revealed defects in the mesenchymal compartments, that could be underlying this impaired lung development phenotype. However, unlike fibrotic conditions where an upregulation of fibroblasts and hyperactivation is observed, we observed a decrease in myofibroblasts precursors, and the remaining myofibroblasts within the developing lung were markedly altered in the *Cpa3*^{Cre} targeted group. Specifically, the myofibroblasts showed an increase in EMT markers and loss of *Cebpb*, indicating a loss of

functional myofibroblast identity in the targeted group (Hu et al., 2004; Hu et al., 2012). These myofibroblasts also showed a decrease in transcriptional expression of collagenases, elastases and laminins in the *Cpa3*^{Cre} targeted lung, which indicated that fibroblast identity shifted from functional to EMT-like and ultimately, rendered them hypoactive. These findings were additionally mirrored at a protein level, where *Cpa3*^{Cre} targeted lungs showed a trend towards reduced in expression of these extracellular matrix proteins. Intriguingly, proteomic analyses showed that targeted pups that survived the first hour after C-section at E18.5 had an intermediate phenotype between the proficient pups and targeted dead pups, further suggestive of incomplete penetrance. Nonetheless, this resulted in a poor sample size to detect the significance of these proteomic defects in the targeted group. Despite the weak statistical power however, we noted that targeted dead pups had a significant decrease in Tgfb1 and an increase in Tgfb2 and Smad2, reflecting a perturbed Tgfb signaling axis in the lungs.

The role of Tgfb in fibrosis has been well established. Integrin-mediated activation of latent Tgfb drives Tgfb signaling via Smad proteins and results in EMT transition and differentiation into hyperactivated myofibroblasts under chronic inflammatory conditions (Kim et al., 2018; Ye & Hu, 2021; L. Gu et al., 2007). Previous work has revealed that in the context of fetal development, the absence of Tgfb1 results in reduced myofibroblast differentiation and subsequently impaired lung development (Tsukiji et al., 2018). Similarly, we found that *Cpa3*^{Cre} targeted lungs had a marked reduction in Tgfb1 and the myofibroblasts were hypoactive. The identity and activation of myofibroblasts is regulated *Cebpb*, which interacts with Tgfb1 (Abraham et al., 2009). Although our proteomic analysis could not determine whether the Tgfb proteins are latent or activated, these findings preliminarily suggests that absence of appropriate Tgfb1 signaling in this developmental context may impair even normal myofibroblast differentiation and result in poor extracellular matrix formation.

The effects of Tgfb may also extend to perturbing epithelial cell identity in lung development (Callaway et al., 2024). The targeted lungs revealed an increase in AP-1 signaling in AT2 cells. AT2 cells typically exhibit stem cell like plasticity within the respiratory tree during lung development and can differentiate into AT1 cells (Sawhney et al., 2025). Aberrant activation of AT2 cells upon injury in inflammatory contexts have been associated with an increase in AP-1 signaling and increased AT2-to-AT1 differentiation (Lynch et al., 2025b). We observed an increase in AT1 cells in the stroma, suggesting that increased AT2 activation may drive AT1 cell differentiation in the targeted lungs. Strikingly, *Cpa3*^{Cre} targeted lungs also had a prominent population of epithelial cells with mesenchymal features. These mesenchymal-like cells expressed transcription factors associated with epithelial-to-mesenchymal transition (EMT) including *Zeb2* and *Snai1* (Saitoh, 2023). Notably, *Tgfb2* is expressed highly in these AT1 and EMT cells, which could explain the aberrant increase in Tgfb2 proteins in *Cpa3*^{Cre} targeted lungs. We speculate that the increased inter-saccular thickening observed in the lung architecture of targeted pups may correspond to the increase in AT1 and EMT-like cells. Additional staining of AT1 cells can allow for quantification of the AT1 cells to confirm whether hyperplasia contributes to increased saccular thickness. Moreover, Masson's trichome staining can provide insight into the fibrotic nature of the impaired connective tissue structure of the fetal lung (Ryota, 2023).

Tgfb is found throughout normal development and may play an important functional role in coordinating epithelial-mesenchymal interactions during fetal lung development (Saito et al., 2018). Indeed, various genetic knockout models targeting isoforms of *Tgfb* show impaired lung development, branching morphogenesis and airway collapse (Bartram and Speer, 2004; Saito et al., 2018). How the reduced expression of Tgfb1 and increased Tgfb2 relate to impaired epithelial-mesenchymal function remains unknown. Nonetheless, Tgfb2

knockout models reveal non-overlapping phenotypes with Tgfb1 knockouts in embryonic stages, with notable defects in developmental processes involving extensive epithelial-mesenchymal interactions (Sanford et al., 1997; Saito et al., 2018). While further work is needed to establish how the two Tgfb isoforms drive epithelial-mesenchymal interactions in saccular development, our work reveals a model in which the two isoforms are unable to compensate for each other to direct normal saccular development.

Taken together, our data support a model in which aberrant Tgfb signalling disrupts normal epithelial-mesenchymal crosstalk during the saccular stages of lung development; however, whether the increased EMT is a driver or consequence of impaired myofibroblast development remains unclear (Figure 16). One possibility is that aberrant Tgfb signaling fails to support myofibroblast differentiation, as seen in previous studies (Tsukiji et al., 2018). The abnormal myofibroblasts may result in improper extracellular matrix formation of the lung stroma which could then induce epithelial stress and EMT. An alternative model posits that impaired Tgfb signaling may drive epithelial cell dysregulation (Callaway et al., 2024) that secondarily alters myofibroblast development and consequently impairs lung development. Dissection of these possibilities will require careful analysis of the temporal progression of the defects, combined with compartment-specific *Tgfb* signaling perturbations to determine the dominant driver of the observed impaired lung development.

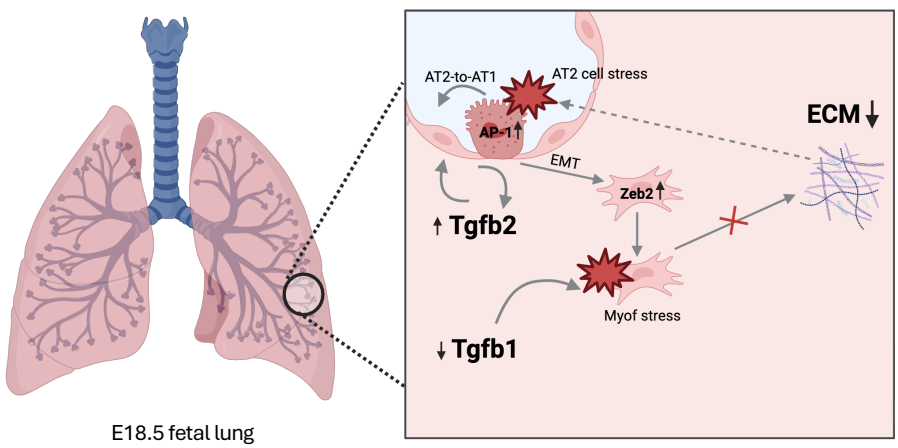

Chapter (3) Figure 16: Schematic overview of the lung developmental defect observed in the *Cpa3*^{Cre} *Rosa26*$^{lsl\text{-}DTA}$ model.

Schematic of fetal lung at E18.5 shows perturbed lung development features. Reduced Tgfb1 expression may result in reduced myofibroblast development which causes impaired extracellular matrix (ECM) formation. The perturbed extracellular matrix may trigger stress in airway epithelial type 2 (AT2) cells which may trigger type 1 (AT1) cell differentiation (via increased AP-1 signalling). The perturbed AT2 and AT1 cells may trigger epithelial-to-mesenchymal (EMT) transition and increase Tgfb2 signaling, which may cumulatively impair myofibroblast development and functions during saccular (late-stage) lung development.

Cpa3^{Cre} *based targeting results in altered hematopoietic outputs*

We sought to understand how targeting *Cpa3*-expressing cells could contribute to impaired lung development. Although we expected to target MCs, we surprisingly found only a modest reduction in MCs across early and late embryonic stages. The increase in

proliferation in MCs within *Cpa3*^{Cre} targeted lungs indicates ongoing replenishment in the MC compartment despite targeting. Moreover, *Cpa3*^{Cre} targeted MCs expressed transcriptional profiles indicative of lower activation status compared to MCs in the proficient littermates, and were CD63^{low} indicative of reduced degranulation *in vivo* (Kraft et al., 2013). Because these changes in MCs could only be detected later in development, i.e., by E18.5, it remains possible that the observed reduction in MC degranulation arises secondarily to the impairment of lung tissue development, rather than serving as the primary causal factor of the developmental defect.

Of note, basophils are closely related to the MC lineage and also expressed *Cpa3,* albeit at lower levels than MCs. Although they may be targeted within our model, basophil-specific targeting is not embryonically lethal (Alvarado-Vazquez et al., 2023), arguing against a primary role of basophils in the observed phenotype.

In contrast, unbiased analysis of the whole proteome revealed a striking reduction in platelet-associated proteins in targeted lungs. Lung megakaryocytes are transcriptionally distinct from liver megakaryocytes at fetal stages and exhibit higher *Tgfb* expression (Yeung et al., 2020). This suggests fundamental differences in the functional profiles of fetal liver and lung megakaryocytes. Moreover, platelets were previously shown to drive *Tgfb* signaling-mediated myofibroblast development during fetal lung development (Tsukiji et al., 2018), a phenotype that closely mirrors the developmental lung defect in our model. We hypothesise that our *Cpa3*^{Cre} targeting model may have potential off-target effects on hematopoietic outputs beyond MC development. Consistent with this, single-cell profiling revealed a modest reduction in compartments in undifferentiated progenitors (udPs) and megakaryocyte progenitors (MkP) as early as E15.5. We note that we cannot exclude the possibility that our findings may be due to limited sampling and underrepresentation of

these populations. Nonetheless, their close clustering to MCs in UMAP space suggests shared transcriptional programmes which may render them susceptible to *Cpa3*^{Cre} targeting in our model.

Previous work has shown that erythropoiesis proceeds with *Gata1* upregulation (Suzuki et al., 2013) while megakaryocytes rely on *Gata2* (Huang et al., 2009; Huang and Crispino, 2008; Ikonomi et al., 2000). Our fetal lung dataset shows a similar pattern of expression where precursors to erythrocytes expressed *Gata1*, while MkPs expressed *Gata2* similarly to MCs, which may explain their selective vulnerability in this model. Moreover, *Gata2* regulates promoter activity of the *Cpa3* gene (Zon et al., 1991), suggesting shared developmental features between these two lineages.

However, *Gata2*$^{-/-}$ mice, are embryonically lethal much earlier in development (Tsai et al., 1994) reflecting the essential role of *Gata2* as a master regulator of megakaryocytes and their critical role in vascularization. Since *Cpa3*^{Cre} targeting does not result in complete loss of MkPs and blood platelets, we hypothesise that we may instead be targeting a transient subset of progenitors which may partially perturb megakaryocyte development. *Cpa3* expression has been reported in yolk sac and liver progenitors that give rise to MkPs and EryPs but is subsequently downregulated upon differentiation (Ma et al., 2025). Given that we observe partial reduction in blood platelets, it will be crucial to determine whether lung megakaryocyte development may be disproportionally targeted by *Cpa3*-specific perturbation of upstream progenitors. Notably, the lung is a major site of platelet biogenesis and contributes to nearly 50% of circulating platelets in adults (Boilard & Machlus, 2021; Lefrançais et al., 2017). While the MCs appear to be capable of replenishing themselves through proliferation, the same repopulation mechanism may not be available to MkPs and megakaryocytes in the lungs. Indeed, megakaryocytes typically enter a senescent state

within their cell-cycle upon maturation (Besancenot et al., 2010) *Cpa3*-based fate mapping will be needed to define the developmental kinetics of how *Cpa3*-progenitor derived megakaryocytes establish and mature within the fetal lung.

Together, these findings suggest that genetic targeting of *Cpa3*$^{+}$ lineages likely perturbs the shared progenitor axis that gives rise to both MCs and MkPs (Figure 17). Given that lung megakaryocytes and platelets are a known source of Tgfb1 in promoting myofibroblast development and septal organogenesis in the fetal lung (Tsukiji et al., 2018), we hypothesise that these off-target perturbations may contribute to impaired Tgfb signaling and subsequent lung developmental defects in our model, ultimately leading to respiratory failure at birth.

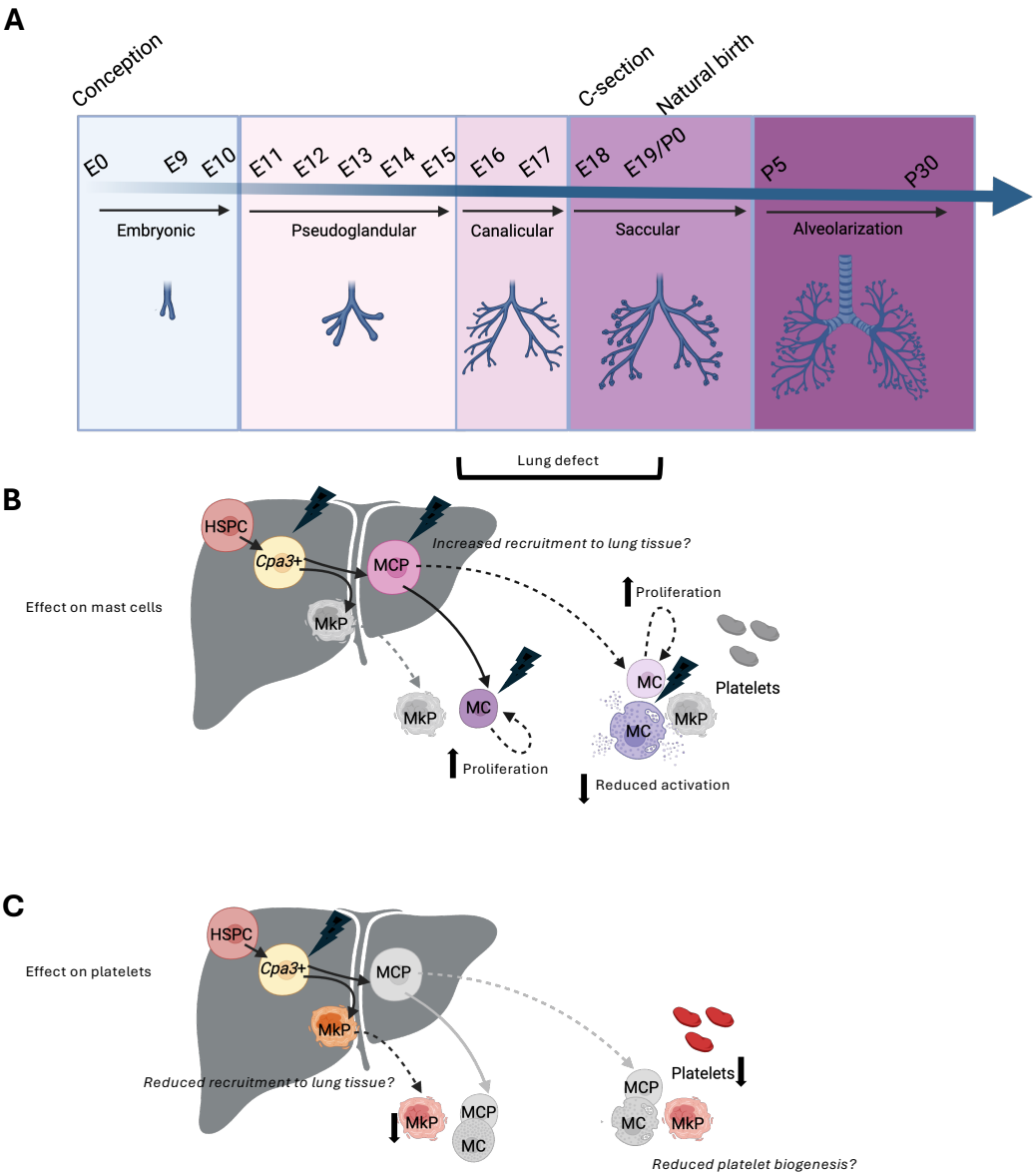

Chapter (3) Figure 17: Schematic overview of the haematopoietic alterations observed in the *Cpa3*^{Cre} *Rosa26*$^{lsl\text{-}DTA}$ model.

(A) Overview of lung development stages during embryogenesis at each embryonic day of development (E) post conception. Fetal lung development progresses from embryonic bud formation (E9.5-E10.5) following which pseudoglandular development occurs (E11.5-E16.5). Late-stage lung development is characterized by the onset of canalicular development (E16.5-17.5) followed by saccular development (E18.5 onwards), and the observed lung developmental defect likely occurs during this window. The fetal liver (grey) shown as the source of progenitors during fetal development. (B) *Cpa3*^{Cre} targeting affects mast cell progenitors (MCPs) and mast cells (MCs) throughout lung development. Perturbation of *Cpa3*-expressing cells was shown to cause a compensatory increase in proliferative capacity of MCs and reduced activation-induced degranulation capacity of MCs in the fetal lung at E18.5. (C) Off-target effects of *Cpa3*^{Cre} targeting on additional *Cpa3*-expressing progenitors that may give rise to megakaryocyte progenitors (MkPs) (interpretation based on fate mapping work from (Ma et al., 2025)). Reduced platelets in circulation may occur as a consequence of *Cpa3*^{Cre} targeting.

An open question that remains is whether MCs contribute to this phenotype in our model. MCs are known to play a role in vascularisation and angiogenesis through their close association with blood vessels and secretion of vasoactive components such as serotonin and histamine (Kunder et al., 2011; Qin et al., 2013). Moreover, platelet-derived products like the platelet activating factor (PAF) can directly trigger MC degranulation and activation (Choi et al., 2025; Kajiwara et al., 2010; Karhausen et al., 2020). Intriguingly, PAF induces histamine release in MCs detected in the lung and peripheral blood but not in the skin (Kajiwara et al., 2010), indicating that platelet and MC interactions may be highly tissue specific. In our model, the reduction of platelets and reduced activation of MCs raises the possibility that these interactions may be disrupted. Poor formation of capillary networks may drive impaired saccular development in conditions like bronchopulmonary dysplasia

(Appuhn et al., 2021), reflecting the importance of coordinated vascular development in the developing lung. Nonetheless, targeting mature, committed populations of MCs alone is unlikely to cause this lung defect nor does it directly impair platelet production, as MC-specific targeting models like *Mcpt5*^{Cre}*Rosa26*$^{lsl\text{-}DTA}$ are viable without overt lung defects, nor do they exhibit a reduction in circulating platelets. Thus, future work should investigate whether combined perturbation of platelets and MC compartments disrupts fetal lung development, supporting the possibility of a shared functional interaction between these lineages in supporting embryonic lung development.

Additional (author) contributions

Animal work: jointly performed by Simran Kapoor and Clara Munz

Preparation of sample cell suspensions and libraries: jointly performed by Simran Kapoor, Clara Munz and Rebecca Gentek

Flow cytometry: jointly performed by Simran Kapoor and Clara Munz

Blood counts: jointly performed by Simran Kapoor and Clara Munz

Histological (paraffin) sectioning: IRR Histology unit (Melanie McMillan)

Histological staining and microscopy: jointly performed by Theresa Eulgem, Solvig Becker, Simran Kapoor

Single cell sorting for 10x sequencing: Clara Munz

Library generation for 10x sequencing: Meryam Beniazza

Sample preparation proteomics and lipidomics: Clara Munz

Materials and Methods

Mouse lines

Original *Cpa3*^{Cre} *Mcl-1*$^{fl/fl}$ mice were originally generated (Lilla et al., 2011) by crossing *Mcl*$^{+/fl}$ mice to *Cpa3*^{Cre} mice (generated by microinjecting the *Cpa3-Cre* transgene into embryonic stem cells in the C57BL/6J background) at Stanford University. *Cpa3*^{Cre} *Mcl-1*$^{fl/fl}$ mice in this study were obtained from Dr Phillip Starkl, MUW (Vienna, Austria), and bred to remove the *Mcl-1*$^{fl/fl}$ allele to generate the *Cpa3*-Cre mice where Cre expression is regulated under the control of the *Cpa3* promoter. *Mcpt5*^{Cre} (Scholten et al., 2008) were obtained from Dr Axel Roers, TUD (Dresden, Germany). *Karma*^{Cre} mice (Mattiuz et al., 2018a)were obtained from Dr Marc Dalod, CIML (Marseille, France).

MC reporter lines

Rosa26$^{lsl\text{-}tdT}$ mice (Madisen et al., 2010) in this study were obtained from Dr Prakash Ramachandran, UoE (Edinburgh, UK). In these mice, a transgene encodes for red fluorescent protein variant tdTomato (tdT), with a LoxP-flanked transcriptional stop cassette upstream of the gene.

Cpa3^{Cre} *Rosa26*$^{lsl\text{-}tdT}$ mice were generated in this study by crossing *Rosa26*$^{lsl\text{-}tdT}$ mice to *Cpa3*^{Cre} mice. Upon Cre-mediated recombination under the *Cpa3* promoter, LoxP-stop-LoxP site specific recombination occurs, and the stop codon is removed, enabling transcription of the red fluorescent tdT protein. *Mcpt5*^{Cre} *Rosa26*$^{lsl\text{-}tdT}$ mice and *Karma*^{Cre} *Rosa26* $^{lsl\text{-}tdT}$ mice were similarly generated.

MC targeting lines

Rosa26$^{lsl\text{-}DTA176}$ (“DTA176”) mice (Wu et al., 2006) in this study were purchased from The Jackson Laboratory (strain #010527). In these mice, a transgene encodes for an attenuated

form of Diphtheria toxin (DTA-176), with a LoxP-flanked transcriptional stop cassette upstream of the gene.

Cpa3^{Cre} *Rosa26*$^{lsl\text{-}DTA176}$ mice are a new line we generated in this study by crossing *Rosa26*$^{lsl\text{-}DTA176}$ mice to *Cpa3*^{Cre} mice. Upon Cre-mediated recombination under the *Cpa3* promoter, LoxP-stop-LoxP site specific recombination occurs, and the stop codon is removed, enabling transcription of Diphtheria toxin. *Mcpt5*^{Cre} *Rosa26*$^{lsl\text{-}DTA176}$ mice and *Karma*^{Cre} *Rosa26*$^{lsl\text{-}DTA176}$ mice were similarly generated.

Animal ethics and housing conditions

All animal work was performed under project license (PPL) number PP1871024 in accordance with the Animals (Scientific Procedures) Act 1986 (ASPA). Mice were bred and housed at the animal facility (BVS Chancellor's Building Animal Facility) in the University of Edinburgh (Edinburgh, UK) under specific pathogen-free conditions at a controlled temperature of 22^{o}C with a 12-hour light/dark cycle. Access to food (irradiated chow pellets) and water (reverse osmosis water) was available *ad libitum*.

Timed pregnancy and C-section

For MC reporter experiments, *Rosa26*$^{lsl\text{-}tdT}$ mice were set up with *Cpa3*^{Cre} mice for timed matings. Matings were set up in the orientation (*Cpa3*$^{Cre/wt}$ x *Rosa26*$^{lsl\text{-}tdT/\ lsl\text{-}tdT}$). Offspring were obtained at the expected Mendelian ratio, yielding approximately 50% *Cpa3* ^{Cre} labelled (*Cpa3*$^{Cre/wt}$ *Rosa26*$^{lsl\text{-}tdT/wt}$) and 50% *Cpa3* ^{Cre} control pups lacking the *Cpa3*-Cre allele (*Cpa3*$^{wt/wt}$ *Rosa26*$^{lsl\text{-}tdT/wt}$).

For MC targeting experiments, *Rosa26*$^{lsl\text{-}DTA176}$ mice were set up with *Cpa3*^{Cre} mice for timed matings. Matings were set up in either orientation (*Cpa3*$^{Cre/wt}$ x *Rosa26*$^{lsl\text{-}DTA17/\ lsl\text{-}DTA176}$ or *Cpa3*-Cre$^{Cre/Cre}$ x *Rosa26*$^{lsl\text{-}DTA176/wt}$). Offspring were obtained at the expected Mendelian

ratio, yielding approximately 50% *Cpa3* ^{Cre} targeted pups (*Cpa3*$^{Cre/wt}$ *Rosa26*$^{lsl\text{-}DTA176/wt}$) pups and 50% *Cpa3* ^{Cre} proficient littermate control pups lacking either the *Cpa3*-Cre allele (*Cpa3*$^{wt/wt}$ *Rosa26*$^{lsl\text{-}DTA176/wt}$) or the *Rosa26*$^{lsl\text{-}DTA176}$ allele (*Cpa3*$^{Cre/wt}$ *Rosa26*$^{wt/wt}$).

Successful mating was confirmed by the presence of a vaginal plug the following morning, recorded as 0.5 days post-conception (E0.5). Plugged females were subsequently monitored and weighed at E12 to confirm pregnancy.

In case of experiments at specific developmental timepoints, C-section workflow was performed as follows. Pregnant females (dams) were culled by cervical dislocation at chosen developmental timepoints (E15.5 or E18.5) and fetuses/newborn pups were delivered by C-section. Genotyping was performed using DNA isolated from the tail of the fetuses.

In case of one-hour observation analyses, each of the pups were individually placed in a 12-well plate on a heating pad to maintain temperature. Pups were monitored for up to 60 minutes, and subsequently culled by decapitation.

Similar mating strategy was for used for analyses using *Mcpt5*^{Cre} mice or *Karma*^{Cre} mice.

Lung float assay

Lungs were dissected from pups during C-section following the one hour observation period and then placed in an Eppendorf tube filled with 1x PBS to assess floation.

Histological staining and microscopy

Lungs of pups were dissected in uteri during C-section prior to the first breath, to avoid inflation-related confounding of lung architecture. Lungs were subsequently fixed in antigen fix (4% paraformaldehyde, CellPath) at room temperature for 45 minutes and dissected into lobes. The left lobe was dehydrated in 70% ethanol and paraffin-embedded for sectioning using a microtome.

Sectioned slides were baked for 45 minutes at 56C for tissue adhesion. After deparaffinization by immersion in xylene, sections were rehydrated in ethanol series (100%, 95%, 80%, 70%) and then stained using standard haematoxylin and eosin (H&E) staining to stain the anatomy of the lung. Slides were stained with haematoxylin for 5 minutes, followed by differentiation in acid alcohol for one minute. Bluing was performed by immersion in Scott's tap water for 2 minutes, followed by eosin staining for 2 minutes. Sections were then dehydrated in reverse ethanol series (70%, 80%, 95%, 100%) and cleared in xylene prior to mounting in Pertex mounting medium.

Stained sections were imaged using Zeiss Axioscan.Z1 slide scanner. Images were analysed using ImageJ fiji software (v2.14.0).

Blood counts

Blood cell counts were measured using the Celltac- α MEK-6550 hematology analyser (Nihon Kohden, Tokyo, Japan). Approximately 10ul of blood was collected from fetuses immediately following decapitation. Blood samples were collected into anticoagulant tubes to avoid clotting-related confounding of blood count reads.

Preparation of sample cell suspensions and libraries

Organs were dissected from the fetuses/pups under a Leica stereomicroscope (10x magnification) and washed in phosphate buffered saline (PBS) (Life Technologies). Each sample (organ) was first mechanically cut into smaller pieces using scissors, followed by enzymatic digestion in in 0.8mg/ml Dispase II (Merck), 5mM $CaCl_2$, 10mM HEPES (Merck), 0.1mg/ml DNaseI (Roche), 3mg/ml Collagenase D (Merck) in RPMI (supplemented with 2%

FCS) at 37°C at 900rpm in a Thermo-Shaker (Grant-bio) for 15 minutes or until digested. The cell suspension obtained from each sample was then filtered through a 100 µm filter and washed in FACS buffer (2% FCS, 2 mM EDTA in PBS) to stop digestion. Cell suspensions were then centrifuged at 500g for 2-5 minutes, resuspended in FACS buffer and transferred to a 98-well v-bottom plate (Corning).

Samples were blocked with 0.5% anti-mouse CD16/32 Trustain Fx (Biolegend), 5% mouse serum (Invitrogen) and 5% rat serum (Merck) in FACS buffer for 20-30 minutes at 4°C. Cells were then washed with FACS buffer and centrifuged at 530g for 5 minutes at 4°C. Cells were then labelled with antibody mix diluted in FACS buffer and Brilliant Stain Buffer (BD) as detailed below for 20-30 minutes at 4°C.

Flow cytometric panel:

Marker	**Fluorophore**	**Supplier**	**Clone number**	**Dilution**
CD45	BUV395	BD Biosciences	30-F11	1:800
CD117 (Kit)	BV650	Biolegend	2B8	1:300
CD11b	BV510	Biolegend	M1/70	1:400
F4/80	BV785	Biolegend	BM8	1:300
CD63	Pe/Cyanine7	Biolegend	NVG-2	1:200
ST2	APC	Biolegend	DIH9	1:200
Live/Dead	APC-Cyanine7	ThermoFisher Scientific		1:800

For flow cytometric analyses, cells were washed with FACS buffer and fixed using antigen fix (4% paraformaldehyde, CellPath) at room temperature for 15 minutes away from light exposure. Cells were washed with FACS buffer and intracellularly stained using conjugated Avidin AlexaFluor AF488 (ThermoFisher Scientific) at 1:10000 dilution in homemade immunohistochemistry (IHC) buffer (0.1M Tris at pH 7.4, constituted with 0.5% bovine serum albumin, 2% Triton X-100 and 0.05g/ml milk powder) for 1 hour at room temperature or overnight at 4C, away from light exposure. Cells were washed and acquired in FACS buffer using the LSRFortessa Flow Cytometer (BD). Prior to acquisition, CountBright Absolute Counting Beads (ThermoFisher Scientific) (10uL equivalent to 10,000 beads) were added for quantification of absolute cell counts.

Sorting panel:

Marker	**Fluorophore**	**Supplier**	**Clone number**	**Dilution**
CD45	BUV395	BD Biosciences	30-F11	1:800
CD117 (Kit)	BV650	Biolegend	2B8	1:300
CD11b	BV510	Biolegend	M1/70	1:400
F4/80	eF450	ThermoFisher Scientific	BM8	1:300
CD63	Pe/Cyanine7	Biolegend	NVG-2	1:200
ST2	APC	Biolegend	DIH9	1:200

For sorting, cells were directly washed with FACS buffer after surface staining only (no fixation and intracellular staining was performed to retain cell viability), and were subsequently acquired in FACS buffer using the FACSAria Cell Sorter (BD). Prior to acquisition, DRAQ7 dye (ThermoFisher) was used in accordance to manufacturer protocol to exclude non-viable cells. Cells were pregated as live singlets and were subsequently sorted as defined below, followed by processing for multiplexing and library construction for E15.5 and E18.5 time points.

scSeq workflow

E15.5 sequencing strategy

Following C-section at E15.5, fetuses were categorized as proficient or targeted (see experimental setup in Figure Y). Cells were FACS sorted as $CD45^+$ (hematopoietic) cells from the lungs, liver and skin of fetuses from the two groups, as detailed in the gating strategy (M&M Figure 1A). Cells were then counted using Luna FX7 to give input cell number 9k.

FACS-sorted cells from different samples were multiplexed using the 10x Genomics Cell Multiplexing Oligos (CMOs), allowing multiplexing of multiple samples belonging to a specified group in a single run. Cells were first tagged by a unique CMO, and then pooled together within a library.

Two libraries (A–B) were generated as follows:

Library A: *Cpa3*^{Cre} proficient pups (pooled) lung ($CD45^+$ cells), liver ($CD45^+$ cells) and skin ($CD45^+$ cells) multiplexed together.

Library B: *Cpa3*^{Cre} targeted pups (pooled) lung ($CD45^+$ cells), liver ($CD45^+$ cells) and skin ($CD45^+$ cells) multiplexed together.

The two libraries (A-B) were prepared using the kits according to manufacturers protocol (10x Genomics) for 10x Genomics scRNA-seq 10X Genomics scRNA-seq 3’ V3.1 at Edinburgh

University Single Cell Facility (IRR North). Samples were sequenced at depth. Sequencing was performed using platform on sequencer (10x Genomics).

E18.5 sequencing strategy

Following C-section at E18.5, pups were monitored for one hour post-delivery. Cells were sorted from littermate pups categorized as proficient or targeted and alive during this period, as well as from targeted pups that died within the hour. Cells were FACS sorted as $CD45^+$ (hematopoietic) and $CD45^-$ (non-hematopoietic) cells from the lungs and skin of pups from the three groups with enrichment for MCs gated as $CD45^+$ $CD11b^-$ $F4/80^-$ $CD117^+$ (Kit^+) $ST2^+$, detailed in the gating strategy (M&M Figure 1B). Cells were then counted using Luna FX7 to give input cell number 9k.

FACS-sorted cells from different samples were multiplexed using the 10x Genomics chip preloaded with color-coded, uniquely barcoded gel beads, allowing multiplexing of multiple samples belonging to a specified group in a single run. Cells were loaded into separate wells, with each sample tagged by a unique barcode.

Four libraries (A–D) were generated as follows:

Library A: *Cpa3*^{Cre} proficient live lung ($CD45^+$ and MC) and skin ($CD45^+$ and MC) samples multiplexed together.

Library B: *Cpa3*^{Cre} targeted live lung ($CD45^+$ and MC) and skin ($CD45^+$ and MC) samples multiplexed together.

Library C: *Cpa3*^{Cre} targeted dead lung ($CD45^+$ and MC) and skin ($CD45^+$ and MC) samples multiplexed together.

Library D: *Cpa3*^{Cre} proficient live lung ($CD45^-$) and *Cpa3*^{Cre} targeted dead lung ($CD45^-$) samples multiplexed together.

The libraries (A-C) were prepared using the kits according to manufacturers protocol (10x Genomics) for 10x Genomics scRNA-seq GEM-X Universal 3’ v4 4 plex at Edinburgh

University Single Cell Facility (IRR North). Libraries were purified using SPRIselect beads. Samples were sequenced at depth. Sequencing was performed using platform on sequencer (10x Genomics).

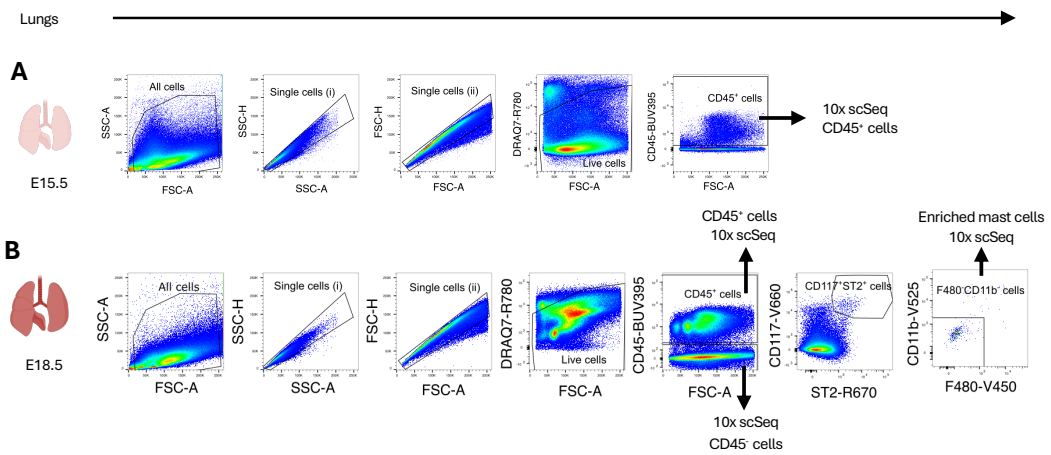

Chapter (3) M&M Figure 1: Gating strategy for sorting CD45$^-$ and CD45$^+$ cells, with enrichment of mast cells in the fetal lung.

Representative flow panels (from proficient mice) illustrating gating strategy used for single cell sequencing experiment. Gating was performed sequentially from left to right. Live, single cells were first selected, followed by CD45$^+$ cells, which were subsequently sorted for 10x single cell sequencing (10x scSeq) downstream preparation for fetal lungs at (A) E15.5 and (B) E18.5. In addition, in E18.5 fetal lungs, CD45$^-$ cells were also sequenced, along with mast cells which were enriched for during sorting by further gating of CD45$^+$ cells as CD117$^+$ ST2$^+$ cells, and macrophages were excluded from this population by gating for F480$^-$CD11b$^-$ mast cells.

<u>scSeq alignment and quality control processing</u>

Sequencing files were demultiplexed and converted to FASTQ files using CellRanger mkfastq pipelines (10x Genomics, v9.01). Reference genome was created using CellRanger mkref pipeline (10x Genomics, v9.01) by combining reference genome (GRCm38) with corresponding genomic sequence of Cre and *Rosa26*$^{lsl\text{-}DTA176}$ transgenes. Sequences were aligned to the reference genome using CellRanger (10x Genomics, v9.01). The raw reads, i.e., the Unique Molecular Identifiers (UMIs) from each library were aligned to the reference genome using CellRanger (10x Genomics, v9.01). Specifically, CellRanger multi-pipline (10x Genomics, v9.01) was used to handle multiplexing and create the raw gene-barcode matrix, comprising the number of UMIs for a specific gene associated with each valid cell barcode from each GEM multiplexed in the library (including background noise from non-true cells like empty GEM droplets). To incorporate data from multiple GEM wells (each representing a library), CellRanger aggr pipeline (10x Genomics, v9.01) was used to create an aggregated matrix.

Downstream analysis was carried out in R (Version 2025.05.1+513) using the Seurat package (v5). First, we performed quality control of the aggregated matrix. The filtered feature-barcode matrix was filtered to remove noise and dead cells with mitochondrial gene levels >7.0 percent were removed. Gene expression was then log-normalised using the NormaliseData(), with the scale factor set to 10000. Dimensional reduction was then performed on this aggregated dataset. Highly variable features were identified via FindVariableFeatures() function selecting the top 3,000 variable genes. Scaling was performed on all genes using ScaleData() function to centre expression of each gene and standardise variance. Finally, we carried out a principal component analysis via RunPCA() function using highly variable features. The inflection point (elbow) in the elbow curve generated was used to determine the number of meaningful PCs to retain (PCs 1:35). The distribution of samples for obvious batch effects was assessed by visualising the distribution

of the samples across the space of the first two PCs (PC1 vs PC2). Doublets were removed by firsti identifying maximum thresholds for total UMI counts (nCount_RNA) and genes (nFeature_RNA), where the threshold was defined as the mean plus three standard deviations of each metric across all cells. These thresholds were rounded to the nearest hundred and cells exceeding either threshold were excluded from downstream analyses. Additional suspected doublets were removed using the DoubletFinder pipeline to retain only single cells.

scSeq Seurat integration and dimensional reduction

In cases where multiple sequencing runs were combined, integration was performed using layer-based canonical correlation analysis (CCA) to account for technical variation between samples. The RNA assay was first split into layers corresponding to each individual sequencing run using the split() function. Each layer was then processed using the workflow described above, including NormalizeData(), FindVariableFeatures(), ScaleData() and RunPCA(). The embeddings were then integrated using IntegrateLayers() function by specifying the CCAIntegration method. The integrated CCA reduction was used for downstream visualisation and clustering to minimize between-group variation while preserving shared biological structure.

<u>scSeq clustering</u>

After quality control, each tissue was subsetted, re-normalised, and subjected to a second round of identification of highly variable features, scaling and PCA to ensure tissue-specific dimensionality reduction. To identify transcriptionally distinct clusters of cells within each tissue, a shared nearest neighbour graph was generated using the FindNeighbours() function on the basis of the biologically meaningful PCs identified (PCs 1:35). Clustering was

then performed using the FindClusters() function on the basis of the Louvain clustering algorithm. Resolution for the FindClusters() function was specified on the basis of most biologically meaningful clusters. Resolution values to define the clustering granularity are specified in respective figure legends. Clusters were visualised using UMAP run via the RunUMAP() function using the top 35 PCs (PCs 1:35).

scSeq differential gene expression analysis

Differential gene expression between clusters was identified using the FindMarkers() function. Marker genes were identified using a Wilcoxon rank-sum test, with p-values adjusted for multiple testing using the Bonferroni method. Genes were required to be expressed in at least 10% of cells in either of the two groups compared (min.pct = 0.1). Top differentially expressed genes were used to annotate each cluster. Where top differentially expressed genes were compared between two clusters, p-value and log2-fold change values used were denoted in legends.

Signature scorecard analysis

Gene signatures were quantified using the AddModuleScore() function, which calculates averaged expression scores for predefined gene sets while controlling for background expression. Gene signature scores were used for downstream visualisation of gene signatures across clusters.

Cell cycle scoring

Cell cycle phase assignment was performed using the CellCycleScoring() function with the updated 2019 canonical cell cycle gene sets (cc.genes.updated.2019). S-phase and G2/M

phase gene lists were assigned using cc.genes.updated.2019$s.genes and cc.genes.updated.2019$g2m.genes, respectively. Cell cycle scores were calculated for each cell and cells were subsequently classified into G1, S or G2/M phases based on their relative S and G2/M scores. Cell cycle scores were used for downstream visualisation of cell-cycle variation across clusters.

scSeq trajectory analysis

Trajectory inference and pseudotime analysis were conducted in R using the Slingshot algorithm. Slingshot was applied to the PCA embedding on extracted Seurat object comprising of the Seurat clusters of interest, to infer the cellular differentiation trajectory between the clusters. Pseudotime values were computed for individual cells along the inferred lineages and visualised for each cluster along pseudotime.

Visualisation

UMAPs were visualised using the DimPlot() function. Feature plots were generated using the FeaturePlot() function. Violin plots were generated using the VlnPlot() function. Dot plots were generated using the DotPlot() function. Volcano plots were generated using the ggplot2() function. Heatmaps were generated using pheatmap() function, where gene expression values were scaled by Z-score normalization. Multi-plot panels were assembled using the patchwork package. Other plots generated were made using base R functions.

Proteomics and lipidomics

Preparation of sample and omics acquisition

Omics data was obtained using samples from neonates that were derived by C-section at E18.5 and followed up for 1 hour observation period. On the basis of genotyping, the pups were stratified into the proficient group (controls), and the targeted group, with the latter including two subgroups based on their survival in the follow up period, i.e. targeted mice that died and targeted mice that remained alive. Sample size of 5 neonates were chosen per group, where each sample represents a biological replicate. From each neonate, lung samples were dissected and snap frozen on dry ice and placed into proteomics tubes. High-resolution mass spectrometry was performed on the samples using the Orbitrap Fusion Lumos Mass Spectrometer (ThermoFisher Scientific), allowing for proteomics and lipidomics analysis. Data Independent Acquistion (DIA) technology was used to acquire the data, i.e., expression of precursors (peptides) and proteins from each sample.

Proteomics and Lipidomics analysis

The DIA data was processed using the DIA-NN algorithm which filtered the data at a 1% false discovery rate using global q-values for the protein groups and global and run-specific q-values for peptides, following which the values were normalised to generate matrices for the protein and peptide values corresponding to each sample. Resulting values were then subject to downstream analyses performed in R (Version 2025.05.1+513).

Normalised values in the matrices were log2-transformed to stabilise variance. Missing values (indicated by NA) were imputed by replacing them with 0.

For dimensionality reduction and visualisation of variance across samples, principal component analysis (PCA) was performed on the protein expression values.

Differential protein expression between samples and/or groups was performed using t-tests on the protein values, and visualised using volcano plots. Statistically significant differential expression of proteins was considered at a significance threshold of adjusted p value <0.05 and absolute log2-fold change >0.5.

Volcano plots and PCA plots were visualized using ggplot2().

Hierarchial clustering heatmaps were generated using pheatmap() to visualize patterns of protein expression across samples. Protein expression values were scaled by Z-score normalization to highlight differences across samples.

Flow cytometry analysis

Flow cytometry data was analysed using FlowJo software (v10).

Statistical analysis

Statistical analyses other than those presented in single cell sequencing analyses and proteomic/lipidomic analyses (see above) were carried out using GraphPad Prism (v10.6.1). Mann-Whitney tests were used to test statistical significance in comparisons between two groups, One-way anova was used to test statistical significance where more than two groups were compared against each other. P-values were considered significant at cutoff value of 0.05, and indicated either numerically, or using * < 0.05, ** <0.005, *** < 0.001, **** < 0.0001, and ns = not significant.

References

Abraham, S. *et al.* (2009) “Evidence for Activation of the TGF-β1 Promoter by C/EBPβ and Its Modulation by Smads,” *Journal of Interferon & Cytokine Research*, 29(1), p. 1. Available at: https://doi.org/10.1089/JIR.2008.0036.

Alvarado-Vazquez, P.A. *et al.* (2023) “Depletion of Mcpt8-expressing cells reduces lung mast cells in mice with experimental asthma,” *Allergy: European Journal of Allergy and Clinical Immunology*, 78(5), pp. 1363–1366. Available at: https://doi.org/10.1111/ALL.15596;WGROUP:STRING:PUBLICATION.

Amin, K. (2012) “The role of mast cells in allergic inflammation,” *Respiratory Medicine*, 106(1), pp. 9–14. Available at: https://doi.org/10.1016/j.rmed.2011.09.007.

Appuhn, S. v. *et al.* (2021) “Capillary Changes Precede Disordered Alveolarization in a Mouse Model of Bronchopulmonary Dysplasia,” *American journal of respiratory cell and molecular biology*, 65(1), pp. 81–91. Available at: https://doi.org/10.1165/RCMB.2021-0004OC.

Arinda, B.N. *et al.* (2022) “Non-traditional roles of immune cells in regeneration: an evolutionary perspective,” *Development (Cambridge)*, 149(8). Available at: https://doi.org/10.1242/DEV.199903/275269.

Atiakshin, D. *et al.* (2022) “Carboxypeptidase A3-A Key Component of the Protease Phenotype of Mast Cells,” *Cells*, 11(3). Available at: https://doi.org/10.3390/CELLS11030570.

Baron, M.H., Vacaru, A. and Nieves, J. (2013) “Erythroid Development in the Mammalian Embryo,” *Blood cells, molecules & diseases*, 51(4), p. 10.1016/j.bcmd.2013.07.006. Available at: https://doi.org/10.1016/J.BCMD.2013.07.006.

Bartram, U. and Speer, C.P. (2004) “The role of transforming growth factor beta in lung development and disease,” *Chest*, 125(2), pp. 754–765. Available at: https://doi.org/10.1378/CHEST.125.2.754.

Besancenot, R. *et al.* (2010) “A Senescence-Like Cell-Cycle Arrest Occurs During Megakaryocytic Maturation: Implications for Physiological and Pathological Megakaryocytic Proliferation,” *PLoS Biology*, 8(9), p. e1000476. Available at: https://doi.org/10.1371/JOURNAL.PBIO.1000476.

Boilard, E. and Machlus, K.R. (2021) “Location is everything when it comes to megakaryocyte function,” *The Journal of Clinical Investigation*, 131(1). Available at: https://doi.org/10.1172/JCI144964.

Cabirol, M.J. *et al.* (2022) “Microglia shape the embryonic development of mammalian respiratory networks,” *eLife*, 11. Available at: https://doi.org/10.7554/ELIFE.80352.

Cairns, J.A. (1998) “Mast cell tryptase and its role in tissue remodelling: Editorial,” *Clinical and Experimental Allergy*, 28(12), pp. 1460–1463. Available at: https://doi.org/10.1046/J.1365-2222.1998.00467.X;JOURNAL:JOURNAL:13652222;WGROUP:STRING:PUBLICATION.

Caldeira, I. *et al.* (2021) “Developmental Pathways Underlying Lung Development and Congenital Lung Disorders,” *Cells 2021, Vol. 10, Page 2987*, 10(11), p. 2987. Available at: https://doi.org/10.3390/CELLS10112987.

Callaway, D.A. *et al.* (2024) “TGF-β controls alveolar type 1 epithelial cell plasticity and alveolar matrisome gene transcription in mice,” *The Journal of Clinical Investigation*, 134(6). Available at: https://doi.org/10.1172/JCI172095.

Calthorpe, R.J. *et al.* (2023) “Complex roles of TGF-β signaling pathways in lung development and bronchopulmonary dysplasia,” *American Journal of Physiology - Lung Cellular and Molecular Physiology*, 324(3), p. L285. Available at: https://doi.org/10.1152/AJPLUNG.00106.2021.

Chin, H.S. and Fu, N.Y. (2021) “Physiological Functions of Mcl-1: Insights From Genetic Mouse Models,” *Frontiers in Cell and Developmental Biology*, 9, p. 704547. Available at: https://doi.org/10.3389/FCELL.2021.704547/FULL.

Choi, H.W. *et al.* (2025) “Platelet-mediated activation of perivascular mast cells triggers progression of sepsis to septic shock in mice,” *Nature Communications 2025* [Preprint]. Available at: https://doi.org/10.1038/S41467-025-66978-0.

Chow, P.C.K. and Bentley, P.J. (2025) “Development necessitates evolutionarily conserved factors,” *Scientific Reports 2025 15:1*, 15(1), pp. 1–14. Available at: https://doi.org/10.1038/s41598-025-92541-4.

Coall, D.A. *et al.* (2015) “Evolution and Prenatal Development,” *Handbook of Child Psychology and Developmental Science*, pp. 1–49. Available at: https://doi.org/10.1002/9781118963418.CHILDPSY303.

Dahlin, J.S. *et al.* (2017) “KIT signaling is dispensable for human mast cell progenitor development,” *Blood*, 130(16), pp. 1785–1794. Available at: https://doi.org/10.1182/BLOOD-2017-03-773374.

Daniel, E. and Cleaver, O. (2019) “Vascularizing organogenesis: Lessons from developmental biology and implications for regenerative medicine,” *Current Topics in Developmental Biology*, 132, pp. 177–220. Available at: https://doi.org/10.1016/bs.ctdb.2018.12.012.

Dwyer, D.F. *et al.* (2016) “Expression profiling of constitutive mast cells reveals a unique identity within the immune system,” *Nature Immunology*, 17(7), pp. 878–887. Available at: https://doi.org/10.1038/ni.3445.

Feyaerts, D. *et al.* (2022) “Establishment of tissue-resident immune populations in the fetus,” *Seminars in Immunopathology*, 44(6), p. 747. Available at: https://doi.org/10.1007/S00281-022-00931-X.

Feyerabend, T.B. *et al.* (2011) “Cre-mediated cell ablation contests mast cell contribution in models of antibody- and T cell-mediated autoimmunity,” *Immunity*, 35(5), pp. 832–844. Available at: https://doi.org/10.1016/j.immuni.2011.09.015.

Gentek, R. *et al.* (2018) “Hemogenic Endothelial Fate Mapping Reveals Dual Developmental Origin of Mast Cells,” *Immunity*, 48(6), pp. 1160-1171.e5. Available at: https://doi.org/10.1016/j.immuni.2018.04.025.

Gieseck, R.L., Wilson, M.S. and Wynn, T.A. (2018) “Type 2 immunity in tissue repair and fibrosis,” *Nature Reviews Immunology*, 18(1), pp. 62–76. Available at: https://doi.org/10.1038/NRI.2017.90;SUBJMETA.

Ginhoux, F. *et al.* (2010) “Fate mapping analysis reveals that adult microglia derive from primitive macrophages,” *Science (New York, N.Y.)*, 330(6005), pp. 841–845. Available at: https://doi.org/10.1126/SCIENCE.1194637.

Ginhoux, F. and Guilliams, M. (2016) “Tissue-Resident Macrophage Ontogeny and Homeostasis,” *Immunity*, 44(3), pp. 439–449. Available at: https://doi.org/10.1016/J.IMMUNI.2016.02.024.

Gu, L. *et al.* (2007) “Effect of TGF-beta/Smad signaling pathway on lung myofibroblast differentiation,” *Acta pharmacologica Sinica*, 28(3), pp. 382–391. Available at: https://doi.org/10.1111/J.1745-7254.2007.00468.X.

Guan, F. *et al.* (2025) “Tissue macrophages: origin, heterogenity, biological functions, diseases and therapeutic targets,” *Signal Transduction and Targeted Therapy 2025 10:1*, 10(1), pp. 93-. Available at: https://doi.org/10.1038/s41392-025-02124-y.

Gutierrez, D.A. *et al.* (2015) “Hematopoietic Kit Deficiency, rather than Lack of Mast Cells, Protects Mice from Obesity and Insulin Resistance,” *Cell Metabolism*, 21(5), pp. 678–691. Available at: https://doi.org/10.1016/j.cmet.2015.04.013.

Herriges, M. and Morrisey, E.E. (2014) “Lung development: orchestrating the generation and regeneration of a complex organ,” *Development*, 141(3), pp. 502–513. Available at: https://doi.org/10.1242/DEV.098186.

Hu, B. *et al.* (2004) “CCAAT/enhancer-binding protein beta isoforms and the regulation of alpha-smooth muscle actin gene expression by IL-1 beta,” *Journal of immunology*

(Baltimore, Md. : 1950), 173(7), pp. 4661–4668. Available at: https://doi.org/10.4049/JIMMUNOL.173.7.4661.

Hu, B. *et al.* (2012) "Mesenchymal-Specific Deletion of C/EBPβ Suppresses Pulmonary Fibrosis," *The American Journal of Pathology*, 180(6), p. 2257. Available at: https://doi.org/10.1016/J.AJPATH.2012.02.010.

Huang, Z. and Crispino, J. (2008) "GATA-2 Controls Proliferation of Megakaryocyte Progenitors and Its Expression Contributes to Human DS-AMKL.," *Blood*, 112(11), pp. 1380–1380. Available at: https://doi.org/10.1182/BLOOD.V112.11.1380.1380.

Ikonomi, P. *et al.* (2000) "Overexpression of GATA-2 inhibits erythroid and promotes megakaryocyte differentiation," *Experimental Hematology*, 28(12), pp. 1423–1431. Available at: https://doi.org/10.1016/S0301-472X(00)00553-1.

st. John, A.L., Rathore, A.P.S. and Ginhoux, F. (2023) "New perspectives on the origins and heterogeneity of mast cells," *Nature Reviews Immunology*, 23(1), pp. 55–68. Available at: https://doi.org/10.1038/S41577-022-00731-2;SUBJMETA.

Kajiwara, N. *et al.* (2010) "Activation of human mast cells through the platelet-activating factor receptor," *Journal of Allergy and Clinical Immunology*, 125(5), pp. 1137-1145.e6. Available at: https://doi.org/10.1016/j.jaci.2010.01.056.

Kapoor, S. *et al.* (2025) "Mast Cells Are Not Essential for Pubertal Mammary Gland Branching," *European Journal of Immunology*, 55(8), p. e70036. Available at: https://doi.org/10.1002/EJI.70036.

Karhausen, J. *et al.* (2020) "Platelets trigger perivascular mast cell degranulation to cause inflammatory responses and tissue injury," *Science Advances*, 6(12), pp. 6314–6332. Available at: https://doi.org/10.1126/SCIADV.AAY6314;JOURNAL:JOURNAL:SCIADV;ISSUE:ISSUE:DOI.

Keller, J.R., Ortiz, M. and Ruscetti, F.W. (1995) "Steel Factor (c-kit Ligand) Promotes the Survival of Hematopoietic Stem/Progenitor Cells in the Absence of Cell Division," *Blood*,

86(5), pp. 1757–1764. Available at: https://doi.org/10.1182/BLOOD.V86.5.1757.BLOODJOURNAL8651757.

Kim, K.K., Sheppard, D. and Chapman, H.A. (2018) “TGF-β1 Signaling and Tissue Fibrosis,” *Cold Spring Harbor Perspectives in Biology*, 10(4), p. a022293. Available at: https://doi.org/10.1101/CSHPERSPECT.A022293.

Kitamura, Y., Go, S. and Hatanaka, K. (1978) *Decrease of Mast Cells in W/ W" Mice and Their Increase by Bone Marrow Transplantation*, *Blood*. Available at: http://ashpublications.org/blood/article-pdf/52/2/447/581579/447.pdf.

Kraft, S. *et al.* (2013) “The Tetraspanin CD63 Is Required for Efficient IgE-Mediated Mast Cell Degranulation and Anaphylaxis,” *The Journal of Immunology*, 191(6), pp. 2871–2878. Available at: https://doi.org/10.4049/jimmunol.1202323.

Krystel-Whittemore, M., Dileepan, K.N. and Wood, J.G. (2016) “Mast cell: A multi-functional master cell,” *Frontiers in Immunology*. Frontiers Media S.A. Available at: https://doi.org/10.3389/fimmu.2015.00620.

Kunder, C.A., St John, A.L. and Abraham, S.N. (2011) “Mast cell modulation of the vascular and lymphatic endothelium,” *Blood*, 118(20), p. 5383. Available at: https://doi.org/10.1182/BLOOD-2011-07-358432.

Lawrence, A.R. *et al.* (2024) “Microglia maintain structural integrity during fetal brain morphogenesis,” *Cell*, 187(4), pp. 962-980.e19. Available at: https://doi.org/10.1016/j.cell.2024.01.012.

Lefrançais, E. *et al.* (2017) “The lung is a site of platelet biogenesis and a reservoir for hematopoietic progenitors,” *Nature*, 544(7648), p. 105. Available at: https://doi.org/10.1038/NATURE21706.

Li, R. *et al.* (2020) “Myofibroblast contraction is essential for generating and regenerating the gas-exchange surface,” *The Journal of Clinical Investigation*, 130(6), p. e132189. Available at: https://doi.org/10.1172/JCI132189.

Li, S. *et al.* (2021) “Universal toxin-based selection for precise genome engineering in human cells,” *Nature Communications 2021 12:1*, 12(1), pp. 497-. Available at: https://doi.org/10.1038/s41467-020-20810-z.

Li, Z. *et al.* (2018) “Adult Connective Tissue-Resident Mast Cells Originate from Late Erythro-Myeloid Progenitors,” *Immunity*, 49(4), pp. 640-653.e5. Available at: https://doi.org/10.1016/j.immuni.2018.09.023.

Lilla, J.N. *et al.* (2011) “Reduced mast cell and basophil numbers and function in Cpa3-Cre; Mcl-1fl/fl mice,” *Blood*, 118(26), p. 6930. Available at: https://doi.org/10.1182/BLOOD-2011-03-343962.

Lilla, J.N. and Werb, Z. (2010) “Mast cells contribute to the stromal microenvironment in mammary gland branching morphogenesis,” *Developmental Biology*, 337(1), pp. 124–133. Available at: https://doi.org/10.1016/j.ydbio.2009.10.021.

Lindahl, P. *et al.* (1997) “Alveogenesis failure in PDGF-A-deficient mice is coupled to lack of distal spreading of alveolar smooth muscle cell progenitors during lung development,” *Development (Cambridge, England)*, 124(20), pp. 3943–3953. Available at: https://doi.org/10.1242/DEV.124.20.3943.

Liu, J. *et al.* (2015) “Mast Cells Participate in Corneal Development in Mice,” *Scientific reports*, 5. Available at: https://doi.org/10.1038/SREP17569.

Lynch, A.M. *et al.* (2025) “AP-1 mediated chromatin changes govern alveolar type 2 cell transition in lung injury-repair,” *bioRxiv*, p. 2025.10.25.684549. Available at: https://doi.org/10.1101/2025.10.25.684549.

Ma, W. *et al.* (2025) “Embryonic mast cells arise from the Cpa3-expressing precursors but not granulocyte-monocyte progenitors,” *Science China Life Sciences* [Preprint]. Available at: https://doi.org/10.1007/s11427-024-2891-1.

Madisen, L. *et al.* (2010) “A robust and high-throughput Cre reporting and characterization system for the whole mouse brain,” *Nature neuroscience*, 13(1), pp. 133–140. Available at: https://doi.org/10.1038/NN.2467.

Mass, E. *et al.* (2016) “Specification of tissue-resident macrophages during organogenesis,” *Science*, 353(6304). Available at: https://doi.org/10.1126/SCIENCE.AAF4238/SUPPL_FILE/MASS.SM.PDF.

Mass, E. and Gentek, R. (2021) “Fetal-Derived Immune Cells at the Roots of Lifelong Pathophysiology,” *Frontiers in Cell and Developmental Biology*, 9, p. 648313. Available at: https://doi.org/10.3389/FCELL.2021.648313/FULL.

Mattiuz, R. *et al.* (2018) “Novel Cre-Expressing Mouse Strains Permitting to Selectively Track and Edit Type 1 Conventional Dendritic Cells Facilitate Disentangling Their Complexity in vivo,” *Frontiers in Immunology*, 9. Available at: https://doi.org/10.3389/fimmu.2018.02805.

McGrath, K.E. *et al.* (2003) “Circulation is established in a stepwise pattern in the mammalian embryo,” *Blood*, 101(5), pp. 1669–1675. Available at: https://doi.org/10.1182/BLOOD-2002-08-2531.

Mosser, D.M., Hamidzadeh, K. and Goncalves, R. (2020) “Macrophages and the maintenance of homeostasis,” *Cellular & Molecular Immunology 2020 18:3*, 18(3), pp. 579–587. Available at: https://doi.org/10.1038/s41423-020-00541-3.

Msallam, R. *et al.* (2020) “Fetal mast cells mediate postnatal allergic responses dependent on maternal IgE,” *Science*, 370(6519), pp. 941–950. Available at: https://doi.org/10.1126/SCIENCE.ABA0864;WEBSITE:WEBSITE:AAAS-SITE;JOURNAL:JOURNAL:SCIENCE;WGROUP:STRING:PUBLICATION.

Nobs, S.P. and Kopf, M. (2021) “Tissue-resident macrophages: guardians of organ homeostasis,” *Trends in Immunology*, 42(6), pp. 495–507. Available at: https://doi.org/10.1016/J.IT.2021.04.007.

Palis, J. *et al.* (2004) “The Megakaryocyte Lineage Arises in the Yolk Sac and Generates an Initial Wave of Large Embryonic Platelets in the Early Mammalian Embryo.,” *Blood*, 104(11), p. 566. Available at: https://doi.org/10.1182/BLOOD.V104.11.566.566.

Paramore, S. v. *et al.* (2024) “Vangl-dependent mesenchymal thinning shapes the distal lung during murine sacculation,” *Developmental cell*, 59(10), p. 1302. Available at: https://doi.org/10.1016/J.DEVCEL.2024.03.010.

Park, M.D. *et al.* (2022) “Macrophages in health and disease,” *Cell*, 185(23), pp. 4259–4279. Available at: https://doi.org/10.1016/J.CELL.2022.10.007.

Pennock, J.L. and Grencis, R.K. (2006) “The mast cell and gut nematodes: damage and defence,” *Chemical immunology and allergy*, 90, pp. 128–140. Available at: https://doi.org/10.1159/000088885.

Qin, L. *et al.* (2013) “The vascular permeabilizing factors histamine and serotonin induce angiogenesis through TR3/Nur77 and subsequently truncate it through thrombospondin-1,” *Blood*, 121(11), pp. 2154–2164. Available at: https://doi.org/10.1182/BLOOD-2012-07-443903.

Rodewald, H.R. and Feyerabend, T.B. (2012) “Widespread Immunological Functions of Mast Cells: Fact or Fiction?,” *Immunity*, pp. 13–24. Available at: https://doi.org/10.1016/j.immuni.2012.07.007.

Ryota, M. (2023) “Techniques of Trichrome Stains in Histopathology and Decoding Fibrosis in Liver, Heart, and Lungs,” *Journal of Interdisciplinary Histopathology*, 11(11). Available at: https://www.ejmjih.com/ejmjih-articles/techniques-of-trichrome-stains-in-histopathology-and-decoding-fibrosis-in-liver-heart-and-lungs-103617.html (Accessed: January 6, 2026).

Saito, A., Horie, M. and Nagase, T. (2018) “TGF-β Signaling in Lung Health and Disease,” *International Journal of Molecular Sciences*, 19(8), p. 2460. Available at: https://doi.org/10.3390/IJMS19082460.

Saitoh, M. (2023) “Transcriptional regulation of EMT transcription factors in cancer,” *Seminars in Cancer Biology*, 97, pp. 21–29. Available at: https://doi.org/10.1016/J.SEMCANCER.2023.10.001.

Sanford, L.P. *et al.* (1997) “TGFβ2 knockout mice have multiple developmental defects that are non-overlapping with other TGFβ knockout phenotypes,” *Development (Cambridge, England)*, 124(13), p. 2659. Available at: https://doi.org/10.1242/DEV.124.13.2659.

Sawhney, A.S. *et al.* (2025) “A molecular circuit regulates fate plasticity in emerging and adult AT2 cells,” *Nature Communications 2025 16:1*, 16(1), pp. 8924-. Available at: https://doi.org/10.1038/s41467-025-64224-1.

Schittny, J.C. (2017) “Development of the lung,” *Cell and Tissue Research*, 367(3), p. 427. Available at: https://doi.org/10.1007/S00441-016-2545-0.

Scholten, J. *et al.* (2008) “Mast cell-specific Cre/loxP-mediated recombination in vivo,” *Transgenic research*, 17(2), pp. 307–315. Available at: https://doi.org/10.1007/S11248-007-9153-4.

Sharma, Y., Astle, C.M. and Harrison, D.E. (2007) “Heterozygous Kit mutants with little or no apparent anemia exhibit large defects in overall hematopoietic stem cell function,” *Experimental hematology*, 35(2), p. 214. Available at: https://doi.org/10.1016/J.EXPHEM.2006.10.001.

Tremblay, L.O. *et al.* (2007) “Respiratory Distress and Neonatal Lethality in Mice Lacking Golgi α1,2-Mannosidase IB Involved in N-Glycan Maturation,” *Journal of Biological Chemistry*, 282(4), pp. 2558–2566. Available at: https://doi.org/10.1074/JBC.M608661200.

Tsai, F.Y. *et al.* (1994) “An early haematopoietic defect in mice lacking the transcription factor GATA-2,” *Nature*, 371(6494), pp. 221–226. Available at: https://doi.org/10.1038/371221A0.

Tsai, M., Valent, P. and Galli, S.J. (2022) “KIT as a master regulator of the mast cell lineage,” *The Journal of allergy and clinical immunology*, 149(6), p. 1845. Available at: https://doi.org/10.1016/J.JACI.2022.04.012.

Tsukiji, N. *et al.* (2018) “Platelets play an essential role in murine lung development through Clec-2/podoplanin interaction,” *Blood*, 132(11), pp. 1167–1179. Available at: https://doi.org/10.1182/BLOOD-2017-12-823369.

Turgeon, B. and Meloche, S. (2009) “Interpreting Neonatal Lethal Phenotypes in Mouse Mutants: Insights Into Gene Function and Human Diseases.” Available at: https://doi.org/10.1152/physrev.00040.2007.-The.

Vu, T.H., Alemayehu, Y. and Werb, Z. (2003) “New insights into saccular development and vascular formation in lung allografts under the renal capsule,” *Mechanisms of Development*, 120(3), pp. 305–313. Available at: https://doi.org/10.1016/S0925-4773(02)00451-3.

Waskow, C. *et al.* (2004) “Rescue of lethal c-KitW/W mice by erythropoietin,” *Blood*, 104(6), pp. 1688–1695. Available at: https://doi.org/10.1182/BLOOD-2004-04-1247.

Wigglesworth, J.S. and Desai, R. (1982) “IS FETAL RESPIRATORY FUNCTION A MAJOR DETERMINANT OF PERINATAL SURVIVAL?,” *The Lancet*, 319(8266), pp. 264–267. Available at: https://doi.org/10.1016/S0140-6736(82)90986-2.

Willis, B.C. and Borok, Z. (2007) “TGF-β-induced EMT: mechanisms and implications for fibrotic lung disease,” *https://doi.org/10.1152/ajplung.00163.2007*, 293(3), pp. 525–534. Available at: https://doi.org/10.1152/AJPLUNG.00163.2007.

Wu, S., Wu, Y. and Capecchi, M.R. (2006) “Motoneurons and oligodendrocytes are sequentially generated from neural stem cells but do not appear to share common lineage-restricted progenitors in vivo,” *Development (Cambridge, England)*, 133(4), pp. 581–590. Available at: https://doi.org/10.1242/DEV.02236.

Ye, Z. and Hu, Y. (2021) “TGF-β1: Gentlemanly orchestrator in idiopathic pulmonary fibrosis (Review),” *International Journal of Molecular Medicine*, 48(1), pp. 1–14. Available at: https://doi.org/10.3892/IJMM.2021.4965/HTML.

Yeung, A.K. *et al.* (2020) “Lung megakaryocytes display distinct transcriptional and phenotypic properties,” *Blood Advances*, 4(24), p. 6204. Available at: https://doi.org/10.1182/BLOODADVANCES.2020002843.

Zon, L.I. *et al.* (1991) “GATA-binding transcription factors in mast cells regulate the promoter of the mast cell carboxypeptidase A gene.,” *Journal of Biological Chemistry*, 266(34), pp. 22948–22953. Available at: https://doi.org/10.1016/S0021-9258(18)54446-X.

Discussion and future perspectives

Mast cell ontogeny and functions in tissue development

Characterising the functions of mast cells (MCs) in physiological contexts has remained challenging in the field of immunology. This difficulty stems from fundamental constraints in the systems available for their study. In the absence of any known naturally occurring MC deficiencies in humans (Rodewald & Feyerabend, 2012), genetic mouse models have been heavily relied upon to investigate MC functions. These genetic models target MCs based on expression of genes essential for their survival and/or functions, which may limit their scope. The most conventionally used genetic models is the c*Kit* deficiency model (Kitamura et al., 1978) which lack MCs constitutively, but also have an impaired HSC compartment with notable off-target effects on other lineages including erythrocytes (Sharma et al., 2007; Waskow et al., 2004). Mice with homozygous *cKit* mutations are severely anaemic and die shortly after birth (Waskow et al., 2004). However, these defects were unlikely to be due to the absence of MCs, as these mice could be rescued by erythropoietin. *cKit* deficient mice also do not completely target MCs during embryonic development, with residual MCs still detected early after birth (Kitamura et al., 1978), suggesting that during prenatal stages, either alternative MC signaling programmes may exist and/or they may be compensated for by each other. Moreover, rescue experiments in this model have typically involved the use of transplant of either donor bone marrow or bone marrow cultured MCs (Du et al., 1996; Kitamura et al., 1978). However, the MCs replenishing these tissues follow an asynchronous pattern of recovery, with abnormal reconstitution in terms of numbers and distribution in tissues over time (Du et al., 1996). Newer genetic models are cKit independent and rely on targeting genes specific to MCs, however even these models have constraints and the work

presented in this thesis highlights that the interpretation of MC phenotypes from these models is more nuanced than previously appreciated.

This synthesis discussion examines how transcriptional programmes governing MC development intersect with genetic targeting strategies to influence observed phenotypes related to MCs. Findings from these models must be interpreted in light of (1) the shared developmental programmes between MCs and other haematopoietic lineages (2) the compensatory capacity of other cells in developmental functions where MCs may also be involved and (3) the timing of perturbation to MC development and potential recovery kinetics, relative to tissue development. Collectively, this work argues that MC function must be understood in the context of developmental timing and tissue niche.

Developmental timing and niche dynamics shape MC identity and function

Developmental timing has a profound effect on the establishment and maintenance of MC identity. Early work on MC identity – whether connective tissue type or mucosal tissue type – was based on the transfer of mast cells and their precursors into an empty connective and mucosal tissue niches in adult *Kit* deficiency mice (Kitamura et al., 1987a, 1987b; Nakano et al., 1985). However, the MCs replenishing these tissues follow an asynchronous pattern of recovery, with abnormal reconstitution in terms of numbers and distribution in tissues over time (Du et al., 1996). These findings illustrate that adult niche reconstitution does not recapitulate developmental processes that establish MC identity and functions *in* vivo.

It is now well-established that MC subsets follow distinct developmental trajectories. Mucosal MCs emerge postnatally in response to cues such as microbiota and inflammation (Bankova et al., 2015; Derakhshan et al., 2021; Gurish et al., 2001; Tauber et al., 2023). In contrast, MCs in connective tissues emerge early during embryonic development and persist

into adulthood (Gentek et al., 2018; Z. Li et al., 2018). Genetic approaches to target MCs should therefore rely on targeting these subsets of MCs *in vivo* to uncover their functional roles, by accounting for both subset identity as well as their developmental timing of origin. One such strategy involves the use of differential gene expression programmes between mucosal and connective tissue MCs. For example, genetic mouse models like *Mcpt5*^{Cre} *Rosa26*$^{lsl\text{-}DTA}$ targeting *Mcpt5*-expressing MCs results in the depletion of mature, connective tissue type MCs but not mucosal tissue type MCs, and revealed that connective tissue MCs may be important for early responses but are non-essential for the complete expulsion of intestinal helminths (Reitz et al., 2017). Similarly, in allergic reactions like contact dermatitis in the skin, this model revealed an essential role of connective tissue MCs in driving contact hypersensitivity (Dudeck et al., 2011). Yet, models like like *Mcpt5*^{Cre} *Rosa26*$^{lsl\text{-}DTA}$ do not show any overt developmental defects, suggesting three possibilities: (1) MCs may either not play a developmental role during this period; (2) they may be compensated for by another cell type; or (3) they may be replenished.

The work in this thesis reveals that genetic targeting of MCs at embryonic versus adult stages yields distinct outcomes. Embryonic targeting of MCs was followed by recovery of MC populations, whereas targeting in adult stages resulted in limited replenishment. This finding has important implications for understanding the functions associated with MCs at distinct developmental stages, i.e., whether MC targeting is studied in prenatal or postnatal contexts.

Adult mast cell depletion

Adult connective tissue MCs exhibit slower turnover kinetics under steady state (Gentek et al., 2018; Kitamura et al., 1977). Moreover, even after inducing the depletion of MCs in adulthood, connective tissue MCs are not rapidly replaced by bone marrow haematopoietic

progenitors, at least in the skin (Gentek et al., 2018). Adult tissues are often more developmentally mature and quiescent, with established cellular lineage hierarchies and reduced niche plasticity under homeostasis. Indeed, MCs seed and mature in fetal skin during a defined developmental window (Gentek et al., 2018; Z. Li et al., 2018; Ma et al., 2025), after which they occupy stable clonal territories under steady state which facilitates their self-maintenance and proliferation over time (Weitzmann et al., 2020). However, the exact nature of the signals that facilitate this self-maintenance are unclear. Other tissue-resident immune cells like macrophages in the brain, peritoneum and skin are also found in regularly spaced territories, where they are thought to be self-maintained by recognising and consuming trophic factors like *CSF-1* produced by fibroblasts in the tissue scaffold (Guilliams et al., 2020). MCs may similarly be able to sense growth factors such as *Kit* ligand (stem cell factor) to maintain their territories within the tissue (Weitzmann et al., 2020). Indeed, *Kit* ligand is expressed by fibroblasts in tissue stroma and plays an important role in promoting MC differentiation (Fujita et al., 1989).

Genetic models targeting connective tissue MCs like the *Mcpt5*^{Cre} *Rosa26*$^{lsl\text{-}DTA}$ (Dudeck et al., 2011; Reitz et al., 2017) showed a significant reduction of these cells in adult tissues, however they did not reveal overt developmental defects, suggesting that adult MCs may not be absolutely essential for homeostatic tissue maintenance, at least not in a unique, non-redundant capacity. However, it may be possible that other cells share the functions that MCs may otherwise perform, reducing selective pressure for rapid MC replenishment. For instance, uterine tissue remodelling is an essential process for fetal development, and is mediated by NK cells and MCs, both of which can compensate for each other in their absence (Meyer et al., 2017). *Karma (Gpr141b)* is another connective tissue MC marker (Mattiuz et al., 2018), and in this thesis (Chapter 2), both constitutive and inducible depletion under the *Karma* gene depleted MCs in the mammary gland but did not have an

effect on mammary gland morphogenesis, at least during puberty. Although we did not notice a critical role of MCs in mammary gland branching, this developmental process is highly conserved across mammals (Slepicka et al., 2021) and it is conceivable that MCs may be acting in concert with some other cells. Notably, we did not find an increase in other immune cells like dendritic cells and macrophages, however we cannot exclude the possibility that the tissue is able to compensate. Comprehensive analysis by increasing the flow panel capacity, complemented by transcriptomic analysis may reveal whether other cells are altered in their numbers and/or functional profiles to compensate for these effects.

Nonetheless, the slow replenishment kinetics of connective tissue MCs in adult mice upon targeting also provide an experimental advantage: these models enable sustained MC depletion which enables the investigation of any critical roles that MCs may facilitate. In contrast, this thesis (Chapter 3) revealed that embryonic tissues exhibit different replenishment kinetics, as discussed in the subsequent section. This suggests that the genetic strategies to investigate MC functions must be selected carefully depending on developmental context.

Embryonic mast cell depletion

In contrast to adult stages, targeting MCs during embryonic development has proven to be challenging. *cKit* deficient mice do not completely target MCs during embryonic development, with residual MCs still detected in neonatal tissues after birth (Kitamura et al., 1978). Moreover, connective tissue MCs express genes like *Mcpt5* early in developing fetal skin (Combs et al., 1965; Gentek et al., 2018; Ma et al., 2025; Rodewald et al., 1996), and work from my thesis (Chapter 2) have revealed that MCs acquire this developmental programme as early as E15.5 in fetal development across tissues. Nonetheless, *Mcpt5*^{Cre} *Rosa26*$^{lsl\text{-}DTA}$ mice retain MCs in fetal tissues (Chapter 2), suggesting the need to target core

MC developmental programmes in fetal stages as they emerge. By spatial-temporal analysis of MC development across neonatal stages, this thesis, collectively with the work of Ma et al. (2025), reveals that *Cpa3* is expressed in the earliest MC progenitors in yolk sac and fetal liver haematopoiesis, suggesting its utility in genetic targeting strategies to perturb MC development embryonically. However, even in our newly generated *Cpa3*^{Cre} *Rosa26*$^{lsl\text{-}DTA}$ model, MCs were not constitutively depleted during fetal development.

One explanation for this outcome is technical. Work from this thesis and Ma et al. (2025) collectively revealed that *Cpa3* expression varies across embryonic MC precursors and maturing MCs, and as such Cre-mediated recombination efficiency may be a limiting technical constraint in *Cpa3*-targeting models. Models like the "Hello Kitty" *Cpa3*^{Cre} *Mcl-1*^{fl} mice (Lilla et al., 2011),and the *Cpa3*^{Cre} *Rosa26*$^{lsl\text{-}DTA}$ mice used in this thesis rely on Cre-mediated recombination under control of the *Cpa3* gene, and robust *Cpa3*-driven Cre activity was detected using reporter alleles. Moreover, cells may show differences in susceptibility to targeting based on floxing out of the anti-apoptotic *Mcl-1* gene (Chin & Fu, 2021), however it is unlikely that cells may be able to resist apoptosis upon expression of Diphtheria toxin (DTA) in cells that undergo Cre-recombination, owing to the high universal sensitivity of cells to this toxin (Li et al., 2021). Moreover, my thesis revealed that even after targeting, the remaining MC populations recovered at E15.5 and E18.5 with increased proliferative capacity, indicating that embryonic targeting of *Cpa3*-expressing MCs likely triggers compensatory expansion rather than sustained ablation.

An alternative explanation is that embryonic niches retain higher plasticity, allowing for rapid replenishment of MCs even after substantial perturbation. In this context, embryonic targeting may reveal the capacity of fetal tissues to restore essential cell populations. Fetal haematopoiesis is highly active during embryonic development and is initiated as early as

E7.5 to give rise to erythrocytes and megakaryocytes and establish circulation, followed by the development of immune cells across the layered haematopoietic waves (Gentek et al., 2018; Hoeffel et al., 2015; Z. Li et al., 2018; McGrath et al., 2003, 2015; Palis et al., 2001). Immune cells like macrophages arising from these fetal haematopoiesis waves may be co-opted to support development of the tissue it seeds, and therefore haematopoiesis may occur to match the demands of the developing tissue (Mass & Gentek, 2021). As such, targeting these population may result in a demand for replenishment, and developing tissues may have the capacity to facilitate recovery of functionally critical immune populations.

Such a phenomenon parallels observations from other tissue-resident immune populations during embryonic development. For example, microglia arise early during fetal development and play essential roles in fetal brain development, where they facilitate synaptic pruning and structural morphogenesis (Cabirol et al., 2022; Lawrence et al., 2024). However, transient depletion of microglia in early stages of fetal development results in eventual repopulation of microglia, following which these cells were able to repair fetal brain lesions (Lawrence et al., 2024). Another example is that of liver macrophages (Kupffer cells) that also emerge during fetal stages (Hoeffel et al., 2015; Mass et al., 2016). Attempts to genetically target these cells in embryonic stages resulted in full, yet transient depletion as they rapidly recovered within a short developmental window (presented by Dr. Elvira Mass at EMBO 2024; personal communications). Moreover, these mice had impaired neonatal tissue development, suggesting that their developmental roles during specific embryonic stages may create sufficient selective pressure to trigger replenishment, and this repopulation capacity may be supported by the developing tissue.

This work collectively suggests that mast cell replenishment mechanisms are likely active during embryogenesis but become progressively restricted after birth. This may be driven by haematopoietically active progenitor pools from fetal hematopoietic waves and permissive niches during fetal development. Additionally, the developmental signals that drive the recruitment of MCs as they establish during embryogenesis may not be active, or at least lower in adult tissues. However, the nature of the how such a permissive niche is established in fetal tissue remains unknown.

The increased proliferative capacity of MCs within the fetal tissues indicates that they are likely responding to a perturbed territorial organization, similar to the mechanisms MCs use to self-maintain in adult tissue (Weitzmann et al., 2020). Indeed, perturbations to steady state have been shown to drive enhanced proliferation in MCs in adult skin (Weitzmann et al., 2020), but also in the case of other fetal-derived immune cells including langerhans cells and epidermal T cells (Gentek et al., 2018b; Ghigo et al., 2013). Moreover, the MC clonal territories, such as those described in adult skin (Weitzmann et al., 2020) may still be establishing themselves at these fetal stages, potentially resulting in increased plasticity. Interestingly, we observed a higher degree of reduction at E18.5, which may reflect a gradual reduction in repopulation capacity over time in the fetal lung. Nonetheless, the increased targeting efficacy may also be a result of increasing *Cpa3* expression levels in MCs at E18.5. Defining whether such MC territories are already specified or still emerging during fetal stages will require are MC reporter-based clonal tracing approaches similar to those used by Weitzmann et al. (2020), but applied across fetal developmental time points. If the territorial organization of MCs are still establishing in this period, the niche may be more active in terms of expressing trophic factors to facilitate the formation of the immune cell populations. Immunofluorescence approaches, together with ligand-receptor analyses from

single cell sequencing, can together help address whether MC repopulation is driven by interactions with the stroma in fetal tissues.

Strategies for improving mast cell functional studies

The findings of this thesis highlight that genetic targeting strategies to uncover the physiological functions of MC during embryogenesis must be interpreted in the context of developmental programmes. The use of our newly generated *Cpa3*^{Cre} *Rosa26*$^{lsl\text{-}DTA}$ model in this thesis revealed two outcomes: (1) apparent repopulation of MCs and (2) concomitant perturbation of non-MC lineages including platelets.

Cpa3-expression marks MCs and their committed precursors during development, but is also transiently expressed in upstream progenitors earlier in the haematopoietically active fetal yolk sac and fetal liver (Ma et al., 2025). These early *Cpa3*-expressing progenitors not only give rise to MCs, but also contribute to megakaryocyte-erythrocyte progenitors (Ma et al., 2025). However, unlike MCs, these megakaryocyte-erythrocyte progenitors cease to express *Cpa3* upon commitment to their lineage. Transcription factor *Gata2* is a master transcriptional regulator in haematopoiesis even in embryonic stages, and is involved in specification of lineages like MCs as well as megakaryocytes (Huang et al., 2009; Y. Li et al., 2015; Ohmori et al., 2015; Tojima et al., 2024). Moreover, *Gata2* regulates promoter activity of the *Cpa3* gene (Zon et al., 1991). However, *Gata2*$^{-/-}$ mice succumb to embryonic lethality (Tsai et al., 1994), and the *Cpa3*^{Cre} *Rosa26*$^{lsl\text{-}DTA}$ model may therefore reflect a perturbation of a branch of *Gata2*-dependent haematopoiesis, where expression of *Cpa3* therefore may mark a transient *Gata2*-developmental branch rather than being strictly MC-specific. Consequently, although our model set out to target MC development, it inadvertently may perturb a broader developmental programme shared across their progenitors that contribute to *Cpa3*$^{-}$ lineages. This may explain the unexpected reduction in platelet numbers

observed in the model, despite the lack of *Cpa3* expression in mature megakaryocyte-erythrocyte progenitors in fetal tissue.

At the same time, as described in the previous section, MCs appear to have a repopulation capacity in the developing fetal tissue. Thus, constitutive targeting during embryogenesis simultaneously may perturb other lineages as well as mask MC-specific functions through compensatory repopulation mechanisms. These findings intriguingly parallel the *cKit* model in some ways, where incomplete embryonic reduction of MCs (Kitamura et al., 1978), together with indirect targeting of the erythrocyte lineage result in early life lethality (Waskow et al., 2004). These phenotypes therefore likely reflect perturbation of temporally restricted, yet shared, hematopoietic branches.

In light of these limitations, an alternate approach is to use complementary genetic model systems to address the non-specificity of genetic models driven by shared gene-programmes between distinct lineages. Work from this thesis (Chapter 1) highlights the utility of such an approach. *cKit* deficiency models exhibit delayed mammary gland branching, a defect attributed to the absence of MCs (Lilla & Werb, 2010). While *cKit* deficiency constitutively impaired MC development in both connective and mucosal tissues (Kitamura et al., 1978), *cKit* is also expressed on stromal cells like the epithelial cells of mammary epithelium (Polat, 2007; Regan et al., 2012; Talaiezadeh et al., 2012). As such, the effects seen by targeting MCs in *cKit* model do not necessarily reflect MCs alone, at least not in a unique, non redundant capacity. The study took advantage of a combination of models, including $Ms4a2^{lsl\text{-}hDTR}$ – targeting basophils and MCs (Dahdah et al., 2014), as well as $Karma^{Cre}$ $Rosa26^{lsl\text{-}DTA}$– targeting MCs and dendritic cells (Mattiuz et al., 2018). By generating a novel system where MCs were genetically targeted based on expression of both *Ms4a2*

and *Karma*, the study could reveal that MCs did not play a unique, non-redundant role in mammary gland morphogenesis.

Although *Mcpt5* is expressed in MCs upon maturation in fetal tissues (Combs et al., 1965; Gentek et al., 2018; Z. Li et al., 2018; Ma et al., 2025), we found residual MC populations could still be detected in the *Mcpt5*^{Cre} *Rosa26* $^{lsl\text{-}DTA}$ mice, providing yet another example of incomplete depletion of MCs embryonically. However, these mice do not exhibit perinatal lethality nor a reduction in platelets, unlike *Cpa3*^{Cre} *Rosa26*$^{lsl\text{-}DTA}$mice. This suggests that the differences observed in the two models likely reflect differences in developmental timing of Cre driver gene expression, resulting in differences in targeting progenitors and downstream lineages.

In relation to the respiratory-distress related lethality observed in the *Cpa3*^{Cre} *Rosa26*$^{lsl\text{-}DTA}$ model (Chapter 3), one possibility is that the impaired lung development underlying the phenotype occurs largely independent of MCs, and is instead driven by the depletion of platelets and megakaryocytes in the lungs. Nonetheless, MCs in our model exhibited reduced activation in fetal tissues. This may simply reflect the state of MCs in an improperly developed fetal lung, or alternatively, MCs may interact functionally with platelets. Testing this latter hypothesis will require combinatorial targeting strategies, as exemplified in the study investigating the role of MCs in mammary gland development (Chapter 1). Attempts to target platelets in the *Mcpt5*^{Cre} *Rosa26* $^{lsl\text{-}DTA}$ model, for instance with use of anti-*Clec1b* antibodies which can target platelets at distinct timepoints (Tsukiji et al., 2018) could reveal whether, when and how these lineages may interact with each other to facilitate tissue development in embryogenesis.

It also remains possible that MCs play other important, yet perhaps more subtle roles in development that are masked by the early onset of severe lethality in the *Cpa3*^{Cre} *Rosa26*$^{lsl\text{-}DTA}$ model. Constitutive targeting from the earliest developmental stages may also allow tissues to adapt, either through the apparent repopulation of the immune cell population as observed for fetal MCs, through compensatory expansion of other cell types, or even via rewiring developmental programmes involved in the tissue formation. Temporal targeting approaches using inducible depletion models may therefore be better suited to reveal the window during which MCs play functional roles. Inducible genetic targeting systems based on the diphtheria toxin receptor (*Rosa26*$^{lsl\text{-}hDTR}$) may be paired with *Cpa3*^{Cre} to induce depletion of MCs at specific developmental stage (Buch et al., 2005). However, such a system was shown to be incompatible with prenatal stages due to systemic toxicity and lethality associated with administering diphtheria toxin to fetuses and neonates (Rebecca Gentek; unpublished).

Alternatively, inducible *Cpa3*-based models such as *Cpa3*^{CreERT2}-*Rosa*$^{lsl\text{-}tdT}$ generated by (Ma et al., 2025) have been used to trace cells derived from *Cpa3*-expressing precursors during fetal development by tamoxifen administration during fetal developmental stages. (Ma et al., 2025) identified that along with MCs, megakaryocyte-erythrocyte progenitors derive from *Cpa3*-expressing precursors at E11.5. By pairing *Cpa3*^{CreERT2} with *Rosa26*$^{lsl\text{-}DTA}$, tamoxifen induction at a later timepoint may prevent targeting of these upstream precursors. However, the temporal boundaries of this shared progenitor contributing to these lineages remains unclear. In addition, it also remains unclear how effectively such a model will perform at targeting MCs. Technical aspects such as inefficient Cre-recombination in this system may limit the efficacy of inducible targeting.

Collectively, these considerations indicate that future work investigating the developmental roles of MCs during fetal stages will likely require transient, stage-specific and complementary combinatorial strategies that account for shared developmental programmes, niche plasticity and compensatory mechanisms.

References

Bankova, L.G. *et al.* (2015) “Maturation of mast cell progenitors to mucosal mast cells during allergic pulmonary inflammation in mice,” *Mucosal Immunology*, 8(3), pp. 596–606. Available at: https://doi.org/10.1038/mi.2014.91.

Buch, T. *et al.* (2005) “A Cre-inducible diphtheria toxin receptor mediates cell lineage ablation after toxin administration,” *Nature Methods 2005 2:6*, 2(6), pp. 419–426. Available at: https://doi.org/10.1038/nmeth762.

Cabirol, M.J. *et al.* (2022) “Microglia shape the embryonic development of mammalian respiratory networks,” *eLife*, 11. Available at: https://doi.org/10.7554/ELIFE.80352.

Chin, H.S. and Fu, N.Y. (2021) “Physiological Functions of Mcl-1: Insights From Genetic Mouse Models,” *Frontiers in Cell and Developmental Biology*, 9, p. 704547. Available at: https://doi.org/10.3389/FCELL.2021.704547/FULL.

Combs, J.W., Lagunoff, D. and Benditt, E.P. (1965) “DIFFERENTIATION AND PROLIFERATION OF EMBRYONIC MAST CELLS OF THE RAT,” *The Journal of Cell Biology*, 25(3), p. 577. Available at: https://doi.org/10.1083/JCB.25.3.577.

Dahdah, A. *et al.* (2014) “Mast cells aggravate sepsis by inhibiting peritoneal macrophage phagocytosis,” *Journal of Clinical Investigation*, 124(10), pp. 4577–4589. Available at: https://doi.org/10.1172/JCI75212.

Derakhshan, T. *et al.* (2021) “Lineage-specific regulation of inducible and constitutive mast cells in allergic airway inflammation,” *Journal of Experimental Medicine*, 218(1). Available at: https://doi.org/10.1084/JEM.20200321.

Du, T. *et al.* (1996) “Tissue-dependent differences in the asynchronous appearance of mast cells in normal mice and in congenic mast cell-deficient mice after infusion of normal bone marrow cells,” *Clinical and Experimental Immunology*, 103(2), p. 316. Available at: https://doi.org/10.1046/J.1365-2249.1996.D01-610.X.

Dudeck, A. *et al.* (2011) “Mast Cells Are Key Promoters of Contact Allergy that Mediate the Adjuvant Effects of Haptens,” *Immunity*, 34(6), pp. 973–984. Available at: https://doi.org/10.1016/j.immuni.2011.03.028.

Fujita, J. *et al.* (1989) “In vitro duplication and in vivo cure of mast-cell deficiency of Sl/Sl(d) mutant mice by cloned 3T3 fibroblasts,” *Proceedings of the National Academy of Sciences of the United States of America*, 86(8), pp. 2888–2891. Available at: https://doi.org/10.1073/PNAS.86.8.2888;WGROUP:STRING:PUBLICATION.

Gentek, R., Ghigo, C., Hoeffel, G., Jorquera, A., *et al.* (2018) “Epidermal γδ T cells originate from yolk sac hematopoiesis and clonally self-renew in the adult,” *The Journal of experimental medicine*, 215(12), pp. 2994–3005. Available at: https://doi.org/10.1084/JEM.20181206.

Gentek, R., Ghigo, C., Hoeffel, G., Bulle, M.J., *et al.* (2018) “Hemogenic Endothelial Fate Mapping Reveals Dual Developmental Origin of Mast Cells,” *Immunity*, 48(6), pp. 1160-1171.e5. Available at: https://doi.org/10.1016/j.immuni.2018.04.025.

Ghigo, C. *et al.* (2013) “Multicolor fate mapping of Langerhans cell homeostasis,” *The Journal of experimental medicine*, 210(9), pp. 1657–1664. Available at: https://doi.org/10.1084/JEM.20130403.

Guilliams, M. *et al.* (2020) “Establishment and Maintenance of the Macrophage Niche,” *Immunity*, 52(3), pp. 434–451. Available at: https://doi.org/10.1016/J.IMMUNI.2020.02.015.

Gurish, M.F. *et al.* (2001) “Intestinal mast cell progenitors require CD49dbeta7 (alpha4beta7 integrin) for tissue-specific homing,” *The Journal of experimental medicine*, 194(9), pp. 1243–1252. Available at: https://doi.org/10.1084/JEM.194.9.1243.

Hoeffel, G. and Ginhoux, F. (2015) “Ontogeny of Tissue-Resident Macrophages,” *Frontiers in Immunology*, 6(SEP), p. 486. Available at: https://doi.org/10.3389/FIMMU.2015.00486.

Huang, Z. and Crispino, J. (2008) “GATA-2 Controls Proliferation of Megakaryocyte Progenitors and Its Expression Contributes to Human DS-AMKL.,” *Blood*, 112(11), pp. 1380–1380. Available at: https://doi.org/10.1182/BLOOD.V112.11.1380.1380.

Kitamura, Y. *et al.* (1977) “Development of mast cells from grafted bone marrow cells in irradiated mice,” *Nature*, 268(5619), pp. 442–443. Available at: https://doi.org/10.1038/268442A0.

Kitamura, Y. *et al.* (1987) “Mutual phenotypic changes between connective tissue type and mucosal mast cells,” *International Archives of Allergy and Immunology*, 82(3–4), pp. 244–248. Available at: https://doi.org/10.1159/000234198.

Kitamura, Y., Go, S. and Hatanaka, K. (1978) *Decrease of Mast Cells in W/ W" Mice and Their Increase by Bone Marrow Transplantation*, *Blood*. Available at: http://ashpublications.org/blood/article-pdf/52/2/447/581579/447.pdf.

Lawrence, A.R. *et al.* (2024) “Microglia maintain structural integrity during fetal brain morphogenesis,” *Cell*, 187(4), p. 962. Available at: https://doi.org/10.1016/J.CELL.2024.01.012.

Li, S. *et al.* (2021) “Universal toxin-based selection for precise genome engineering in human cells,” *Nature Communications 2021 12:1*, 12(1), pp. 497-. Available at: https://doi.org/10.1038/s41467-020-20810-z.

Li, Y. *et al.* (2015) “The STAT5-GATA2 pathway is critical in basophil and mast cell differentiation and maintenance,” *Journal of immunology (Baltimore, Md. : 1950)*, 194(9), pp. 4328–4338. Available at: https://doi.org/10.4049/JIMMUNOL.1500018.

Li, Z. *et al.* (2018) “Adult Connective Tissue-Resident Mast Cells Originate from Late Erythro-Myeloid Progenitors,” *Immunity*, 49(4), pp. 640-653.e5. Available at: https://doi.org/10.1016/j.immuni.2018.09.023.

Lilla, J.N. *et al.* (2011) “Reduced mast cell and basophil numbers and function in Cpa3-Cre; Mcl-1fl/fl mice,” *Blood*, 118(26), p. 6930. Available at: https://doi.org/10.1182/BLOOD-2011-03-343962.

Lilla, J.N. and Werb, Z. (2010) “Mast cells contribute to the stromal microenvironment in mammary gland branching morphogenesis,” *Developmental Biology*, 337(1), pp. 124–133. Available at: https://doi.org/10.1016/j.ydbio.2009.10.021.

Ma, W. *et al.* (2025) “Embryonic mast cells arise from the Cpa3-expressing precursors but not granulocyte-monocyte progenitors,” *Science China Life Sciences* [Preprint]. Available at: https://doi.org/10.1007/s11427-024-2891-1.

Mass, E. *et al.* (2016) “Specification of tissue-resident macrophages during organogenesis,” *Science*, 353(6304). Available at: https://doi.org/10.1126/SCIENCE.AAF4238/SUPPL_FILE/MASS.SM.PDF.

Mass, E. and Gentek, R. (2021) “Fetal-Derived Immune Cells at the Roots of Lifelong Pathophysiology,” *Frontiers in Cell and Developmental Biology*, 9, p. 648313. Available at: https://doi.org/10.3389/FCELL.2021.648313/FULL.

Mattiuz, R. *et al.* (2018) “Novel Cre-Expressing Mouse Strains Permitting to Selectively Track and Edit Type 1 Conventional Dendritic Cells Facilitate Disentangling Their Complexity in vivo,” *Frontiers in Immunology*, 9. Available at: https://doi.org/10.3389/fimmu.2018.02805.

McGrath, K.E. *et al.* (2003) “Circulation is established in a stepwise pattern in the mammalian embryo,” *Blood*, 101(5), pp. 1669–1675. Available at: https://doi.org/10.1182/BLOOD-2002-08-2531.

McGrath, K.E. *et al.* (2015) “Distinct sources of hematopoietic progenitors emerge before HSCs and provide functional blood cells in the mammalian embryo,” *Cell reports*, 11(12), p. 1892. Available at: https://doi.org/10.1016/J.CELREP.2015.05.036.

Meyer, N. *et al.* (2017) “Safeguarding of fetal growth by mast cells and natural killer cells: Deficiency of one is counterbalanced by the other,” *Frontiers in Immunology*, 8(JUN). Available at: https://doi.org/10.3389/fimmu.2017.00711.

Nakano, T. *et al.* (1985) “Fate of bone marrow-derived cultured mast cells after intracutaneous, intraperitoneal, and intravenous transfer into genetically mast cell-deficient W/Wv mice. Evidence that cultured mast cells can give rise to both connective tissue type and mucosal mas…,” *The Journal of experimental medicine*, 162(3), pp. 1025–1043. Available at: https://doi.org/10.1084/JEM.162.3.1025.

Ohmori, S.N.Y. *et al.* (2015) “GATA2 is critical for the maintenance of cellular identity in differentiated mast cells derived from mouse bone marrow,” *Blood*, 125(21), pp. 3306–3315. Available at: https://doi.org/10.1182/BLOOD-2014-11-612465.

Palis, J. *et al.* (2001) “Spatial and temporal emergence of high proliferative potential hematopoietic precursors during murine embryogenesis,” *Proceedings of the National Academy of Sciences of the United States of America*, 98(8), p. 4528. Available at: https://doi.org/10.1073/PNAS.071002398.

Polat, A. (2007) “c-KIT expression in columnar cell lesions of the breast accompanied by benign and malignant breast diseases,” *Pathology Research and Practice*, 203(11), pp. 765–769. Available at: https://doi.org/10.1016/j.prp.2007.08.010.

Regan, J.L. *et al.* (2012) “C-Kit is required for growth and survival of the cells of origin of Brca1-mutation-associated breast cancer,” *Oncogene*, 31(7), pp. 869–883. Available at: https://doi.org/10.1038/onc.2011.289.

Reitz, M. *et al.* (2017) “Mucosal mast cells are indispensable for the timely termination of Strongyloides ratti infection,” *Mucosal Immunology*, 10(2), pp. 481–492. Available at: https://doi.org/10.1038/mi.2016.56.

Rodewald, H.R. *et al.* (1996) “Identification of a committed precursor for the mast cell lineage,” *Science*, 271(5250), pp. 818–822. Available at: https://doi.org/10.1126/SCIENCE.271.5250.818.

Rodewald, H.R. and Feyerabend, T.B. (2012) “Widespread Immunological Functions of Mast Cells: Fact or Fiction?,” *Immunity*, pp. 13–24. Available at: https://doi.org/10.1016/j.immuni.2012.07.007.

Sharma, Y., Astle, C.M. and Harrison, D.E. (2007) “Heterozygous Kit mutants with little or no apparent anemia exhibit large defects in overall hematopoietic stem cell function,” *Experimental hematology*, 35(2), p. 214. Available at: https://doi.org/10.1016/J.EXPHEM.2006.10.001.

Slepicka, P.F., Somasundara, A.V.H. and dos Santos, C.O. (2021) “The molecular basis of mammary gland development and epithelial differentiation,” *Seminars in Cell & Developmental Biology*, 114, pp. 93–112. Available at: https://doi.org/10.1016/J.SEMCDB.2020.09.014.

Talaiezadeh, A., Jazayeri, S.N. and Nateghi, J. (2012) “Expression of c-kit protein in cancer vs. normal breast tissue,” *Wspolczesna Onkologia*, 16(4), pp. 306–309. Available at: https://doi.org/10.5114/wo.2012.30058.

Tauber, M. *et al.* (2023) “Landscape of mast cell populations across organs in mice and humans,” *Journal of Experimental Medicine*, 220(10). Available at: https://doi.org/10.1084/jem.20230570.

Tojima, R. *et al.* (2024) “Roles of C/EBPα, GATA2, TGF-β-signaling, and epigenetic regulation in the expression of basophil-specific protease genes.” Available at: https://doi.org/10.1101/2024.02.24.581851.

Tsai, F.Y. *et al.* (1994) “An early haematopoietic defect in mice lacking the transcription factor GATA-2,” *Nature*, 371(6494), pp. 221–226. Available at: https://doi.org/10.1038/371221A0.

Tsukiji, N. *et al.* (2018) “Platelets play an essential role in murine lung development through Clec-2/podoplanin interaction,” *Blood*, 132(11), pp. 1167–1179. Available at: https://doi.org/10.1182/BLOOD-2017-12-823369.

Waskow, C. *et al.* (2004) “Rescue of lethal c-KitW/W mice by erythropoietin,” *Blood*, 104(6), pp. 1688–1695. Available at: https://doi.org/10.1182/BLOOD-2004-04-1247.

Weitzmann, A. *et al.* (2020) “Mast Cells Occupy Stable Clonal Territories in Adult Steady-State Skin,” *Journal of Investigative Dermatology*, 140(12), pp. 2433-2441.e5. Available at: https://doi.org/10.1016/j.jid.2020.03.963.

Zon, L.I. *et al.* (1991) “GATA-binding transcription factors in mast cells regulate the promoter of the mast cell carboxypeptidase A gene.,” *Journal of Biological Chemistry*, 266(34), pp. 22948–22953. Available at: https://doi.org/10.1016/S0021-9258(18)54446-X.